Hydroxamic acid-functionalized Copolymers for Metal Chelation:
From Monomer Development to Thermoresponsive Materials and Biomedical Applications

Dissertation
zur Erlangung des Grades
„Doktor der Naturwissenschaften"
im Promotionsfach Chemie

am Fachbereich
Chemie, Pharmazie, Geographie und Geowissenschaften
der Johannes Gutenberg-Universität
in Mainz

Jennifer Keth

geb. in Worms

Mainz, Januar 2021

JOHANNES GUTENBERG UNIVERSITÄT MAINZ

JG|U

This thesis was carried out from October 2017 to January 2021 in the group of Professor Holger Frey at the Department of Chemistry, Johannes Gutenberg University, Mainz.

Reviewer 1: Prof. Dr. Holger Frey
Reviewer 2: ███████████████

Date of Oral Examination: 11.03.2021

Referring to §10 section 3d of the Doctoral Degree Regulations (24.07.2007), I hereby declare that I wrote the dissertation submitted without any unauthorized external assistance and used only sources acknowledged in the work. All textual passages which are appropriated verbatim or paraphrased from published and unpublished texts as well as all information obtained from oral sources are duly indicated and listed in accordance with bibliographical rules. I have not or had not submitted the work now submitted as dissertation to other state or academic examinations. I had not submitted the dissertation now submitted or parts of it to any other faculty or department.

Für meine Familie

DANKSAGUNGEN

Außerdem danke ich ███████████ und ███████████ für die SEM-Aufnahmen der polymeren Nanopartikel.

Ich möchte mich bei ██████████ für die Hilfe im Labor und das tolle Engagement bedanken, das er meinem Forschungsthema entgegenbrachte.

Ganz besonders möchte ich mich bei ████████████████████████████ neben der tatkräftigen Unterstützung im Laboralltag auch für die vielen lustigen Momente bedanken. Ihr seid aus dem Arbeitskreis einfach nicht wegzudenken. Vielen Dank für euren unermüdlichen Einsatz! Ebenso danke ich ███████████ für die Unterstützung bei vielen organisatorischen Fragestellungen und ██████████████ für die Durchführung der MALDI-ToF-MS-Messungen.

Ich werde besonders die Hüttenseminare, Konferenzen, Fastnachtsfeiern, Seewochenenden, Oktoberfeste, AK-Ausflüge und Weihnachtsfeiern in Erinnerung behalten. Ich hoffe sehr, dass diese tollen Traditionen im Arbeitskreis nach der Corona-Krise wieder aufgenommen werden. Mein besonderer Dank gilt hierbei ████████████ ██ ██████████████ für die angenehme Atmosphäre in Labor und Büro sowie für die zahlreichen Events außerhalb der Universität. Ihr habt die Zeit unvergesslich gemacht.

Mein Dank gilt auch meinen Freunden, die mich während meines Studiums begleitet haben. Ganz besonders möchte ich hierbei ████████████████████████████ ████████████████ hervorheben. Ohne euch wäre die Zeit nur halb so lustig gewesen. Vielen Dank!

Außerdem möchte ich mich bei meinen Freunden außerhalb des Arbeitskreises und des Studiums bedanken. Vielen Dank ███████████████████.

Mein größter Dank gilt ███████████ die mich zu jeder Zeit unterstützt haben. Ohne eure Hilfe und euer Zutun wäre mein Studium und meine Promotion nicht möglich gewesen. Vielen Dank für Alles!

Abschließend möchte ich mich noch von ganzem Herzen bei ██████████ für sein Verständnis und seine Unterstützung in jeder Lebenslage bedanken. Danke, dass du für mich da bist und mir immer mit Rat und Tat zur Seite stehst.

# CONTENTS

MOTIVATION AND OBJECTIVES

Nature enables the bioavailability of iron via several types of "siderophores" (greek: "iron carriers"). Especially the catechol moiety exhibits excellent complexation behavior towards iron and enables the iron metabolism in various microorganisms. As another example, 3,4-dihydroxyphenyl-L-alanine (DOPA) is an essential part in the mussel foot protein that enables strong adhesion at various surfaces under extreme conditions. Based on these properties, catechol moieties have become interesting compounds for synthetic polymer structures, i.e. for antifouling surface coatings or adhesive hydrogels.[1] Besides their unique complexation capability, the catechol moiety possesses a drawback that severely limits its technical use in industry. The facile oxidation to quinones complicates its handling and therefore impedes application in various fields.

In nature, another functional group is known that exhibits excellent complexation abilities: hydroxamic acids. These moieties possess slightly lower complex stability constants than their catechol analogues, but they are stable against oxidative processes in air in a wide pH range.[2] These compounds are already well established to treat iron overload diseases, as in the treatment of thalassemia. Despite the poor oral availability, the hydroxamic acid-bearing deferoxamine is currently the "gold standard" for iron chelation therapy.[3] Besides their relevance in medical applications, their strong interaction with metal ions opens a wide range of applications in the field of materials science. For example, they were used for the separation of rare-earth metals, for waste water treatment[4] and also as linking agents in dye-sensitized solar cells[5] and metal organic frameworks[6].

Despite their fascinating complexation capability, only a few works regarding hydroxamic acids-functionalized polymers are known. The first report on polymeric hydroxamic acids date back to 1942.[7] In the 1970s, Winston *et al.* with their in-depth investigations contributed fundamentally to the understanding of poly(hydroxamic acid)s as metal chelators.[8] Usually, hydroxamic acid functionalities are introduced via tedious and non-quantitative postmodification reactions with hydroxylamine, starting from poly(methacrylate)s or poly(acrylamide)s. Unfortunately, these postmodification reactions lead to side products and non-quantitative conversion.[9] Therefore, it is an important objective to introduce hydroxamic acid moieties directly into a polymer structure, avoiding postmodification efforts. Furthermore, the introduction of hydroxamic acids via postmodifications leads to limited possibilities for adjusting the polarity of the polymers, since functional groups such as esters or amides are required for the reaction with hydroxylamine. The copolymerization of hydroxamic acids with comonomers of different hydrophilicities could offer a powerful tool to adjust the solubility behavior of the metal chelating polymers precisely and

in one step. Due to the current lack of a method for direct incorporation of hydroxamic acids into well-defined hydrophobic or hydrophilic polymers, the following question arises that is addressed in the first part of this work (**Scheme 1**):

"*How can one directly incorporate hydroxamic acids both into hydrophobic and hydrophilic polymers while obtaining control over the number and position of the functionalities and the molecular weight of the polymers?*"
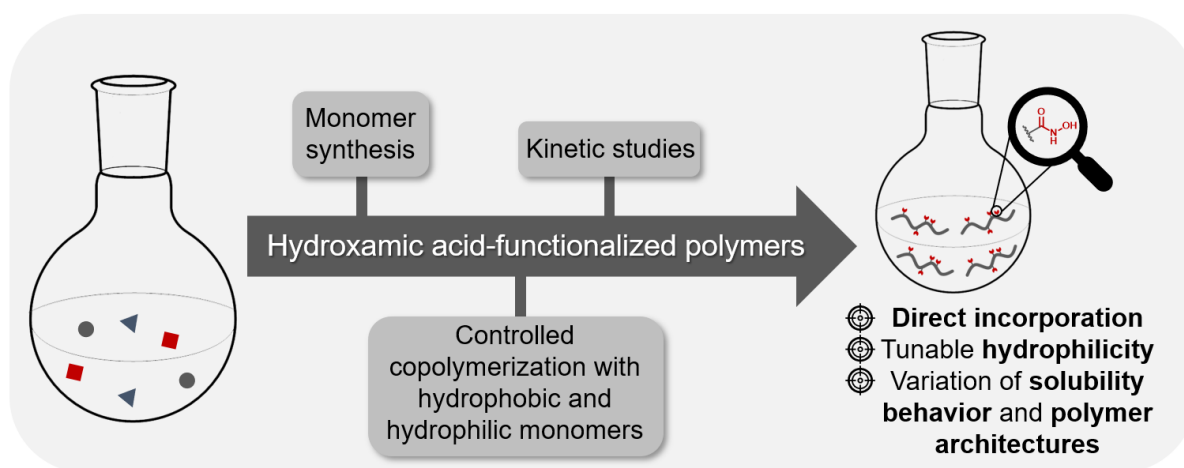
SCHEME 1 Schematic procedure to develop hydroxamic acid-functionalized copolymers with different polarities and polymer architectures.

In the last decades, stimuli-responsive materials became very important in applied materials science. For thermoresponsive materials, hydrophilicity and the structural shape of the polymers in aqueous media were controlled by temperature as an external trigger.[10] These properties enable various bio-applications, such as enzyme recycling, protein chromatography, controlled bio-adhesion, hyperthermia-induced drug delivery and tissue engineering.[10] Since its discovery in the 1960s, poly(*N*-isopropylacrylamide) (PNIPAM) became the most prominent example for thermoresponsive materials and is construed as "gold standard" in this research area. However, several drawbacks of these materials, such as the irreversible phase transition or the strong influence of end groups on the thermal behavior for smaller polymers, paved the way for the extensive research for alternative thermoresponsive materials.[10] Various research groups focused on the preparation of poly(oligo ethylene glycol methacrylate) (POEGMA) as an alternative to PNIPAM.[11-13] Unlike linear poly(ethylene glycol), POEGMA is composed of a carbon-carbon backbone with multiple oligo (ethylene glycol) side chains in a brush-like structure. The oligo(ethylene glycol) segments (up to 85% in weight) lead to the water-soluble and biocompatible character of these materials.[14] Thus, POEGMA combines the thermoresponsive properties of PNIPAM with the biocompatibility of linear PEG. The combination of aqueous solubility

and metal chelating motifs, using temperature as an external trigger could open a variety of application fields. In terms of materials and medical sciences, water-insoluble hydroxamic acid-functionalized copolymers could be attractive candidates for surface adhesion or as nanocarriers for magnetic nanoparticles in pharmacological applications. Therefore, it is crucial to investigate both potential applications and the properties of both water-soluble and water-insoluble hydroxamic acid-functionalized copolymers. In this context we will focus on the following question (**Scheme 2**):

"*How can one adjust and apply the versatile properties of water-soluble and water-insoluble hydroxamic acid-functionalized copolymers in the fields of materials and medical sciences?*"
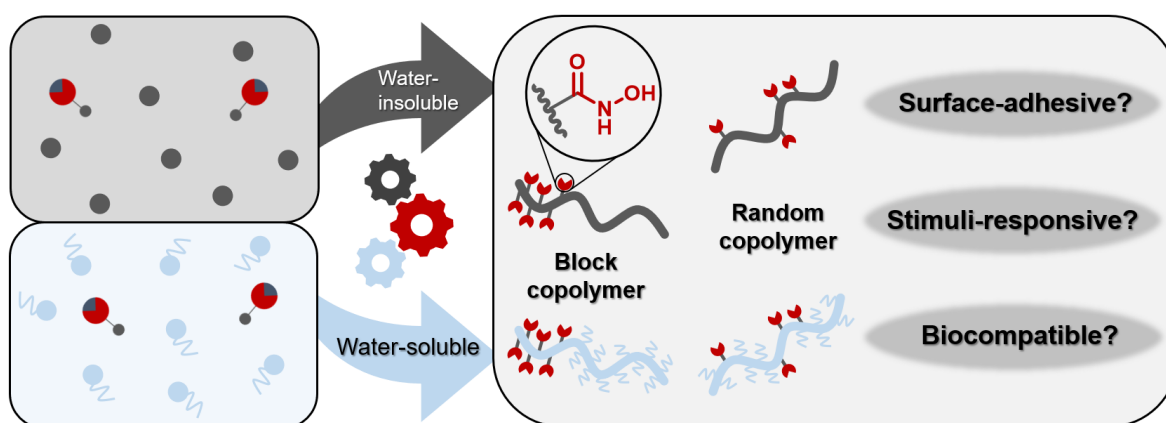
SCHEME 2   Schematic illustration of the strategy to obtain water-soluble and water-insoluble hydroxamic acid-functionalized copolymers with varied polymer architectures.

In this work, chapter 1 and 2 focus on the essential properties of hydroxamic acids and a general approach to synthesize well-defined hydrophobic or hydrophilic copolymers with control over the number and the position of hydroxamic acids. The versatile properties and potential applications of water-soluble and water-insoluble hydroxamic acid-functionalized copolymers are presented in chapter 3 and 4 of this work.

REFERENCES

(1) Niederer, K.; Schüll, C.; Leibig, D.; Johann, T.; Frey, H. Catechol Acetonide Glycidyl Ether (CAGE): A Functional Epoxide Monomer for Linear and Hyperbranched Multi-Catechol Functional Polyether Architectures. *Macromolecules* **2016**, *49*, 1655–1665.

(2) Neilands, J. B. Hydroxamic Acids in Nature. Science 1967, 156, 1443–1447.

(3) Abbina, S.; Abbasi, U.; Gill, A.; Wong, K.; Kalathottukaren, M. T.; Kizhakkedathu, J. N. Design of Safe Nanothera-peutics for the Excretion of Excess Systemic Toxic Iron. *ACS central science* **2019**, *5*, 917–926.

(4) Rahman, M. L.; Sarkar, S. M.; Yusoff, M. M.; Abdullah, M. H. Optical detection and efficient removal of transition metal ions from water using poly(hydroxamic acid) ligand. *Sens. Actuators, B* **2017**, *242*, 595–608.

(5) Brewster, T. P.; Konezny, S. J.; Sheehan, S. W.; Martini, L. A.; Schmuttenmaer, C. A.; Batista, V. S.; Crabtree, R. H. Hydroxamate anchors for improved photoconversion in dye-sensitized solar cells. *Inorg. Chem.* **2013**, *52*, 6752–6764.

(6) Pereira, C. F.; Howarth, A. J.; Vermeulen, N. A.; Almeida Paz, F. A.; Tomé, J. P. C.; Hupp, J. T.; Farha, O. K. Towards hydroxamic acid linked zirconium metal-organic frameworks. *Mater. Chem. Front.* **2017**, *117*, 10401.

(7) Coffman, D. D. Polymeric Hydroxamic Acids. US2402604 A, **1946**.

(8) Winston, A.; Mazza, E. T. Hydroxamic acid polymers. *J. Polym. Sci. Pol. Chem.* **1975**, *13*, 2019–2030.

(9) Mello, R. S.; Orth, E. S.; Loh, W.; Fiedler, H. D.; Nome, F. Polymers containing hydroxamate groups: nanoreactors for hydrolysis of phosphoryl esters. *Langmuir* **2011**, *27*, 15112–15119.

(10) Lutz, J.-F.; Weichenhan, K.; Akdemir, Ö.; Hoth, A. About the Phase Transitions in Aqueous Solutions of Thermore-sponsive Copolymers and Hydrogels Based on 2-(2-methoxyethoxy)ethyl Methacrylate and Oligo(ethylene glycol) Methacrylate. *Macromolecules* **2007**, *40*, 2503–2508.

(11) Wang, X.-S.; Lascelles, S. F.; Jackson, R. A.; Armes, S. P. Facile synthesis of well-defined water-soluble polymers via atom transfer radical polymerization in aqueous media at ambient temperature. *Chem. Commun.* **1999**, 1817–1818.

(12) Wang, X.-S.; Armes, S. P. Facile Atom Transfer Radical Polymerization of Methoxy-Capped Oligo(ethylene glycol) Methacrylate in Aqueous Media at Ambient Temperature. *Macromolecules* **2000**, *33*, 6640–6647.

(13) Tao, L.; Mantovani, G.; Lecolley, F.; Haddleton, D. M. Alpha-aldehyde terminally functional methacrylic polymers from living radical polymerization: application in protein conjugation "pegylation". *J. Am. Chem. Soc.* **2004**, *126*, 13220–13221.

(14) Lutz, J.-F. Polymerization of oligo(ethylene glycol) (meth)acrylates: Toward new generations of smart biocompat-ible materials. *J. Polym. Sci. Pol. Chem.* **2008**, *46*, 3459–3470.

ABSTRACT

With the first experiments demonstrating the existence of macromolecules in 1920 by Hermann Staudinger, a success story started that persists until today. In our everyday life, polymers became omnipresent. The broad application fields range from packaging materials to the use in medicine and pharmaceutics. Relying on a variety of polymerization techniques, tailored polymer structures can be synthesized and precisely adjusted to the respective application field of interest. With the variation of monomers, composition, molecular weights and polymer architectures, material properties can be tuned in a targeted manner.

This thesis focuses on the synthesis of hydroxamic acid-based monomer structures and their polymerization to well-defined metal-chelating materials. Hydroxamic acids possess outstanding importance in nature as functional group in "siderophores" (greek: iron carriers) to enhance the bioavailability of Fe(III) in the metabolism of various microorganisms. **Chapter 1** reviews the essential characteristics of hydroxamic acids in terms of their structural properties, the synthesis and the applications in both medical and materials sciences.

The combination of the underrated hydroxamic acid moiety with polymers has been reported only in a limited number of works to date. Hydroxamic acids (HA) are mainly introduced via postmodification reactions with hydroxylamine, leading to side reactions and mostly ill-defined materials. **Chapter 2** deals with the incorporation of hydroxamic acids into poly(methacrylate)s via copolymerization, yielding well-defined structures (**Scheme 1**).
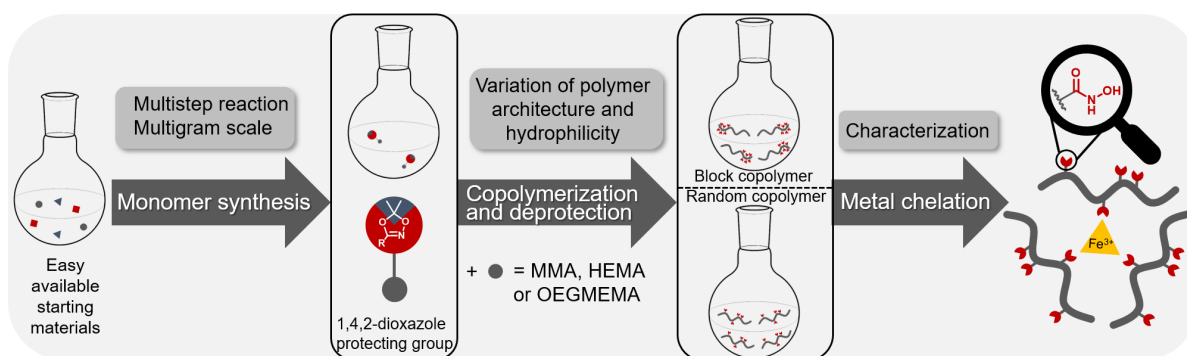
SCHEME 1 Schematic illustration of the synthesis strategy to generate metal-chelating hydroxamic acid-functionalized polymers with varied polarity and polymer architecture.

For this purpose, a monomer was designed that exhibits (i) a methacrylate polymerizable group, (ii) an ethylene glycol spacer unit to separate the polymerizing group from (iii) the protected hydroxamic acid moiety. The hydroxamic acid functionalities were present as 1,4,2-dioxazole moieties to withstand the reaction conditions in a RAFT polymerization. With this approach, hydrox-

amic acids can be attached to poly(methacrylate)s, controlling both the number and the position of the HA functionalities. ^{1}H NMR kinetic measurements confirmed the random incorporation of the hydroxamic acid-functionalized monomer in copolymerizations with methyl methacrylate (MMA), hydroxyethyl methacrylate (HEMA) and oligo (ethylene glycol) methyl ether methacrylate (OEGMEMA), respectively. The multifunctional polymers demonstrate a strong adhesion at iron and copper surfaces, confirmed by contact angle measurements.

The properties of copolymers consisting of hydroxamic acids and OEGMEMA as a non-linear PEG-based macromonomer were further investigated in **Chapter 3** (**Scheme 2**). The OEGMEMA moieties in the copolymers enable a reversible temperature-induced switch between the soluble and the collapsed aggregated state (LCST). The hydrophilicity of the copolymers can therefore be controlled by temperature as a simple external trigger. The system revealed a reversible phase transition during heating and cooling cycles. It was shown, that the LCST was influenced by the molecular weight, the polymer architecture and the degree of deprotection. In addition, the incorporation of hydroxamic acids into the copolymers enables metal chelation through O,O-coordination of hydroxamic acids with various metal ions. Investigation via isothermal calorimetry titration (ITC) confirmed the high binding affinity between poly(hydroxamic acid)s and Fe(III). The combination of aqueous solubility and metal chelating properties opens a variety of applications in both materials and medical sciences. Studies of the complexation behavior of the copolymers towards Fe(III) as well as cell viability studies demonstrate the suitability of hydroxamic acids bearing POEGMEMA for biomedical application.
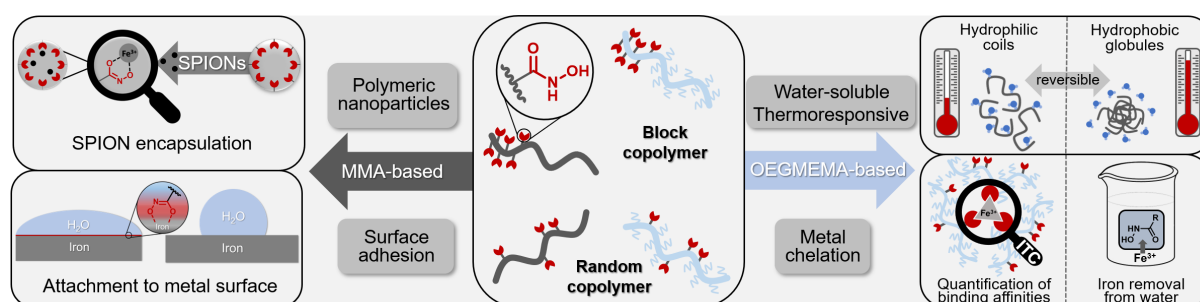
SCHEME 2 Schematic illustration of the properties and potential applications of hydrophobic and hydrophilic hydroxamic acid-functionalized copolymers.

Chapter 4 deals with the synthesis of polymeric nanoparticles for the encapsulation of superparamagnetic iron oxide nanoparticles (SPIONs) via the introduction of hydroxamic acids as numerous iron receptor sites (**Scheme 2**). Investigations both via electron microscopy and UV-Vis spectroscopy confirmed enhanced SPION uptake into the functional polymeric nanoparticles already at low hydroxamic acid amounts of 5%$_{mol}$, compared to non-functional analogues. Inves-

tigations via fluorescence-based flow cytometry and metabolic activity tests on murine spleen cells provide information regarding the cell-specific accumulation and confirmed low toxicity of these materials.

Appendix. This work was the result of a collaboration with ███████████ preceding other chapters of this thesis. The publication reveals a general concept for the introduction of hydroxamic acids into polymers. Protected hydroxamic acid moieties were used as key structure for the synthesis of multifunctional polymers. Oxyanionic and controlled radical polymerization techniques provided control over the number and the position of hydroxamic acid moieties in the polymer. The coating of surfaces and nanoparticles as well as T cell proliferation assays demonstrate the versatile advantages and the low toxicity of hydroxamic acid-functionalized polymers.

ZUSAMMENFASSUNG

Mit der ersten Dokumentation von Makromolekülen im Jahr 1920 durch Hermann Staudinger begann eine Erfolgsgeschichte, die bis heute andauert. In unserem täglichen Leben wurden Polymere allgegenwärtig. Die vielseitigen Anwendungsbereiche reichen von Verpackungsmaterialien bis hin zur Verwendung in medizinischen und pharmazeutischen Bereichen. Durch eine Vielzahl verschiedener Techniken können maßgeschneiderte Polymerstrukturen synthetisiert und präzise an das jeweilige Anwendungsgebiet angepasst werden. Mit der Variation von Monomeren, Zusammensetzungen, Molekulargewichten und Polymer-Architekturen können viele Materialeigenschaften gezielt eingestellt werden.

Diese Arbeit beschreibt die Synthese von Hydroxamsäure-basierten Monomeren und deren Polymerisation zu definierten Komplexbildnern. Hydroxamsäuren haben in der Natur eine herausragende Bedeutung als funktionelle Gruppe in „Siderophoren" (griechisch: Eisenträger), um die Bioverfügbarkeit von Fe(III) im Metabolismus verschiedener Mikroorganismen zu verbessern. In **Kapitel 1** werden die strukturellen Eigenschaften, die chemische Synthese und Anwendungen von Hydroxamsäuren sowohl im medizinischen als auch in materialwissenschaftlichen Kontexten vorgestellt.

Die Kombination von Hydroxamsäuren mit Polymeren wird nur in wenigen Arbeiten beschrieben. Bislang wurden Hydroxamsäuren hauptsächlich über polymeranaloge Modifikationen mit Hydroxylamin eingeführt, die zu Nebenreaktionen und undefinierten Materialien führen. In **Kapitel 2** wird eine Strategie zum direkten Einbau von Hydroxamsäuren in Poly(methacrylate) (**Abbildung 1**) vorgestellt. Hierfür wurde ein Monomer entwickelt, das (i) eine polymerisierende Methacrylat-Gruppe, (ii) eine Ethylenglykol-Einheit zur Separierung der polymerisierenden Gruppe von (iii) der Hydroxamsäure-Funktionalität besitzt. Um den Reaktionsbedingungen während einer RAFT-Polymerisation standzuhalten, wurden die Hydroxamsäure-Funktionalitäten in 1,4,2-Dioxazol-Schutzgruppen überführt. Mit dieser Strategie konnten Hydroxamsäure-funktionelle Poly(methacrylate) mit Kontrolle über die Anzahl und die Position der Funktionalitäten synthetisiert werden. Kinetische ^{1}H-NMR-Messungen bestätigen den statistischen Einbau des Hydroxamsäure-funktionellen Monomers in Copolymerisationen mit Methylmethacrylat (MMA), Hydroxyethylmethacrylat (HEMA) bzw. Oligo(ethylen glykol)methylethermethacrylat (OEGMEMA). Die multifunktionellen Polymere zeigen eine starke Haftung an Eisen- und Kupferoberflächen, die durch Kontaktwinkel-Messungen verfolgt wurde.
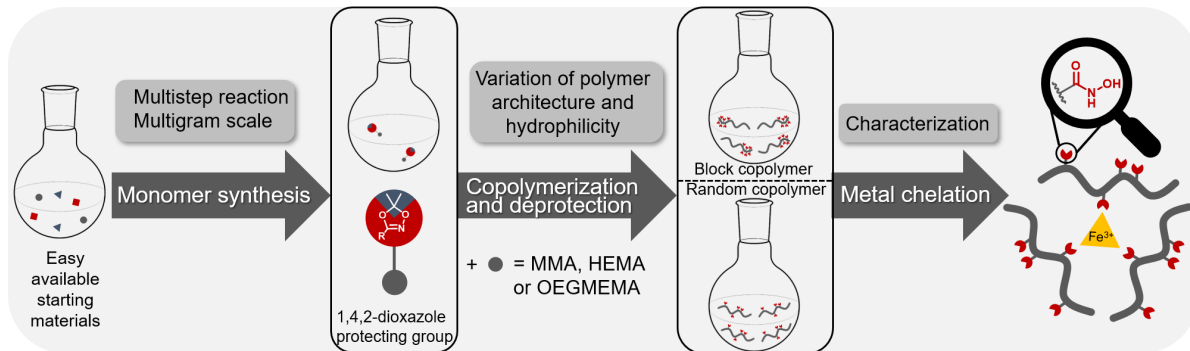
ABBILDUNG 1 Schematische Darstellung der Strategie zur Synthese von Hydroxamsäure-funktionalisierten Polymeren mit unterschiedlichen Polaritäten und Polymerarchitekturen.

Die Eigenschaften von Copolymeren bestehend aus den nicht-linearen PEG-basierten Makromonomeren OEGMEMA und Hydroxamsäuren werden in **Kapitel 3** weiter untersucht (**Abbildung 2**). Die OEGMEMA-Einheiten innerhalb der Copolymere ermöglichen einen reversiblen, temperaturinduzierten Wechsel zwischen dem löslichen und dem kollabierten aggregierten Zustand. Die Hydrophilie der Copolymere kann daher über die Temperatur als einfachen, externen Parameter gesteuert werden. Das System zeigt einen reversiblen Phasenübergang während der Heiz- und Kühlprozesse. Die Trübungspunkte werden durch das Molekulargewicht, die Polymerarchitektur und den Grad der Hydroxamsäure-Entschützung beeinflusst. Neben den thermoresponsiven Eigenschaften der Materialien, ermöglicht der Einbau von Hydroxamsäuren die Komplexbildung mit verschiedenen Metallionen. Untersuchungen mittels isothermer Titrationskalorimetrie (ITC) bestätigen die hohe Bindungsaffinität zwischen Poly(hydroxamsäure) und Fe(III). Die Kombination von wasserlöslichen und komplexierenden Eigenschaften kann eine Vielzahl von Anwendungsbereichen sowohl in den Material- als auch in den medizinischen Wissenschaften eröffnen. Grundlegende Studien zur Komplexierung von Fe(III) und Tests zur Bestimmung der metabolischen Aktivität von murinen Milzzellen zeigen die vielseitigen Vorteile der Kombination von Hydroxamsäuren mit POEGMEMA.

Kapitel 4 befasst sich mit der Synthese von Hydroxamsäure-funktionellen Nanopartikeln zur Einkapselung von superparamagnetischen Eisenoxid-Nanopartikeln (SPION) (**Abbildung 2**). Untersuchungen sowohl mittels Elektronenmikroskopie als auch mittels UV-Vis-Spektroskopie bestätigen eine erhöhte SPION-Aufnahme bei Nanopartikeln mit einem Hydroxamsäure-Anteil von $5\%_{mol}$ im Vergleich zu nicht funktionellen Analoga. Untersuchungen mittels fluoreszenzbasierter Durchflusszytometrie und Tests zur Bestimmung der metabolischen Aktivität von murinen Milzzellen geben Aufschluss über die zellspezifische Akkumulation und bestätigen die geringe Toxizität dieser Materialien.
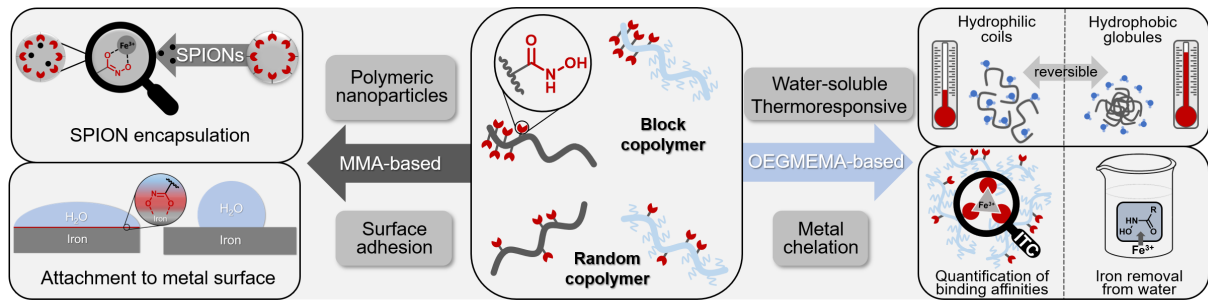
ABBILDUNG 2 Schematische Darstellung der Eigenschaften und der möglichen Anwendungen von hydrophoben und hydrophilen Hydroxamsäure-funktionalisierten Copolymeren.

Appendix. Diese Arbeit resultierte aus einer Zusammenarbeit mit ▮▮▮▮▮▮▮▮ und beschreibt ein allgemeines Konzept für die Einführung von Hydroxamsäuren in Polymere. Geschützte Hydroxamsäure-Einheiten wurden als zentrale Komponenten für die Synthese multifunktioneller Polymere verwendet. Oxyanionische und kontrollierte radikalische Polymerisationstechniken lieferten eine Kontrolle über die Anzahl und die Position der Hydroxamsäure-Einheiten im Polymer. Die Beschichtung von Oberflächen und Nanopartikeln sowie T-Zell Proliferationstests zeigen die vielseitigen Vorteile und die geringe Toxizität Hydroxamsäure-funktionalisierter Polymere.

GRAPHICAL ABSTRACT

CHAPTER 1 | Introduction of hydroxamic acids
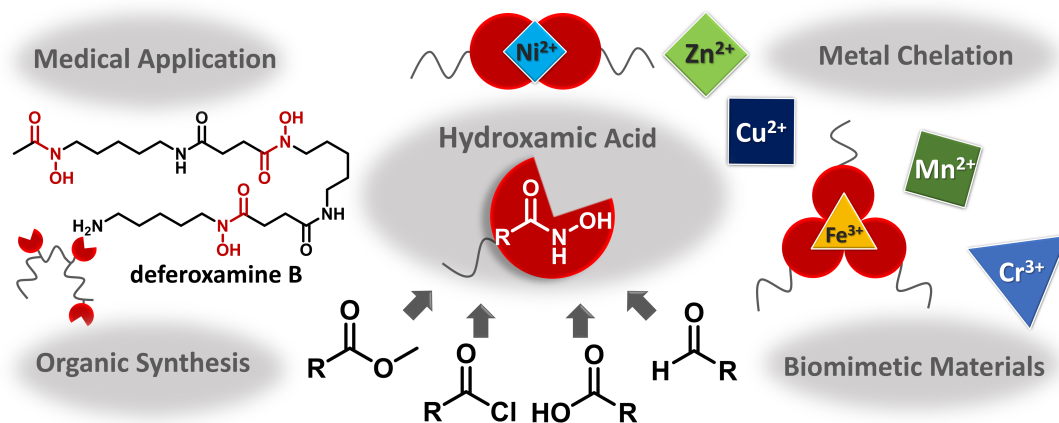
CHAPTER 2 | Introduction of hydroxamic acids into poly(methacrylate)s
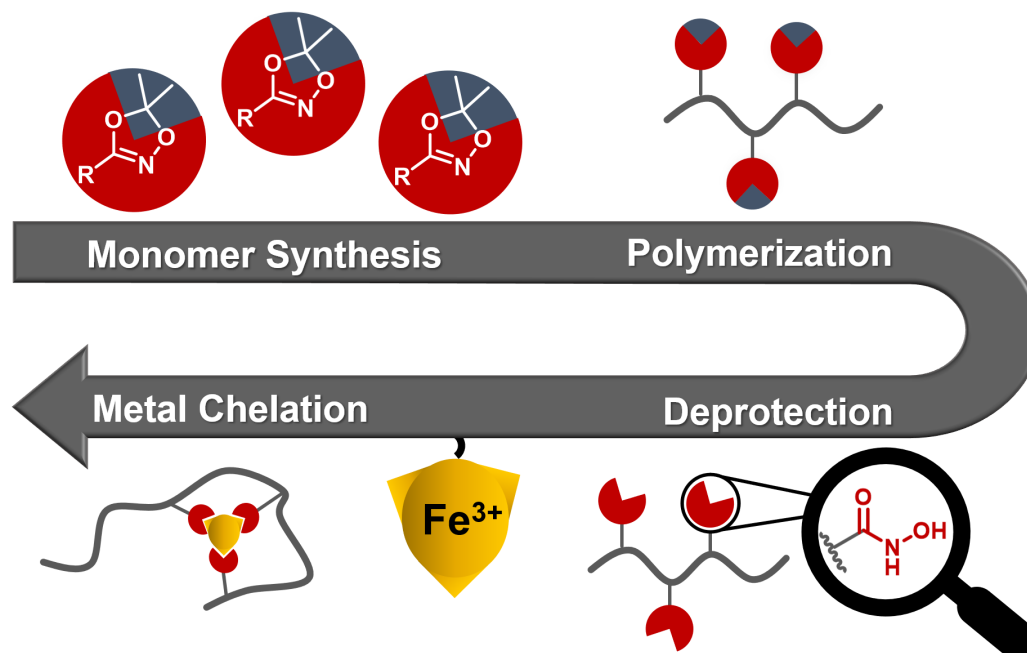
CHAPTER 3 | Water-soluble hydroxamic acid-functionalized poly(methacrylate)s
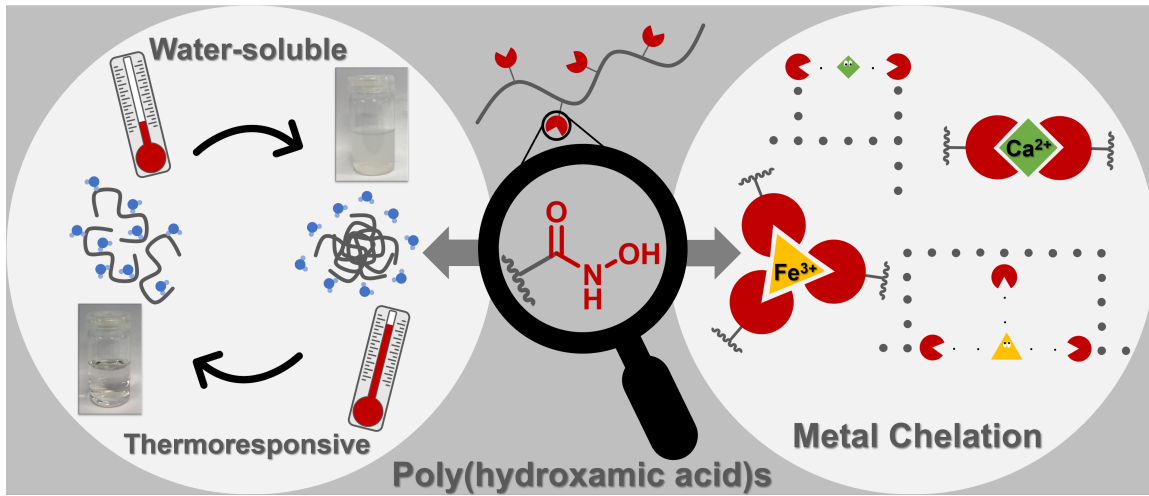
CHAPTER 4 | Polymeric nanoparticles for SPION encapsulation
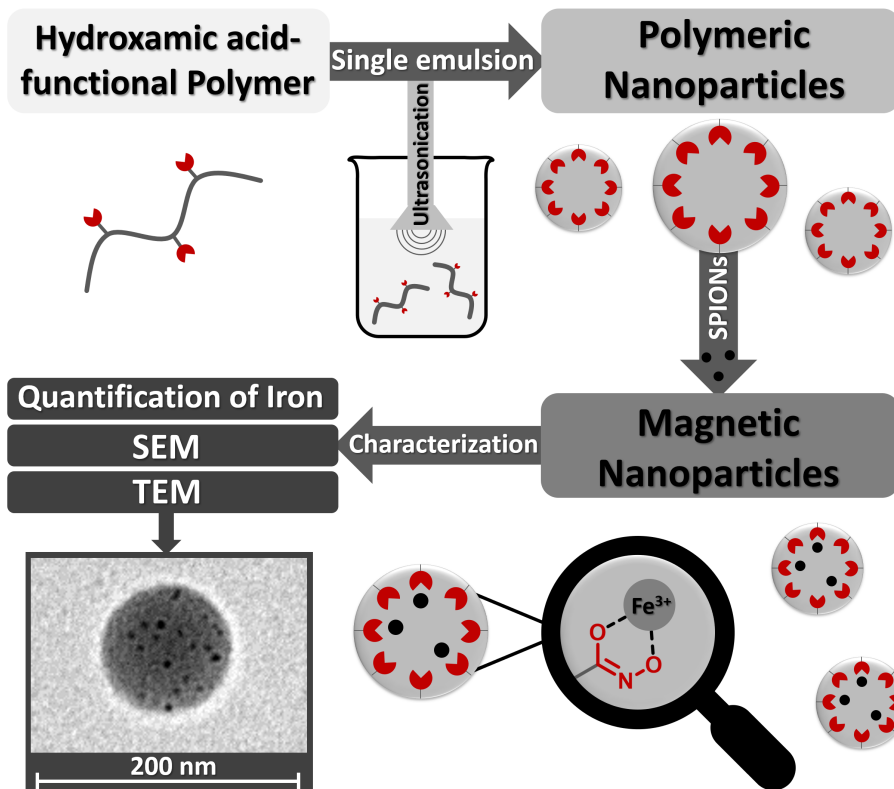
APPENDIX | Introduction of hydroxamic acids into polymers

R = H, CH$_3$, CH$_2$-OH

✓ Non-toxic, biocompatible

✓ Alternative to catechols

✓ Excellent coating & chelation

1 Fe + 1 HA

1 Fe + 3 HA

Nanoparticles

CHAPTER 1

INTRODUCTION OF HYDROXAMIC ACIDS

CHAPTER 1

Hydroxamic Acid – An Underrated Moiety? Marrying Bioinorganic Chemistry and Polymer Science

Jennifer Keth[1], Tobias Johann[1] and Holger Frey[1*]

[1]Department of Chemistry, Johannes Gutenberg-University, Duesbergweg 10-14, 55124 Mainz, Germany

Even 150 years after their discovery, hydroxamic acids are mainly known as the starting material for the Lossen rearrangement in textbooks. However, hydroxamic acids feature a plethora of existing and potential applications ranging from medical purposes to materials science, based on their excellent complexation properties. This underrated functional moiety can undergo a broad variety of organic transformations and possesses unique coordination properties for a large variety of metal ions, *e.g.* Fe (III), Zn(II), Mn(I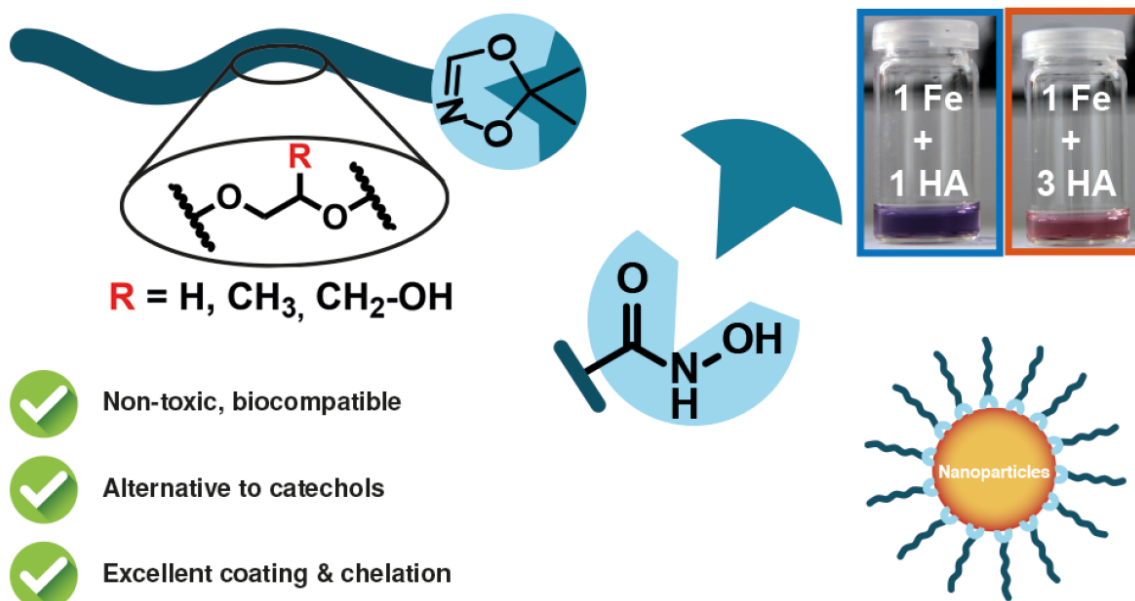I) and Cr(III). This renders it ideal for biomedical applications in the field of metal-associated diseases or the inhibition of metalloenzymes, as well as for the separation of metals. Considering their chemical stability and reactivity, their biological origin and both medical and industrial applications, this review aims at highlighting hydroxamic acids as highly promising chelators in the fields of both medical and materials science. Furthermore, the state of the art in combining hydroxamic acids with a variety of polymer structures is discussed and a perspective regarding their vast potential at the interface of bioinorganic and polymer chemistry is given.

INTRODUCTION

Heinrich Lossen discovered hydroxamic acids (**Scheme 1**) in 1869 as the reaction product of hydroxylamine and diethyl oxalate. Wilhelm Lossen created the term "hydroxamic acid" due to the acidic behavior, the amide related structure and the preparation by treatment of carbonyl compounds with hydroxylamine.[1] They are often also denoted "*N*-hydroxyamides" or "*N*-acyl hydroxylamine".
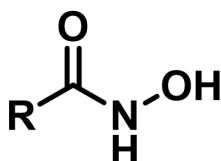

SCHEME 1   Lewis structure of the hydroxamic acid moiety.[2]

Hydroxamic acids are generally not considered as a prominent functional group in organic chemistry. They are mostly known as the starting material for the so-called Lossen rearrangement. This review summarizes the versatile properties of hydroxamic acids and their use in organic and polymer chemistry as well as their current and prospective application in medicine and material science.

Structural properties.

Hydroxamic acids are typically crystalline solids. Their behavior is complicated by the existence of three tautomeric forms: The *Z* (**Scheme 2a**) and *E* (**Scheme 2b**) amide and the oxime diol (**Scheme 2c**) form that is called "hydroximic acid". The tautomers differ in reactivity, especially towards deprotonation. The diol form is usually not found in solution or solid state, but it can be used as a starting material for further reactions (*vide infra*).[3] The ratio of *E* to *Z* tautomer varies with temperature and concentration in solution.[4] At lower temperatures the tautomers are also detectable via ^{1}H NMR spectroscopy.[3] *p*-Hydroxybenzohydroxamic acid is mostly found as the *E* tautomer at -60 °C in acetone (*Z*:*E*=4:96). Similar results have been reported for benzohydroxamic acid and salicylhydroxamic acid as well.[3] X-ray crystallography suggests that in the solid state the *Z* amide is found exclusively. The typical bond length of the C-N bond is 1.32 Å, confirming the amide type bond character and thus limited rotational freedom of the C-N bond.[5] The different tautomer distribution in solution (mostly *E*) compared to solid state (exclusive *Z*) can be accounted to *E*-*E* dimers which are formed in solution and stabilized via hydrogen bonds.[3]

a
Z Amide

b
E Amide

c
Hydroximic acid

a'

b'
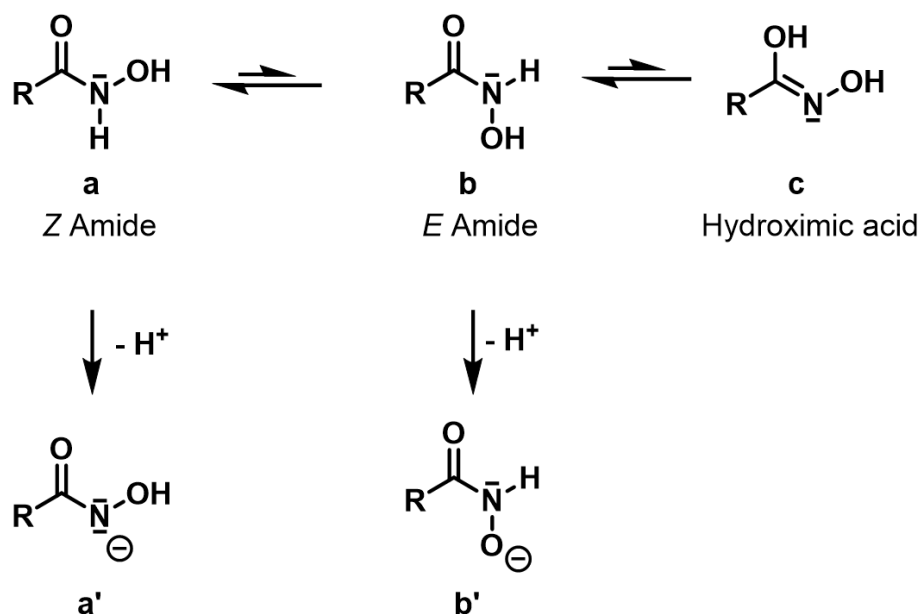
**SCHEME 2**   Tautomers of hydroxamic acids and their different deprotonated forms.[2]

Acid-base behavior.

Even though hydroxamic acids have been known since 1869, their acid-base properties are still not well understood.[3] As their name implies, hydroxamic acids can react as Brønsted acids to form the so-called "hydroxamates" (**Scheme 2a', 2b'**). The typical pK_s-values range from 7 to 9, whereas the related amides are generally 6 magnitudes less acidic.[2] In their unsubstituted NH-OH form, deprotonation can occur either at the amide N-H or the hydroxyl group. Deprotonation of the N-H group is favored in DMSO or in the gas state, while in water or alcohols the deprotonation at the hydroxyl group in analogy to carboxylic acids predominates. Double negatively charged hydroxamic acids, simultaneously deprotonated at the amide and hydroxyl groups, are only known in rare cases due to specific metal-ligand interactions.[6–10]

Ab initio calculations by Venturini *et al.* suggest that the *Z* tautomer is preferentially deprotonated at the N-H-group (**Scheme 2a'**), while the *E* tautomer favors deprotonation at the hydroxyl group (**Scheme 2b'**).[3] Protonation by strong acids occurs only at the carbonyl oxygen. The pK_s-value for protonation was reported as pK_s = -2.1 ± 0.1.[7]

Chemical stability and reactivity.

Hydroxamic acids do not exhibit unlimited stability under strongly acidic or basic conditions. Their chemical behavior under these conditions is very similar to the related amides, carboxylic acids or carboxylates.[2,11]
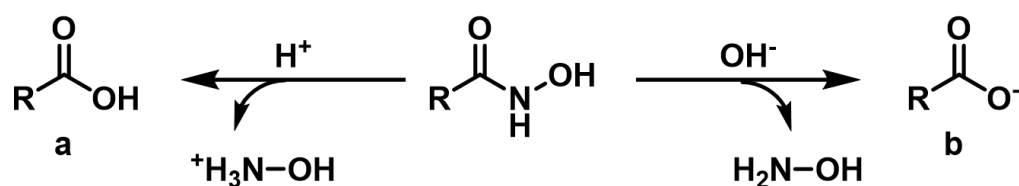
SCHEME 3 Reaction pathway of hydroxamic acids under strongly acidic or basic conditions.

The acidic hydrolysis (**Scheme 3a**) follows first-order kinetics with regard to the proton concentration with protonation at the carbonyl group being the kinetically limiting reaction step. The rate constant for the hydrolysis of benzohydroxamic acid was estimated as $k_{89\,°C} = 1.92 \cdot [H^+] \cdot h^{-1}$ with a half-life of 22 minutes at 89 °C in 1 M HCl.[12] The base-catalyzed degradation (**Scheme 3b**) is more complex due to the underlying tautomer equilibria. For the hydrolysis of benzohydroxamic acid in 0.12 M NaOH at 89 °C a half-life of 16.5 hours was determined. At neutral pH values hydroxamic acids are known to be stable*.[12] Besides their reaction with nucleophiles, hydroxamic acids can also act as nucleophiles themselves. Acylation usually proceeds to form O-acylhydroxamic acids - typical reagents for the Lossen rearrangement. In fact, this prominent name reaction was coined in 1872 when W. Lossen heated dibenzohydroxamic acid (**Scheme 4a**), and phenyl isocyanate was released (**Scheme 4b**), then described as a strong tear gas.[13]
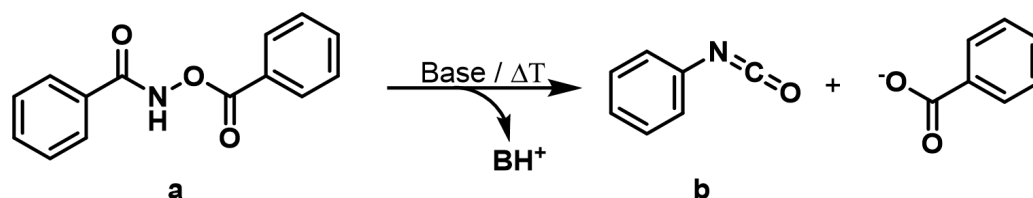

SCHEME 4 Lossen rearrangement of O-benzoylbenzoic hydroxamic acid (historically called "dibenzohydroxamic acid" by W. Lossen).

The rearrangement proceeds in a concerted mechanism under catalysis with bases or acids and heating. A nitrene intermediate is not known.[14] The rearrangement is spontaneous when highly active acid halides or phosphorus halides are used for acylation.[15] Alkylation first forms O-alkylated products, followed by additional N-alkylated structures.[16]

---

*The rate constants for basic and acidic conditions were determined only at 88.6 °C by Berndt and Fuller.[12] No degradation was found at neutral pH for 24 h at 88.6 °C was found. Importantly, from this behavior also high stability at physiological conditions can be concluded.

Complexation properties.

Apart from their use as precursors for isocyanate synthesis, hydroxamic acids are well-known for their outstanding complexation properties. Hydroxamic acids typically form complexes as bidentate ligands via *O,O*-coordination to form very stable 5 membered ring structures (**Scheme 5a**). Their stability is approximately 7 orders of magnitude higher compared to carboxylic acids that only form a 4 membered ring (**Scheme 5b**).[17,18] Chelation can only proceed from the single deprotonated Z tautomer, which is formed dynamically via the tautomer equilibrium.[10,19]

a   **b**
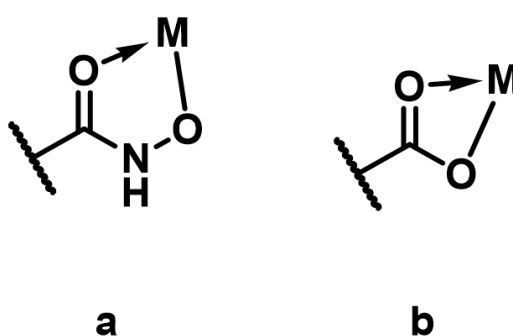
SCHEME 5 Coordination structure of hydroxamic acids (**a**) versus carboxylic acids (**b**).

The most prominent complexes are formed with Fe(III) and are also often found in nature to increase the bioavailability of insoluble iron compounds. Complexes with nearly every metal are known. With Fe(III), Cr(III), Co(III), In(III), Si(IV), Ge(IV) typically octahedral complexes are formed, while quadratic planar complexes with Cu(II) and heteroleptic complexes with V(V), Co(II), Co(III), Ni(II), Mo(VI), Rh(III), Rh(III), Sn(IV), W(VI), Os(III), Pt(II) and U(IV) are known. Notably, the complexes of Ni(II), Pt(II) and Pd(II) do not form classical *O,O*-bidentate coordination spheres.[10] The Fe(III) complexes with benzohydroxamic acid are distorted octahedral high spin (Δ-f ac) complexes with facial arrangement of the hydroxamic acids. The magnetic moment was determined as 5.8 μ_B.[10,20] For bivalent metals, the stability constants follow the Irving-Williams scheme (Cu(II) > Ni(II) > Zn(II) > Mn(II) > Mg(II)).[19,21–23]

In a seminal work directed at surface interaction, Whitesides *et al.* reported the following affinity order for surface interaction aiming at the formation of self-assembled monolayers (SAMs) by hydroxamic acids: CuO_x > AgO_x > AlO_x > ZrO_x ~ FeO_x > TiO_x > Au.[17]

TABLE 1 Stability constants (log K) for a variety of metal complexes for acetohydroxamic acid (AHA), benzohydroxamic acid (BHA) and catechol.[18,19,21,24,25]

Complex	Fe(III)	Mn(II)	Zn(II)	Cu(II)	Ni(II)	Z(IV)	U(IV)O$_2$
[M(AHA)]	11.4	4.0	5.2	7.9	5.2		
[M(AHA)$_2$]	21.1	6.9	9.5	14.1	9.2		
[M(AHA)$_3$]	28.3		11.6		11.7		
[M(BHA)]	11.1	6.0	7.6	10.0	7.2	12.4	8.7
[M(BHA)$_2$]	20.4	10.5	13.2	18.1	12.3	24.1	16.8
[M(BHA)$_3$]	27.8						
[M(Catechol)]	20.0	7.7	9.9	13.9	8.9		15.9
[M(Catechol)$_2$]	34.7	13.6	17.4	24.9	14.4		
[M(Catechol)$_3$]	43.8						

Hydroxamic acids form less stable complexes than catechols, but in contrast they are not prone to oxidation. Furthermore, their complexation properties are less sensitive to the pH value compared to catechols. The most stable complexes are formed at basic pH values, but even at a pH value as low as 2 complexation occurs.[19] Due to their complexation behavior with metal ions, hydroxamic acids have been investigated as linking agents both in dye-sensitized solar cells (DSSC) and metal-organic frameworks (MOF) in recent years.[26–28]

The usually highly colored complexes are also used for the analysis of metal ion concentrations. For vanadium(V) the detection limit is approx. 0.15 ppm, if bound by N-phenylbenzohydroxamic acid. The typical extinction coefficient of these charge-transfer complexes is in the order of 10^4 M^{-1} cm^{-1}.[29] The *in situ* formation of hydroxamic acids and their subsequent conversion to colored complexes is also commonly used in detection reagents for amides, lactones, carboxylic acids, esters, and anhydrides.[30]

Hydroxamic acids in nature.

Hydroxamic acids play a crucial role in nature. Mono-, bis- and tris-hydroxamic acids are known. Their ability to form highly stable complexes with iron designates them as a key chelator in iron metabolism. Besides catechols, they are considered as one of the two major classes of Fe(III) complexing groups in siderophores that enable microbial iron transport[31,32]. Iron is an essential element for life. It represents the key component for redox processes in various enzymes, that are essential for the transport of oxygen.[33] Iron is very abundant in nature, but simultaneously only available in the form of highly water insoluble compounds, thus its bioavailability is extremely limited.[34,35] To overcome this issue, hydroxamic acids are used both by microorganisms and plants to solubilize iron and thus facilitate iron uptake. They are also featured in growth factors, antibiotics, antibiotic antagonists, proliferation factors and tumor inhibitors.[36] One prominent

example of a naturally occurring hydroxamic acid is ferrichrome, which is produced by various fungi of the *Aspergillus*, *Ustilago* and *Penicillum* family. Ferrichrome, a cyclic hexapeptide, features three hydroxamic acids for the efficient binding of Fe(III).[37] Release of iron is usually induced by reduction of Fe(III) to Fe(II) and subsequent transfer to porphyrin-based coenzymes or prosthetic moieties. Ferrichrome acts as a potent growth factor down to 1 nM total concentration by increasing the bioavailability of iron in *Arthrobacter terregens*.[36] This extremely high activity even at low concentration is achieved due to specialized receptors for the uptake of ferrichrome. The ferric hydroxamate uptake (Fhu) receptor is a prominent β-barrel protein pore (**Figure 1**), which is expressed by microorganisms to efficiently uptake iron bound via siderophores.[38,39] Motivated by the enormous importance of hydroxamic acid-based siderophores in nature, a broad scope of synthetic, biomimetic siderophores was developed in recent years.[41]
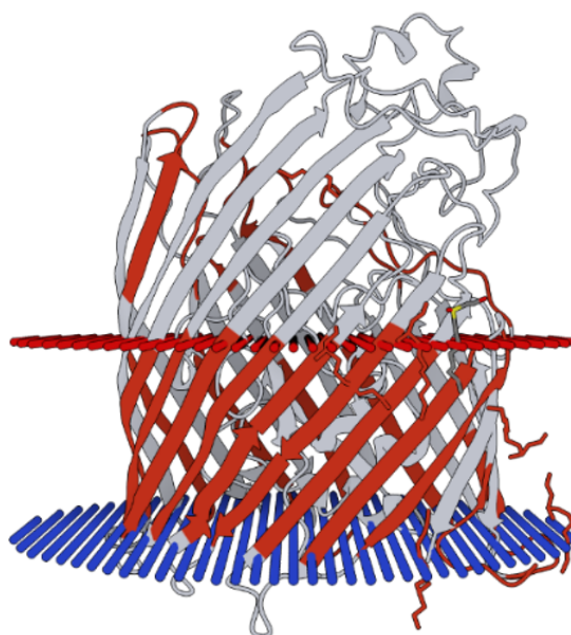

FIGURE 1 3D representation of Fhu type A receptor from E.Coli. A barrel is formed by 22 antiparallel β-strands containing a globular plug that consists of five α-helices and 6 β-strands. With ferrichrome uptake, an α-helix from the globular plug is unfolded.[39,40]

Biosynthesis of hydroxamic acids.

Hydroxamic acids in nature are typically found in their *N*-alkylated structure, *i.e.* as secondary *N*-hydroxyamides as a result of the biosynthesis pathway.[36] The biosynthesis of hydroxamic acids was investigated at the example of the production of deferoxamine E (DFO-E) in *Streptomyces coelicolor*. Starting from *L*-Lysine (**Scheme 6a**), cadaverine (**Scheme 6b**) is generated via decarboxylation. One amino moiety is then oxidized by the enzyme *DesB*, which is similar to typi-

cal FAD-dependent amine-monooxygenases. This *N*-hydroxyl derivative (**Scheme 6c**) is now further reacted via classic peptide biosynthesis pathways with succinyl-coenzyme A (**Scheme 6d**) to form the *N*-alkylated hydroxamic acid (**Scheme 6e**). Further steps finally lead to deferoxamine.[42]
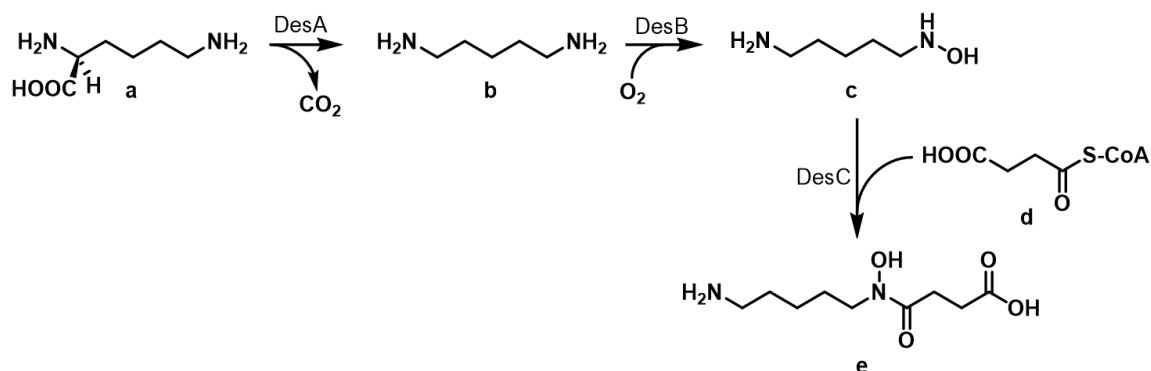
SCHEME 6   Biosynthesis pathway of secondary hydroxamic acids.[42]

Hydroxamic acids in medicine.

All currently known medical applications of hydroxamic acids rely on their outstanding chelation properties, which renders them ideally suited as potent metalloenzyme inhibitors.
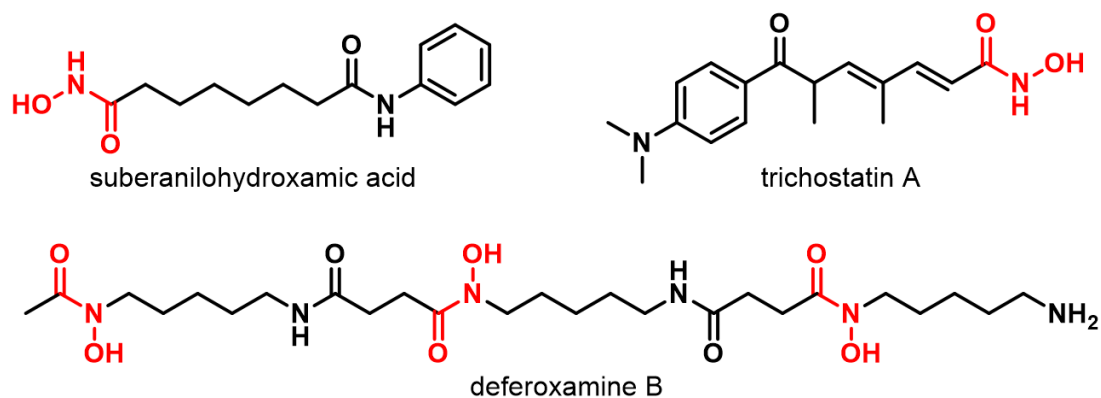

FIGURE 2   Hydroxamic acids with possible and actual medical applications. Suberanilohydroxamic acid (SAHA) and deferoxamine are commonly used in medicine, while trichostatin A is in preclinical development.[43-45]

The inhibition of histone deacetylases (HDAC) by hydroxamic acids has been reported and is currently a key component in the treatment of several types of cancer, for example, severe cases of cutaneous T cell lymphoma.[46] HDACs play a crucial role in many DNA related diseases and are highly associated with tumor development. Suberanilohydroxamic acid (SAHA, Vorinostat

(Merck), Zolinza (USA), tradenames) (**Figure 2**) is a potent inhibitor for HDAC1 and HDAC8 with an IC_{50} of 100 nM. SAHA binds the central zinc atom while maintaining two hydrogen bonds to neighboring histidine groups at the active site of HDAC8 (**Scheme 7**). This increases the overall binding affinity and thus explains the low IC_{50} values, a unique feature of hydroxamic acids.[47]
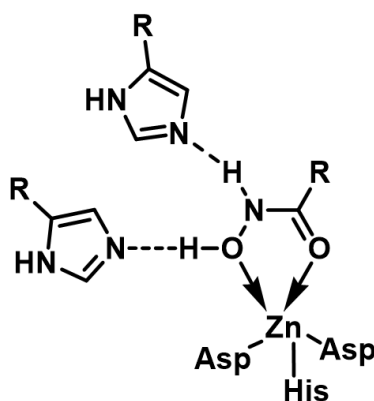

SCHEME 7   Binding modus of the hydroxamic acid moiety of SAHA at the active site of HDAC8.[47]

SAHA is known to pass the blood-brain barrier and can be applied orally via conjugation with cyclodextrin. In first animal studies, SAHA has been shown to significantly reduce motor deficits by inhibiting HDACs in brain tissue.[48] Besides their use as HDAC inhibitors, hydroxamic acids have also been investigated as inhibitors of Zn(II)-based matrix metalloproteinases, carboanhydrases, Ni(II) based ureases, hydrolases, lipoxygenases, and cyclooxygenases.[10] Also, anti-tuberculosis, fungicide, and anti-carcinogenic properties have been reported.[49]

Another prominent use of hydroxamic acids is their application as medicine for iron overload diseases.[35,49] Deferoxamine (DFO) shows high stability constant for iron complexes ($pK = 31$) and is listed as an essential medicine by the WHO.[50] DFO is commonly produced by removing the iron bound in ferrioxamine which is only accessible in industrial scale via biosynthesis by *Streptomyces pilosus*.[51] The therapy using DFO is a therapeutic milestone in preventing lethal iron accumulation in patients who frequently need blood transfusions, as is the case in thalassemias, inherited blood disorders characterized by decreased hemoglobin production. DFO is also used to treat aluminum-associated toxicity in patients that are undergoing frequent dialysis.[50,52] Furthermore, in preliminary studies treatment with DFO has been proven beneficial for the patients' recovery in case of strokes or other internal bleedings. It is assumed that local iron accumulation in tissue can be reduced and thus iron-induced neurotoxic effects are limited.[53] Besides their biological activity via chelation, hydroxamic acids have also been investigated as reagents for NO release by ruthenium(III) catalysis. Via ruthenium(II)-nitrosyl complex a carboxylic acid and NO are released, which induces hypotensive effects.[54]

Chemical synthesis of hydroxamic acids.

Generally, routes for the synthesis of hydroxamic acids employ the reaction of a carbonyl compound with hydroxylamine or its derivatives. In case of highly reactive carbonyl compounds such as acyl chlorides, the reaction with hydroxylamine leads to mixtures of mono-, di- or trisubstituted products due to multiple acylations of the *in-situ* formed hydroxamic acid.[13] To ensure selective preparation of hydroxamic acids, *O*-protected hydroxylamine must be employed with subsequent cleavage of the protecting group (**Scheme 8D**).[17] Single step preparation can be achieved by starting from the ester derivative (**Scheme 8B**). In this hydroxylaminolysis based mechanism, *O*-acylhydroxylamine is formed first, which is subsequently transformed to the thermodynamically more stable hydroxamic acid.[2,55,56] Common solvents for this reaction are alcohols, typically methanol. In the case of water-soluble esters the reaction can also be performed in aqueous solution.[55,57] Aprotic solvents are not suitable due to the low solubility of hydroxylamine in those.[58] The inherent high crystallinity of hydroxamic acids facilitates purification via recrystallization.[57]
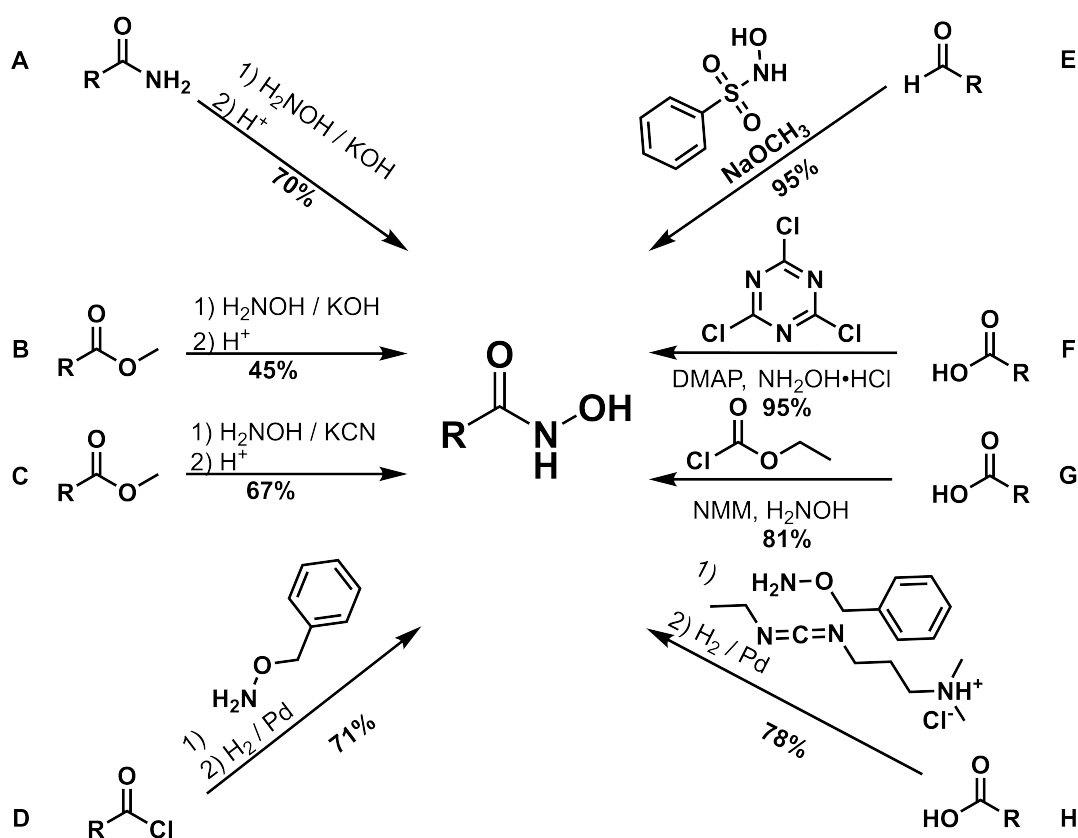

SCHEME 8 Various synthetic approaches for the preparation of hydroxamic acids.

Syntheses starting from esters usually employ basic conditions to ensure deprotonation of hydroxylamine. Without catalysis, the reaction proceeds under neutral conditions only at very low rates.[59] KCN can be added as a suitable catalyst to accelerate the transformation even at neutral pH (**Scheme 8C**).[60] The preparation of hydroxamic acids from esters was also reported in microreactors with increased yield and lowered reaction times.[61] Also the one-step preparation of hydroxamic acids with adjacent stereocenters was described by use of benzyl-protected hydroxylamine with LiHMDS at -78 °C.[62] Amides are another known starting material for the synthesis of hydroxamic acids (**Scheme 8A**).[63,64] Preparation under mild conditions is usually performed by coupling protected hydroxylamines with carboxylic acids (**Scheme 8H**).[17] Besides carbodiimide-based coupling methods, mixed anhydrides have been employed successfully (**Scheme 8G, 8F**).[59,65,66] A historical route for the synthesis of hydroxamic acids from aldehydes was described by Angeli in 1896 and Rimini in 1901 (**Scheme 8E**).[67-69] In this Angeli-Rimini name reaction, aldehydes are oxidized to hydroxamic acids by using N-hydroxybenzenesulfonamide, while the corresponding sulfinic acid is formed. The purification of the reaction product obtained by this route is typically troublesome, which renders it mainly suitable as a detection reaction for TLC analysis. Newer approaches have overcome the purification issues by using resin-bound N-hydroxybenzenesulfonamide.[69]

Protecting group chemistry.

Classically, hydroxamic acids are introduced in the last step of a synthetic sequence due to their reactivity and limited stability against harsh conditions.[70] Especially for further reaction steps, protected hydroxamic acids must be employed. The use of protected hydroxylamines like N-BOC-O-TBS-hydroxylamine is suitable, if the maintained carbonyl group is tolerated in further reaction steps.[71] Especially under nucleophilic or basic conditions, the carbonyl group must also be protected to ensure stability of the hydroxamic acid moiety.
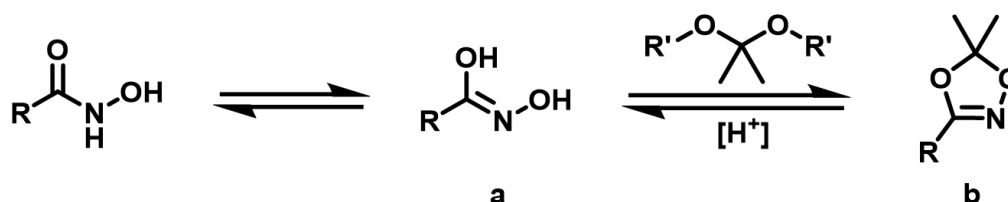
SCHEME 9   Synthesis scheme for the preparation of 1,4,2-dioxazoles from hydroxamic acids via transketalization. The hydroximic tautomer (a) is converted to the ketal-like 1,4,2-dioxazole (b) by using ketals of acetone and acidic catalysis.

Currently, the conversion of hydroxamic acids to a 1,4,2-dioxazole for protecting purpose, described in a single publication by Couturier *et al.*, is the only known suitable protecting strategy that tolerates nucleophilic reaction conditions.[72] 1,4,2-dioxazoles can be prepared via [2+3] cycloaddition of nitrile oxides with activated carbonyl compounds[73] or by photolysis of acyl azides in presence of ketones.[74] Starting from the hydroxamic acid, the conversion to 1,4,2-dioxazole was investigated by Mukaiyama *et al.*.[75] In this transketalization reaction, the diol-tautomer "hydroximic acid" of hydroxamic acids proceeds to form cyclic ketals (**Scheme 9**). 1,4,2-dioxazoles show limited stability at higher temperatures due to Lossen type rearrangements, but excellent stability under basic and nucleophilic conditions at ambient temperature.[72,75-77] Cleavage of the protecting group can be achieved via acidic treatment, analogous to the well-known acetals and ketals.[72]

Preparation of polymers bearing hydroxamic acids and their general properties.

Initial reports on macromolecules bearing hydroxamic acids date back to 1942.[78] Nearly all reported approaches introduced hydroxamic acids into polymers via post-polymerization modification of polyacryl derivatives with hydroxylamine. Seminal in-depth investigations of the properties of polymers bearing multiple hydroxamic acids were reported by Winston *et al.* in 1975. In this work, poly(hydroxamic acid)s were prepared via modification of free radically synthesized NHS-active ester based polymers with *N*-methylhydroxylamine.[79] In subsequent works, the flexibility of the linker connecting the hydroxamic acids to the poly(methacrylate) backbone was shown to be crucial for the formation of stable octahedral complexes with iron (**Figure 3**, P-9, P-11, and P-13).[80] No difference in the complexation constant was found for the non-methylated hydroxamic acid counterparts (**Figure 3**, P-11 (N'H)).[81] The lack of the methyl group tethered to the polymer backbone (**Figure 3**, Pa-11) was shown to have no impact on the stability constant of the respective iron(III)-complexes.

In the case of tris-iron(III)hydroxamato complexes, gel formation was observed.[82] Winston *et al.* also investigated the time-dependent dynamics of iron(III) based crosslinking. Due to dynamic exchange of the crosslinking sites from intermolecular network points to intra-molecular loops, the viscosity of the polymer-iron solution decreased over time.[83] This effect is ascribed to the fair stability constants of the hydroxamic acid complexes (**Table 1**), allowing for a dynamic exchange of the coordination sites. Strictly speaking, thermodynamically driven loops are formed via dynamic exchange of Fe(III) complexes by the hydroxamic acids groups tethered to one single polymer chain, leading to an intramolecular link instead of crosslinking points.
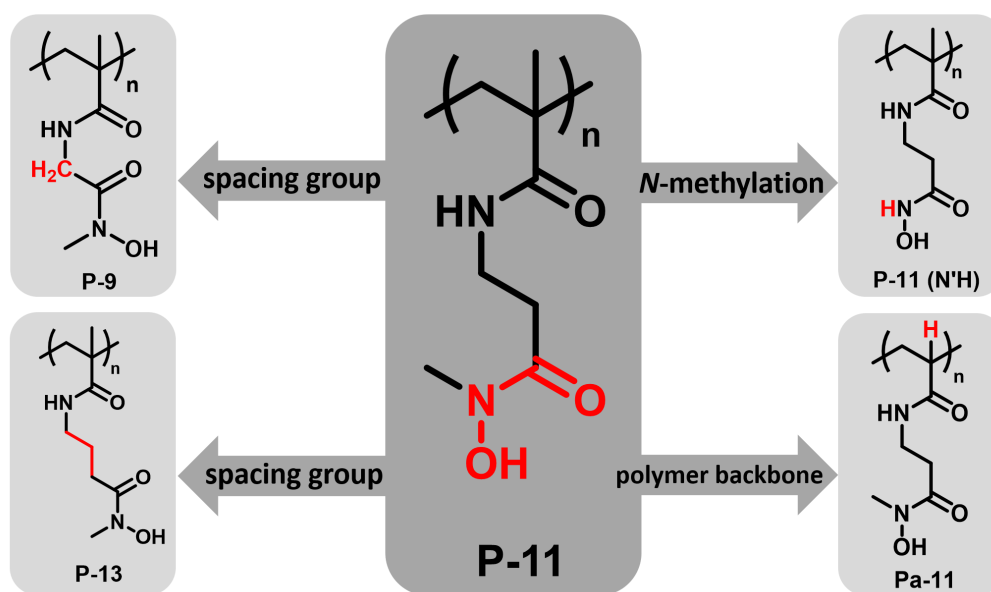
FIGURE 3 Hydroxamic acid-functionalized polymers varied by the length of the spacing group, the methylation of the hydroxamic acid nitrogen and the nature of the polymer backbone synthesized by Winston *et al.*.[79,81,82]

Besides these comprehensive works, other reports of polymers bearing hydroxamic acids are mainly focused on the preparation of poly(hydroxamic acid)s from poly(methylmethacrylate)s or poly(acrylamide)s.[63,64,84,85] These types of poly(hydroxamic acid)s were employed as a starting material for peptide synthesis and for acyl transfer reactions.[86,87] Goddard and coworkers reported the post-polymerization modification of poly(propylene)-*graft*-poly(methylacrylate)s under basic conditions with hydroxylamine to form the hydroxamic acid-functionalized analogue as an active packaging material.[88] Unfortunately, most post-polymerization modifications of polymers are not straightforward and commonly not quantitative. The well-known conversion of amides into hydroxamic acids does not proceed smoothly when performed on poly(acrylamide)s, as shown by Nome *et al.*. Due to neighboring effects, an alternating order of hydroxamic acid and carboxylic acid was obtained instead.[85] On the other hand, it is an important observation that direct radical polymerization of monomers with unprotected hydroxamic acid functional groups failed due to radical transfer to the hydroxamic acid moiety during polymerization, causing inhibition of the polymerization, as shown by Wiley, Davis and coworkers.[89]
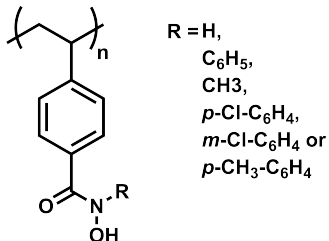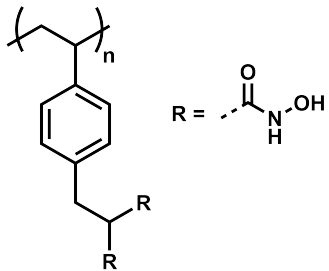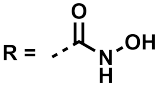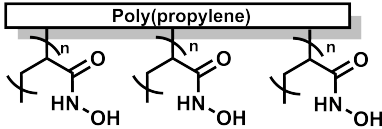
Application of poly(hydroxamic acid)s for metal scavenging.

Rare earth metals are becoming increasingly important for the production of electronic devices. The use of resin-bound poly(hydroxamic acid)s was investigated as a suitable approach for the separation and purification of rare earth metals from solution.[90-92] In several works, cross-linked

chloroformoyl styrene particles were modified in multistep procedures to bear hydroxamic acids and were subsequently used for the separation of Ce(IV) from La(III) and Nd(III) from Y(III) (**Table 2**).[93-96] Also, removal of uranium from salt water was demonstrated as a possible application of resin bound hydroxamic acids (**Table 2**).[41,97] The affinity order for the binding of rare earth metals with a resin load of up to 10% was reported as La(III) > Nd(III) > Sm(III) > Gd(III) > Tb(III).[98] Similar applications have been shown with starch-*graft*-PMA polymers that were modified by hydroxylamine to hydroxamic acids.[99]

The synthesis of poly(hydroxamic acid)-functionalized ion-exchange resins for the separation of V(V), Fe(II), Fe(III), Mo(VI), Ti(IV), Hg(II), Cu(II) and Ca(II) was reported by Meloan *et al.* long ago. They investigated the elution behavior of several metal ions employing hydroxamic acid and carboxylic acid-functionalized resins. Elution times of Fe(III), Cu(II), and Ce(IV) were increased when using the hydroxamic acid-functionalized resins, compared to the carboxylic acid-functionalized analogues.[41,100] Furthermore, hydroxamic acids as metal chelating ligands were utilized in another context. The prevention of oxidative degradation reactions has been shown with poly(propylene)-*graft*-poly(hydroxamic acid) films (**Table 2**). In the latter work, the hydroxamic acid moieties acted as chelating ligands on the surface to reduce lipid oxidation.[88,101]

TABLE 2 Overview of applications for various poly(hydroxamic acid)s.[88,93,97]

Polymer Structure	Application
R = H, C6H5, CH3, *p*-Cl-C6H4, *m*-Cl-C6H4 or *p*-CH3-C6H4	Separation of rare earth metals via resin-bound poly(hydroxamic acid)s[93]
R = (hydroxamic acid structure)	Removal of uranium from seawater[97]
Poly(propylene) (hydroxamic acid structure)	Active packing material to reduce lipid oxidation[88]

Therapeutic use of polymers bearing hydroxamic acids.

Unlike the well-established low molecular weight hydroxamic acids, no polymers bearing hydroxamic acids are currently used in medicine.[102] However, Kizhakkedathu *et al.* recently demonstrated that conjugates based on polyethers with deferoxamine are a promising approach for the therapy of iron overload diseases.[103] Poly(oligo (ethylene glycol) methacrylate) (POEGMA) polymers with up to 26 molecules of DFO (**Figure 4**, **A1** and **A2**), as well as hyperbranched poly(glycerol) conjugated with up to 300 molecules of DFO have been reported (**Figure 4B**).[103-105] Impressively, these DFO-polyether conjugates showed a 100-fold decrease in toxicity and 500-fold increased plasma half time compared to free DFO, while maintaining similar iron binding efficacy.[102,104-106]
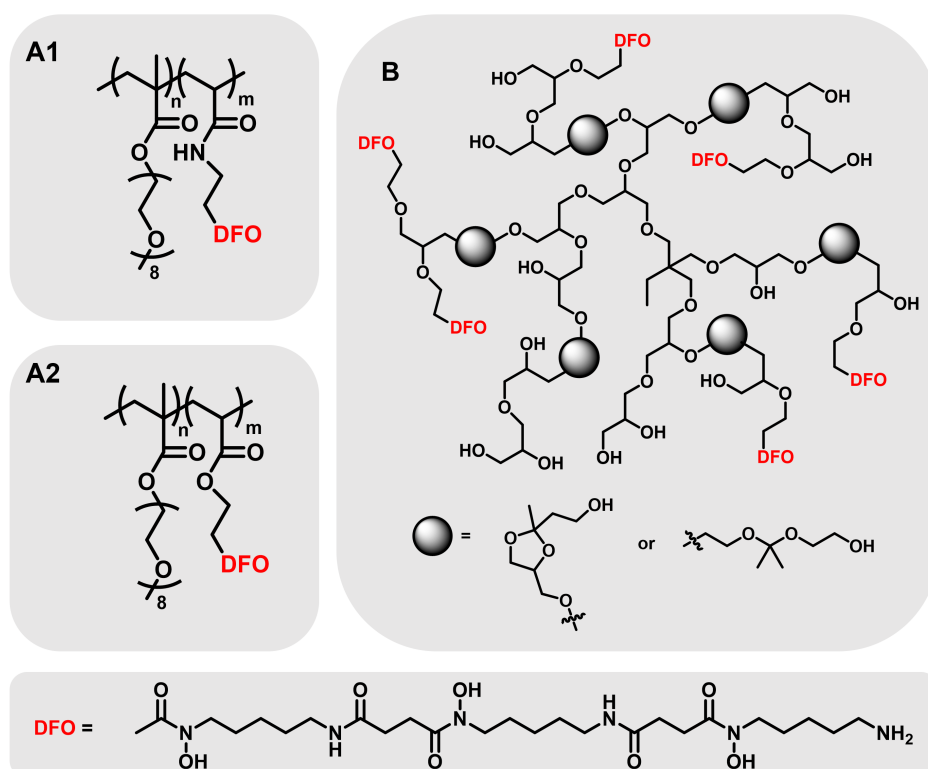

FIGURE 4 Polymer structures of various biodegradable iron chelators. **A)** PEG based acrylic conjugates consisting of oligo(ethylene glycol) methyl ether methacrylate and deferoxamine (DFO)-functionalized *N*-ethylacrylamide (**A1**) or ethylacrylate (**A2**) respectively.[104] **B)** DFO-functionalized hyperbranched poly(glycerol) nanoconjugates with cleavable linkages.[103]

Besides the use of DFO as a binding motif for iron, other systems employed resin-bound hydroxamic acids as orally applied hydrogels for iron binding.[107] Several other applications like inhibition of matrix-metalloproteases[108], synthesis of drug conjugates[109–111] and self-healing hydro-

gels based on salicylhydroxamic acids and boronic acid derivatives were proposed.[112] In recent works, our group developed a general approach to protected hydroxamic acid-based monomers suitable for both anionic and radical polymerization techniques. The concept relies on the above-mentioned 1,4,2-dioxazoles[69] (cf. **Scheme 9**) as protected hydroxamic acids to introduce multiple hydroxamic acids into well-defined polymer architectures, based for instance on polyethers and poly(methacrylate)s.[110] Using this approach, multiple hydroxamic acids were introduced at poly(ethylene glycol) (PEG) via copolymerization of ethylene oxide with an epoxide monomer containing a 1,4,2-dioxazole-protected hydroxamic acid (HAAGE).[112] AB and ABA type di- and triblock copolymers as well as statistical copolymers of HAAGE and ethylene oxide were prepared (M_n from 2600 to 12000 g mol^{-1}, dispersity Đ < 1.2). After the polymerization deprotection was achieved by mild acidic treatment, releasing multiple free hydroxamic acids tethered to the polyether backbone. The chelation properties of different polymer architectures (statistical vs. diblock and ABA triblock) were studied and compared with regard to the number and position of hydroxamic acids. Remarkably, separation of the hydroxamic acid units by at least 5 ethylene glycol monomer units was found to be essential for high Fe(III) binding efficiency, while block copolymers were observed to be the best-suited architecture for polymer network and hydrogel formation via Fe(III) chelation.[112] To sum up, this synthetic approach permits control over both the content and position of the hydroxamic acid groups at the polymer backbone (**Scheme 10**).[113–115]
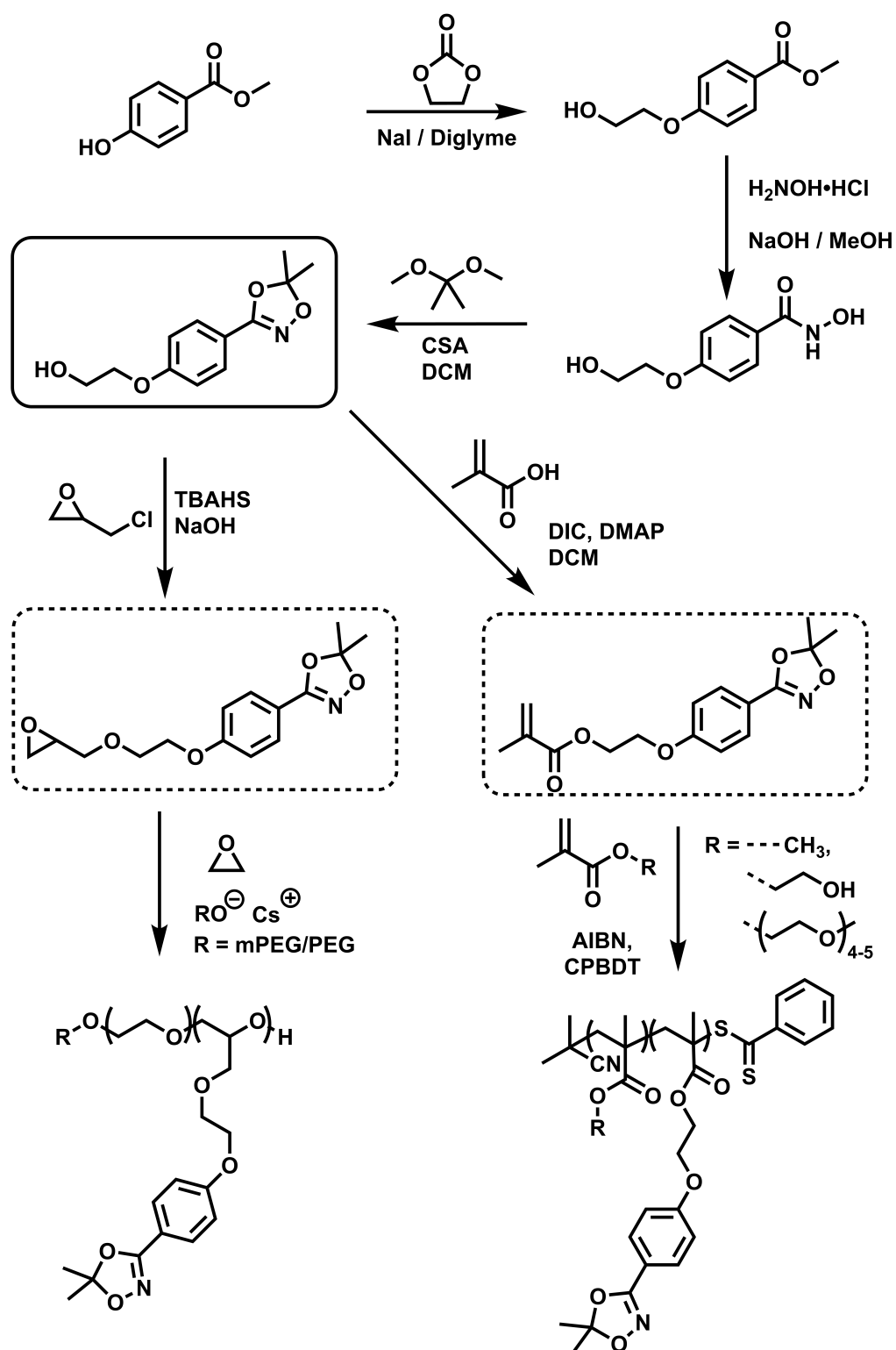
SCHEME 10 Synthetic route for the preparation of epoxide and methacrylate hydroxamic acid-functionalized monomers and the corresponding polymers via oxyanionic polymerization or RAFT.[113]

CONCLUSIONS AND FUTURE PERSPECTIVES

Hydroxamic acids are widely present in nature and besides the widely studied catechol moieties, play a key role in the iron metabolism, securing the bioavailability of iron. Learning from nature, they have been proven to be a suitable and versatile functional group for small molecules, but also for polymers, *e.g.* as a building block in organic chemistry, particularly for metal chelation. Applications range from highly specialized, therapeutic medical objectives to industrial purposes, relying on the complexation of a large variety of metals. While a solid base of knowledge has been built up, the field of hydroxamic acids still offers ample challenges for further investigation and development, particularly with respect to well-defined polymer architectures for a large variety of therapeutic concepts. To address these challenges, we have recently introduced a molecular "construction kit" for protected hydroxamic acid monomers that can be installed in a well-defined manner at homo- and block copolymers. The respective general approach enables the synthesis of a variety of polymer architectures (*e.g.* statistical or block- and star copolymers) and is applicable to different polymer systems such as *e.g.*, poly(methacrylate)s and polyethers. We believe that functional protected hydroxamic acids in the form of 1,4,2-dioxazoles represent a key building block to enable the introduction of hydroxamic acids both via radical as well as oxyanionic polymerization techniques. Other valuable, recent approaches include the attachment of deferoxamine to established, biocompatible polymer structures, as detailed above. Clearly, the combination of polymers with hydroxamic acids represents an emerging field with great promise. In addition, hydroxamic acids may be viewed as an intriguing alternative to the widely studied, "mussel-inspired", albeit oxidatively instable catechols,[116] which currently represent the dominating class of chelators and surface adhesive structures in materials science.

REFERENCES

(1) Lossen, H. Ueber die Oxalohydroxamsäure;. *Liebigs Ann. Chem.* **1869**, 150, 314–322.

(2) Bauer, L.; Exner, O. The Chemistry of Hydroxamic Acids and N-Hydroxyimides. *Angew. Chem. Int. Ed. Engl.* **1974**, 13, 376–384.

(3) García, B.; Secco, F.; Ibeas, S.; Muñoz, A.; Hoyuelos, F. J.; Leal, J. M.; Senent, M. L.; Venturini, M. Structural NMR and ab initio study of salicylhydroxamic and p-hydroxybenzohydroxamic acids: evidence for an extended aggregation. *J. Org. Chem.* **2007**, 72, 7832–7840.

(4) García, B.; Ibeas, S.; Muñoz, A.; Leal, J. M.; Ghinami, C.; Secco, F.; Venturini, M. NMR studies of phenylbenzohydroxamic acid and kinetics of complex formation with nickel(II). *Inorg. Chem.* **2003**, 42, 5434–5441.

(5) Göttlicher, S.; Paulus, H. Verfeinerung der Kristallstruktur von (Ethylendiamin)zink(II)-benzohydroxamat-hydrat, $ZnC_{23}H_{29}N_5O_7$. *Chem. Ber.* **1982**, 115, 393–395.

(6) Bordwell, F. G.; Fried, H. E.; Hughes, D. L.; Lynch, T. Y.; Satish, A. V.; Whang, Y. E. Acidities of carboxamides, hydroxamic acids, carbohydrazides, benzenesulfonamides, and benzenesulfonohydrazides in DMSO solution. *J. Org. Chem.* **1990**, 55, 3330–3336.

(7) García, B.; Ibeas, S.; Hoyuelos, F. J.; Leal, J. M.; Secco, F.; Venturini, M. Hydroxamic Acids as Weak Base Indicators: Protonation in Strong Acid Media. *J. Org. Chem.* **2001**, 66, 7986–7993.

(8) Decouzon, M.; Exner, O.; Gal, J. F.; Maria, P. C. The gas-phase acidity and the acidic site of acetohydroxamic acid: A FT-ICR study. *J. Org. Chem.* **1990**, 55, 3980–3981.

(9) Caudle, M. T.; Crumbliss, A. L. Dissociation Kinetics of (N-Methylacetohydroxamato)iron(III) Complexes: A Model for Probing Electronic and Structural Effects in the Dissociation of Siderophore Complexes. *Inorg. Chem.* **1994**, 33, 4077–4085.

(10) Codd, R. Traversing the coordination chemistry and chemical biology of hydroxamic acids. *Coord. Chem. Rev.* **2008**, 252, 1387–1408.

(11) Buglass, A. J.; Hudson, K.; Tillett, J. G. The acid-catalysed hydrolysis and protonation behaviour of hydroxamic acids. *J. Chem. Soc., B:* **1971**, 123–126.

(12) Berndt, D. C.; Fuller, R. L. The Kinetics and Mechanism of the Hydrolysis of Benzohydroxamic Acid 1. *J. Org. Chem.* **1966**, 31, 3312–3314.

(13) Lossen, W. Ueber Benzoylderivate des Hydroxylamins. *Liebigs Ann. Chem.* **1872**, 161, 347–362.

(14) Bauer, L.; Miarka, S. V. Stereospecific Lossen Rearrangements. *J. Org. Chem.* **1959**, 24, 1293–1296.

(15) Samuel, D.; Silver, B. L. The Elucidation of the Reaction of Benzohydroxamic Acid with Benzenesulfonyl Chloride and with Diisopropyl Phosphofluoridate Using Oxygen-18 as Tracer. *J. Am. Chem. Soc.* **1963**, 85, 1197–1198.

(16) Johnson, J. E.; Springfield, J. R.; Hwang, J. S.; Hayes, L. J.; Cunningham, W. C.; McClaugherty, D. L. Alkylation of benzohydroxamic acid. *J. Org. Chem.* **1971**, 36, 284–294.

(17) Folkers, J. P.; Gorman, C. B.; Laibinis, P. E.; Buchholz, S.; Whitesides, G. M.; Nuzzo, R. G. Self-Assembled Monolayers of Long-Chain Hydroxamic Acids on the Native Oxide of Metals. *Langmuir* **1995**, 11, 813–824.

(18) Smith, R. M.; Martell, A. E. *Critical Stability Constants*; Critical Stability Constants 6; Springer: Boston, MA, 1989.

(19) Kurzak, B.; Kozłowski, H.; Farkas, E. Hydroxamic and aminohydroxamic acids and their complexes with metal ions. *Coord. Chem. Rev.* **1992**, 114, 169–200.

(20) Chatterjee, B. Donor properties of hydroxamic acids. *Coord. Chem. Rev.* **1978**, 26, 281–303.

(21) Agrawal, Y. K.; Tandon, S. G. Solution stability constants of complexes of benzohydroxamic acid with some divalent metal ions. *J. Inorg. Nucl. Chem.* **1972**, 34, 1291–1295.

(22) Irving, H.; Williams, R. J. P. Order of Stability of Metal Complexes. *Nature* **1948**, 162, 746–747.

(23) Harty, M.; Bearne, S. L. Measuring benzohydroxamate complexation with Mg^{2+}, Mn^{2+}, Co^{2+}, and Ni^{2+} using isothermal titration calorimetry. *J. Therm. Anal. Calorim.* **2016**, 123, 2573–2582.

(24) Schwarzenbach, G.; Schwarzenbach, K. Hydroxamatkomplexe I. Die Stabilität der Eisen(III)-Komplexe einfacher Hydroxamsäuren und des Ferrioxamins B. *Helv. Chim. Acta* **1963**, 46, 1390–1400.

(25) Baroncelli, F.; Grossi, G. The complexing power of hydroxamic acids and its effect on the behaviour of organic extractants in the reprocessing of irradiated fuels—I the complexes between benzohydroxamic acid and zirconium, iron (III) and uranium (VI). *J. Inorg. Nucl. Chem.* **1965**, 27, 1085–1092.

(26) Koenigsmann, C.; Ripolles, T. S.; Brennan, B. J.; Negre, C. F. A.; Koepf, M.; Durrell, A. C.; Milot, R. L.; Torre, J. A.; Crabtree, R. H.; Batista, V. S.; Brudvig, G. W.; Bisquert, J.; Schmuttenmaer, C. A. Substitution of a hydroxamic acid anchor into the MK-2 dye for enhanced photovoltaic performance and water stability in a DSSC. *Phys. Chem. Chem. Phys.* **2014**, 16, 16629–16641.

(27) Pereira, C. F.; Howarth, A. J.; Vermeulen, N. A.; Almeida Paz, F. A.; Tomé, J. P. C.; Hupp, J. T.; Farha, O. K. Towards hydroxamic acid linked zirconium metal–organic frameworks. *Mater. Chem. Front.* **2017**, 1, 1194–1199.

(28) Kongprakaiwoot, N.; Noll, B. C.; Brown, S. N. Tetradentate bis(hydroxamate) and hydroxamate-diketonate ligands and their titanium(IV) complexes. *Inorg. Chem.* ***2008, 47, 11902–11909.***

(29) Abbasi, S. Extraction and spectrophotometric determination of vanadium(V) with N-[p-(N,N-dimethylanilino)-3-methoxy-2-naphtho]hydroxamic acid. *Anal. Chem.* **1976**, 48, 714–717.

(30) Merck, E. Company Brochure, *Dyeing Reagents for Thin Layer and Paper Chromatography*; Darmstadt, 1974.

(31) Raymond, K. N.; Carrano, C. J. Coordination chemistry and microbial iron transport. *Acc. Chem. Res.* **1979**, 12, 183–190.

(32) Raymond, K. N.; Allred, B. E.; Sia, A. K. Coordination Chemistry of Microbial Iron Transport. *Acc. Chem. Res.* **2015**, 48, 2496–2505.

(33) Nelson, D. L.; Cox, M. M.; Lehninger, A. L. *Lehninger principles of biochemistry*, 6., internat. ed.; Freeman; Macmillan Higher Education: New York, Basingstoke, 2013.

(34) Lide, D. R., Ed. *CRC handbook of chemistry and physics: A ready-reference book of chemical and physical data*, 85. ed.; CRC Press: Boca Raton, 2004.

(35) Miller, M. J. Syntheses and therapeutic potential of hydroxamic acid based siderophores and analogs. *Chem. Rev.* **1989**, 89, 1563–1579.

(36) Neilands, J. B. Hydroxamic Acids in Nature. *Science* **1967**, 156, 1443–1447.

(37) van der Helm, D.; Baker, J. R.; Eng-Wilmot, D. L.; Hossain, M. B.; Loghry, R. A. Crystal structure of ferrichrome and a comparison with the structure of ferrichrome A. *J. Am. Chem. Soc.* **1980**, 102, 4224–4231.

(38) Messerschmidt, A.; Huber, R.; Poulas, T.; Wieghardt, K.; Cygler, M.; Bode, W., Eds. *Handbook of Metalloproteins*; John Wiley & Sons, Ltd: Chichester, 2006.

(39) Locher, K. P.; Rees, B.; Koebnik, R.; Mitschler, A.; Moulinier, L.; Rosenbusch, J. P.; Moras, D. Transmembrane signaling across the ligand-gated FhuA receptor: crystal structures of free and ferrichrome-bound states reveal allosteric changes. *Cell* **1998**, 95, 771–778.

(40) Locher, K. P.; Rees, B.; Koebnik, R.; Mitschler, A.; Moulinier, L.; Rosenbusch, J. P.; Moras, D. FhuA from E. Coli; Worldwide Protein Data Bank, `https://www.wwpdb.org/pdb?id=pdb_00001by3` (accessed May 27, 2020).

(41) Sockwell, A. K.; Wetzler, M. Beyond Biological Chelation: Coordination of f-Block Elements by Polyhydroxamate Ligands. *Chemistry* (Weinheim an der Bergstrasse, Germany) **2019**, 25, 2380–2388.

(42) Barona-Gómez, F.; Wong, U.; Giannakopulos, A. E.; Derrick, P. J.; Challis, G. L. Identification of a cluster of genes that directs desferrioxamine biosynthesis in Streptomyces coelicolor M145. *J. Am. Chem. Soc.* **2004**, 126, 16282–16283.

(43) Drummond, D. C.; Noble, C. O.; Kirpotin, D. B.; Guo, Z.; Scott, G. K.; Benz, C. C. Clinical development of histone deacetylase inhibitors as anticancer agents. *Annu. Rev. Pharmacol. Toxicol.* **2005**, 45, 495–528.

(44) Chang, J.; Varghese, D. S.; Gillam, M. C.; Peyton, M.; Modi, B.; Schiltz, R. L.; Girard, L.; Martinez, E. D. Differential response of cancer cells to HDAC inhibitors trichostatin A and depsipeptide. *Br. J. Cancer* **2012**, 106, 116–125.

(45) Damaskos, C.; Garmpis, N.; Valsami, S.; Kontos, M.; Spartalis, E.; Kalampokas, T.; Kalampokas, E.; Athanasiou, A.; Moris, D.; Daskalopoulou, A.; Davakis, S.; Tsourouflis, G.; Kontzoglou, K.; Perrea, D.; Nikiteas, N.; Dimitroulis, D. Histone Deacetylase Inhibitors: An Attractive Therapeutic Strategy Against Breast Cancer. *Anticancer Res.* **2017**, 37, 35–46.

(46) Marks, P. A.; Breslow, R. Dimethyl sulfoxide to vorinostat: development of this histone deacetylase inhibitor as an anticancer drug. *Nat. Biotechnol.* **2007**, 25, 84–90.

(47) Vannini, A.; Volpari, C.; Filocamo, G.; Casavola, E. C.; Brunetti, M.; Renzoni, D.; Chakravarty, P.; Paolini, C.; Francesco, R. de; Gallinari, P.; Steinkühler, C.; Di Marco, S. Crystal structure of a eukaryotic zinc-dependent histone deacetylase, human HDAC8, complexed with a hydroxamic acid inhibitor. *Proc. Natl. Acad. Sci.* **2004**, 101, 15064–15069.

(48) Hockly, E.; Richon, V. M.; Woodman, B.; Smith, D. L.; Zhou, X.; Rosa, E.; Sathasivam, K.; Ghazi-Noori, S.; Mahal, A.; Lowden, P. A. S.; Steffan, J. S.; Marsh, J. L.; Thompson, L. M.; Lewis, Cathryn M.; Marks, Paul A.; Bates, Gillian P. Suberoylanilide hydroxamic acid, a histone deacetylase inhibitor, ameliorates motor deficits in a mouse model of Huntington's disease. *Proc. Natl. Acad. Sci.* **2003**, 100, 2041–2046.

(49) Marmion, C. J.; Griffith, D.; Nolan, K. B. Hydroxamic Acids - An Intriguing Family of Enzyme Inhibitors and Biomedical Ligands. *Eur. J. Inorg. Chem.* **2004**, 2004, 3003–3016.

(50) World Health Organization. Model List of Essential Medicines. `http://www.who.int/medicines/publications/essentialmedicines/en/` (accessed January 1, 2016).

(51) Yawalkar, S. J. Milestones in the research and development of desferrioxamine. *Nephrol. Dial. Transplant.* **1993**, 8 Suppl 1, 40–42.

(52) Poggiali, E.; Cassinerio, E.; Zanaboni, L.; Cappellini, M. D. An update on iron chelation therapy. *Blood transfusion* **2012**, 10, 411–422.

(53) Wu, H.; Wu, T.; Xu, X.; Wang, J.; Wang, J. Iron toxicity in mice with collagenase-induced intracerebral hemorrhage. *J. Cereb. Blood Flow Metab.* **2011**, 31, 1243–1250.

(54) Marmion, C. J.; Murphy, T.; Docherty, J. R.; Nolan, K. B. Hydroxamic acids are nitric oxide donors. Facile formation of ruthenium(II)-nitrosyls and NO-mediated activation of guanylate cyclase by hydroxamic acids. *Chem. Commun.* **2000**, 1153–1154.

(55) Hauser, C. R.; Renfrow, W. B., JR. Synthesis of Benzohydroxamic acid. *Org. Synth.* **1939**, 19, 15.

(56) Jeanrenaud, A. Ueber die Einwirkung des Hydroxylamins auf Säureäther. *Ber. Dtsch. Chem. Ges.* **1889**, 22, 1270–1284.

(57) Kreye, O.; Wald, S.; Meier, M. A. R. Introducing Catalytic Lossen Rearrangements: Sustainable Access to Carbamates and Amines. *Adv. Synth. Catal.* **2013**, 355, 81–86.

(58) Blome; Buddenberg; Hartter; Kropf; Müller; Weickmann; Zeller, Eds. *Methoden der Organischen Chemie (Houben-Weyl)*, IV/1a: Oxidation; Georg Thieme Verlag: Stuttgart, 1981.

(59) Reddy, A.S.; Kumar, M.S.; Reddy, G.R. A convenient method for the preparation of hydroxamic acids. *Tetrahedron Lett.* **2000**, 41, 6285–6288.

(60) Ho, C. Y.; Strobel, E.; Ralbovsky, J.; Galemmo, R. A. Improved solution- and solid-phase preparation of hydroxamic acids from esters. *J. Org. Chem.* **2005**, 70, 4873–4875.

(61) Riva, E.; Gagliardi, S.; Mazzoni, C.; Passarella, D.; Rencurosi, A.; Vigo, D.; Martinelli, M. Efficient continuous flow synthesis of hydroxamic acids and suberoylanilide hydroxamic acid preparation. *J. Org. Chem.* **2009**, 74, 3540–3543.

(62) Gissot, A.; Volonterio, A.; Zanda, M. One-step synthesis of O-benzyl hydroxamates from unactivated aliphatic and aromatic esters. *J. Org. Chem.* **2005**, 70, 6925–6928.

(63) Domb, A.; Cravalho, E.; Langer, R. The synthesis of poly(hydroxamic acid) from poly(acrylamide). *J. Polym. Sci. Pol. Chem.* **1988**, 26, 2623–2630.

(64) Domb, A.; Langer, R.; Cravalho, E.; Gershon, G.; Mathiowitz, E.; Laurencin, C. Method of making Hydroxamic Acid Polymers from Primary Amide Polymers: U.S. Patent 5,128,420, Jul 7, 1992.

(65) Luca, L. de; Giacomelli, G.; Taddei, M. An Easy and Convenient Synthesis of Weinreb Amides and Hydroxamates. *J. Org. Chem.* **2001**, 66, 2534–2537.

(66) Giacomelli, G.; Porcheddu, A.; Salaris, M. Simple one-flask method for the preparation of hydroxamic acids. *Org. Lett.* **2003**, 5, 2715–2717.

(67) Angeli, A. Sopra la nitroidrossilammina. *Gazz. Chim. Ital.* **1896**, 26, 17–25.

(68) Rimini, E. Sopra una nuova reazione delle aldeidi. *Gazz. Chim. Ital.* **1901**, 31, 84.

(69) Porcheddu, A.; Giacomelli, G. Angeli-Rimini's reaction on solid support: a new approach to hydroxamic acids. *J. Org. Chem.* **2006**, 71, 7057–7059.

(70) Sandler, S. R.; Karo, W. *Organic functional group preparations 12*; Acad. Press: Orlando.

(71) Altenburger, J. M.; Mioskowski, C.; d'Orchymont, H.; Schirlin, D.; Schalk, C.; Tarnus, C. Useful hydroxylamine derivatives for the synthesis of hydroxamic acids. *Tetrahedron Lett.* **1992**, 33, 5055–5058.

(72) Couturier, M.; Tucker, J. L.; Proulx, C.; Boucher, G.; Dubé, P.; Andresen, B. M.; Ghosh, A. 5,5-Dimethyl-1,4,2-dioxazoles as Versatile Aprotic Hydroxamic Acid Protecting Groups. *J. Org. Chem.* **2002**, 67, 4833–4838.

(73) Huisgen, R.; Mack, W.; Anneser, E. 1.3-Dipolare Additionen der Nitriloxyde an CS-Doppelbindungen. *Angew. Chem.* **1961**, 73, 656–657.

(74) Clauss, K.-U.; Buck, K.; Abraham, W. The photochemistry of acyl azides — IX. Direct and sensitized photolytic generation of acylnitrenes for cycloaddition reactions. *Tetrahedron* **1995**, 51, 7181–7192.

(75) Nohira, H.; Inoue, K.; Hattori, H.; Okawa, T.; Mukaiyama, T. The Synthesis and the Thermal Decomposition of 1, 3, 4-Dioxazole Derivatives. *Bull. Chem. Soc. Jpn.* **1967**, 40, 664–668.

(76) Geffken, D.; Froböse, J. Cyclisierung von N-(1-Methoxy-1-methylethoxy)carboxamiden zu 5,5-Dimethyl-1,4,2-dioxazolen. *J. Prakt. Chem.* **1994**, 336, 550–552.

(77) Geffken, D.; Froböse, J. (O-Arylcarbamoyl)acetonoxime aus 3-Aryl-1-(1-methoxy-1-methyl-ethoxy) harnstoffen und 3-Aryl-1-hydroxyharnstoffen. Anmerkungen zu einem Patentanspruch. *J. Prakt. Chem.* **1993**, 335, 555–557.

(78) Coffman, D. D. Polymeric Hydroxamic Acids US2402604 A.

(79) Winston, A.; Mazza, E. T. Hydroxamic acid polymers. *J. Polym. Sci. Pol. Chem.* **1975**, 13, 2019–2030.

(80) Winston, A.; McLaughlin, G. R. Hydroxamic acid polymers. II. Design of a polymeric chelating agent for iron. *J. Polym. Sci. Pol. Chem.* **1976**, 14, 2155–2165.

(81) Varaprasad, D. V. P. R.; Rosthauser, J. W.; Winston, A. Hydroxamic acid polymers. Effect of structure on the chelation of iron in water: II. *J. Polym. Sci. Pol. Chem.* **1984**, 22, 2131–2143.

(82) Winston, A.; Kirchner, D. Hydroxamic Acid Polymers. Effect of Structure on the Selective Chelation of Iron in Water. *Macromolecules* **1978**, 11, 597–603.

(83) Rosthauser, J. W.; Winston, A. Crosslinking of hydroxamic acid copolymers through iron chelation. *Macromolecules* **1981**, 14, 538–543.

(84) Kern, W.; Schulz, R. C. Synthetische makromolekulare Stoffe mit reaktiven Gruppen. *Angew. Chem.* **1957**, 69, 153–171.

(85) Mello, R. S.; Orth, E. S.; Loh, W.; Fiedler, H. D.; Nome, F. Polymers containing hydroxamate groups: nanoreactors for hydrolysis of phosphoryl esters. *Langmuir* **2011**, 27, 15112–15119.

(86) Narita, M.; Teramoto, T.; Okawara, M. Syntheses and Reactions of Functional Polymers. LXVI. Activation of Carboxylic Acid by Means of Polymers Containing Hydroxamic Acid Residue and N-Hydroxysuccinimide Residue. *Bull. Chem. Soc. Jpn.* **1972**, 45, 3149–3155.

(87) Sophiamma, P.N.; Sreekumar, K. Polystyrene-based hydroxamic esters: Preparation and application as acyl transfer reagents. *React. Funct. Polym.* **1997**, 35, 169–177.

(88) Lin, Z.; Decker, E. A.; Goddard, J. M. Preparation of metal chelating active packaging materials by laminated photografting. *J. Coat. Technol. Res.* **2016**, 13, 395–404.

(89) Iskander, G. M.; Kapfenstein, H. M.; Davis, T. P.; Wiley, D. E. Synthesis and copolymerization of methacryloyl hydroxamic acids. *J. Appl. Polym. Sci.* **2000**, 78, 751–758.

(90) Lee, T. S.; Hong, S. I. Synthesis of porous poly(hydroxamic acid) from poly(ethyl acrylate-co-divinylbenzene). *Polym. Bull.* **1994**, 32, 273–279.

(91) Lee, T. S.; Hong, S. I. Porous Chelating Resins from Poly(Acrylonitrile- co -Ethyl Acrylate- co -Divinylbenzene). *J. Macromol. Sci., Part A: Pure Appl.Chem.* **1995**, 32, 379–392.

(92) Lee, T. S.; Hong, S. I. Synthesis and metal binding behavior of hydroxamic acid resins from poly(ethyl acrylate) crosslinked with divinylbenzene and hydrophilic crosslinking agent. *J. Polym. Sci. Pol. Chem.* **1995**, 33, 203–210.

(93) Agrawal, Y. K.; Kaur, H.; Menon, S.K. Poly(styrene-p-hydroxamic acids): Synthesis, and ion exchange separation of rare earths. *React. Funct. Polym.* **1999**, 39, 155–164.

(94) Shah, A.; Devi, S. Separation of lead and copper on a series of chelating ion-exchange resins. Part I. *Analyst* **1985**, 110, 1501.

(95) Shah, A.; Devi, S. Poly(hydroxamic acid) chelating resins. Part II. Separation of zinc from cadmium and of cobalt from copper and nickel. *Analyst* **1987**, 112, 325.

(96) Trivedi, U.V.; Menon, S.K.; Agrawal, Y. K. Polymer supported calix[6]arene hydroxamic acid, a novel chelating resin. *React. Funct. Polym.* **2002**, 50, 205–216.

(97) Hirotsu, T.; Katoh, S.; Sugasaka, K.; Sakuragi, M.; Ichimura, K.; Suda, Y.; Fujishima, M.; Abe, Y.; Misonoo, T. Synthesis of dihydroxamic acid chelating polymers and the adsorptive property for uranium in sea water. *J. Polym. Sci. Pol. Chem.* **1986**, 24, 1953–1966.

(98) Alakhras, F. A.; Dari, K. A.; Mubarak, M. S. Synthesis and chelating properties of some poly(amidoxime-hydroxamic acid) resins toward some trivalent lanthanide metal ions. *J. Appl. Polym. Sci.* **2005**, 97, 691–696.

(99) Lutfor, M. R.; Silong, S.; Yunus, W. M. Z. W.; Rahman, M. Z. A.; Ahmad, M.; Haron, M. J. New polymer bearing hydroxamic acid chelating resin for binding of heavy metal ions. *J. Chem. Res.* **2001**, 2001, 450–451.

(100) Petrie, G.; Locke, D.; Meloan, C. E. Hydroxamic Acid Chelate Ion Exchange Resin. *Anal. Chem.* **1965**, 37, 919–920.

(101) Tian, F.; Decker, E. A.; Goddard, J. M. Controlling lipid oxidation via a biomimetic iron chelating active packaging material. *J. Agric. Food Chem.* **2013**, 61, 12397–12404.

(102) Hamilton, J. L.; Kizhakkedathu, J. N. Polymeric nanocarriers for the treatment of systemic iron overload. *Mol. Cell. Therapies* **2015**, 3, 3.

(103) Abbina, S.; Abbasi, U.; Gill, A.; Wong, K.; Kalathottukaren, M. T.; Kizhakkedathu, J. N. Design of Safe Nanotherapeutics for the Excretion of Excess Systemic Toxic Iron. *ACS Cent. Sci.* **2019**, 5, 917–926.

(104) Rossi, N. A. A.; Mustafa, I.; Jackson, J. K.; Burt, H. M.; Horte, S. A.; Scott, M. D.; Kizhakkedathu, J. N. In vitro chelating, cytotoxicity, and blood compatibility of degradable poly(ethylene glycol)-based macromolecular iron chelators. *Biomaterials* **2009**, 30, 638–648.

(105) Imran ul-haq, M.; Hamilton, J. L.; Lai, B. F. L.; Shenoi, R. A.; Horte, S. A.; Constantinescu, I.; Leitch, H. A.; Kizhakkedathu, J. N. Design of long circulating nontoxic dendritic polymers for the removal of iron in vivo. *ACS Nano* **2013**, 7, 10704–10716.

(106) Hamilton, J. L.; Ul-Haq, M. I.; Creagh, A. L.; Haynes, C. A.; Kizhakkedathu, J. N. Iron Binding and Iron Removal Efficiency of Desferrioxamine Based Polymeric Iron Chelators: Influence of Molecular Size and Chelator Density. *Macromol. Biosci.* **2017**, 17, 1600244.

(107) Polomoscanik, S. C.; Cannon, C. P.; Neenan, T. X.; Holmes-Farley, S. R.; Mandeville, W. H.; Dhal, P. K. Hydrox-amic acid-containing hydrogels for nonabsorbed iron chelation therapy: synthesis, characterization, and biological evaluation. *Biomacromolecules* **2005**, 6, 2946–2953.

(108) Skarja, G. A.; Brown, A. L.; Ho, R. K.; May, M. H.; Sefton, M. V. The effect of a hydroxamic acid-containing polymer on active matrix metalloproteinases. *Biomaterials* **2009**, 30, 1890–1897.

(109) Kenawy, e.-R.; Abdel-Hay, F.; el-Newehy, M.; Ottenbrite, R. M. Effect of pH on the drug release rate from a new polymer–drug conjugate system. *Polym. Int.* **2008**, 57, 85–91.

(110) Kenawy, e.-R.; el-Newehy, M.; Abdel-Hay, F.; Ottenbrite, R. M. A new degradable hydroxamate linkage for pH-controlled drug delivery. *Biomacromolecules* **2007**, 8, 196–201.

(111) Eichenbaum, G. M.; Kiser, P. F.; Shah, D.; Simon, S. A.; Needham, D. Investigation of the Swelling Response and Drug Loading of Ionic Microgels: The Dependence on Functional Group Composition. *Macromolecules* **1999**, 32, 8996–9006.

(112) Roberts, M. C.; Hanson, M. C.; Massey, A. P.; Karren, E. A.; Kiser, P. F. Dynamically Restructuring Hydrogel Networks Formed with Reversible Covalent Crosslinks. *Adv. Mater.* **2007**, 19, 2503–2507.

(113) Johann, T.; Keth, J.; Bros, M.; Frey, H. A general concept for the introduction of hydroxamic acids into polymers. *Chem. Sci.* **2019**, 10, 7009–7022.

(114) Keth, J.; Johann, T.; Frey, H. Metal chelators via RAFT polymerization: Introducing hydroxamic acids into poly(methacrylate)s. **2020**, submitted for publication.

(115) Johann, T.; Kemmer-Jonas, U.; Barent, R.; Frey, H. Multi-functional Fe(III)-binding polyethers relying on hydrox-amic acid-based epoxides. *Macromol. Rapid Commun.* **2019**, 1900282.

(116) Lee, H.; Dellatore, S. M.; Miller, W. M.; Messersmith, P. B. Mussel-inspired surface chemistry for multifunctional coatings. *Science* **2007**, 318, 426–430.

CHAPTER 2

INTRODUCTION OF HYDROXAMIC ACIDS INTO
POLY(METHACRYLATE)S

CHAPTER 2

To be submitted

Poly(methacrylate) Metal Chelators via RAFT Polymerization: Introducing Hydroxamic Acids

Jennifer Keth[1],   Tobias Johann[1],   Manfred Wagner[2]   and   Holger Frey[1*]

[1]Department of Chemistry, Johannes Gutenberg University, Duesbergweg 10-14, 55128 Mainz, Germany
[2]Max Planck Institute for Polymer Research Ackermannweg 10, 55128 Mainz, Germany
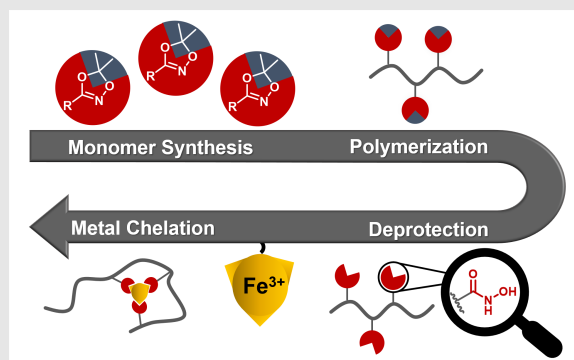
The synthesis of a tailored hydroxamic acid-functionalized methacrylate-based monomer (MAHAA) is presented as a tool to introduce multiple metal chelating motifs to vinyl-based polymers. The free hydroxamic acid moieties were converted to 1,4,2-dioxazole protecting groups to prevent undesired radical transfer reactions among the heteroatoms of hydroxamic acid moieties during radical polymerizations. The reversible addition-fragmentation transfer (RAFT) polymerization technique was applied to copolymerize the hydroxamic acid-functional monomer MAHAA with methyl methacrylate (MMA), hydroxyethyl methacrylate (HEMA) and oligo (ethylene glycol) methyl ether methacrylate (OEGMEMA), respectively. This enabled control over the number and position of the metal chelating motifs at the polymer backbone. Hydrophobic copolymers based on MMA as well as hydrophilic copolymers based on HEMA and OEGMEMA were prepared in the molecular weight range from 2,700 to 9,900 g mol^{-1} with dispersities below 1.35. Up to 50%$_{mol}$ of the hydroxamic acid moiety was incorporated in the methacrylate copolymers. In addition, *in* situ ^{1}H NMR kinetic measurements were performed to investigate the copolymerization behavior of MAHAA with MMA, HEMA and OEGMEMA respectively. Subsequent to the copolymerization the protecting groups were completely removed by an acidic workup to generate hydroxamic acid-functionalized copolymers. In proof-of-principle-experiments, the attachment of hydroxamic acid-functionalized copolymers onto various metal surfaces was confirmed by contact angle measurements.

INTRODUCTION

In the last decades, the number of works in the field of polymer chemistry in combination with metal complexation has received increasing attention. Especially catechol-based polymer structures were widely investigated with respect to complexation and metal interaction.[1–6] The catechol moiety is known as the essential part of the mussel foot protein in nature, which attaches to a vast variety of surfaces based on its strong chelating behavior.[1,2] Related to catechols, hydroxamic acids also play an important role as iron-transporting structures in nature, for instance in several types of "siderophores" (greek: "iron carriers") secreted by microorganisms.[7,8] However, the highly storage stable hydroxamic acids represent an excellent alternative to the easily oxidized catechol derivatives.[1,9]

Currently, hydroxamic acids are the key component of deferoxamine employed for the treatment of iron-metabolism associated diseases.[10,11] Besides their medical use, their strong interaction with various metals opens a wide range of different applications in the field of material science. Brown *et al.*[12] investigated the complexing behavior of hydroxamates in comparison with diketonates as ligands to bind to Ti(IV). Furthermore, the hydroxamic acid moiety has been successfully used in various applications, e.g. as a linking agent in dye sensitized solar cell (DSSC) systems or in metal organic frameworks (MOF).[13,14] Most applications rely on the complexation capability of hydroxamic acids due to the formation of a stable five-membered ring with various metal ions, e.g. Fe(III), Zn(II), Mn(II) and Cr(III).[8,15] Besides the use of low molecular weight hydroxamic acids, their combination with polymers has also been developed.[16] Several works by Winston *et al.*[11,17,18] demonstrated the versatility of hydroxamic acid containing polymers and their capability to complex various metal ions.

Polymers with metal complexing and surface-adhesive groups are relevant for a myriad of applications. For instance, the polymers are applicable as surface coatings[19,20] or ion exchange resins.[21-25] Nome and coworkers investigated the postmodification of polymers to obtain hydroxamic acid functionalities. Due to the high nucleophilic activity, an alternating carboxylic and hydroxamic acid copolymer structure was observed as a result of the neighboring effect, reducing the overall yield and impeding the transformation to hydroxamic acids.[26] Several works describe the introduction of hydroxamic acids at polymers by postmodification reactions.[27] As described by Nome and coworkers, this approach leads to side products or non-quantitative conversion and therefore to a limited degree of functionalization. Regarding the drawbacks of the preparation of poly(hydroxamic acid)s via postmodification strategies, the question arises how to introduce hydroxamic acids directly and in a more controlled manner during the polymerization process. In our group, the direct incorporation of hydroxamic acids into poly(ether)s has already

been established via oxyanionic polymerizations. In these previous works, a 1,4,2-dioxazole group was chosen as a suitable protecting group to withstand the reaction conditions during the polymerization.[8,28,29] In this report we introduce a broadly applicable hydroxamic acid-functionalized methacrylate monomer and a variety of copolymerizations via controlled radical polymerization techniques. Employing radical polymerization techniques for hydroxamic acid-based monomers, Davis *et al.* observed incomplete conversions and suggested a limiting side reaction based on the transfer of radicals among the different heteroatoms of the hydroxamic acid functionality induced by the labile hydrogen of the hydroxamic acid moiety. As a result, inhibition and transfer reactions reduced the overall hydroxamic acid moieties in the polymer.[30] Consequently, we chose 1,4,2-dioxazoles as suitable protecting groups to withstand the presence of radicals during polymerization.[28] After the polymerization, this protecting group can easily be cleaved by an acidic workup to release the hydroxamic acid moieties.

RESULTS AND DISCUSSION

In the following discussion, the development of the methacrylate monomer structure, free and controlled radical copolymerization, cleavage of the protecting group and finally the application of the obtained materials will be discussed in detail.

Monomer synthesis

Functional monomers are commonly employed to introduce multiple functional groups along a vinyl polymer backbone. Among the common groups for radical polymerization, methacrylate- and styrene-based monomers are of special interest. Therefore, we initially screened synthesis pathways to combine a hydroxamic acid moiety with a polymerizable group. In the following, the synthesis of methacrylate-based (**I** in **Scheme 1**) and styrene-based (**II** in **Scheme 1**) hydroxamic acid-functionalized monomers are discussed in detail.
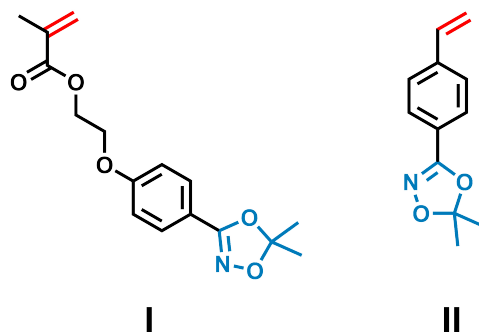
SCHEME 1 Chemical structure of a hydroxamic acid-functionalized methacrylate derivative (MAHAA, **I**) and a styrene derivative (StHAA, **II**). Polymerizing groups are shown in red, protected hydroxamic acid moieties in blue.

The methacrylate monomer was synthesized in 4 steps, starting from inexpensive and commercially available chemicals. In general, the synthesis of hydroxamic acids can be based on different functional groups. In literature, amides, aldehydes, acyl chlorides as well as carboxylic acids are known as suitable substrates.[15,30-33] Here, ester functionalities were utilized to synthesize hydroxamic acid moieties by the reaction with hydroxylamine under basic conditions. The sequence of the synthesis steps is of key importance to prevent competitive esterification between hydroxamic acid moieties and free hydroxyl groups. As a consequence, the hydroxamic acid moiety was protected before the Steglich esterification was carried out (**Scheme 2**). Furthermore, the protection of the hydroxamic acid moiety is important to prevent side reactions during the polymerization, i.e. the transfer of radicals among the heteroatoms of the hydroxamic acid moiety.[30] A protected hydroxyl-functionalized hydroxamic acid (**1d** in **Scheme 2**) was prepared in the first three steps and was previous introduced in our group as a common precursor for monomer synthesis as well as for the initiation of an anionic ring opening polymerization (**1d** in **Scheme 2**).[28] The subsequent Steglich esterification was established to this system as a reaction under mild conditions that leads to the methacrylate-based monomer MAHAA (**I** in **Scheme 2**). The synthesis of this monomer was scalable with an overall yield of 37%.
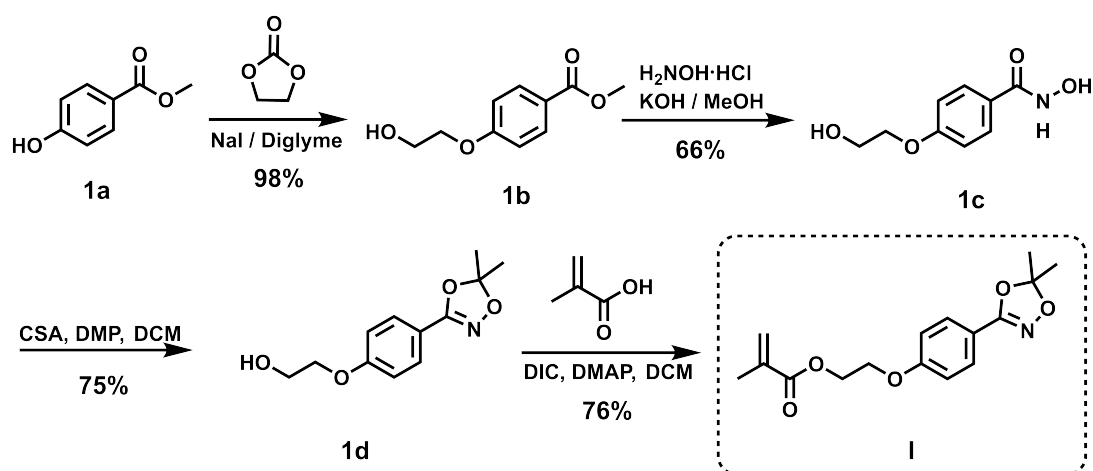
SCHEME 2 Synthetic route for the preparation of methacrylate hydroxamic acid acetonide (MAHAA, **I**) in 4 steps.

Figure 1 presents the ^{1}H NMR spectrum of the synthesized monomer structure with a full assignment of the signals. The presence of the singlet signal at 1.6 ppm (corresponding to the protons of the methyl groups attachted to the 1,4,2-dioxazole group (**a** in **Figure 1**)) confirmed the stability of the protecting group against the reaction conditions in a Steglich esterification.
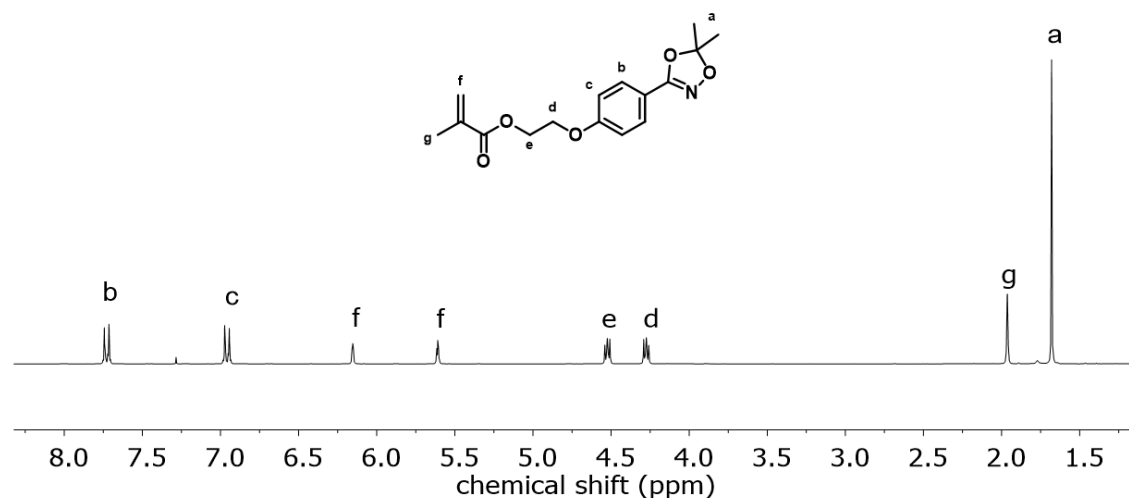
FIGURE 1 ^{1}H NMR spectrum of MAHAA (**I**) (300 MHz, CDCl$_3$).

Summarizing, the methacrylate-based monomer MAHAA was designed to exhibit (i) a polymerizable group (ii) a protected hydroxamic acid moiety to withstand the polymerization conditions and (iii) an ethylene glycol linker to separate both groups and thus limit a steric interference. The combination of this properties led to a versatile and new hydroxamic acid-functionalized monomer.

Furthermore, we focused on styrene derivatives as a universal and well-studied monomer type which is compatible with different polymerization techniques, such as anionic or radical polymerization techniques.[34,35] The protected hydroxamic acid functionality is attached in the *para*-position to the polymerizing group of styrene (**II** in **Scheme 1**). The hydroxamic acid-functionalized styrene monomer (**II**) was synthesized in 5 steps starting from methyl *p*-toluate. In the first steps, the ester was converted to the hydroxamic acid and subsequently protected via transketalization to yield the 1,4,2-dioxazole structure (**Scheme 1**). During our initial studies, we found the transformation of the methyl group to the polymerizing vinyl bond to be the limiting factor preventing scale-up. Especially, the employed Wittig reaction leads to high amounts of triphenylphosphine oxide, which requires tedious purification effort limiting the yields furthermore (see *Supporting Information* for experimental details). Despite these problems, the product was established as a new suitable monomer in radical polymerization reactions.

During the course of our investigation, we found the combination of methacrylates with a hydroxamic acid moiety to be more efficient in terms of synthesis procedures, purification effort and yields compared to the styrene derivative. Therefore, we decided to focus exclusively on the methacrylate-based hydroxamic acid-functionalized monomer and its polymerization via controlled radical techniques in the following discussion.

Compatibility in a RAFT polymerization

In our studies, the polymerizing group of MAHAA was designed to possess structural analogy to MMA, HEMA and OEGMEMA to facilitate compatibility and enable the reaction conditions established for the RAFT polymerization. ^{1}H and ^{13}C NMR spectroscopy was utilized to estimate and to compare the electronic structure of the methacrylate monomers with MAHAA. As a result, no significant difference (less than 0.08 ppm difference in ^{1}H NMR and less than 0.70 ppm difference in ^{13}C NMR) in the chemical shifts was observed (**Table 1**). Therefore, similar polymerization behavior of MAHAA was expected as for MMA, HEMA and OEGMEMA.

TABLE 1 Chemical shifts for signals **a**, **b** and **b'** in ^{1}H NMR and **A**, **B**, **B'** and **C** in ^{13}C NMR spectra of different methacrylate monomers (300 MHz, CDCl$_3$).

Monomer	a [ppm]	b, b' [ppm]	A [ppm]	B [ppm]	B' [ppm]	C [ppm]
MAHAA	1.94	5.59, 6.13	18.29	126.31	135.98	167.36
OEGMEMA	1.93	5.56, 6.11	18.30	125.71	136.12	167.32
MMA	1.90	5.51, 6.05	18.35	125.47	136.26	167.93
HEMA	1.94	5.59, 6.14	18.34	126.14	136.07	167.86
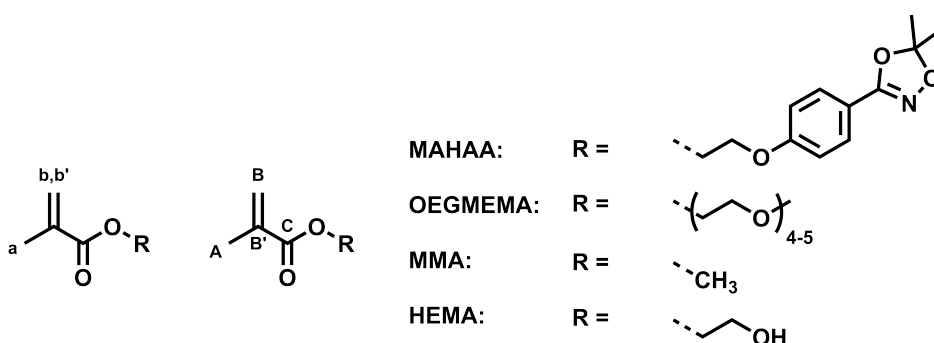
Polymer synthesis

The choice of a suitable RAFT agent depends strongly on the reactivity of the monomers.[37] In our studies, the chain transfer agent (CTA) 2-Cyano-2-propyl benzodithioate (CPBDT) was successfully applied for the RAFT copolymerization of methacrylates and derivatives due to similar radical reactivities of CTA (R·) and monomer (M·). Furthermore, RAFT was chosen as method of choice to enable the preparation of controlled statistical and block copolymers. The RAFT polymerization technique is compatible with various monomer structures, such as acrylates, methacrylates, styrenes and acrylamides.[37] We have chosen MMA, HEMA and OEGMEMA as comonomers for MAHAA to synthesize copolymers with varying hydrophilicities and different solubility behavior (**Scheme 3**). The short PEG chains (4-5 repeating units) in OEGMEMA in a brush-like structure mediate water solubility, whereas MMA-based and HEMA-based copoly-

mers were water-insoluble. Thus, the properties of the copolymers can be tuned with the choice of the comonomers. The copolymers were varied with respect to their molecular weights and the amount of incorporated amount of hydroxamic acid groups, which varied from 5-50%$_{mol}$ in a molecular weight range of 2,700 to 9,900 g mol^{-1}. In all cases, SEC characterization proved narrow molecular weight distributions with dispersities between 1.11 and 1.35 (**Table 2**). The copolymers were characterized by size exclusion chromatography (SEC) as well as 1D and 2D NMR spectroscopy (see *Supporting Information* for details).
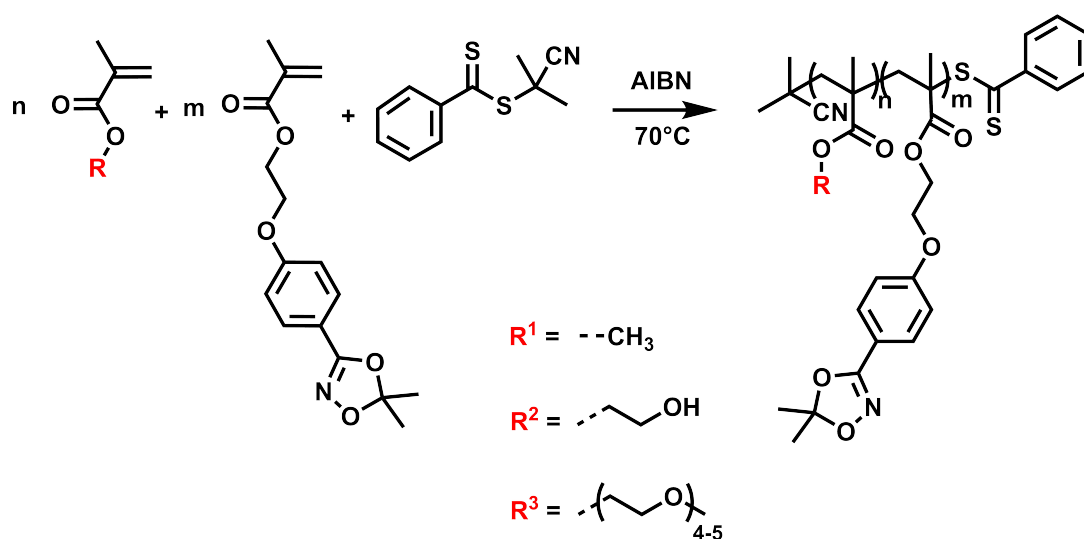
SCHEME 3   Synthesis of hydroxamic acid-functionalized copolymers containing MMA (R^1), HEMA (R^2) or OEGMEMA (R^3) mediated by RAFT polymerization.

TABLE 2   Synthesized hydroxamic acid-functionalized copolymers.

Polymer	$M_{n,theo.}$ [g mol^{-1}]	M_n[a] [g mol^{-1}]	M_n[b] [g mol^{-1}]	$Đ$[b]	MAHAA[a] [%$_{mol}$]	Yield[%]
P(MMA$_{35}$-*co*-MAHAA$_3$)	5000	4600	4900	1.11	8	94
P(MMA$_{54}$-*co*-MAHAA$_4$)	10000	6700	8300	1.13	7	81
P(MMA$_{12}$-*co*-MAHAA$_{13}$)	5700	5200	5300	1.20	50	97
P(HEMA$_{18}$-*co*-MAHAA$_1$)	2500	2700	4400	1.27	5	90
P(HEMA$_{64}$-*co*-MAHAA$_5$)	5000	9900	8300	1.35	7	99
P(HEMA$_{10}$-*co*-MAHAA$_{10}$)	5700	4400	3100	1.26	50	97
P(OEGMEMA$_{19}$-*co*-MAHAA$_3$)	5000	6600	4700	1.22	14	83
P(OEGMEMA$_{24}$-*co*-MAHAA$_4$)	10000	8300	6800	1.19	14	93
P(OEGMEMA$_9$-*co*-MAHAA$_9$)	5700	5400	6400	1.12	50	95
P(MMA)$_{56}$-*b*-P(MAHAA)$_{10}$	10000	8700	8300	1.18	18	85

a. Determined via ^{1}H NMR end group analysis. **b.** SEC (THF), P(MMA) calibration, DMF as solvent was used in the case of HEMA and OEGMEMA containing polymers.

The copolymers containing MMA and MAHAA (**Scheme 3**, R^1) were synthesized in a molecular weight range from 4,600 to 9,900 g mol^{-1}, with dispersities below 1.14 (**Table 2**). The block copolymer was synthesized successfully in two steps. First, a P(MMA) homopolymer was synthesized that was utilized as macroCTA in the following polymerization with MAHAA. In all cases, the SEC traces showed monomodal distributions for all statistical and block copolymers (**Figure 2**).
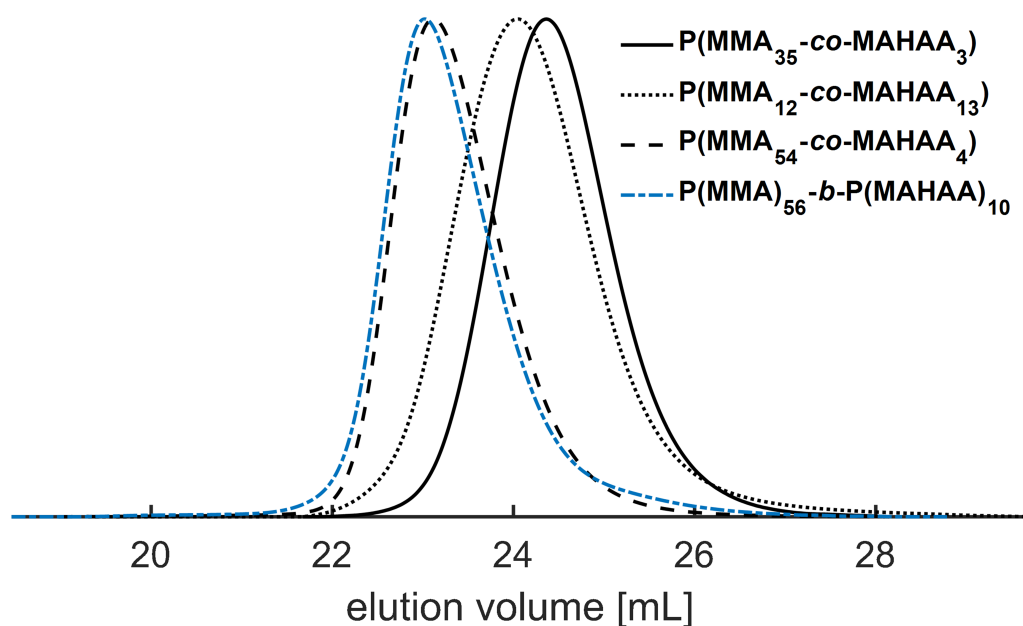
FIGURE 2 SEC traces of the hydroxamic acid-functionalized copolymers containing MMA with different architectures (THF, P(MMA) calibration, UV detector).

Copolymerizations of MAHAA with HEMA and OEGMEMA, respectively were carried out to increase the polarity of the resulting copolymers and to change the solubility behavior of the resulting copolymers. MAHAA was copolymerized successfully with HEMA, confirmed via ^{1}H NMR spectroscopy and SEC measurements (**Figure 3**, **Figure S33**). Explorative works of Armes and coworkers[38,39] demonstrated the convenient synthesis of well-defined and water-soluble P(OEGMEMA) structures by the ATRP technique in the late 1990s. Lutz *et al.* investigated the properties of polymers consisting of OEGMEMA and 2-(2-methoxy-ethoxy)ethyl methacrylate in detail. These copolymers combine the advantages of PEG in terms of biocompatibility and low toxicity with thermoresponsive behavior in water.[40,41] Here, we report the synthesis of P(OEGMEMA-*co*-MAHAA) structures that combine aqueous solubility with metal chelating properties. To this end, OEGMEMA (**Scheme 3**, R^3) was employed for the copolymerization with MAHAA. Successful copolymerization was proven via ^{1}H NMR spectroscopy and

SEC measurements (**Figure 3**, **Figures S33** and **S34**). To conclude, the results of these proof-of-principle experiments, MAHAA was copolymerized successfully with methacrylate derivatives via the RAFT polymerization technique with control over the position and number of hydroxamic acid moieties among the polymer backbone. Slight deviations between theoretical molecular weights and determined molecular weights might be due to the partial monomer consumption through AIBN (CTA/I = 10). No cleavage of the protecting group was detected after the polymerization (see *Supporting Information* **Figure S15**). Hence, the 1,4,2-dioxazole group is stable under the polymerization conditions of the RAFT technique.
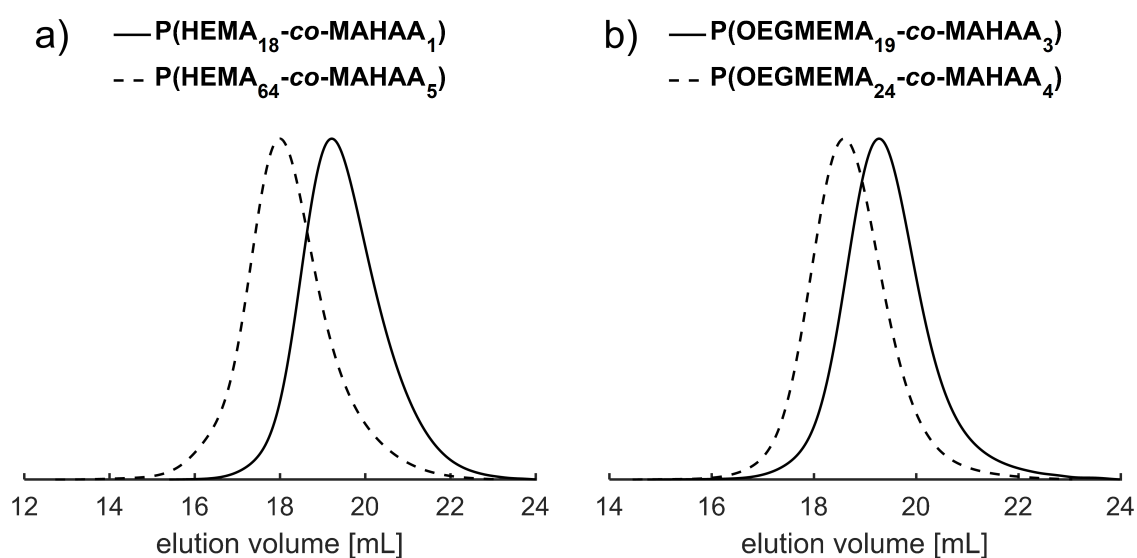
FIGURE 3 SEC traces of the hydroxamic acid-functionalized polymers. Copolymers of MAHAA with HEMA respectively OEGMEMA are shown (DMF, P(MMA) calibration, UV detector).

Kinetic studies

In previous works, we demonstrated for hydroxamic acid-substituted polyethers that the polymer architecture has an impact on the complex formation between hydroxamic acids and metal ions due to inter- or intramolecular network formation.[42] Both polymer architecture and the distribution of MAHAA at the polymer chains determine the complex formation between hydroxamic acids and metal ions. We performed *in situ* ^{1}H NMR kinetic measurements to investigate the copolymerization behavior of MAHAA with M1 (MMA, HEMA or OEGMEMA). For all measurements observed the same decrease of monomer concentrations of MAHAA and M1 with time, revealing the expected random incorporation of the monomers (**Figure 4**).
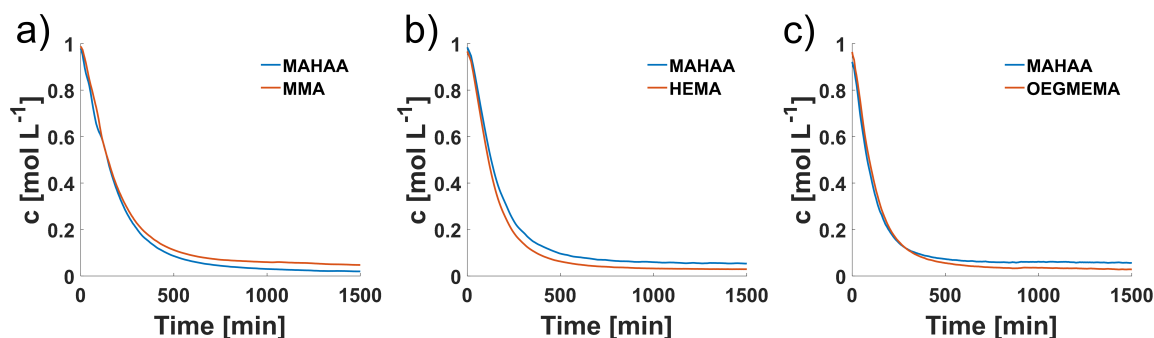
FIGURE 4 Monomer concentrations of MAHAA and MMA (a), HEMA (b) or OEGMEMA (c) versus time in a RAFT polymerization.

The reactivity ratios were determined from kinetic data with the method established by Jaacks in the early 1970s (**Table 3**).[43] Based on this fundamental equation, the reactivity ratios between the homopropagation (k_{11} and k_{22}) and the crossover propagation (k_{12} and k_{21}) with $r_1 = k_{11}/k_{12}$ and $r_2 = k_{22}/k_{21}$ were calculated (see *Supporting Information* for further details on kinetic data evaluation).

TABLE 3 Reactivity ratios determined by *in situ* ^{1}H NMR kinetic measurements. The values were calculated by the Jaacks method.[43] M1 = MMA, HEMA or OEGMEMA. A 50:50 molar ratio of [M1:MAHAA] was used. The polymerizations were performed at 70 °C in dioxane-d_8.

Polymer	r_{M1}	r_{MAHAA}
P(MMA$_{12}$-co-MAHAA$_{13}$)	$0.87 \pm 3.1 \cdot 10^{-3}$	$1.14 \pm 4.1 \cdot 10^{-3}$
P(OEGMEMA$_9$-co-MAHAA$_9$)	$1.01 \pm 5.1 \cdot 10^{-3}$	$0.99 \pm 5.0 \cdot 10^{-3}$
P(HEMA$_{10}$-co-MAHAA$_{10}$)	$1.19 \pm 1.2 \cdot 10^{-3}$	$0.84 \pm 8.2 \cdot 10^{-4}$

In the copolymerizations studied all reactivity ratios were close to unity, demonstrating random incorporation of the monomers. These results are in line with the expected copolymerization behavior of the monomers due to the similar chemical and electronic structure of the polymerizing double bonds (**Table 1**). In addition, we conclude from the equal preference between homo- and crossover propagation that the MAHAA incorporation in the copolymer structure is not sterically hindered (**Table 3**). Summarizing, the kinetic data evaluation confirmed the expected random incorporation of MAHAA in the copolymerization with MMA, HEMA and OEGMEMA, respectively.

Deprotection and liberation of hydroxamic acid side chains

After the polymerization, the 1,4,2-dioxazole protecting groups were removed to release the hydroxamic acid moieties. The cleavage of the protecting groups was carried out via the reaction

with *DL*-campher sulfonic acid (CSA) under mild conditions at room temperature for 24 h. The deprotection was followed via ^{1}H NMR spectroscopy by sampling after different reaction times (**Figure 5**).
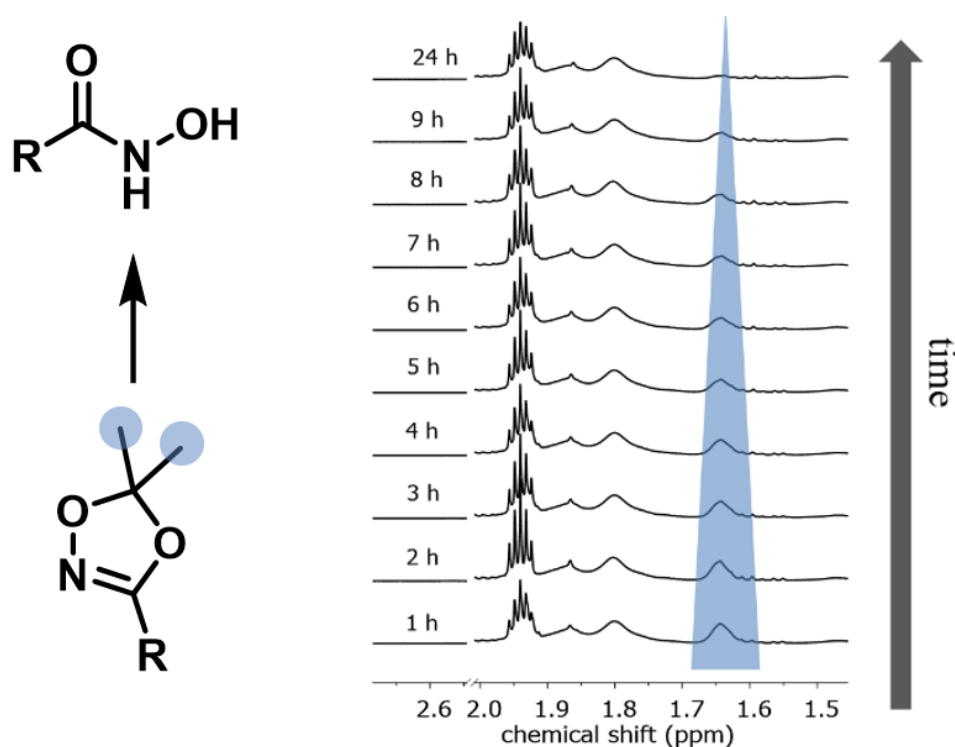
FIGURE 5 ^{1}H NMR spectra overlay showing the removal of the protecting group (highlighted in blue) of P(MMA-*co*-MAHAA) (300 MHz, CD$_3$CN).

The signal at 1.61 ppm (highlighted in blue in **Figure 5**) corresponds to the protons of the 1,4,2-dioxazole protecting group. After approximately 24 h, the signal of the 1,4,2-dioxazole structure had vanished, and the deprotected polymer P(MMA-*co*-MAHA) was obtained. To further investigate the cleavage of the protecting group, quantitative ^{1}H NMR analysis was performed. For the cleavage of the ketal structure, the common mechanism was assumed. Hence, the reaction is assumed to follow a pseudo-first order kinetics when performed in excess of protons. The integrals were normalized and correlated to the concentration of the 1,4,2-dioxazole in solution. A logarithmic representation (**Figure 6**) shows a linear behavior as expected with first order kinetics (y = -0.0009821x-0.03605). As a first estimation, it is possible to calculate the half life time of the deprotection, showing that 50% of all the protecting groups are cleaved after approximately 12 h.
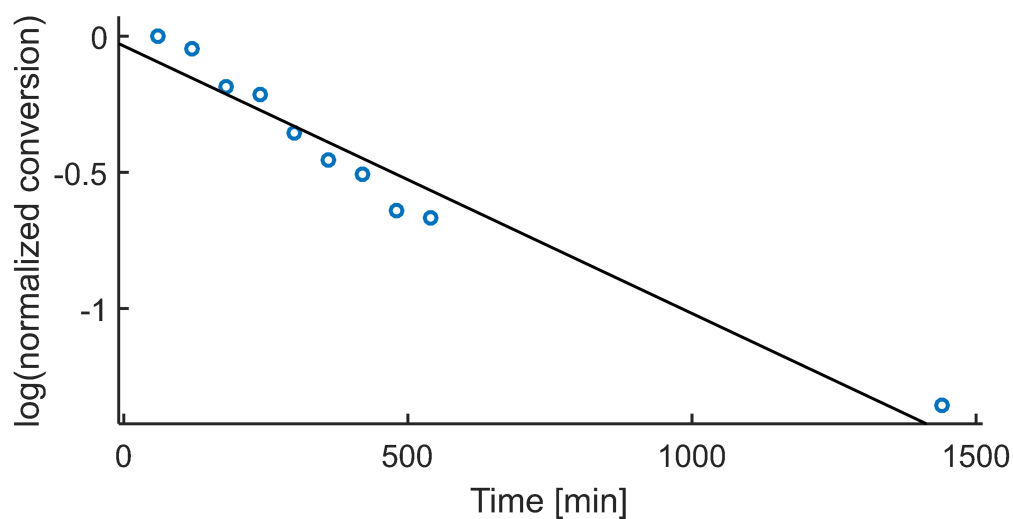
FIGURE 6 Decreasing intensity of the protecting group signals with time. A linear fit was used (y = -0.0009821x - 0.03605).

The deprotection reaction of the HEMA- and OEGMEMA-based copolymers were performed with the addition of a 0.1 M HCl solution at room temperature. After 24 h the protecting groups were completely removed (**Figures S21** and **S23**).

Surface adhesion tests

As a final demonstration, the adhesion behavior of the prepared P(MMA-*co*-MAHA) copolymers was tested. Coating of metal surfaces has been widely investigated in the last few years, aiming for surfaces with tailored chemical properties to suppress nonspecific biological interactions or protein adsorptions due to the incorporation of functional groups in the coating layer.[44] A major obstacle in long-term coating is the lack of suitable groups that lead to sustainable adhesion with the surfaces, especially under wet conditions.[45] Different metal surfaces were coated with the methacrylate based hydroxamic acid-functionalized P(MMA-*co*-MAHA). Iron, copper and brass surfaces were employed to investigate the adhesion behavior of the hydroxamic acid-functionalized polymer. For the sample preparation, metal samples were added to either (i) a P(MMA-*co*-MAHA) solution, (ii) a P(MMA) solution or (iii) a reference solution without polymer. All surfaces were rinsed several times with dichloromethane and dried before further characterization (see *Supporting Information* for experimental details). For contact angle measurements, a water droplet was placed on the metal surfaces to gain information on the polarity of the surface by its specific contact angle. An interaction between metal and hydroxamic acid was observed for each metal surface, manifest in a change in the contact angle between the reference and the

P(MMA-*co*-MAHA) coated metal plate (**Table 4**). The P(MMA) coated metal samples led to no significant change in the contact angle, indicating no attachment of P(MMA) on the metal surfaces. Only the hydroxamic acid functionalized polymers showed an interaction with the metal surfaces. In conclusion, the proof-of-principle experiments showed successful attachment of hydroxamic acid-functionalized polymers on the metal surfaces, confirmed by a change of the specific contact angle.

TABLE 4   Contact angle measurements on copper, iron and brass plates coated with P(MMA$_{90}$-*co*-MAHA$_8$) respectively P(MMA)$_{63}$.

Polymer	Copper	Iron	Brass
Reference	73 ± 7°	62 ± 5°	76 ± 2°
P(MMA)$_{63}$	74 ± 5°	61 ± 3°	74 ± 7°
P(MMA$_{90}$-*co*-MAHA$_8$)	59 ± 3°	55 ± 2°	63 ± 6°

CONCLUSIONS

We demonstrate the successful synthesis of a methacrylate based hydroxamic acid-functionalized monomer (MAHAA), which is accessible in 4 steps from inexpensive and conveniently available starting materials with yields of 37% over all steps. The monomer was copolymerized with MMA, HEMA and OEGMEMA, respectively via the RAFT polymerization technique. This approach enabled the direct incorporation of hydroxamic acids into poly(methacrylate)s with control over the molecular weight as well as the number and the position of the hydroxamic acid moieties in the copolymers. Kinetic data evaluation confirmed random incorporation of MAHAA in copolymerizations with MMA, HEMA and OEGMEMA respectively. As a proof-of-principle concept, we have demonstrated the adhesion of hydroxamic acid-functionalized polymers at metal surfaces, such as copper, iron and brass, confirmed by contact angle measurements. The combination of hydroxamic acids with polymer chemistry is a powerful tool to introduce multiple metal chelating motifs, controlling the number and position of the moieties. The highly storage stable hydroxamic acids and polymeric analogues represent an alternative to catechol-based structures.

ACKNOWLEDGEMENTS

REFERENCES

(1) Leibig, D.; Müller, A. H. E.; Frey, H. Anionic Polymerization of Vinylcatechol Derivatives: Reversal of the Monomer Gradient Directed by the Position of the Catechol Moiety in the Copolymerization with Styrene. *Macromolecules* **2016**, *49*, 4792–4801.

(2) Niederer, K.; Schüll, C.; Leibig, D.; Johann, T.; Frey, H. Catechol Acetonide Glycidyl Ether (CAGE): A Functional Epoxide Monomer for Linear and Hyperbranched Multi-Catechol Functional Polyether Architectures. *Macromolecules* **2016**, *49*, 1655–1665.

(3) Holten-Andersen, N.; Mates, T. E.; Toprak, M. S.; Stucky, G. D.; Zok, F. W.; Waite, J. H. Metals and the integrity of a biological coating: the cuticle of mussel byssus. *Langmuir* **2009**, *25*, 3323–3326.

(4) Holten-Andersen, N.; Harrington, M. J.; Birkedal, H.; Lee, B. P.; Messersmith, P. B.; Lee, K. Y. C.; Waite, J. H. pH-induced metal-ligand cross-links inspired by mussel yield self-healing polymer networks with near-covalent elastic moduli. *Proc. Natl. Acad. Sci. U. S. A.* **2011**, *108*, 2651–2655.

(5) Maier, G. P.; Butler, A. Siderophores and mussel foot proteins: the role of catechol, cations, and metal coordination in surface adhesion. *J. Biol. Inorg. Chem.* **2017**, 739–749.

(6) Faure, E.; Falentin-Daudré, C.; Jérôme, C.; Lyskawa, J.; Fournier, D.; Woisel, P.; Detrembleur, C. Catechols as versatile platforms in polymer chemistry. *Prog. Polym. Sci.* **2013**, *38*, 236–270.

(7) Miller, M. J. Syntheses and therapeutic potential of hydroxamic acid based siderophores and analogs. *Chem. Rev.* **1989**, *89*, 1563–1579.

(8) Keth, J.; Johann, T.; Frey, H. Hydroxamic Acid: An Underrated Moiety? Marrying Bioinorganic Chemistry and Polymer Science. *Biomacromolecules* **2020**, *21*, 2546–2556.

(9) Schweigert, N.; Zehnder, A. J. B.; Eggen, R. I. L. Chemical properties of catechols and their molecular modes of toxic action in cells, from microorganisms to mammals. Minireview. *Environ. Microbiol.* **2001**, *3*, 81–91.

(10) Neilands, J. B. Hydroxamic Acids in Nature. *Science* **1967**, *156*, 1443–1447.

(11) Winston, A.; Mazza, E. T. Hydroxamic acid polymers. *J. Polym. Sci. Pol. Chem.* **1975**, *13*, 2019–2030.

(12) Brown, D. A.; Coogan, R. A.; Fitzpatrick, N. J.; Glass, W. K.; Abukshima, D. E.; Shiels, L.; Ahlgrén, M.; Smolander, K.; Pakkanen, T. T.; Pakkanen, T. A.; *et al.* Conformational behaviour of hydroxamic acids: ab initio and structural studies. *J. Chem. Soc., Perkin Trans. 2* **1996**, *105*, 2673–2679.

(13) Pereira, C. F.; Howarth, A. J.; Vermeulen, N. A.; Almeida Paz, F. A.; Tomé, J. P. C.; Hupp, J. T.; Farha, O. K. Towards hydroxamic acid linked zirconium metal-organic frameworks. *Mater. Chem. Front.* **2017**, *117*, 10401.

(14) Brewster, T. P.; Konezny, S. J.; Sheehan, S. W.; Martini, L. A.; Schmuttenmaer, C. A.; Batista, V. S.; Crabtree, R. H. Hydroxamate anchors for improved photoconversion in dye-sensitized solar cells. *Inorg. Chem.* **2013**, *52*, 6752–6764.

(15) Folkers, J. P., Gorman, C. B., Laibinis, P. E., Buchholz, S., Whitesides, G. M., Nuzzo, R. G. Self-assembled monolayers of long-chain hydroxamic acids on the native oxides of metals. *Langmuir* **1995**, *11*, 813–824.

(16) Coffman, D. D. Polymeric Hydroxamic Acids. US2402604 A, **1942**.

(17) Winston, A.; McLaughlin, G. R. Hydroxamic acid polymers. II. Design of a polymeric chelating agent for iron. *J. Polym. Sci. Pol. Chem.* **1976**, *14*, 2155–2165.

(18) Winston, A.; Kirchner, D. Hydroxamic Acid Polymers. Effect of Structure on the Selective Chelation of Iron in Water. *Macromolecules* **1978**, *11*, 597–603.

(19) Tian, F.; Decker, E. A.; Goddard, J. M. Controlling lipid oxidation via a biomimetic iron chelating active packaging material. *J. Agric. Food Chem.* **2013**, *61*, 12397–12404.

(20) Tian, F.; Decker, E. A.; Goddard, J. M. Development of an iron chelating polyethylene film for active packaging applications. *J. Agric. Food Chem.* **2012**, *60*, 2046–2052.

(21) Agrawal, Y.K.; Kaur, H.; Menon, S.K. Poly(styrene-p-hydroxamic acids): synthesis, and ion exchange separation of rare earths. *React. Funct. Polym.* **1999**, *39*, 155–164.

(22) Vernon, F.; Eccles, H. Chelating ion-exchangers containing n-substituted hydroxylamine functional groups. *Anal. Chim. Acta* **1976**, *83*, 187–193.

(23) Kumar, S. A.; Pandey, S. P.; Shenoy, N. S.; Kumar, S. D. Matrix separation and preconcentration of rare earth elements from seawater by poly hydroxamic acid cartridge followed by determination using ICP-MS. *Desalination* **2011**, *281*, 49–54.

(24) Agrawal, Y. K.; Kapoor, H. L. Stability constants of rare earths with hydroxamic acids. *J. Inorg. Nucl. Chem.* **1977**, *39*, 479–482.

(25) Alakhras, F. A.; Dari, K. A.; Mubarak, M. S. Synthesis and chelating properties of some poly(amidoxime-hydroxamic acid) resins toward some trivalent lanthanide metal ions. *J. Appl. Polym. Sci.* **2005**, *97*, 691–696.

(26) Mello, R. S.; Orth, E. S.; Loh, W.; Fiedler, H. D.; Nome, F. Polymers containing hydroxamate groups: nanoreactors for hydrolysis of phosphoryl esters. *Langmuir* **2011**, *27*, 15112–15119.

(27) Skarja, G. A.; Brown, A. L.; Ho, R. K.; May, M. H.; Sefton, M. V. The effect of a hydroxamic acid-containing polymer on active matrix metalloproteinases. *Biomaterials* **2009**, *30*, 1890–1897.

(28) Johann, T.; Keth, J.; Bros, M.; Frey, H. A general concept for the introduction of hydroxamic acids into polymers. *Chem. Sci.* **2019**, *10*, 7009–7022.

(29) Johann, T.; Kemmer-Jonas, U.; Barent, R. D.; Frey, H. Multifunctional Fe(III)-Binding Polyethers from Hydroxamic Acid-Based Epoxide Monomers. *Macromolecular rapid communications* **2020**, *41*, e1900282.

(30) Iskander, G. M.; Kapfenstein, H. M.; Davis, T. P.; Wiley, D. E. Synthesis and copolymerization of methacryloyl hydroxamic acids. *J. Appl. Polym. Sci.* **2000**, *78*, 751–758.

(31) Giacomelli, G.; Porcheddu, A.; Salaris, M. Simple one-flask method for the preparation of hydroxamic acids. *Organic letters* **2003**, *5*, 2715–2717.

(32) Porcheddu, A.; Giacomelli, G. Angeli-Rimini's reaction on solid support: a new approach to hydroxamic acids. *J. Org. Chem.* **2006**, *71*, 7057–7059.

(33) Domb, A. J.; Cravalho, E. G.; Langer, R. The synthesis of poly(hydroxamic acid) from poly(acrylamide). *J. Polym. Sci. Pol. Chem.* **1988**, *26*, 2623–2630.

(34) Hirao, A.; Loykulnant, S.; Ishizone, T. Recent advance in living anionic polymerization of functionalized styrene derivatives. *Prog. Polym. Sci.* **2002**, *27*, 1399–1471.

(35) Moad, G.; Rizzardo, E.; Thang, S. H. Living Radical Polymerization by the RAFT Process - A Second Update. *Aust. J. Chem.* **2009**, *62*, 1402.

(34) Perrier, S. 50th Anniversary Perspective : RAFT Polymerization—A User Guide. *Macromolecules* **2017**, *50*, 7433–7447.

(35) Sun, Y.-M.; Huang, J.-J.; Lin, F.-C.; Lai, J.-Y. Composite poly(2-hydroxyethyl methacrylate) membranes as rate-controlling barriers for transdermal applications. *Biomaterials* **1997**, *18*, 527–533.

(36) Wang, X.-S.; Armes, S. P. Facile Atom Transfer Radical Polymerization of Methoxy-Capped Oligo(ethylene glycol) Methacrylate in Aqueous Media at Ambient Temperature. *Macromolecules* **2000**, *33*, 6640–6647.

(37) Wang, X.-S.; Lascelles, S. F.; Jackson, R. A.; Armes, S. P. Facile synthesis of well-defined water-soluble polymers via atom transfer radical polymerization in aqueous media at ambient temperature. *Chem. Commun.* **1999**, 1817–1818.

(38) Lutz, J.-F. Thermo-Switchable Materials Prepared Using the OEGMA-Platform. *Adv. Mater.* **2011**, *23*, 2237–2243.

(39) Pissuwan, D.; Boyer, C.; Gunasekaran, K.; Davis, T. P.; Bulmus, V. In vitro cytotoxicity of RAFT polymers. *Biomacromolecules* **2010**, *11*, 412–420.

(41) Jaacks, V. A Novel Method of Determination of Reactivity Ratios in Binary and Ternary Copolymerizations. *Makromol. Chem.* **1972**, *161*, 161–172.

(42) Steube, M.; Johann, T.; Plank, M.; Tjaberings, S.; Gröschel, A. H.; Gallei, M.; Frey, H.; Müller, A. H. E. Kinetics of Anionic Living Copolymerization of Isoprene and Styrene Using in Situ NIR Spectroscopy: Temperature Effects on Monomer Sequence and Morphology. *Macromolecules* **2019**, *52*, 9299–9310.

(43) Fernández-Monreal, C.; Martínez, G.; Sánchez-Chaves, M.; López Madruga, E. Solvent effect on the free-radical copolymerization of 2-hydroxyethyl methacrylate with t -butyl acrylate. *J. Polym. Sci. Pol. Chem.* **2001**, *39*, 2043–2048.

(44) Lee, H.; Dellatore, S. M.; Miller, W. M.; Messersmith, P. B. Mussel-inspired surface chemistry for multifunctional coatings. *Science* **2007**, *318*, 426–430.

(45) Waite, J. H. Nature's underwater adhesive specialist. *Int. J. Adhes. Adhes.* **1987**, *7*, 9–14.

SUPPORTING INFORMATION

Materials

All reagents were used without further purification, unless otherwise stated. All chemicals and solvents were purchased from Abcr, Acros, Aldrich, Fisher Scientific, Fluka, Riedel-de-Haën or Roth. Deuterated solvents were purchased from Deutero GmbH. MMA, HEMA and OEGMEMA were filtered through a basic alumina column to remove the stabilizer. If not mentioned the compounds were used as received.

Instrumentation

NMR analysis. ^{1}H NMR spectra at 300 MHz and ^{13}C NMR spectra at 75 MHz were recorded on a Bruker Avance III HD 300 (5 mm BBFO-Head with z-gradient) at 23 °C. ^{1}H NMR spectra at 400 MHz and ^{13}C NMR spectra at 100 MHz were recorded on a Bruker Avance III HD 400 (5 mm BBFO-Smartprobe with z-gradient) at 23 °C. All NMR spectra were referenced to the residual proton signals of the deuterated solvent.

Size exclusion chromatography (SEC). SEC was performed in DMF (1 mL/min, 50 °C) containing 1 g/L lithium bromide as additive. An Agilent 1100 series SEC system including a HEMA 300/100/40 Å column cascade, an UV (254 nm) and a RI detector was used. Furthermore, SEC was performed in THF (1 mL/min, 20 °C) containing 1 g/L lithium bromide as additive. A MZ-gel SD plus column, an UV (254 nm) and a RI detector was used. Calibration was carried out using P(MMA) standards provided by Polymer Standard Service (PSS).

Contact angle measurement. Contact angle measurements were carried out by performing the sessile drop method. Each metal wafer was put into a P(MMA) respectively a P(MMA-*co*-MAHA) solution in DCM overnight at rt. The wafers were rinsed several times with DCM to remove non-adhered polymer and dried under air. The contact angles were measured by dropping one droplet of MilliQ-water on the surface of each metal plate. The angle between solid and liquid phase was determined. All measurements were repeated at least five times.

EXPERIMENTAL SECTION

Monomer synthesis: Methacrylate hydroxamic acid acetonide (MAHAA) I.
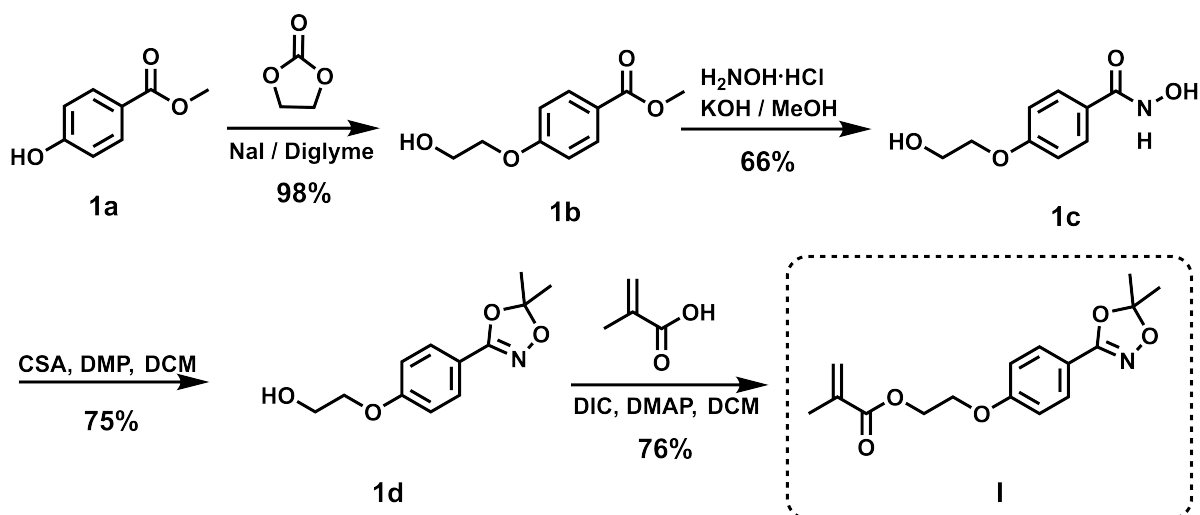
SCHEME S1   Synthetic route for the preparation of methacrylate hydroxamic acid acetonide (MAHAA) in 4 steps.

Synthesis of Methyl 4-(2-hydroxyethoxy)benzoate (1b).
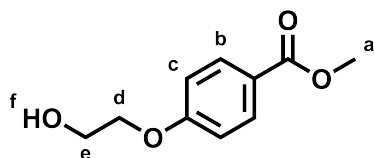
According to the literature[1], 80 g (0.53 mol, 1.00 eq) of methyl 4-hydroxybenzoate, 48.62 g (0.55 mol, 1.05 eq) of ethylene carbonate, 7.88 g (0.053 mol, 0.10 eq) of sodium iodide and 96 mL of diglyme were put in a three-neck flask equipped with a reflux condenser. The mixture was left for 20 h at 110 °C and afterwards for 3 h at 170 °C. The solvent was removed under reduced pressure. After the addition of 300 mL of ethyl acetate the mixture was washed with 50 mL water, 50 mL NaHCO$_3$ and 50 mL of NaCl. After drying over Na$_2$SO$_4$ the solvent was removed under reduced pressure. Methyl 4-(2-hydroxyethoxy)benzoate was obtained in yields of 100.94 g (0.51 mol, 98%).

^{1}H NMR (300 MHz, DMSO-d_6): δ [ppm] = 7.91 (*AA'BB'*, 2H, ArC^{3,5}*H*, b), 7.02 (*AA'BB'*, 2H, ArC^{2,6}*H*, c), 4.91 (*s*, 1H, O-*H*, f), 4.04 (*m*, 2H, O-C*H*$_2$, d), 3.80 (*s*, 3H, O-C*H*$_3$, a), 3.71 (*m*, 2H, HO-C*H*$_2$, e).

Synthesis of *N*-hydroxy-4-(2-hydroxyethoxy)benzamide (1c).
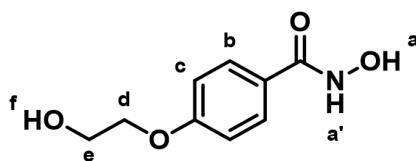
According to the literature[1], 50 g (0.72 mol, 2.00 eq) hydroxyl amine were dissolved in 500 mL of methanol in a 2 L Schlenk flask. 60.56 g (1.08 mol, 3.00 eq) of potassium hydroxide were dissolved in 200 mL methanol and were put under ice cooling to the hydroxyl amine solution. After filtration through a frit (porosity 3) the filtrate was mixed with 70.59 g (0.36 mol, 1.00 eq) methyl 4-(2-hydroxyethoxy)benzoate previously dissolved in 100 mL methanol. After stirring for 6 days at rt the mixture was quenched carefully with a $NaHSO_4$ solution (85.00 g, 2.00 eq) up to pH 3-4. The solvent was removed under reduced pressure. The solid was put in an extraction thimble (soxhlet extractor) and was extracted for 3 days with THF as a solvent. The yield was 46.12 g (0.23 mol, 66%).

^{1}H NMR (300 MHz, DMSO-d_6): δ [ppm] = 11.05 (*s*, 1H, N*H*-OH, a'), 8.82 (*s*, 1H, NH-O*H*, a), 7.72 (*AA'BB'*, 2H, ArC^{3,5}*H*, b), 6.99 (*AA'BB'*, 2H, ArC^{2,6}*H*, c), 4.88 (*s*, 1H, O-*H*, f), 4.01 (*m*, 2H, O-C*H$_2$*, d), 3.71 (*m*, 2H, HO-C*H$_2$*, e).

Synthesis of 2-(4-(5,5-dimethyl-1,4,2-dioxazol-3-yl)phenoxy)ethan-1-ol (1d).
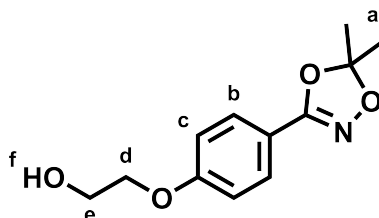
1d was prepared in a modified procedure from literature.[1] In a 2 L Schlenk flask, 18.00 g (0.09 mol, 1.00 eq) *N*-hydroxy-4-(2-hydroxyethoxy)benzamide were dissolved in 1 L dichloromethane. Afterwards 28.52 g (0.27 mol, 3.00 eq) 2,2-dimethoxypropane and 22.27 g (0.10 mol, 1.05 eq) *DL*-campher sulfonic acid were added. The mixture was stirred for 12 h at rt. The mixture was added to 480 mL of a 2 M NaOH solution. The yield was 16.07 g (0.075 mol, 75%).

^{1}H NMR (300 MHz, DMSO-d_6): δ [ppm] = 7.61 (*AA'BB'*, 2H, ArC^{3,5}*H*, b), 7.06 (*AA'BB'*, 2H, ArC^{2,6}*H*, c), 4.91 (*s*, 1H, O-*H*, f), 4.04 (*m*, 2H, O-C*H$_2$*, d), 3.73 (*m*, 2H, HO-C*H$_2$*, e), 1.60 (*s*, 6H, *H$_3$*C-CO$_2$-C*H$_3$*, a).

Synthesis of 2-(4-(5,5-dimethyl-1,4,2-dioxazol-3-yl)phenoxy)ethyl methacrylate (MAHAA) (I).
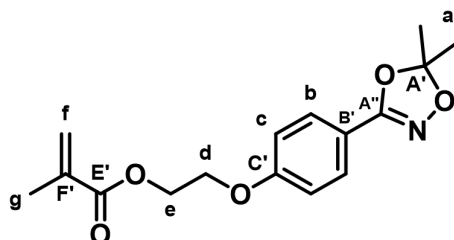
The reaction was carried out in a modified procedure according to the synthesis of Neises and Steglich.[2] In a 50 mL Schlenk flask, 6.06 g (0.026 mol, 1.10 eq) 2-(4-(5,5-dimethyl-1,4,2-dioxazol-3-yl)phenoxy)ethan-1-ol, 2.00 g (0.023 mol, 1.00 eq) methacrylic acid and 0.23 g (1.9 mmol, 0.08 eq) 4-dimethylaminopyridine (DMAP) were dissolved in 15 mL dichloromethane. Under ice cooling it was added 3.23 g (0.026 mol, 1.10 eq) N,N'-Diisopropylcarbodiimide (DIC) in a time period of 5 minutes. After stirring for 15 minutes under ice cooling, the mixture was stirred for 5 h at rt. The mixture was filtrated through a frit (porosity: 3) and the filtrate was washed twice with 100 mL of a saturated sodium hydrogen carbonate solution. The organic phase was dried over $MgSO_4$ and the solvent was removed under reduced pressure. The solid was purified by column chromatography (SiO_2, PE:EA = 9:1). Methacrylate hydroxamic acid acetonide (MAHAA, **I**) could be obtained in yields of 5.35 g (0.018 mol, 76%).

^{1}H NMR (300 MHz, $CDCl_3$): δ [ppm] = 7.73 ($AA'BB'$, 2H, $ArC^{3,5}H$, b), 6.93 ($AA'BB'$, 2H, $ArC^{2,6}H$, c), 6.15 (dq, J = 1.9, 1.0 Hz, 1H, $C=CH_2$, f), 5.60 (dq, J = 1.6 Hz, 1H, $C=CH_2$, f), 4.57-4.48 (m, 2H, $O-CH_2$, e), 4.28 (m, 2H, $O-CH_2$, d), 1.96 (dd, J = 1.6, 1.0 Hz, 3H, $C-CH_3$, g), 1.68 (s, 6H, $H_3C-CO_2-CH_3$, a).

^{13}C NMR (75 MHz, $CDCl_3$) δ [ppm] = 167.36 ($C=O$, E'), 161.01 (ArC^1-O, C'), 158.16 ($OC=N$, A"), 135.98 ($C=CH_2$, F'), 128.52 ($ArC^{3,5}$, B), 126.31 ($C=CH_2$, F), 116.52 (ArC^4-C, B'), 115.29 ($H_3C-CO_2-CH_3$, A'), 114.77 ($ArC^{2,6}$, C), 66.13 ($Ar-O-CH_2$, D), 62.92 ($Ar-O-CH_2-CH_2$, E), 24.91 ($H_3C-CO_2-CH_3$, A), 18.39 ($C-CH_3$, G).

IR-ATR $\tilde{v}$ [cm^{-1}] = 2961 (CH_3), 1714 ($C=O$), 1515 ($C=C$), 1165 ($C-O-C$), 813 ($C-H_{Ar}$).

R_f (PE:EA = 9:1) = 0.36.

Monomer synthesis: Styrene hydroxamic acid acetonide (StHAA) (II).
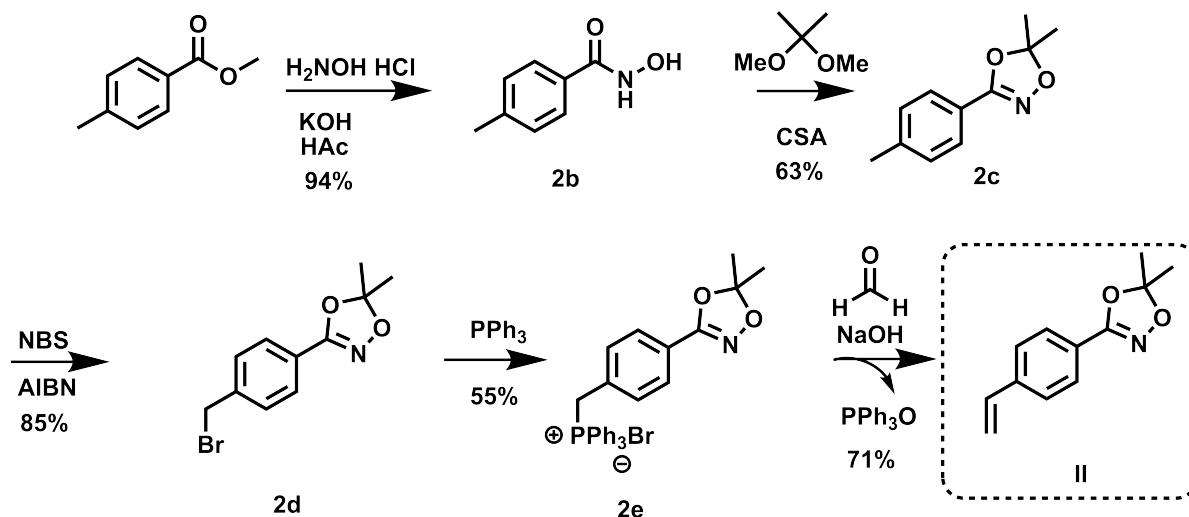
SCHEME S2   Synthetic route for the preparation of styrene hydroxamic acid acetonide (StHAA) in 5 steps.

Synthesis of *N*-hydroxy-4-methylbenzamide (2b).
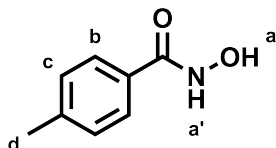
2b was prepared in a modified procedure according to the literature.[3] 46.56 g (0.67 mol 0.67 eq) hydroxyl amine and 56.11 g (1.00 mol, 1.00 eq) of potassium hydroxide were separately dissolved in 190 mL methanol. The potassium hydroxide solution were put under ice cooling to the hydroxyl amine solution. After 30 minutes, the mixture was filtrated through a frit (porosity 3). The filtrate was mixed with 49.56 g (0.33 mol, 0.33 eq) methyl 4-methylbenzoate. After stirring overnight at rt, the mixture was filtrated and 150 mL of a 1.25 M acetic acid solution were added and heated to reflux. After cooling in an ice bath *N*-hydroxy-4-methylbenzamide (**2b**) could be obtained in yields of 46.78 g (0.31 mol, 94%).

^{1}H NMR (300 MHz, DMSO-d_6): δ [ppm] = 10.14 (*s*, 2H, N*H*-O*H*, a+a'), 7.71-61 (*AA'BB'*, 2H, ArC^{2,6}*H*, b), 7.30-7.20 (*AA'BB'*, 2H, ArC^{3,5}*H*, c), 2.34 (*s*, 3H, ArC-C*H*$_3$, d).

Synthesis of 5,5-dimethyl-3-(*p*-tolyl)-1,4,2-dioxazole (2c).
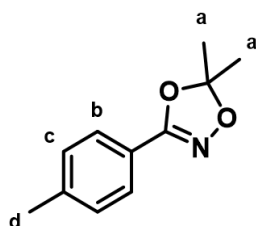
The preparation of **2c** was carried out in a modified procedure according from the literature.[4] In a 1 L Schlenk flask, 5.49 g (36.32 mmol, 1.00 eq) *N*-hydroxy-4-methylbenzamide and 350 mL dichloromethane were mixed and 11.34 g (0.11 mol, 3.00 eq) 2,2-dimethoxypropane and 8.43 g (36.32 mmol, 1.00 eq) *DL*-campher sulfonic acid were added. After 2 h of stirring at rt, the mixture was added to 180 mL of a 2 M NaOH solution. The mixture was stirred overnight. The organic layer was washed with NaOH and brine. The organic layer was dried over Na_2SO_4 and filtered. The solvent was removed via rotary evaporation. 5,5-dimethyl-3-(p-tolyl)-1,4,2-dioxazole (**2c**) could be obtained as a colorless solid in yields of 4.35 g (22.75 mmol, 63%).

^{1}H NMR (300 MHz, CDCl$_3$): δ [ppm] = 7.74-7.64 (*AA'BB'*, 2H, ArC^{2,6}*H*, b), 7.19 (*AA'BB'*, 2H, ArC^{3,5}*H*, c), 2.41 (*s*, 3H, ArC-C*H$_3$*, d), 1.67 (*s*, 6H, *H$_3$*C-CO$_2$-C*H$_3$*, a).

Synthesis of 3-(4-(bromomethyl)phenyl)-5,5-dimethyl-1,4,2-dioxazole (2d).
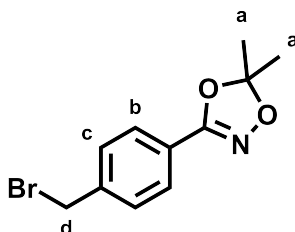
The synthesis of **2d** was carried out in a modified preparation from literature. In a 500 mL three-neck flask, 5.00 g (26.10 mmol, 1.00 eq) 5,5-dimethyl-3-(*p*-tolyl)-1,4,2-dioxazole were dissolved in 250 mL cyclohexane. 8.38 g (47.10 mmol, 1.80 eq) *N*-bromosuccinimide and 0.77 g (4.70 mmol, 0.18 eq) 2,2'-Azobis(2-methylpropionitrile) (AIBN) were added and heated to reflux for 22 h. The solid was filtered. The filtrate was added to a concentrated NaHCO$_3$ solution. The solution was extracted with diethyl ether. The organic layer was dried over Na_2SO_4 and filtered. The solvent was removed via rotary evaporation. 3-(4-(bromomethyl)phenyl)-5,5-dimethyl-1,4,2-dioxazole (**2d**) could be obtained as a yellow liquid in yields of 5.99 g (22.20 mmol, 85%).

^{1}H NMR (300 MHz, CDCl$_3$): δ [ppm] = 7.80-7.75 (*AA'BB'*, 2H, ArC^{2,6}*H*, b), 7.50-7.44 (*AA'BB'*, 2H, ArC^{3,5}*H*, c), 4.52 (*s*, 2H, ArC-C*H$_2$*, d), 1.68 (*s*, 6H, *H$_3$*C-CO$_2$-C*H$_3$*, a).

Synthesis of (4-(5,5-dimethyl-1,4,2-dioxazol-3-yl)benzyl)triphenylphosphonium bromide (2e).
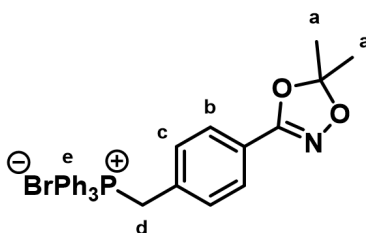
The synthesis of **2e** was carried out in a modified preparation from literature. In a 500 mL three-neck flask, 7.36 g (27.20 mmol, 1.00 eq) 3-(4-(bromomethyl)phenyl)-5,5-dimethyl-1,4,2-dioxazole were dissolved in 200 mL of dry acetone. 7.86 g (30.00 mmol, 1.10 eq) triphenylphosphine were added. The mixture was heated to reflux for 90 minutes. After cooling to rt, the solid was filtered and washed with petroleum ether. The product (4-(5,5-dimethyl-1,4,2-dioxazol-3-yl)benzyl)triphenylphosphonium bromide (**2e**) could be obtained as a colorless solid in yields of 7.93 g (14.89 mmol, 55%).

^{1}H NMR (300 MHz, DMSO-d_6): δ [ppm] = 7.98-7.63 (*m*, 15H, P-(ArC^{2,3,4,5,6}*H*)$_3$, e), 7.61-7.52 (*AA'BB'*, 2H, ArC^{2,6}*H*, b), 7.12 (*AA'BB'*, ArC^{3,5}*H*, c), 5.30 (*d*, J = 16.2 Hz, 2H, ArC-C*H*$_2$, d), 1.61 (*s*, 6H, *H*$_3$C-CO$_2$-C*H*$_3$, a).

Synthesis of 5,5-dimethyl-3-(4-vinylphenyl)-1,4,2-dioxazole (StHAA) (II).
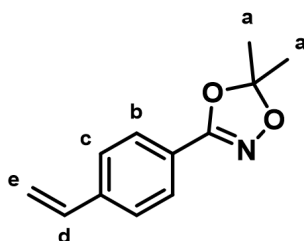
The synthesis of **II** was carried out in a modified preparation from literature.[5] In a 250 mL flask, 4.85 g (9.11 mmol, 1.00 eq) (4-(5,5-dimethyl-1,4,2-dioxazol-3-yl)benzyl)triphenylphosphnium bromide (**2e**) were added to 55 mL (1.52 mol, 164.86 eq) of a 37-41% aqueous formaldehyde solution. 3.03 g (7.58 mmol, 8.32 eq) NaOH were dissolved in 30 mL water. The solution was slowly added to the reaction mixture and stirred at rt overnight. The mixture was extracted with dichloromethane and dried over Na$_2$SO$_4$ and filtered. The solvent was removed via rotary evaporation. The product was purified by column chromatography (SiO$_2$, PE:EA = 99:1). 5,5-dimethyl-3-(4-vinylphenyl)-1,4,2-dioxazole (StHAA) (**II**) could be obtained as colorless solid with yields of 1.33 g (6.51 mmol, 71%).

^{1}H NMR (300 MHz, CDCl$_3$): δ [ppm] = 7.79-7.68 (*AA'BB'*, 2H, ArC^{2,6}*H*, b), 7.50-7.40 (*AA'BB'*, 2H, ArC^{3,5}*H*, c), 6.73 (*dd*, J = 17.6, 10.9 Hz, 1H, ArC-C*H*=CH$_2$, d), 5.83 (*dd*, J = 17.6, 0.8 Hz, 1H, C=C*H*$_2$, e), 5.35 (*dd*, J = 10.9, 0.7 Hz, 1H, C=C*H*$_2$, e), 1.68 (*s*, 6H, *H*$_3$C-CO$_2$-C*H*$_3$, a).

R$_f$ (PE:EA = 99:1) = 0.43.

RAFT copolymerization of MMA and MAHAA (P(MMA-*co*-MAHAA)).
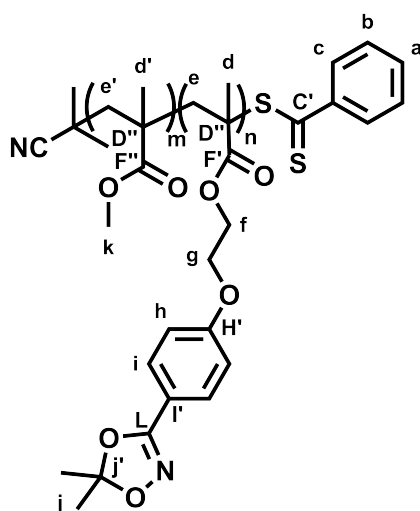
In a 10 mL Schlenk tube 100.00 mg (0.328 mmol, 0.10eq) MAHAA, 295.10 mg (2.948 mmol, 0.90 eq) MMA, 10.49 mg (0.047 mmol, 0.15 eq) 2-Cyano-2-propyl benzodithioate (CPBDT) and 0.78 mg (0.009 mmol, 0.03 eq) AIBN were dissolved in 1.5 mL dioxane. After three freeze pump thaw cycles the mixture was stirred for 24 h at 70 °C. After precipitation in ice cold methanol (45 mL, -20 °C), the product was recovered by centrifugation (4500 RPM, 10 minutes).

^{1}H NMR (300 MHz, CDCl$_3$): δ [ppm] = 7.85 (*m*, ArC^{2,6}*H*, c), 7.70 (*AA'BB'*, ArC^{3,5}*H*, i), 7.50 (*m*, ArC^4*H*, a), 7.34 (*m*, ArC^{3,5}*H*, b), 6.93 (*AA'BB'*, ArC^{2,6}*H*, h), 4.29 (*s*, Ar-O-C*H*$_2$-CH$_2$, f), 4.20 (*s*, Ar-O-C*H*$_2$, g), 3.57 (*s*, O-C*H*$_3$, k), 1.78 (*m*, C-C*H*$_2$, e+e'), 1.65 (*s*, *H*$_3$C-CO$_2$-C*H*$_3$, j), 0.99 (*m*, C-C*H*$_3$, d+d').

^{13}C NMR (75 MHz, CDCl$_3$): δ [ppm] = 178.20 (*C*=O, F'+F"), 177.90 (*C*=O, F'+F"), 177.08 (*C*=O, F'+F"), 160.87 (Ar*C*^{4}, I'), 158.13 (O*C*=N, L), 128.55 25 (Ar*C*^{3,5}, B), 128.43 (Ar*C*^{3,5}, I), 126.79 (Ar*C*^{2,6}, C), 116.56 (Ar*C*-O, H'), 115.30 (H$_3$C-CO$_2$-CH$_3$, J'), 114.76 (Ar*C*^{2,6}, H), 65.47 (Ar-O-*C*H$_2$, G), 63.24 (Ar-O-CH$_2$-*C*H$_2$, F), 54.47 (*C*H$_2$, E+E'), 51.92 (O-*C*H$_3$, K), 44.98 (*C*, D"), 24.93 (H$_3$*C*-CO$_2$-CH$_3$, J), 18.79 (*C*-CH$_3$, (D+D')$_a$), 16.56 (*C*-CH$_3$, (D+D')$_{syn}$).

IR-ATR $\tilde{\nu}$ [cm^{-1}] = 2956 (CH$_3$), 2250 (C≡N), 1732 (C=O), 1452 (C=C), 1255 (C-O-C), 1118 (C-O-C), 906 (C-H$_{Ar}$), 726 (C-H$_{Ar}$).

RAFT copolymerization of HEMA and MAHAA (P(HEMA-*co*-MAHAA)).
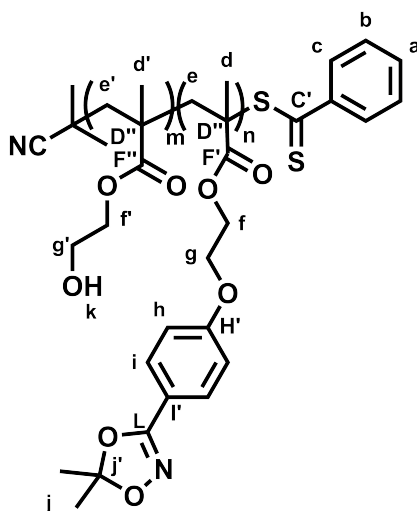
In a 10 mL Schlenk tube 100.00 mg (0.328 mmol, 0.10eq) MAHAA, 383.6 mg (2.948 mmol, 0.90eq) HEMA, 10.70 mg (0.048 mmol, 0.15 eq) CPBDT and 0.40 mg (0.005 mmol, 0.01eq) AIBN were dissolved in 1.5 mL dioxane. After three freeze pump thaw cycles the mixture was stirred for 24 h at 70 °C. After precipitation in ice cold diethylether (45 mL, -20 °C), the product was recovered by centrifugation (4500 RPM, 10 minutes).

^{1}H NMR (300 MHz, DMSO-d_6): δ [ppm] = 7.81 (*m*, ArC^{2,6}*H*, c), 7.66 (*AA'BB'*, ArC^{3,5}*H*, i), 7.64 (*m*, ArC^4*H*, a), 7.47 (*m*, ArC^{3,5}*H*, b), 7.08 (*s*, ArC^{2,6}*H*, h), 4.88-4.73 (*s*, O*H*, k), 4.35-4.15 (*s*, Ar-O-C*H$_2$*-C*H$_2$*, f+g), 4.03-3.77 (*s*, O-C*H$_2$*, f'), 3.66-3.48 (*s*, HO-C*H$_2$*, g'), 2.01 – 1.67 (*m*, C-C*H$_2$*, e+e'), 1.63 (*s*, *H$_3$*C-CO$_2$-C*H$_3$*, j), 0.87 (*m*, C-C*H$_3$*, d+d').

^{13}C NMR (75 MHz, DMSO-d_6): δ [ppm] = 177.40 (*C*=O, F'+F"), 177.15 (*C*=O, F'+F"), 176.38 (*C*=O, F'+F"), 160.72 (O*C*=N, L), 128.78 (Ar*C*^{3,5}, B), 128.09 (Ar*C*^{3,5}, I), 126.27 (Ar*C*^{2,6}, C), 115.07 (H$_3$C-CO$_2$-*C*H$_3$, J'), 66.27 (O-*C*H$_2$-CH$_2$-OH, F'), 65.42 (O-*C*H$_2$-CH$_2$-OH, F+G), 58.60 (O-CH$_2$-*C*H$_2$-OH, G'), 53.39 (*C*H$_2$, E+E'), 44.55 (*C*, D"), 44.12 (*C*, D"), 24.39 (H$_3$*C*-CO$_2$-CH$_3$, J), 18.21 (*C*-CH$_3$, (D+D')$_a$), 16.12 (*C*-CH$_3$, (D+D')$_{syn}$).

RAFT copolymerization of OEGMEMA and MAHAA (P(OEGMEMA-*co*-MAHAA)).

In a 10 mL Schlenk tube 15.00 mg (0.049 mmol, 0.05eq) MAHAA, 280.00 mg (0.933 mmol, 0.95 eq) OEGMEMA, 6.53 mg (0.03 mmol, 0.60 eq) CPBDT and 0.24 mg (0.003 mmol, 0.06 eq) AIBN were dissolved in 1.5 mL dioxane. After three freeze pump thaw cycles the mixture was stirred for 24 h at 70 °C. After precipitation in ice cold diethylether (45 mL, -20 °C), the product was recovered by centrifugation (4500 RPM, 10 minutes).
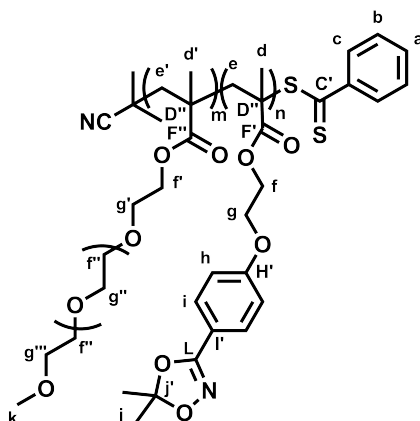
^{1}H NMR (300 MHz, CDCl$_3$): δ [ppm] = 7.83 (*s*, ArC^{2,6}*H*, c), 7.68 (*AA'BB'*, ArC^{3,5}*H*, i), 7.50 (*s*, ArC^4*H*, a), 7.34 (*s*, ArC^{3,5}*H*, b), 6.94 (*AA'BB'*, ArC^{2,6}*H*, h), 4.36-4.17 (*s*, Ar-O-C*H$_2$*-C*H$_2$*, f+g), 4.16-3.97 (*s*, O-C*H$_2$*, f'), 3.69-3.58 (*s*, O-C*H$_2$*-C*H$_2$*-O, g'+f''+g''), 3.57-3.50 (*s*, O-C*H$_2$*, g'''), 3.40-3.34 (*s*, O-C*H$_3$*, k), 2.15-1.71 (*m*, C-C*H$_2$*, e+e'), 1.65 (*s*, *H$_3$*C-CO$_2$-C*H$_3$*, j), 1.13-0.72 (*m*, C-C*H$_3$*, d+d').

^{13}C NMR (75 MHz, CDCl$_3$): δ [ppm] = 177.16 (*C*=O, F'+F''), 176.34 (*C*=O, F'+F''), 174.46 (*C*=O, F'+F''), 128.42 (Ar*C*^{3,5}, I), 114.65 (H$_3$*C*-CO$_2$-CH$_3$, J'), 71.91 (*s*, O-*C*H$_2$, G'''), 70.56 (*s*, O-*C*H$_2$-*C*H$_2$-O, F''+G''), 68.47 (O-*C*H$_2$-*C*H$_2$-O, G'), 63.87 (O-*C*H$_2$, F'), 59.01 (O-*C*H$_3$, K), 54.10 (*C*H$_2$, E+E'), 44.78 (*C*, D''), 24.84 (H$_3$*C*-CO$_2$-CH$_3$, J), 18.31 (C-*C*H$_3$, (D+D')$_a$), 16.33 (C-*C*H$_3$, (D+D')$_{syn}$).

RAFT block copolymerization of MMA and MAHAA (P(MMA)-*b*-P(MAHAA)).
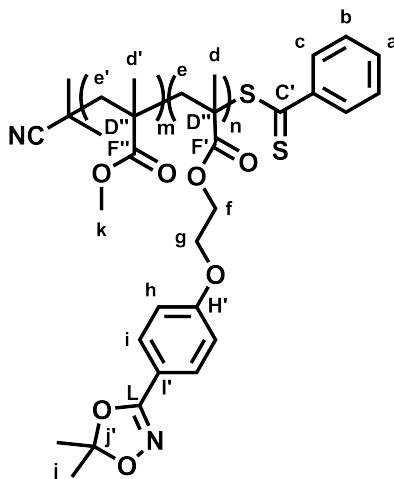
In a 10 mL Schlenk tube, 30.00 mg (0.098+mmol, 14.21 eq) MAHAA, 39.12 mg (0.007 mmol, 1.00 eq) macroCTA (P(MMA)) and 0.1 mg (6.09 · 10^{-4} mmol, 0.09 eq) AIBN were dissolved in 1.5 mL dioxane. After three freeze pump thaw cycles the mixture was stirred for 24 h at 70 °C. After precipitation in ice cold diethylether (45 mL, -20 °C), the product was recovered by centrifugation (4500 RPM, 10 minutes).

^{1}H NMR (400 MHz, CDCl$_3$): δ [ppm] = 7.78 (*s*, ArC^{2,6}*H*, c), 7.68 (*AA'BB'*, ArC^{3,5}*H*, i), 7.39 (*s*, ArC^{3,5}*H*, b), 6.90 (*AA'BB'*, ArC^{2,6}*H*, h), 4.52-3.98 (*m*, Ar-O-C*H$_2$*-C*H$_2$*, f+g), 3.62 (*s*, O-C*H$_3$*, k), 2.17-1.77 (*m*, C-C*H$_2$*, e+e'), 1.66 (*s*, *H$_3$*C-CO$_2$-C*H$_3$*, j), 1.18-0.63 (*m*, C-C*H$_3$*, d+d').

^{13}C NMR (100 MHz, CDCl$_3$): δ [ppm] =178.26 (*C*=O, F'+F"), 177.97 (*C*=O, F'+F"), 158.13 (O*C*=N, L), 128.55 (Ar*C*^{2,6}, C), 116.53 (Ar*C*-O, H'), 115.36 (*H$_3$*C-*C*O$_2$-CH$_3$, J'), 114.75 (Ar*C*^{2,6}, H), 67.24 (Ar-O-*C*H$_2$-*C*H$_2$, G+F), 54.53 (*C*H$_2$, E+E'), 51.98 (O-*C*H$_3$, K), 45.02 (*C*, D"), 44.69 (*C*, D"), 24.96 (H$_3$*C*-CO$_2$-CH$_3$, J), 18.87 (C-*C*H$_3$, (D+D')$_a$), 16.66 (C-*C*H$_3$, (D+D')$_{syn}$).

Deprotection of P(MMA-*co*-MAHAA).
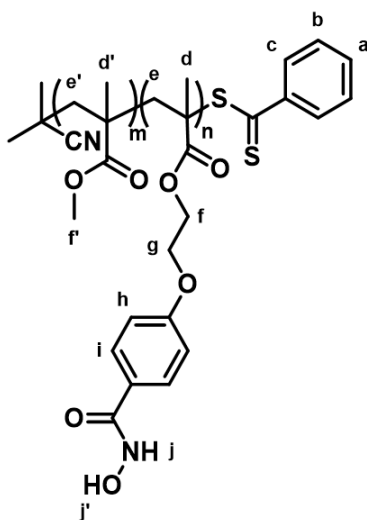
50 mg of the polymer were dissolved in 1.2 mL acetonitrile and 0.2 mL methanol. 8 mg of *DL*-campher sulfonic acid (CSA) were added and the mixture was stirred at rt for 44 h. CSA was removed by dialysis (MWCO: 1000 g mol^{-1}) in 24 h from methanol.

^{1}H NMR (300 MHz, DMSO-*d$_6$*): δ [ppm] = 11.09 (*s*, N*H*, j), 10.07 (*s*, O*H*, j'), 7.85 (*s*, ArC^{2,6}*H*, c), 7.74 (*AA'BB'*, ArC^{3,5}*H*, i), 7.65 (*s*, ArC^4*H*, a), 7.48 (*s*, ArC^{3,5}*H*, b), 6.99 (*AA'BB'*, ArC^{2,6}*H*, h), 4.48-4.11 (*m*, Ar-O-C*H$_2$*-C*H$_2$*, f+g), 3.77-3.35 (*s*, O-C*H$_3$*, k), 2.07-1.55 (*m*, C-C*H$_2$*, e+e'), 1.07 – 0.44 (*m*, C-C*H$_3$*, d+d').

^{13}C NMR (75 MHz, DMSO-*d$_6$*): δ [ppm] = 177.61 (*C*=O, F'+F"), 176.64 (*C*=O, F'+F"), 144.62 (*C*=S, C'), 129.25 (Ar*C*^{3,5}, B), 129.12 (Ar*C*^{3,5}, I), 126.73 (Ar*C*^{2,6}, C), 125.71 (Ar*C*^{4}, I'), 114.56 (Ar*C*^{2,6}, H), 54.09 (*C*H$_2$, E+E'), 52.22 (O-*C*H$_3$, K), 44.34 (*C*, D"), 18.92 (C-*C*H$_3$, (D+D')$_a$), 16.59 (C-*C*H$_3$, (D+D')$_{syn}$).

IR-ATR $\tilde{v}$ [cm^{-1}] = 2997 (O-H, N-H), 2949 (CH$_3$), 1725 (C=O), 1433 (C=C), 1238 (C-O-C), 1149 (C-O-C), 989 (C-H$_{Ar}$), 841 (C-H$_{Ar}$), 750 (C-H$_{Ar}$).

Deprotection of P(HEMA-*co*-MAHAA).
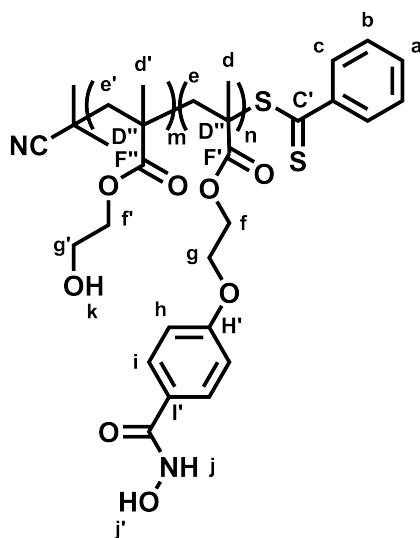
28 mg of the polymer were dissolved in 2 mL methanol and 2 mL of a 0.1 M HCl solution. The mixture was stirred for 24 h. The solution was extracted with 4 mL DCM for three times and the organic layer was dried over Na_2SO_4. The solvent was removed via rotary evaporation.

^{1}H NMR (400 MHz, DMSO-d_6): δ [ppm] = 11.11 (*s*, N*H*, j), 8.93 (*s*, O*H*, j'), 7.82 (*s*, Ar$C^{2,6}H$, c), 7.74 (*AA'BB'*, Ar$C^{3,5}H$, i), 7.64 (*s*, ArC^4H, a), 7.48 (*s*, Ar$C^{3,5}H$, b), 7.01 (*AA'BB'*, Ar$C^{2,6}H$, h), 5.06-4.55 (*s*, O*H*, k), 4.08-3.72 (*s*, O-C*H$_2$*, f'), 3.72-3.48 (*s*, O-C*H$_2$*-C*H$_2$*-O, f+g+g'), 2.12-1.58 (*m*, C-C*H$_2$*, e+e'), 1.09-0.55 (*m*, C-C*H$_3$*, d+d').

^{13}C NMR (100 MHz, DMSO-d_6): δ [ppm] = 177.20 (*C*=O, F'+F''), 176.36 (*C*=O, F'+F''), 131.40, 128.83 (Ar$C^{3,5}$, B), 128.70 (Ar$C^{3,5}$, I), 126.28 (Ar$C^{2,6}$, C), 114.17 (Ar$C^{2,6}$, H), 66.28 (Ar-O-CH_2, G), 61.40 (Ar-O-CH_2-CH_2, F), 58.51 (O-CH_3, K), 53.43 (CH_2, E+E'), 44.55 (*C*, D''), 18.04 (C-CH_3, (D+D')$_a$), 16.12 (C-CH_3, (D+D')$_{syn}$).

Deprotection of P(OEGMEMA-*co*-MAHAA).

28 mg of the polymer were dissolved in 2 mL methanol and 2 mL of a 0.1 M HCl solution. The mixture was stirred for 24 h. The solution was extracted with 4 mL DCM for three times and the organic layer was dried over Na_2SO_4. The solvent was removed via rotary evaporation.

^{1}H NMR (300 MHz, DMSO-d_6): δ [ppm] = 11.07 (*s*, N*H*, j), 8.90 (*s*, O*H*, j'), 7.81 (*s*, Ar$C^{2,6}H$, c), 7.73 (*AA'BB'*, Ar$C^{3,5}$, i), 7.64 (*s*, ArC^4H, a), 7.46 (*s*, Ar$C^{3,5}$, b), 6.96 (*AA'BB'*, Ar$C^{2,6}H$, h), 4.40-4.15 (*m*, O-C*H$_2$*-C*H$_2$*-O, f+g), 4.14-3.81 (*s*, O-C*H$_2$*, f'), 3.70-3.57 (*s*, O-C*H$_2$*-C*H$_2$*, g'), 3.55-3.47 (*s*, O-C*H$_2$*-C*H$_2$*-O, f''+g''), 3.46-3.36 (*s*, O-C*H$_2$*, g'''), 3.29-3.14 (*s*, O-C*H$_3$*, k), 2.07-1.65 (*m*, C-C*H$_2$*, e+e'), 1.62, 1.07-0.51 (*m*, C-C*H$_3$*, d+d').

^{13}C NMR (75 MHz, DMSO-d_6): δ [ppm] = 177.22 (C=O, F'+F"), 176.44 (C=O, F'+F"), 129.05 (Ar$C^{3,5}$, B), 126.65 (Ar$C^{2,6}$, C), 125.63 (ArC^4, I'), 114.49 (Ar$C^{2,6}$, H), 71.77 (O-CH$_2$, G"'), 70.28 (O-CH$_2$-CH$_2$-O, F"+G"), 68.28 (O-CH$_2$-CH$_2$-O, G'), 64.20 (O-CH$_2$, F'), 58.50 (O-CH$_3$, K), 55.38 (CH$_2$, E+E'), 44.54 (C, D"), 18.45 (C-CH$_3$, (D+D')$_a$), 16.64 (C-CH$_3$, (D+D')$_{syn}$).
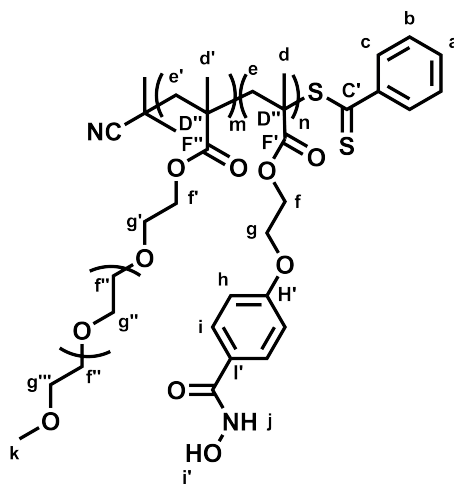
Free radical polymerization of StHAA (II).

120 mg (0.59 mmol, 29.48 eq) StHAA were dissolved in 5 mL anisole. 3.3 mg (0.02 mmol, 1 eq) of AIBN were added. After three freeze pump thaw cycles the mixture was stirred for 22 h at 80 °C and 2 h at 100 °C.

^{1}H NMR (400 MHz, CDCl$_3$): δ [ppm] = 7.46 (Ar$C^{2,6}H$, b), 6.47 (Ar$C^{3,5}H$, c), 1.67 (H$_3$C-CO$_2$-CH$_3$, a), 1.41 (C-CH$_2$-CH, e+d).
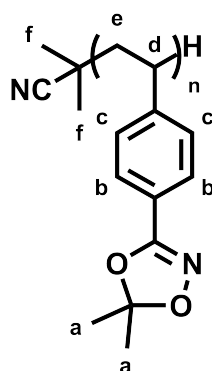
Preparation of the ^{1}H NMR kinetic studies.

In a NMR kinetic tube, MMA, MAHAA, CPBDT and AIBN (47.5:2.5:1:0.1) were dissolved in dioxane-d_8. After three freeze-pump-thaw cycles, the polymerizations were started at 70 °C for 24 h monitored by ^{1}H NMR spectroscopy.

Characterization
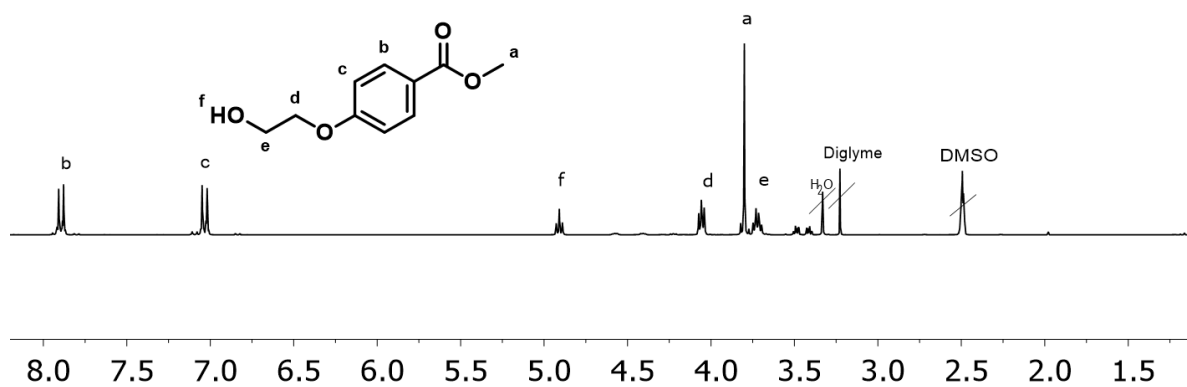
FIGURE S1 ^{1}H NMR spectrum of Methyl 4-(2-hydroxyethoxy)benzoate (**1b**) (300 MHz, DMSO-d_6).
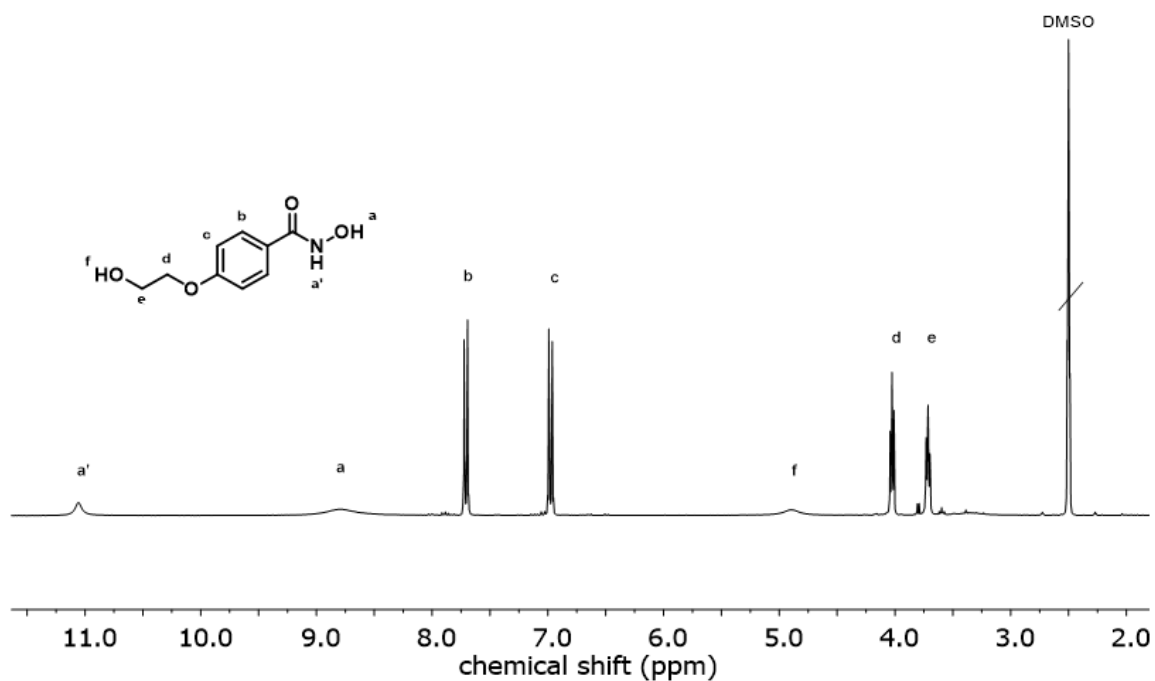
FIGURE S2 ^{1}H NMR spectrum of N-hydroxy-4-(2-hydroxyethoxy)benzamide (**1c**) (300 MHz, DMSO-d_6).
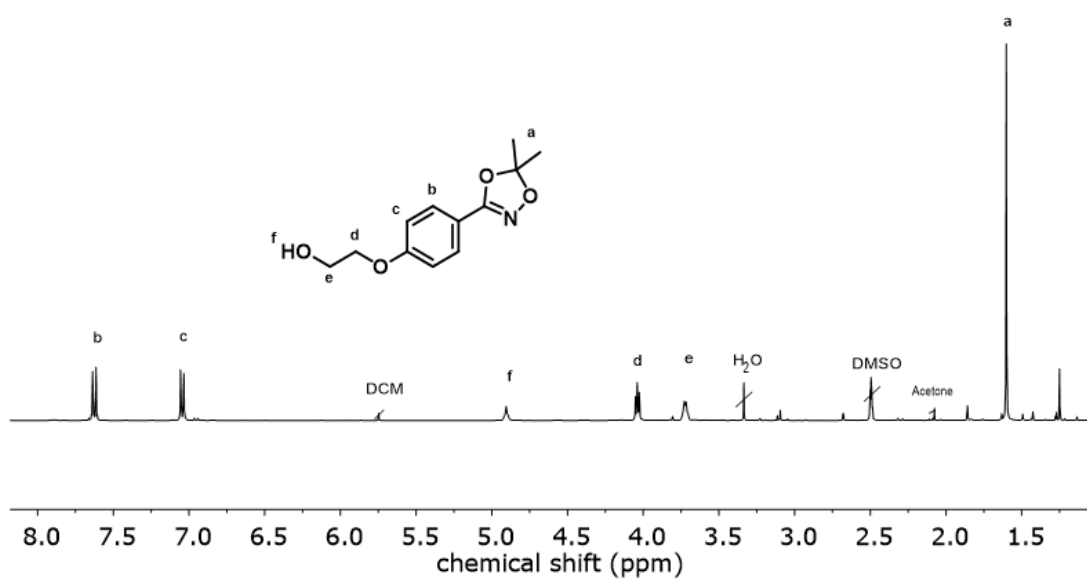
FIGURE S3 ^{1}H NMR spectrum of 2-(4-(5,5-dimethyl-1,4,2-dioxazol-3-yl)phenoxy)ethan-1-ol (**1d**) (300 MHz, DMSO-d_6).
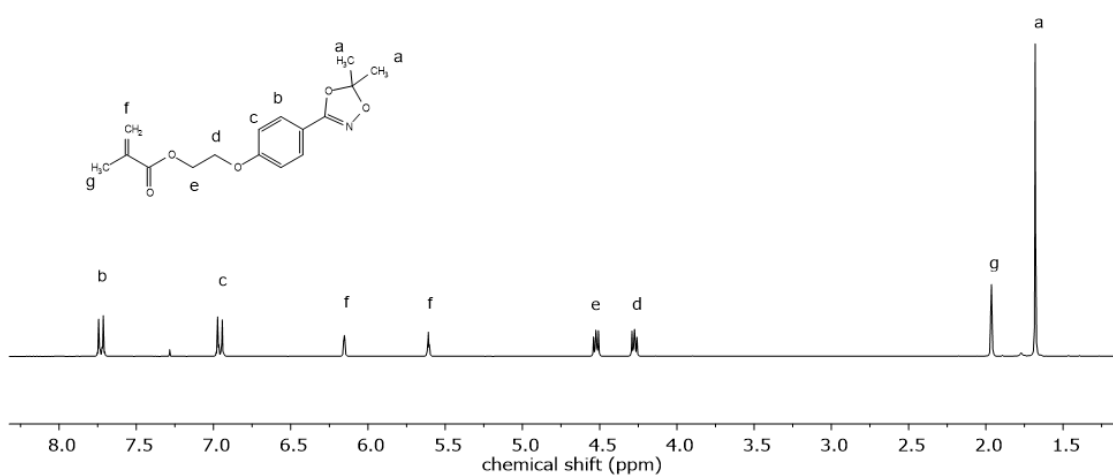
FIGURE S4 ^{1}H NMR spectrum of MAHAA (**I**) (300 MHz, CDCl$_3$).
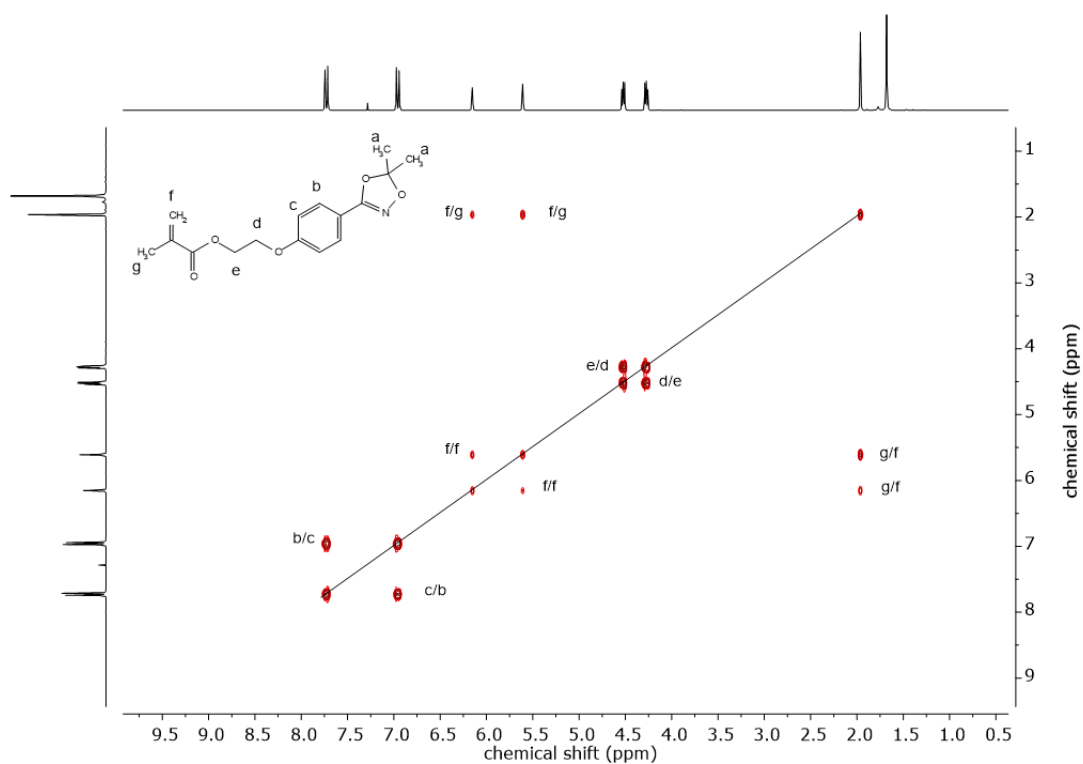
FIGURE S5 ^{1}H-^{1}H COSY NMR spectrum of MAHAA (**I**) (300 MHz, CDCl$_3$).
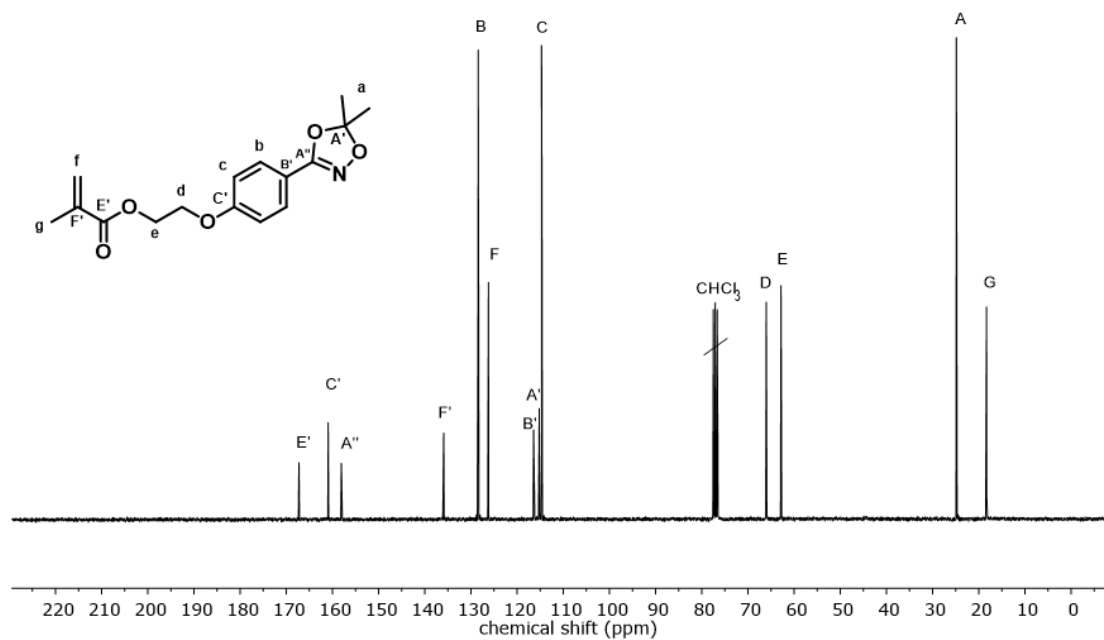
FIGURE S6 ^{13}C NMR spectrum of MAHAA (**I**) (75 MHz, CDCl$_3$).
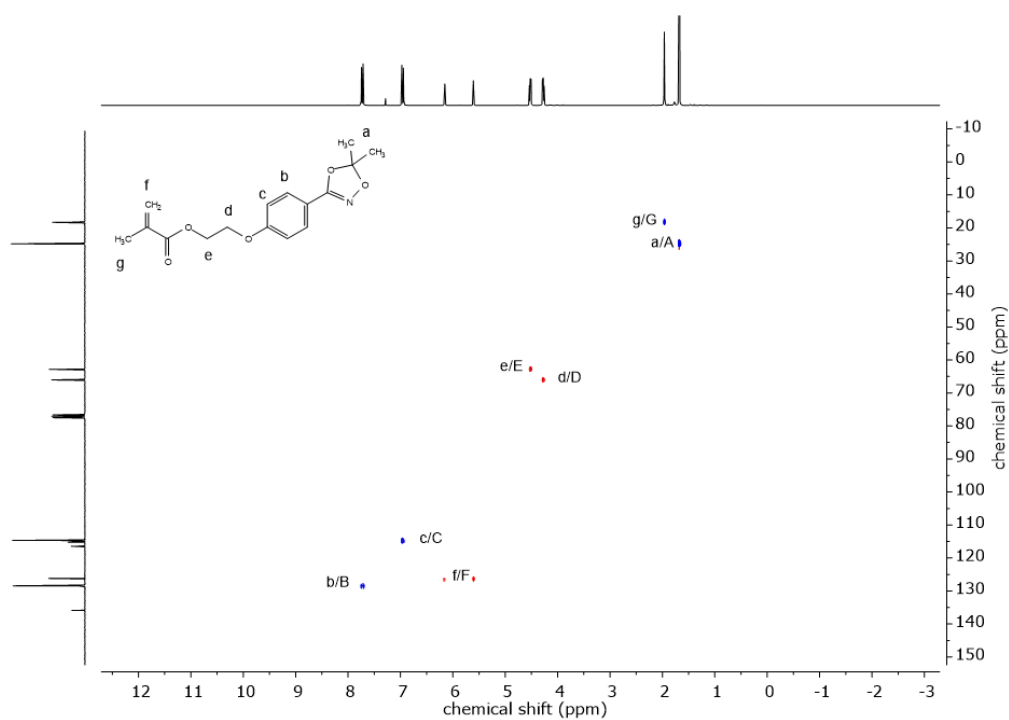
FIGURE S7 ^{1}H-^{13}C NMR HSQC spectrum of MAHAA (**I**) (300 MHz, 75 MHz, CDCl$_3$).
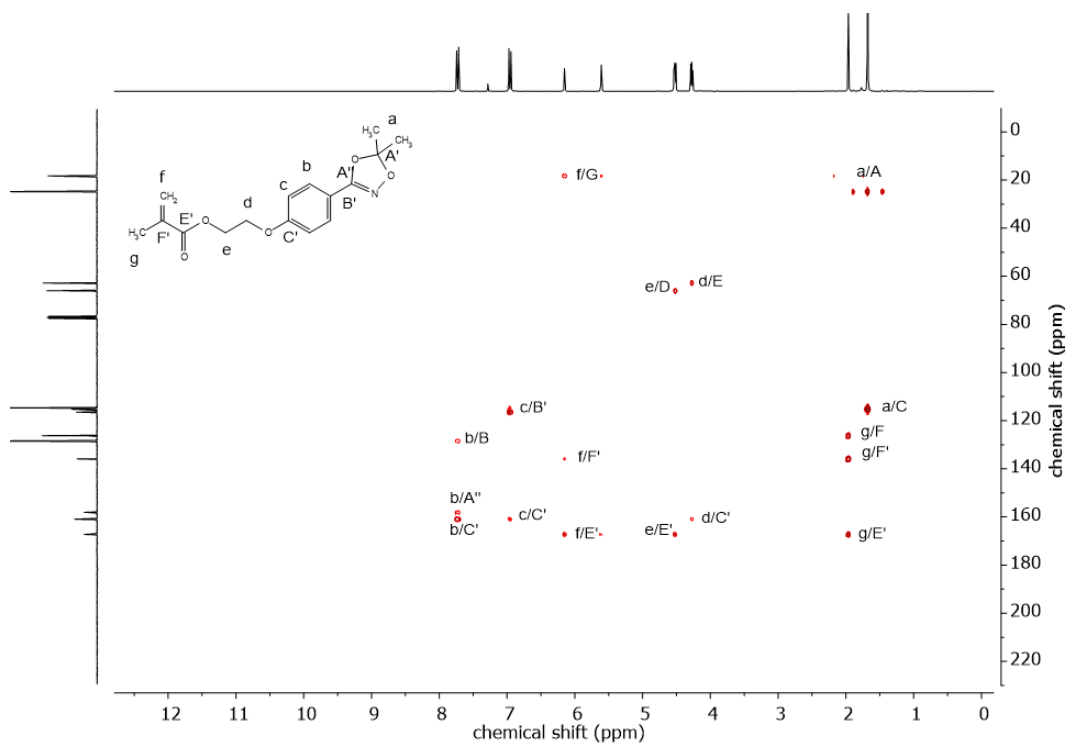
FIGURE S8 ^{1}H-^{13}C NMR HMBC spectrum of MAHAA (**I**) (300 MHz, 75 MHz, CDCl$_3$).
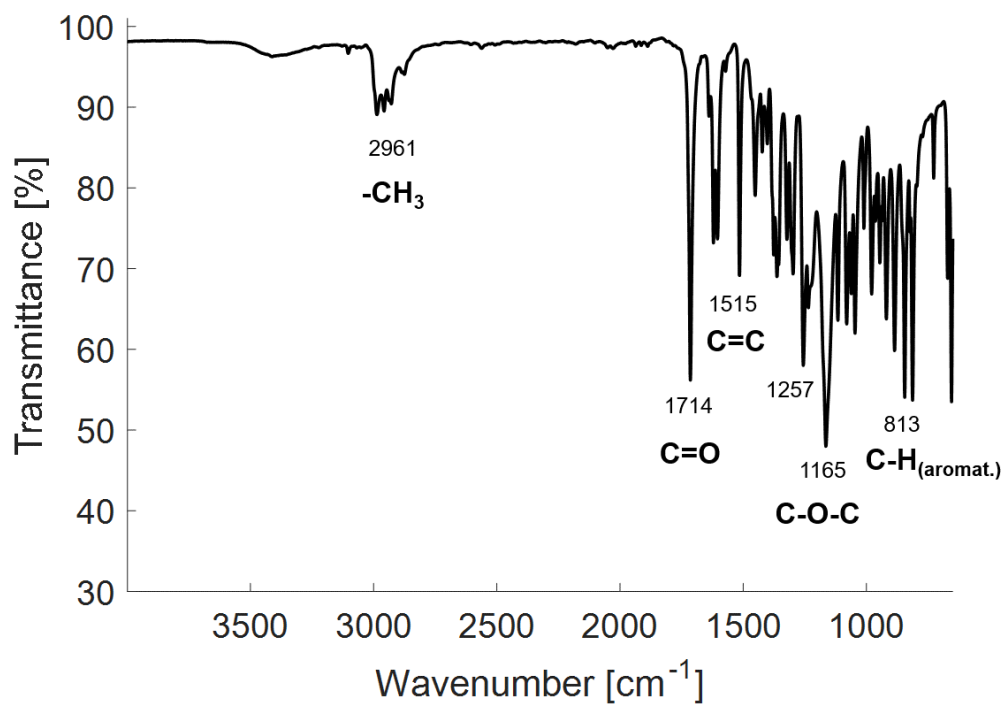
FIGURE S9 FT-ATR-IR spectrum of MAHAA (**II**).
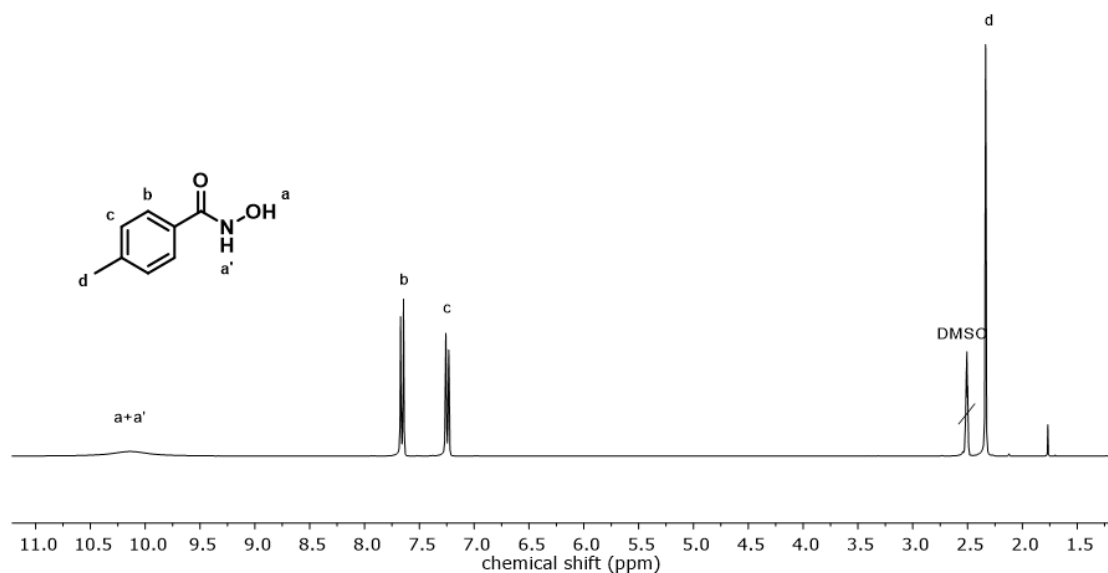
FIGURE S10 ^{1}H NMR spectrum of *N*-hydroxy-4-methylbenzamide (**2b**) (300 MHz, DMSO-d_6).
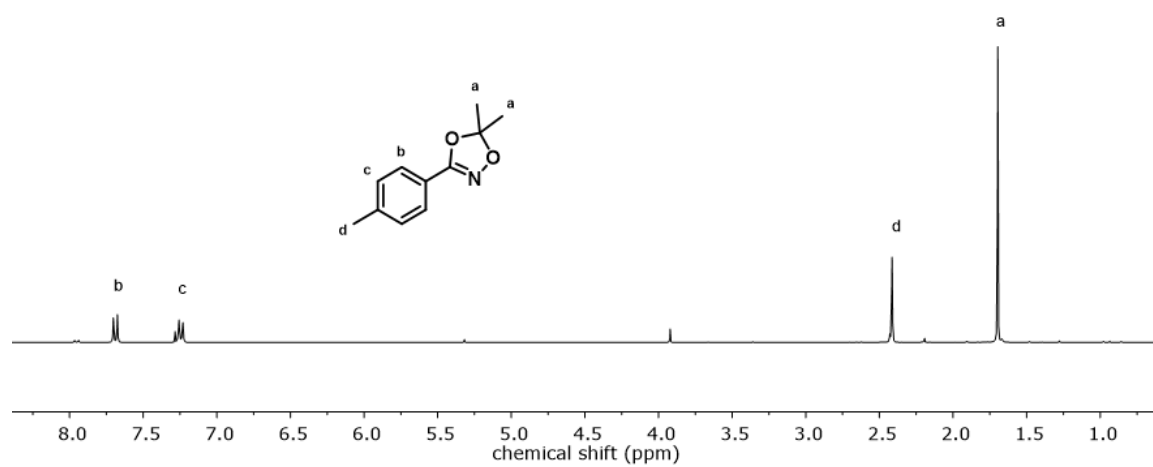
FIGURE S11 ^{1}H NMR spectrum of 5,5-dimethyl-3-(*p*-tolyl)-1,4,2-dioxazole (**2c**) (300 MHz, CDCl$_3$).
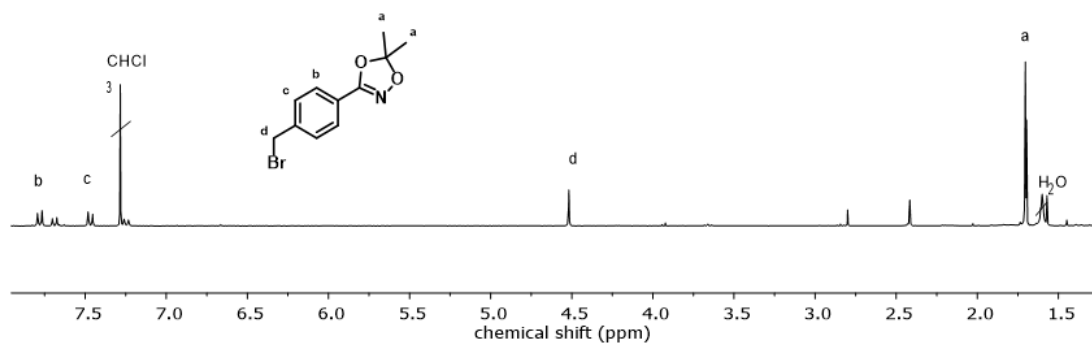
FIGURE S12 ^{1}H NMR spectrum of 3-(4-(bromomethyl)phenyl)-5,5-dimethyl-1,4,2-dioxazole (**2d**) (300 MHz, CDCl$_3$).
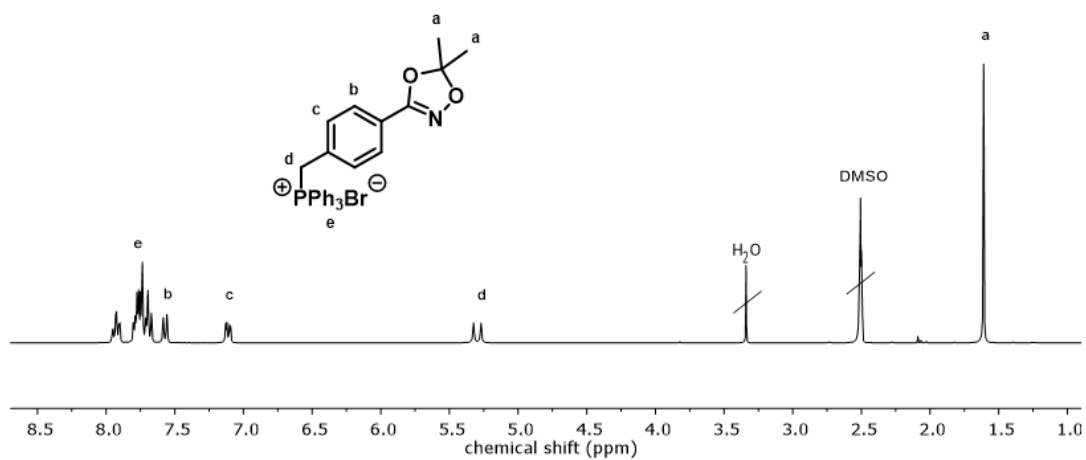
FIGURE S13 ^{1}H NMR spectrum of (4-(5,5-dimethyl-1,4,2-dioxazol-3-yl)benzyl)triphenylphosphonium bromide (**2e**) (300 MHz, DMSO-d_6).
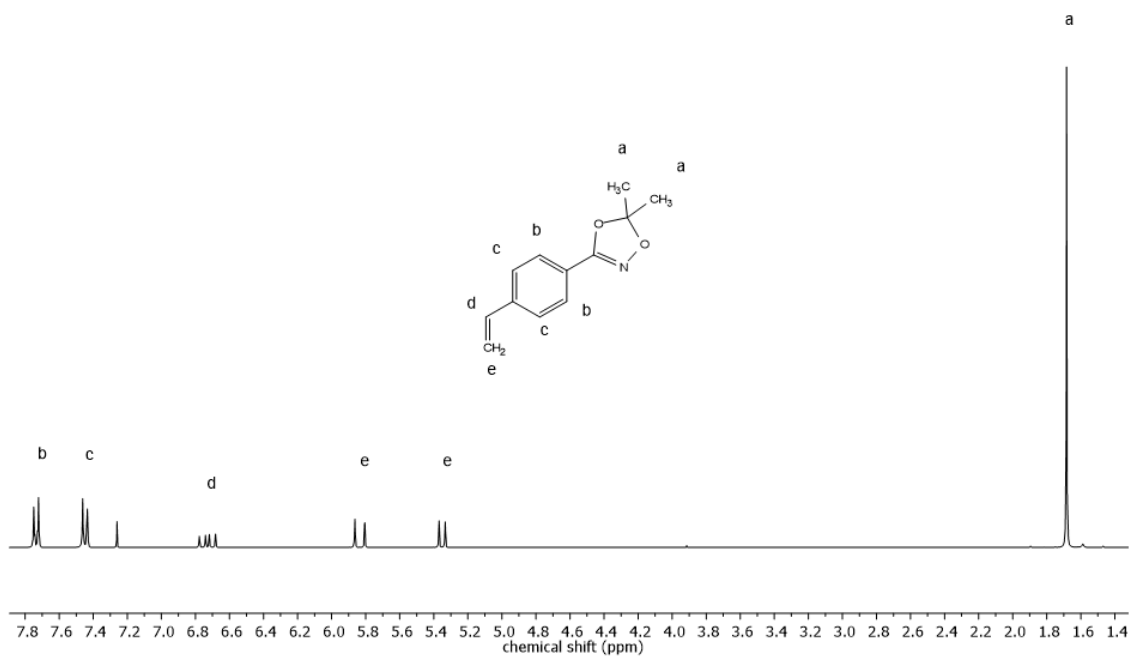
FIGURE S14 ^{1}H NMR spectrum of StHAA (**II**) (300 MHz, CDCl$_3$).
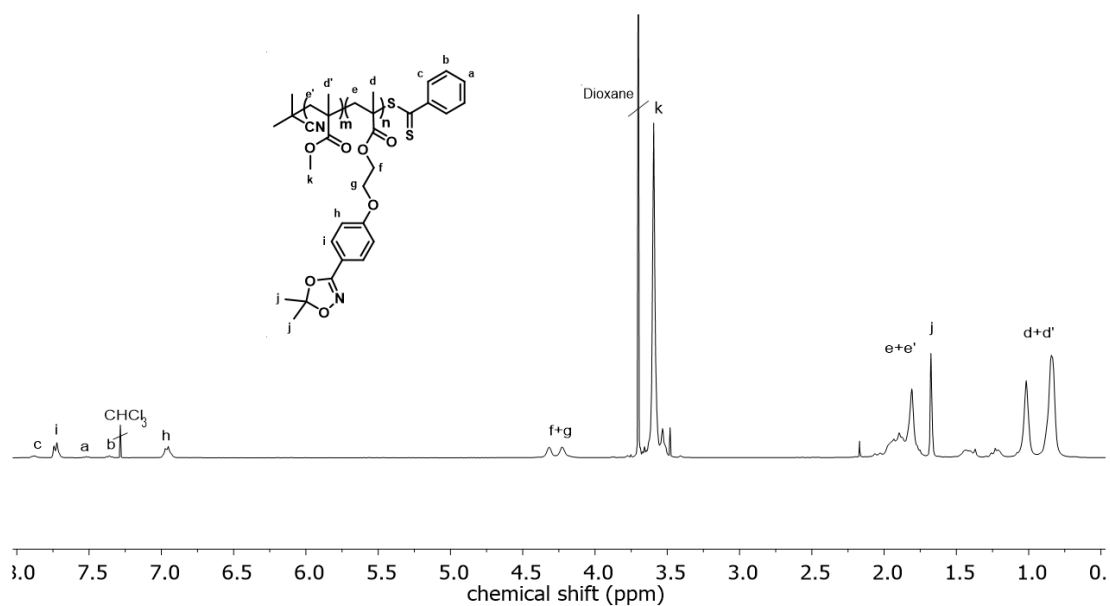
FIGURE S15 ^{1}H NMR spectrum of P(MMA-*co*-MAHAA) (400 MHz, CDCl$_3$).
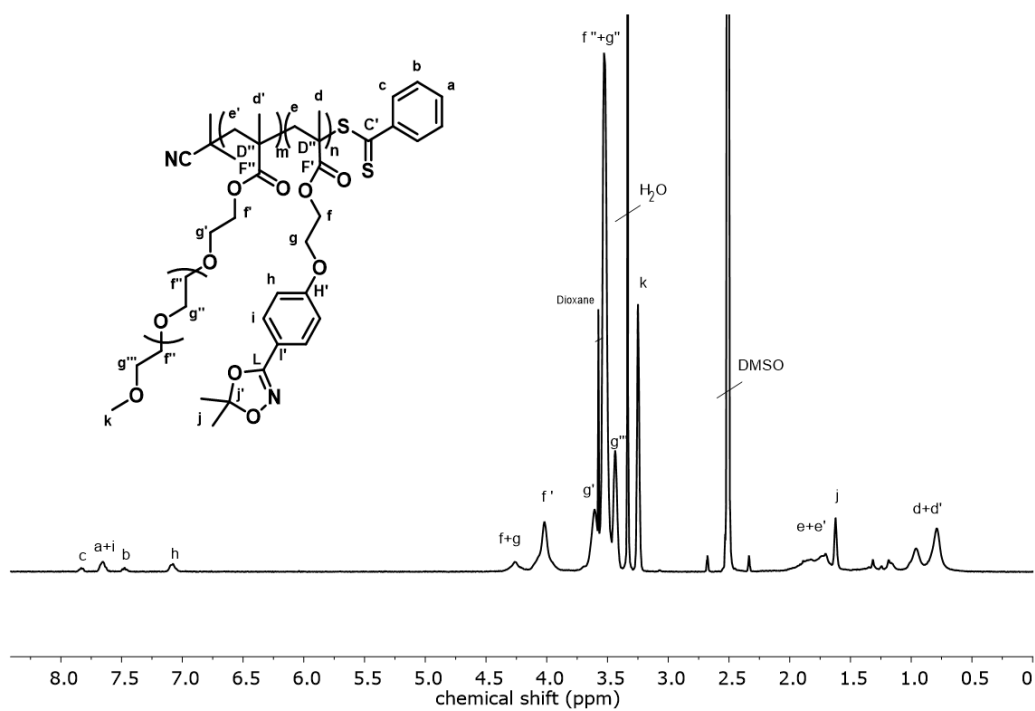
FIGURE S16 ^{1}H NMR spectrum of P(OEGMEMA-*co*-MAHAA) (400 MHz, DMSO-d_6).
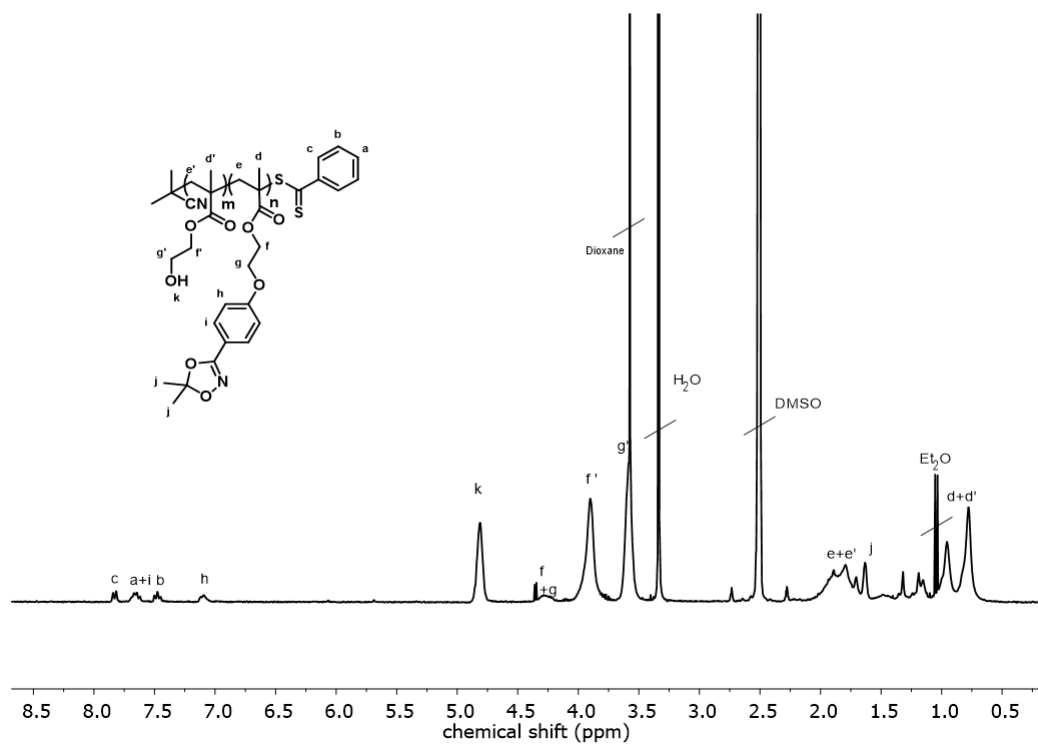
FIGURE S17 ^{1}H NMR spectrum of P(HEMA-*co*-MAHAA) (300 MHz, DMSO-d_6).
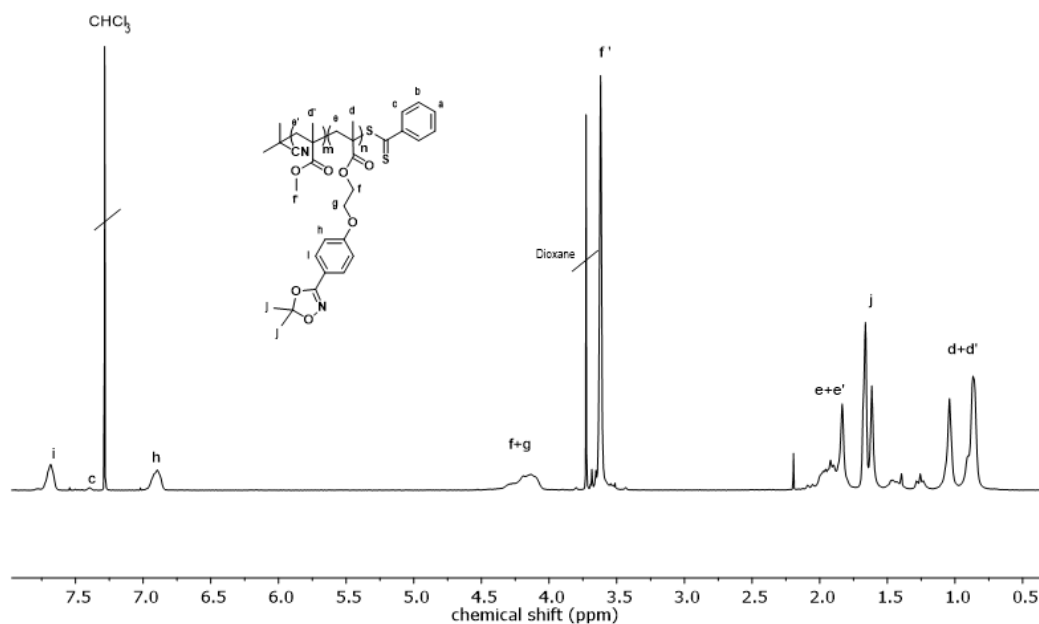
FIGURE S18 ^{1}H NMR spectrum of P(MMA)-*b*-P(MAHAA) (400 MHz, CDCl$_3$).
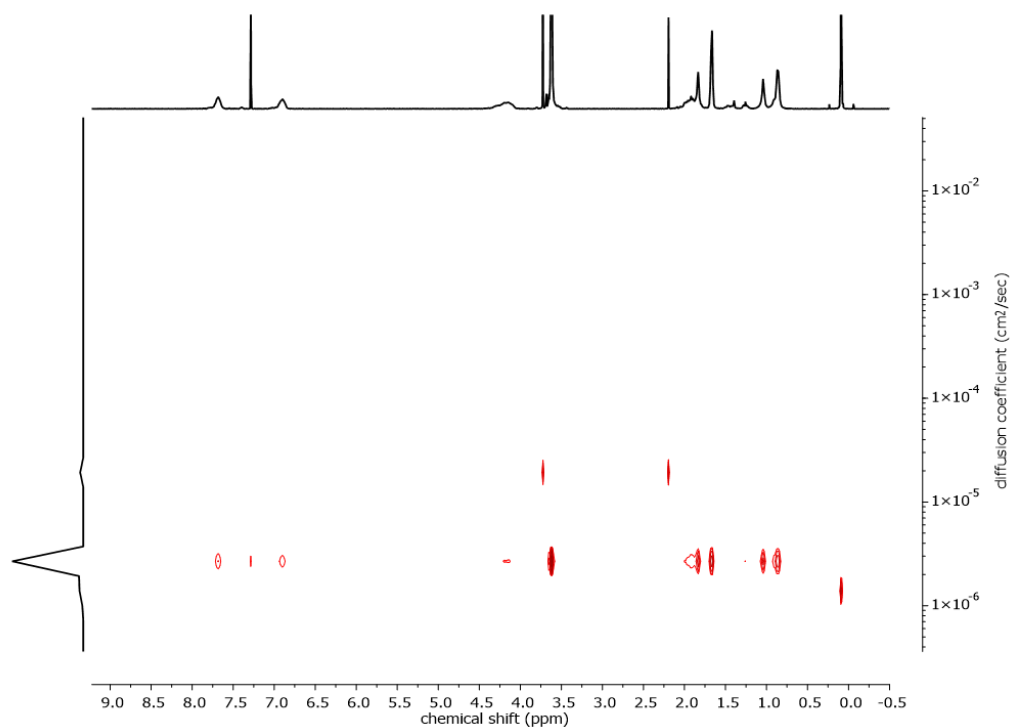
FIGURE S19 ^{1}H DOSY NMR spectrum of P(MMA)-*b*-P(MAHAA) (400 MHz, CDCl$_3$).
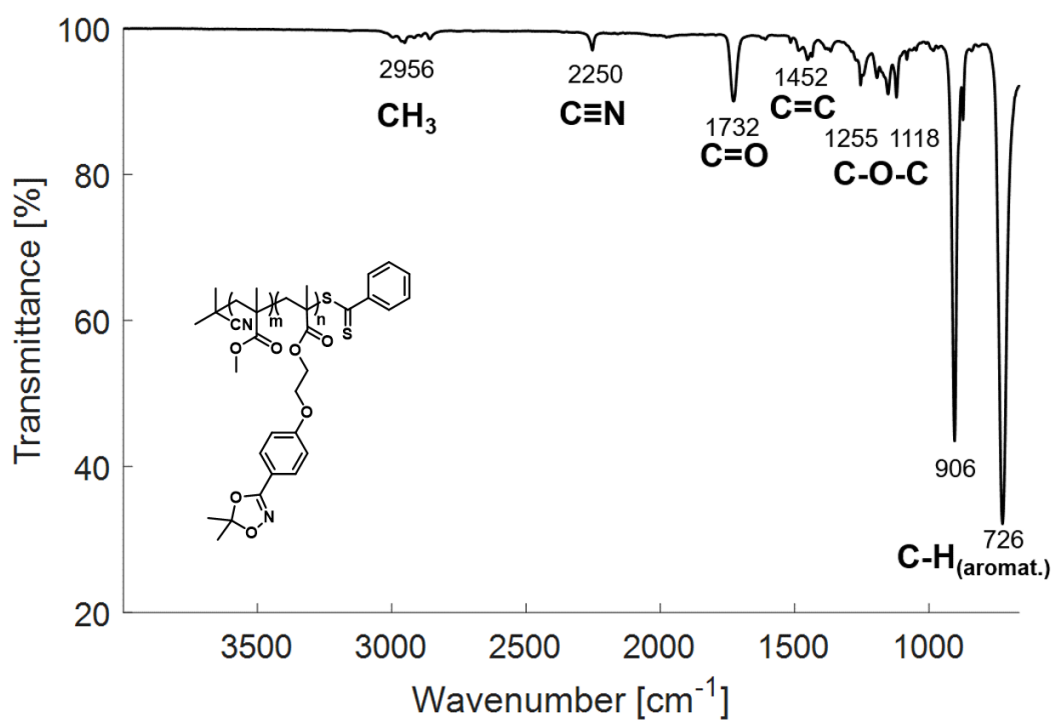
FIGURE S20 FT-ATR-IR spectrum of P(MMA-co-MAHAA).
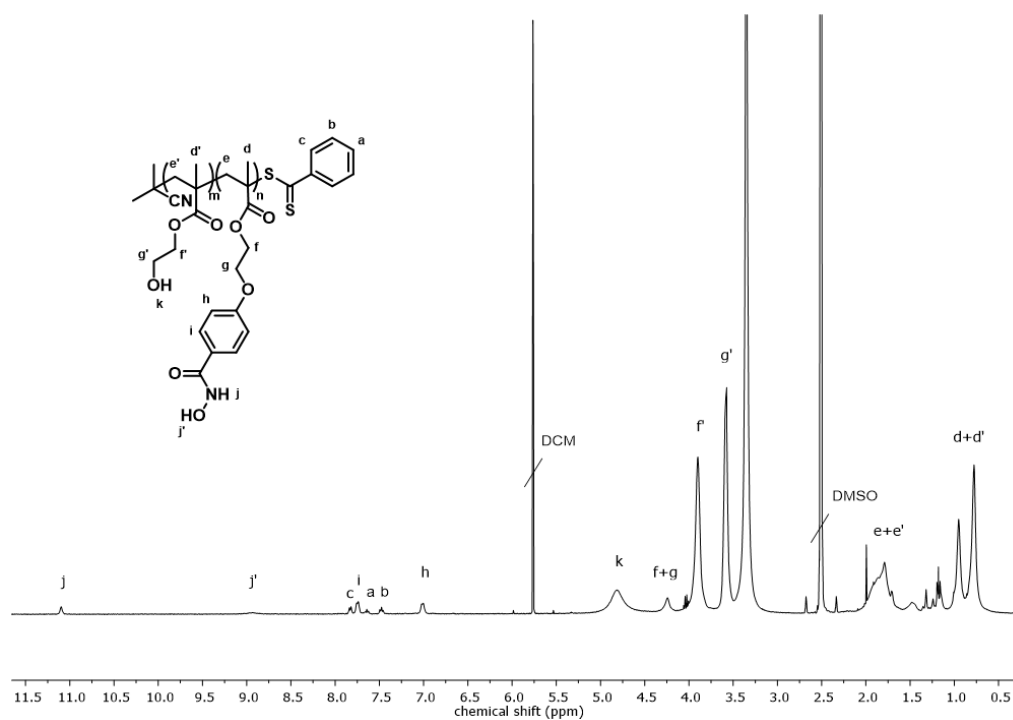
FIGURE S21 ^{1}H NMR spectrum of P(HEMA-*co*-MAHA) (300 MHz, DMSO-d_6).
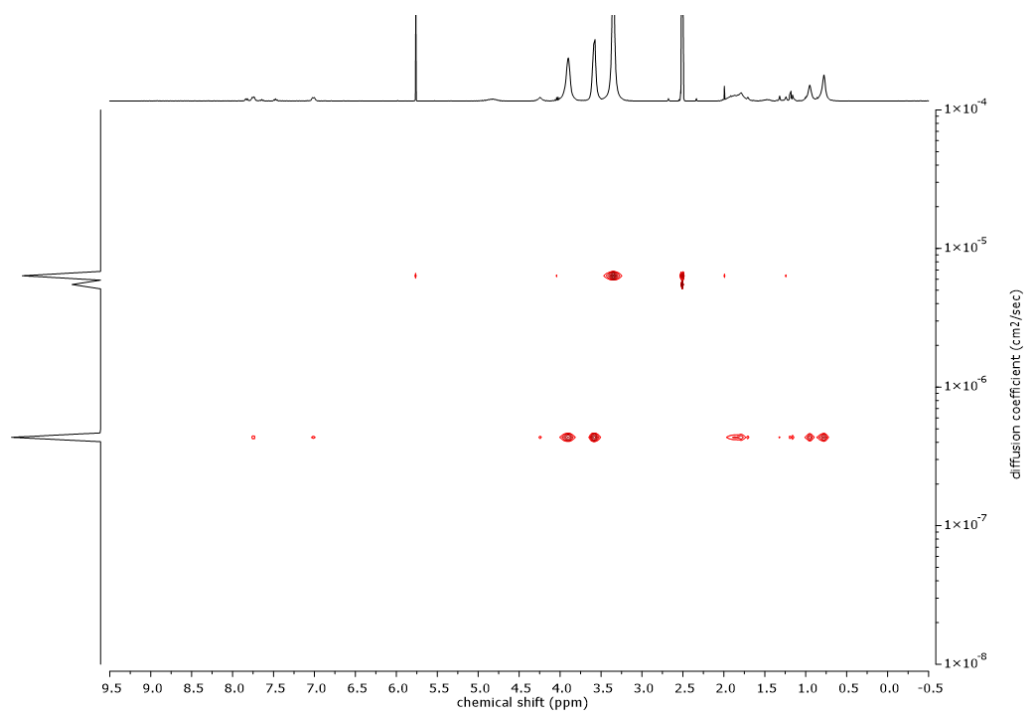
FIGURE S22 ^{1}H DOSY NMR spectrum of P(HEMA-*co*-MAHA) (400 MHz, DMSO-d_6).
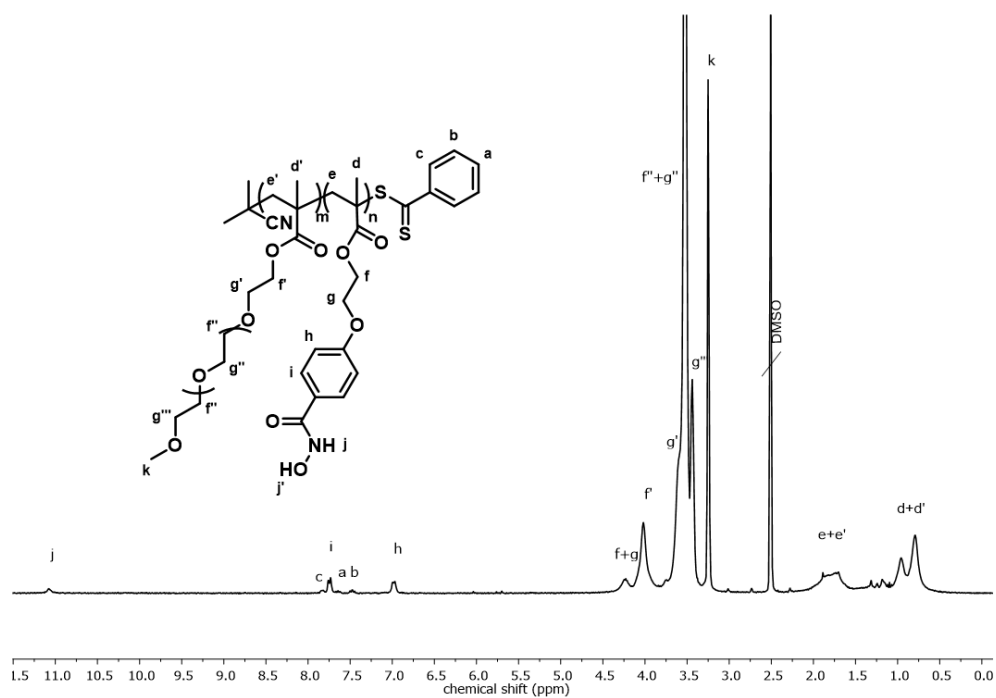
FIGURE S23 ^{1}H NMR spectrum of P(OEGMEMA-*co*-MAHA) (300 MHz, DMSO-d_6).
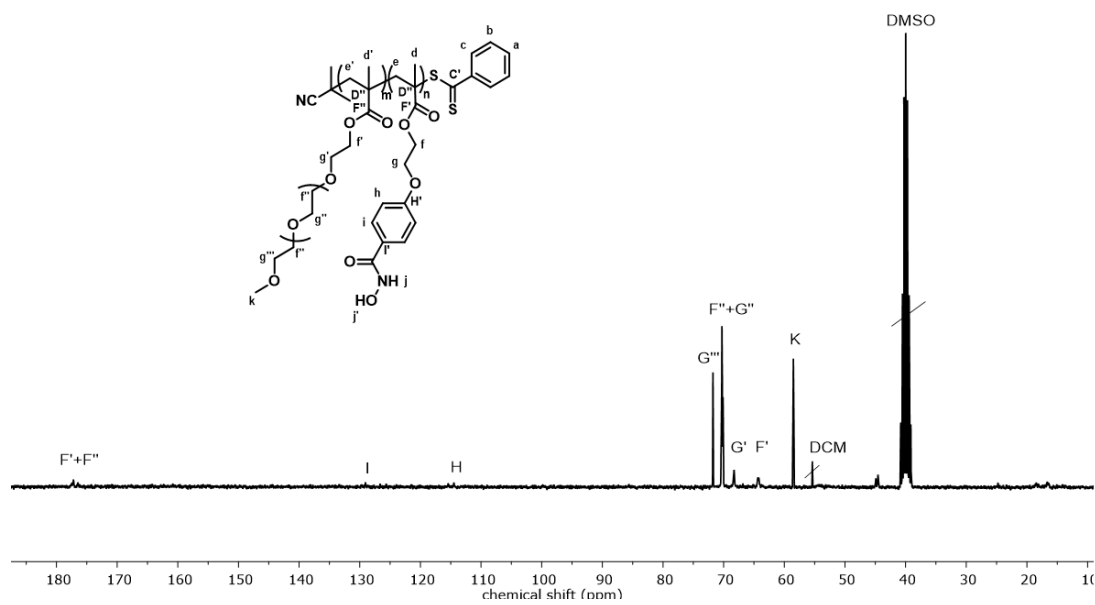
FIGURE S24 ^{13}C NMR spectrum of P(OEGMEMA-*co*-MAHA) (75 MHz, DMSO-d_6).
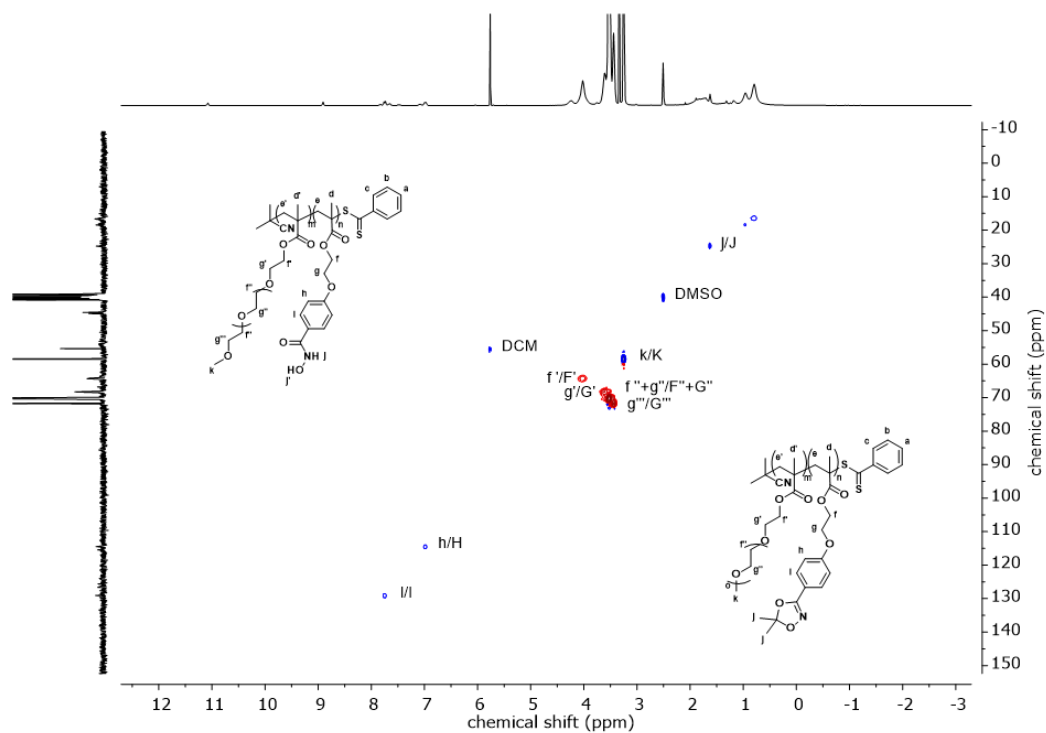
FIGURE S25 ^{1}H-^{13}C NMR HSQC spectrum of P(OEGMEMA-*co*-MAHA) (300 MHz, 75 MHz, DMSO-d_6).
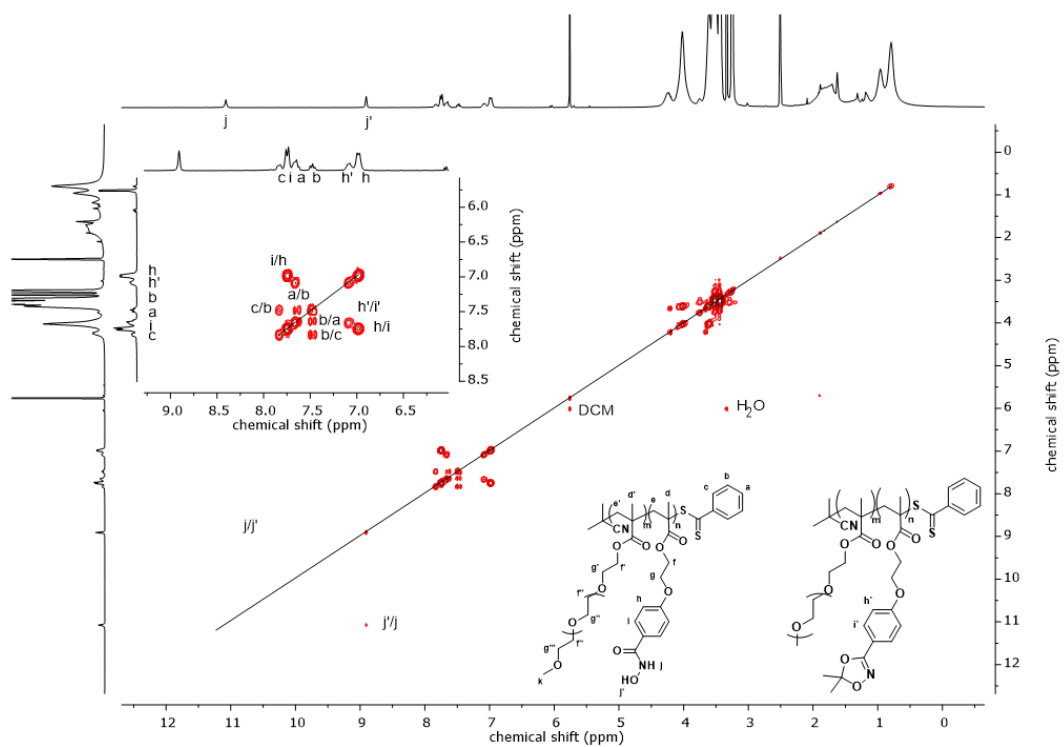
FIGURE S26 ^{1}H-^{1}H COSY NMR spectrum of P(OEGMEMA-*co*-MAHA) (300 MHz, DMSO-d_6).
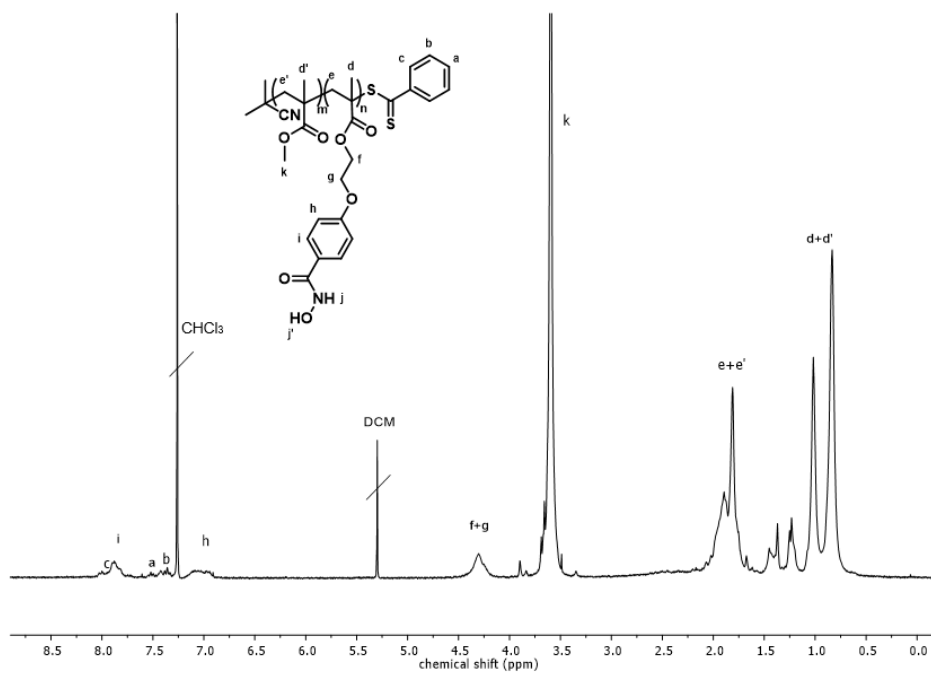
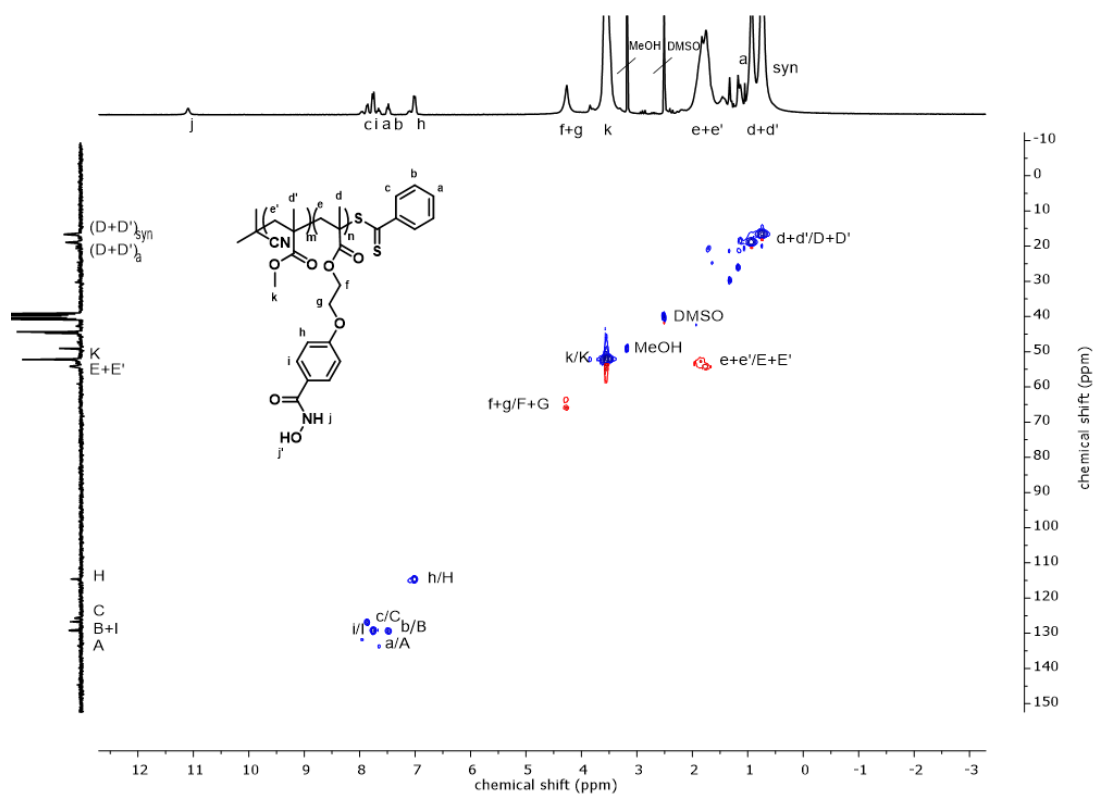**FIGURE S27** ^{1}H NMR spectrum of P(MMA-*co*-MAHA) (300 MHz, CDCl$_3$).

FIGURE S28 ^{1}H-^{13}C NMR HSQC spectrum of P(MMA-*co*-MAHA) (300 MHz, 75 MHz, DMSO-d_6).
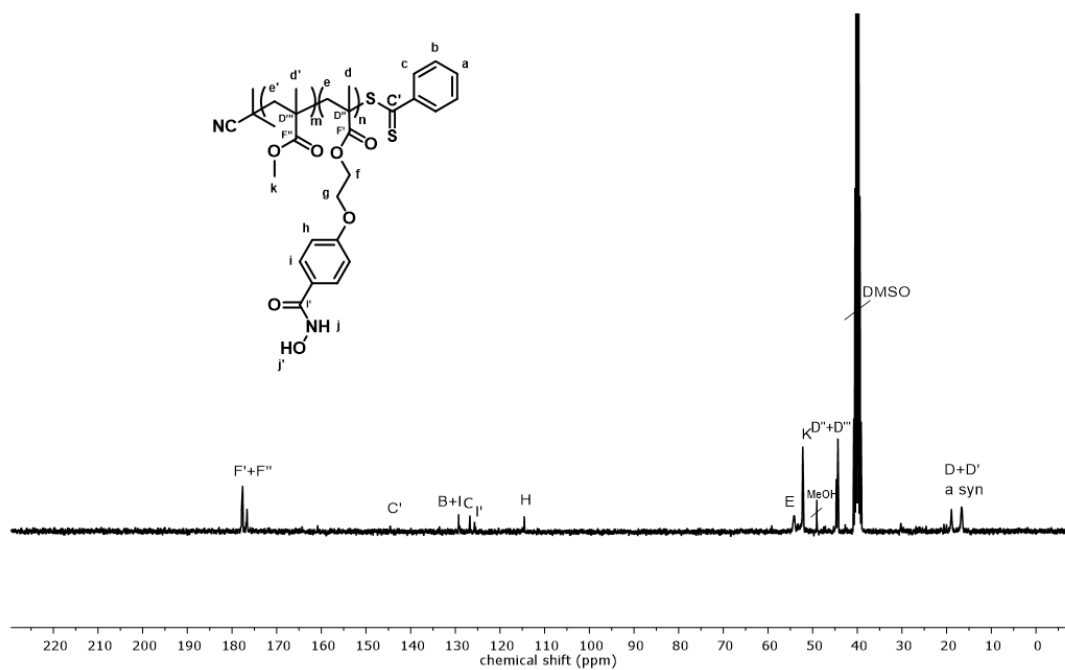
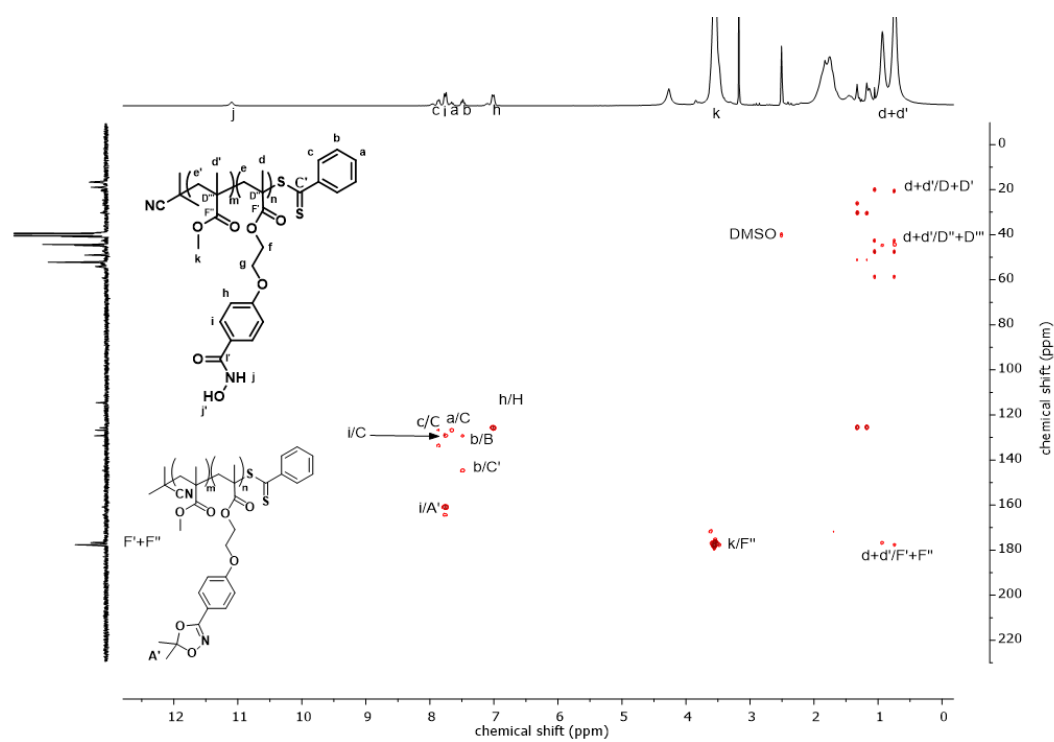**FIGURE S29** ^{13}C NMR spectrum of P(MMA-*co*-MAHA) (75 MHz, DMSO-d_6).

FIGURE S30 ^{1}H-^{13}C NMR HMBC spectrum of P(MMA-*co*-MAHA) (300 MHz, 75 MHz, DMSO-d_6).
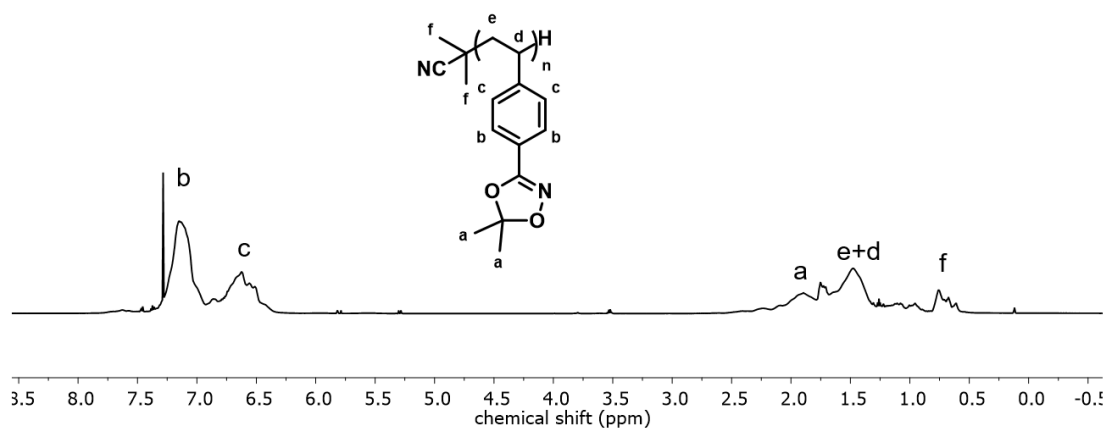
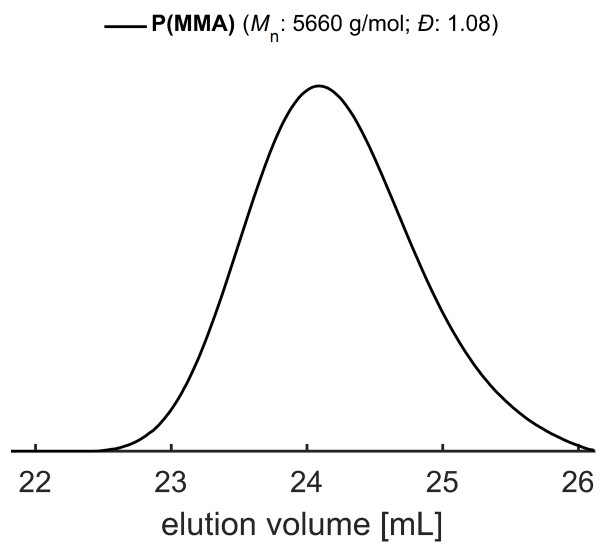**FIGURE S31** ^{1}H NMR spectrum of P(StHAA) (400 MHz, CDCl$_3$).

FIGURE S32 SEC curve of the macroCTA P(MMA), (THF, P(MMA) calibration, RI detector).
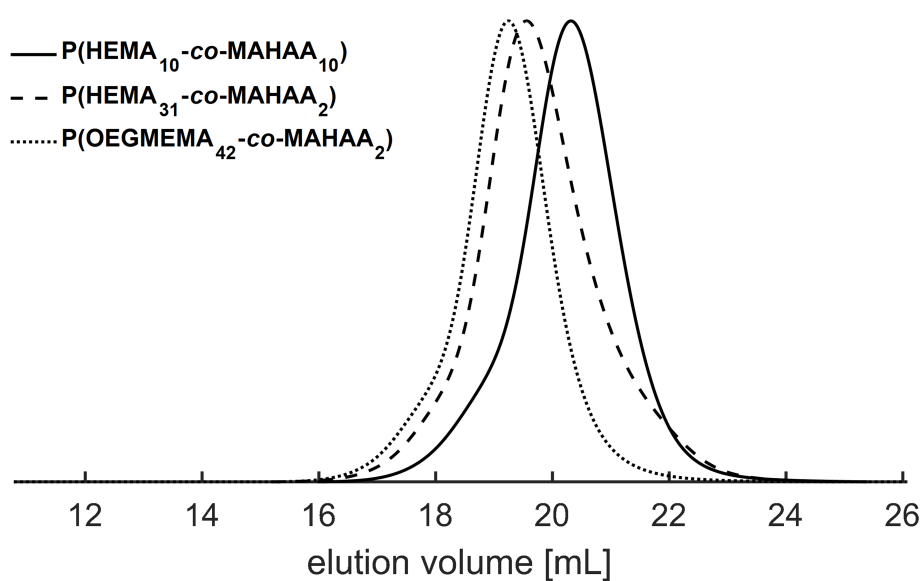
FIGURE S33 SEC traces of P(HEMA$_{10}$-*co*-MAHAA$_{10}$), P(HEMA$_{31}$-*co*-MAHAA$_2$) and P(OEGMEMA$_{42}$-*co*-MAHAA$_2$) (DMF, P(MMA) calibration, UV detector).
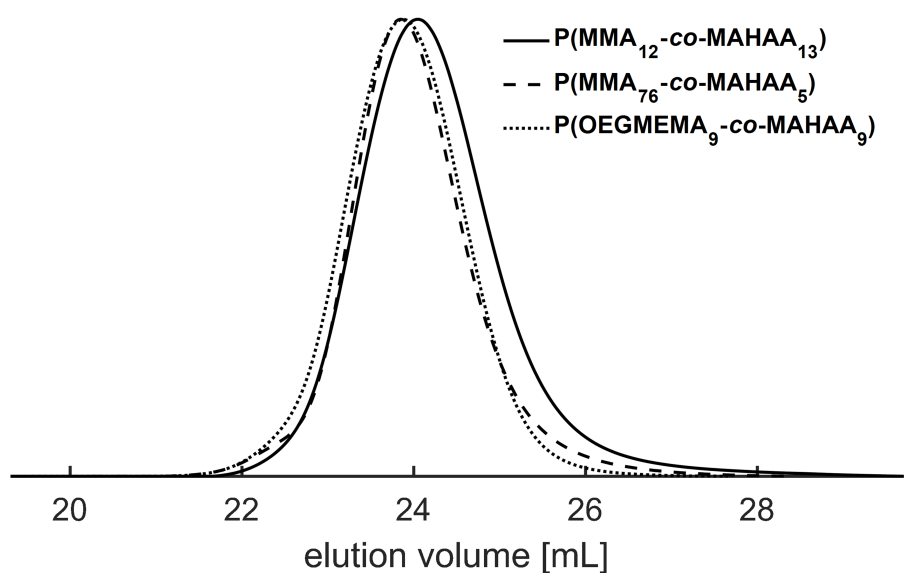
FIGURE S34 SEC traces of P(MMA$_{12}$-*co*-MAHAA$_{13}$), P(MMA$_{76}$-*co*-MAHAA$_5$) and P(OEGMEMA$_9$-*co*-MAHAA$_9$) (THF, P(MMA) calibration, UV detector).
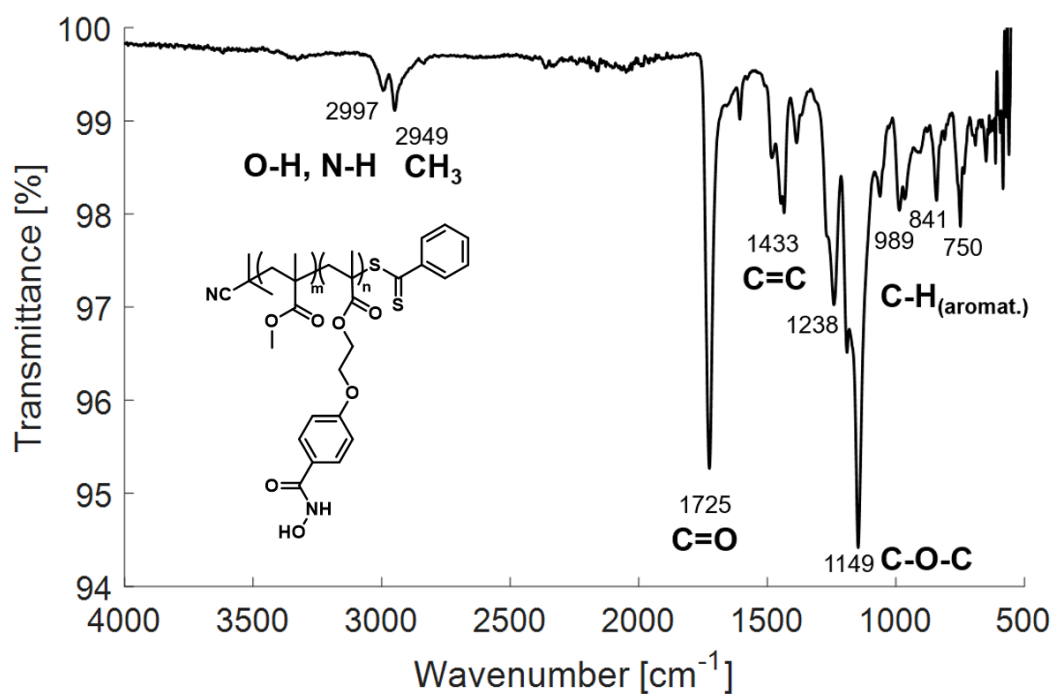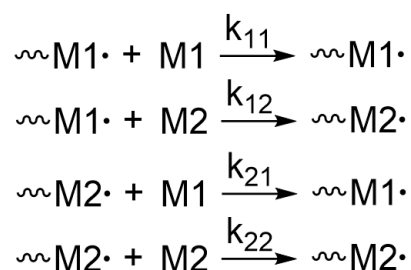
FIGURE S35   FT-ATR-IR spectrum of P(MMA-co-MAHA).

^{1}H NMR kinetic studies

The polymerization was followed online by ^{1}H NMR spectroscopy to study the incorporation behavior of the two different monomers. We can investigate copolymerization behavior by determining the reactivity ratios r_1 and r_2 that are defined as ratios between the homopropagation (k_{11} and k_{22}) and the corresponding crossover propagation (k_{12} and k_{21}) (**Eq. 1.1 and 1.2**). In other words, r_1 and r_2 describe the reactivity of the radicals at the polymer chain end towards monomer 1 or 2, respectively. If $r_1 > 1$, there is a higher probability of the radical M1· to attack monomer M1 instead of M2. Consequently, these ratios can be seen as an expression of how likely a monomer will react with itself or the other monomer. The fundamental propagation possibilities of the radical at the polymer chain end can be seen in **Scheme S3**.

$$\sim\!M1\cdot \; + \; M1 \xrightarrow{\;k_{11}\;} \sim\!M1\cdot$$

$$\sim\!M1\cdot \; + \; M2 \xrightarrow{\;k_{12}\;} \sim\!M2\cdot$$

$$\sim\!M2\cdot \; + \; M1 \xrightarrow{\;k_{21}\;} \sim\!M1\cdot$$

$$\sim\!M2\cdot \; + \; M2 \xrightarrow{\;k_{22}\;} \sim\!M2\cdot$$

SCHEME S3   Fundamental reaction scheme of the formation of copolymers constiting of monomer M1 and monomer M2.

$$r_1 = \frac{k_{11}}{k_{12}} \tag{1.1}$$

$$r_2 = \frac{k_{22}}{k_{21}} \tag{1.2}$$

In this studies, the reactivity ratios r_1 and r_2 were determined with the method established by Jaacks in the early 1970s.[6] The fundamental equation takes the initial monomer concentration $[MX]_0$ and the concentration of unreacted monomer after the polymerization $[MX]_t$ into account (**Eq. (1.3)**).

$$\log\left(\frac{[M1]_t}{[M1]_0}\right) = r_1 \cdot \log\left(\frac{[M2]_t}{[M2]_0}\right) \tag{1.3}$$

The reactivity ratio r_2 was determined under the condition $r_1 \cdot r_2 = 1$. The determination of the reactivity ratios was performed by integration of the particular monomer signals. In the case of the copolymers containing MMA and MAHAA, the protons of the double bonds appeared separated in the ^{1}H NMR spectra (**Figures S35** and **S36**). On the other hand, the protons of the double bond for HEMA and MAHAA, respectively OEGMEMA and MAHAA overlaid in the spectra. Therefore, the signal of the protons of the methylene group of MAHAA (blue in **Figures S37-S40**) were subtracted from the overlaid signals highlighted in (red in **Figures S37-S40**) to determine the reactivity ratios.

TABLE S1 Reactivity ratios determined by *in situ* ^{1}H NMR kinetic measurements. The values were calculated by the Jaacks method.[6] M1 = MMA, HEMA or OEGMEMA, respectively. The polymerizations were performed at 70 °C in dioxane-d_8 for 24 h.

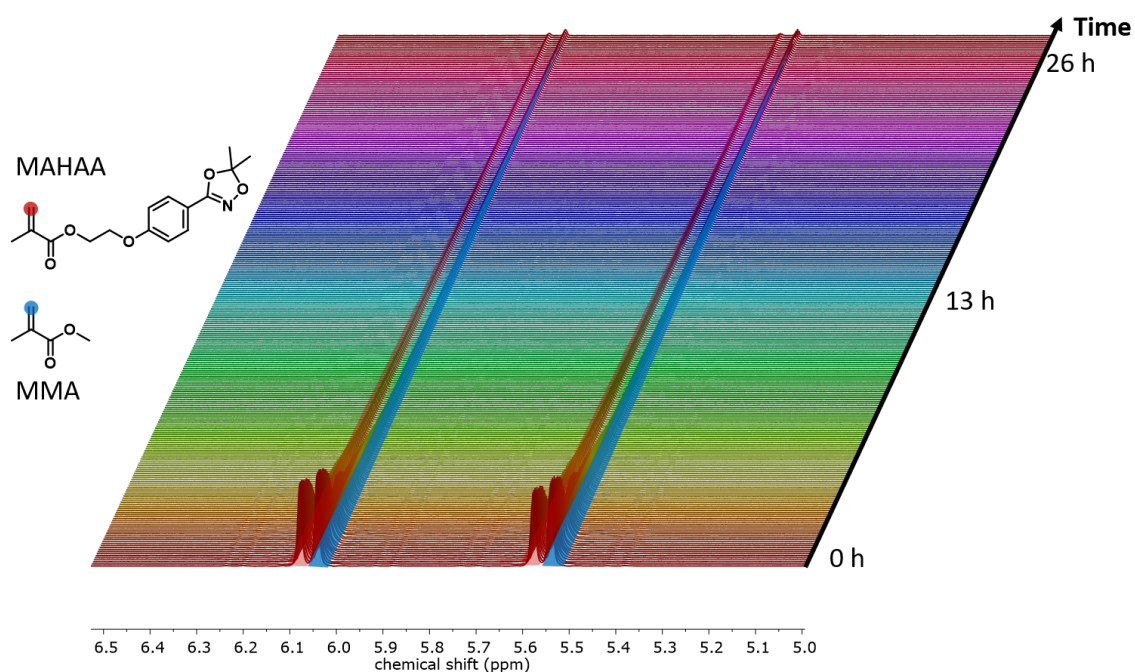| Polymer	[M1:MAHAA]	r_{M1}	r_{MAHAA}
P(MMA$_{76}$-*co*-MAHAA$_5$)	95:5	$0.90 \pm 2.3 \cdot 10^{-3}$	$1.11 \pm 2.9 \cdot 10^{-3}$
P(OEGMEMA$_{42}$-*co*-MAHAA$_2$)	95:5	$0.86 \pm 3.8 \cdot 10^{-3}$	$1.16 \pm 5.1 \cdot 10^{-3}$
P(HEMA$_{31}$-*co*-MAHAA$_2$)	95:5	$1.25 \pm 2.6 \cdot 10^{-2}$	$0.80 \pm 1.4 \cdot 10^{-2}$

FIGURE S36 ^{1}H NMR spectra overlay of the polymerization of MMA and MAHAA to P(MMA$_{12}$-*co*-MAHAA$_{13}$) mediated by RAFT (500 MHz, dioxane-d_8). Significant signals corresponding to the protons of the double bond of the monomers MMA (**blue**) and MAHAA (**red**) are shown.

FIGURE S37 ^{1}H NMR spectra overlay of the polymerization of MMA and MAHAA to P(MMA$_{76}$-*co*-MAHAA$_5$) mediated by RAFT (500 MHz, dioxane-d_8). Significant signals corresponding to the protons of the double bond of the monomers MMA (**blue**) and MAHAA (**red**) are shown.
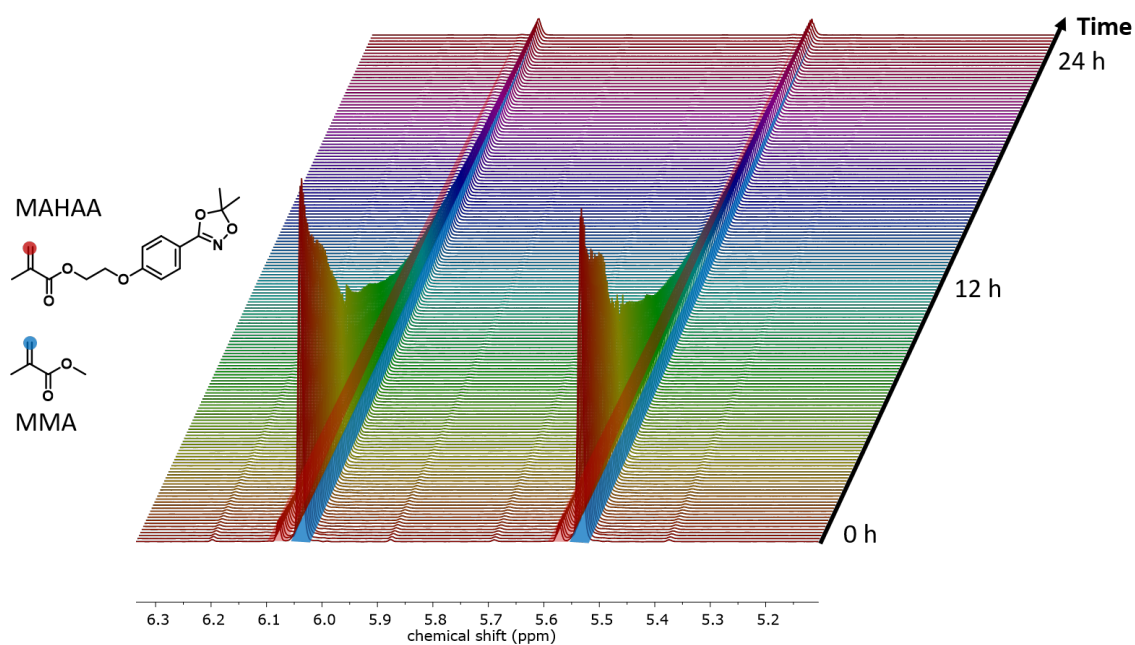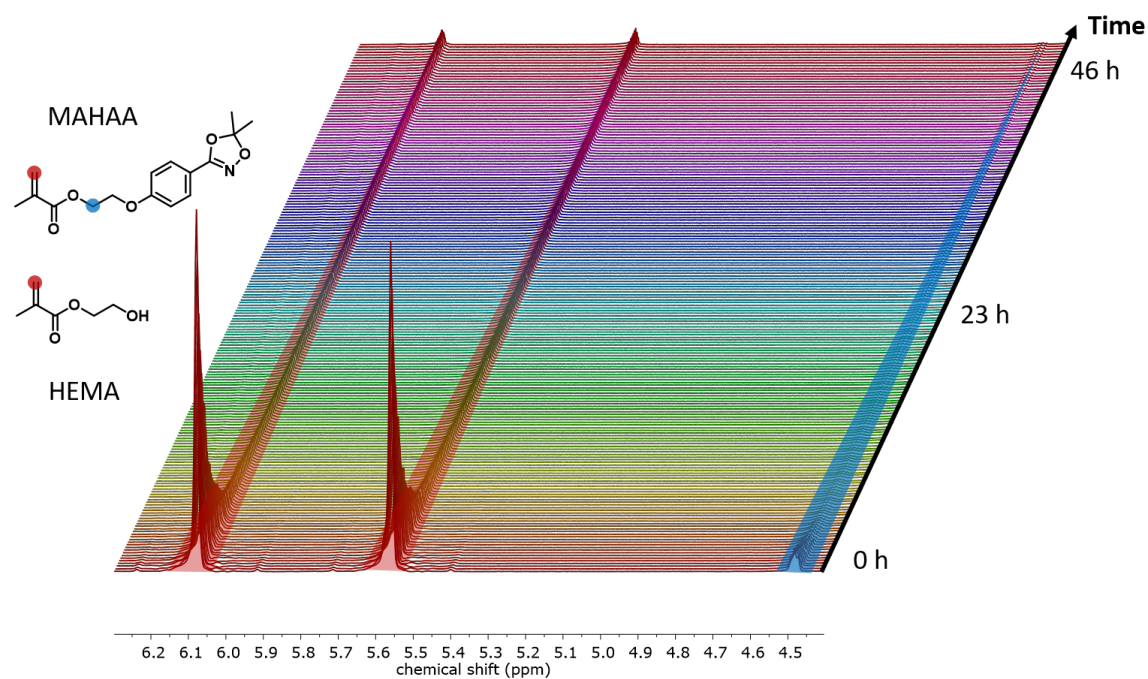
FIGURE S38 ^{1}H NMR spectra overlay of the polymerization of HEMA and MAHAA to P(HEMA$_{31}$-*co*-MAHAA$_2$) mediated by RAFT (500 MHz, dioxane-d_8). Significant signals corresponding to the protons of the double bond of both monomers (**red**) and protons of the methylene group of MAHAA (**blue**) are shown.

FIGURE S39 ^{1}H NMR spectra overlay of the polymerization of HEMA and MAHAA to P(HEMA$_{10}$-*co*-MAHAA$_{10}$) mediated by RAFT (500 MHz, dioxane-d_8). Significant signals corresponding to the protons of the double bond of both monomers (**red**) and protons of the methylene group of MAHAA (**blue**) are shown.
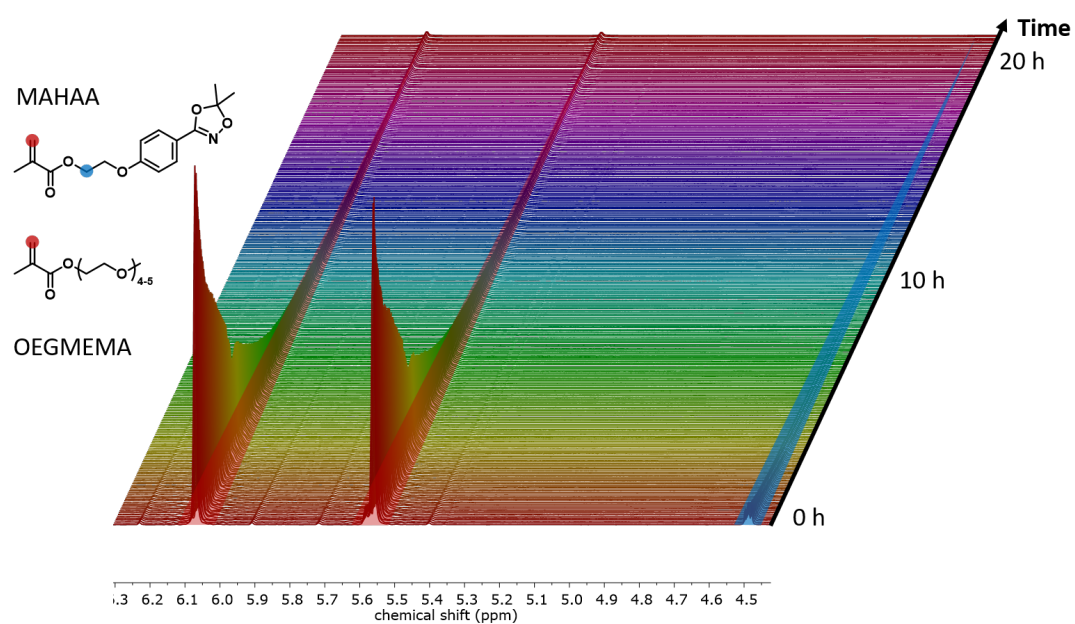
FIGURE S40 ^{1}H NMR spectra overlay of the polymerization of OEGMEMA and MAHAA to P(OEGMEMA$_{42}$-*co*-MAHAA$_2$) mediated by RAFT (500 MHz, dioxane-d_8). Significant signals corresponding to the protons of the double bond of both monomers (**red**) and protons of the methylene group of MAHAA (**blue**) are shown.
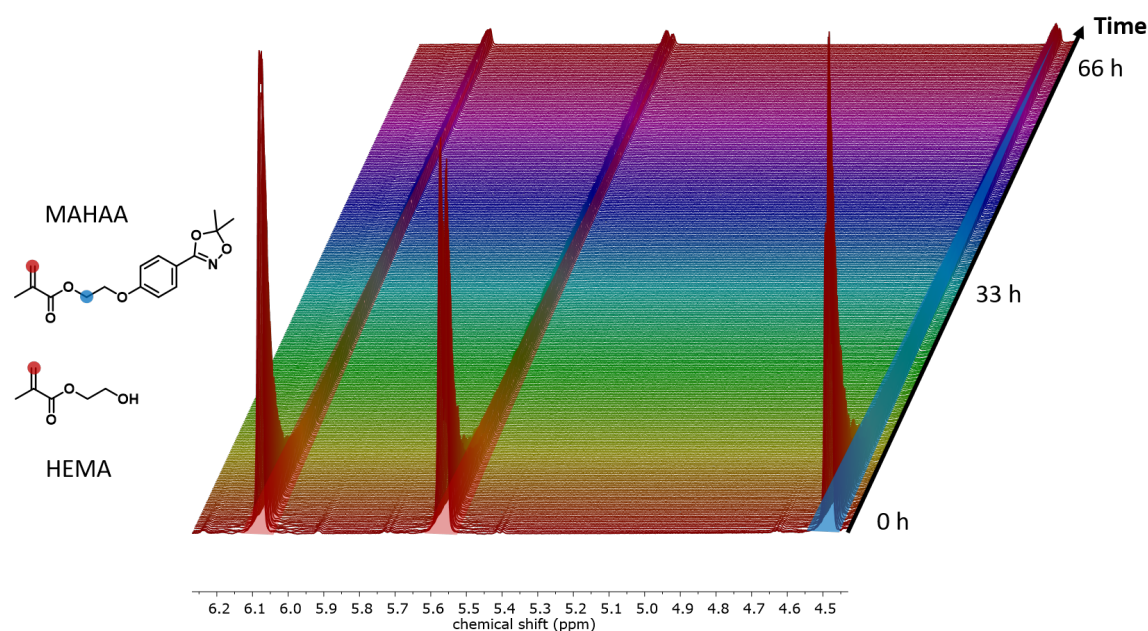

FIGURE S41 ^{1}H NMR spectra overlay of the polymerization of OEGMEMA and MAHAA to P(OEGMEMA$_9$-*co*-MAHAA$_9$) mediated by RAFT (500 MHz, dioxane-d_8). Significant signals corresponding to the protons of the double bond of both monomers (**red**) and protons of the methylene group of MAHAA (**blue**) are shown.
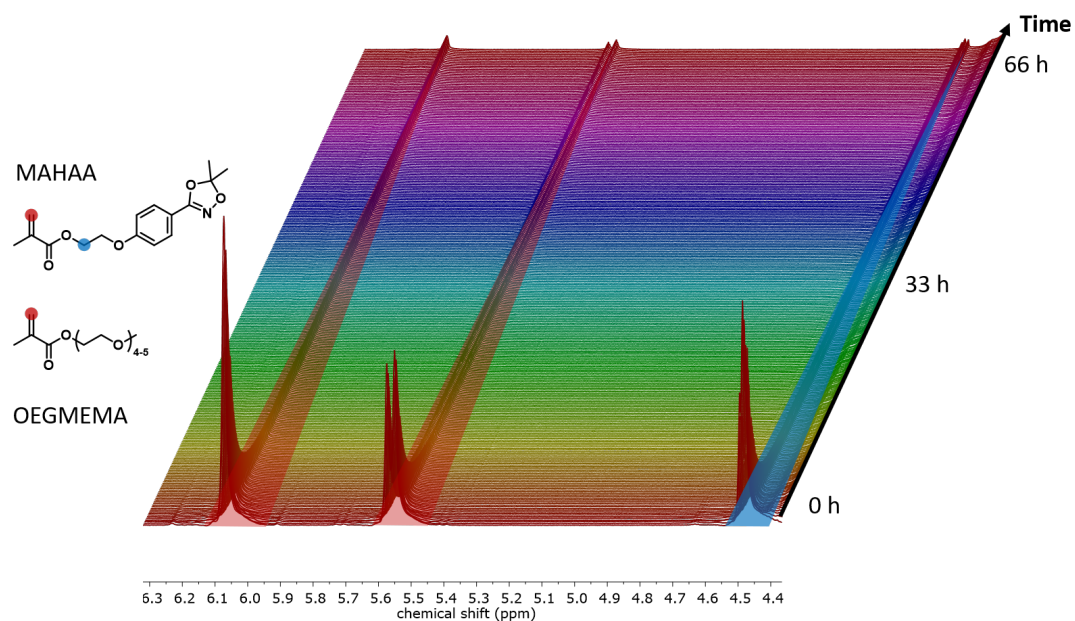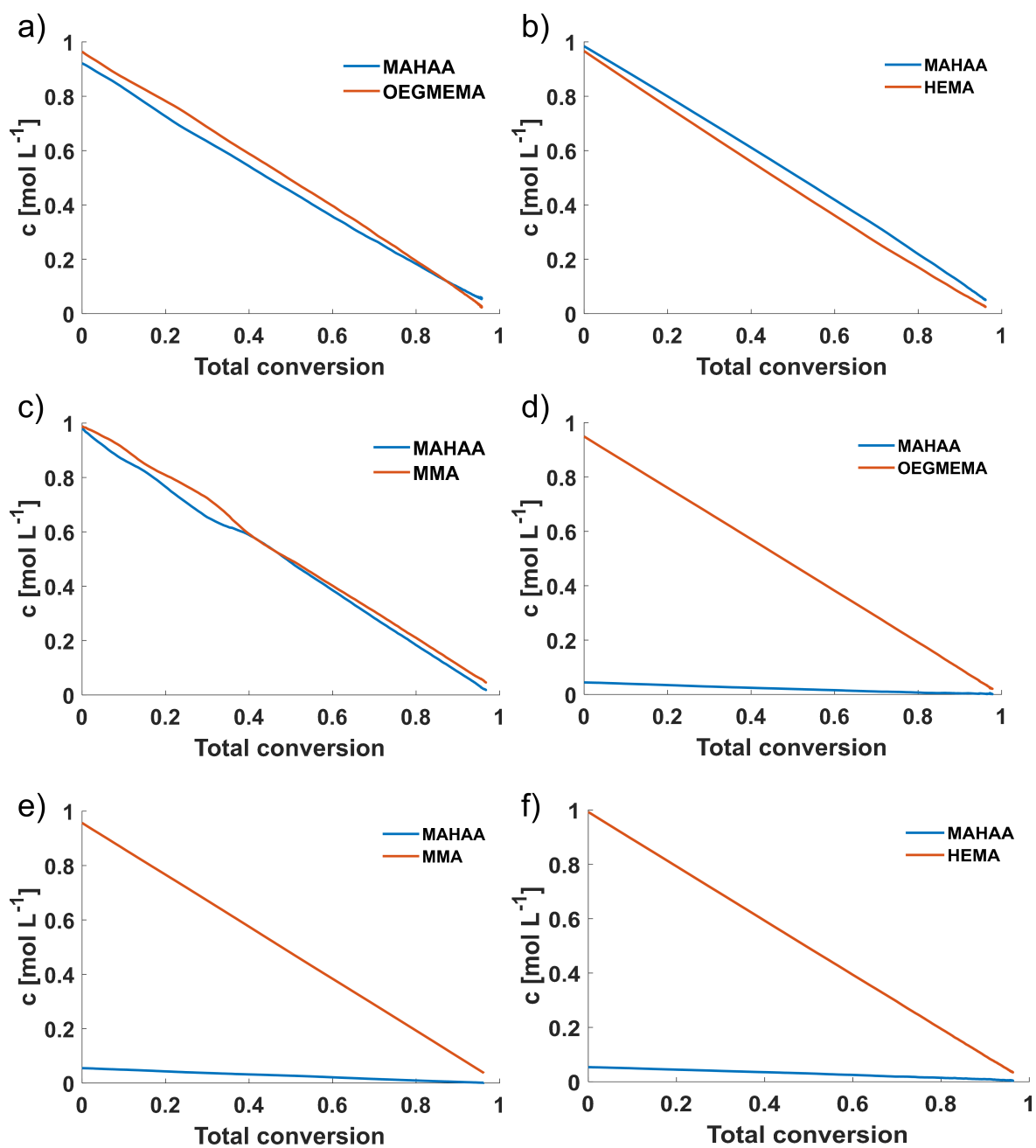
FIGURE S42 Individual monomer concentration versus the total conversion during the copolymerization of MAHAA with M1 to obtain P(OEGMEMA$_9$-*co*-MAHAA$_9$) (**a**), P(HEMA$_{10}$-*co*-MAHAA$_{10}$) (**b**), P(MMA$_{12}$-*co*-MAHAA$_{13}$) (**c**), P(OEGMEMA$_{42}$-*co*-MAHAA$_2$) (**d**), P(MMA$_{76}$-*co*-MAHAA$_5$) (**e**) and P(HEMA$_{31}$-*co*-MAHAA$_2$) (**f**).
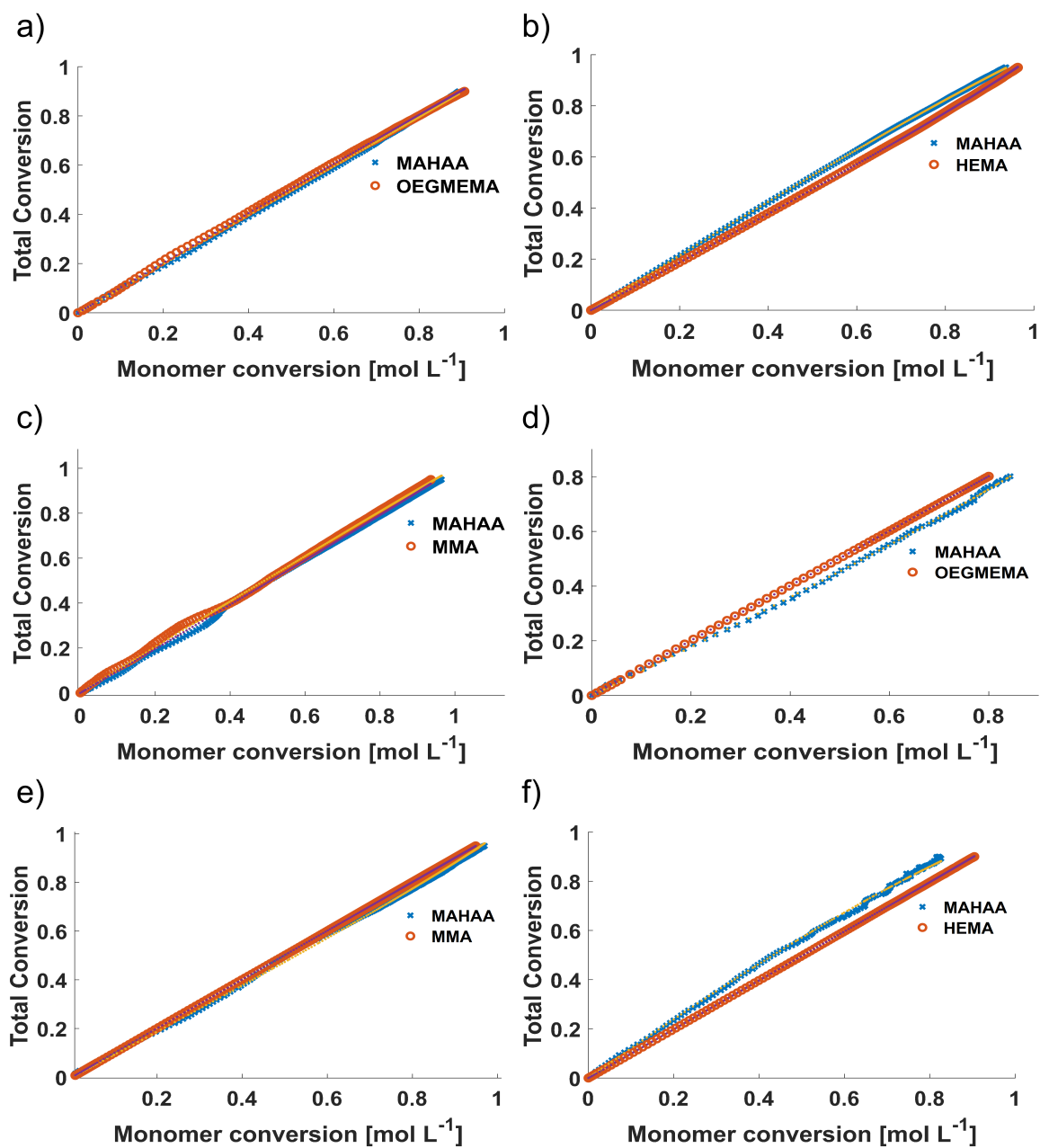
FIGURE S43   Total conversion versus monomer conversion for the copolymerization of P(OEGMEMA$_9$-co-MAHAA$_9$) (**a**), P(HEMA$_{10}$-co-MAHAA$_{10}$) (**b**), P(MMA$_{12}$-co-MAHAA$_{13}$) (**c**), P(OEGMEMA$_{42}$-co-MAHAA$_2$) (**d**), P(MMA$_{76}$-co-MAHAA$_5$) (**e**) and P(HEMA$_{31}$-co-MAHAA$_2$) (**f**).
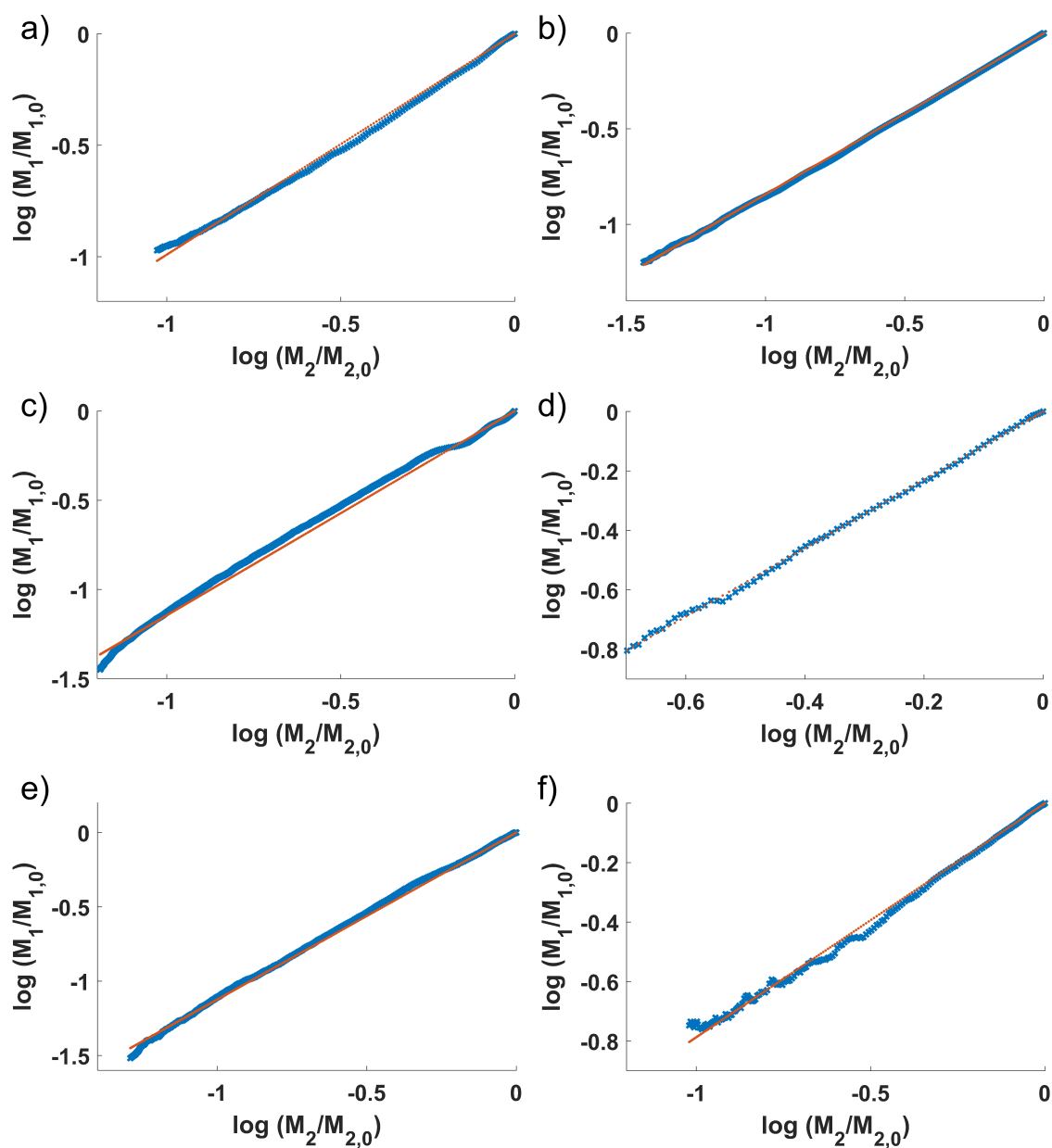
FIGURE S44 Jaacks plots concerning the initial monomer concentration $[MX]_0$ and the concentration of unreacted monomer after the polymerization $[MX]_t$ into account. Logarithmic plots are shown for the copolymerization of P(OEGMEMA$_9$-co-MAHAA$_9$) (**a**), P(HEMA$_{10}$-co-MAHAA$_{10}$) (**b**), P(MMA$_{12}$-co-MAHAA$_{13}$) (**c**), P(OEGMEMA$_{42}$-co-MAHAA$_2$) (**d**), P(MMA$_{76}$-co-MAHAA$_5$) (**e**) and P(HEMA$_{31}$-co-MAHAA$_2$) (**f**).
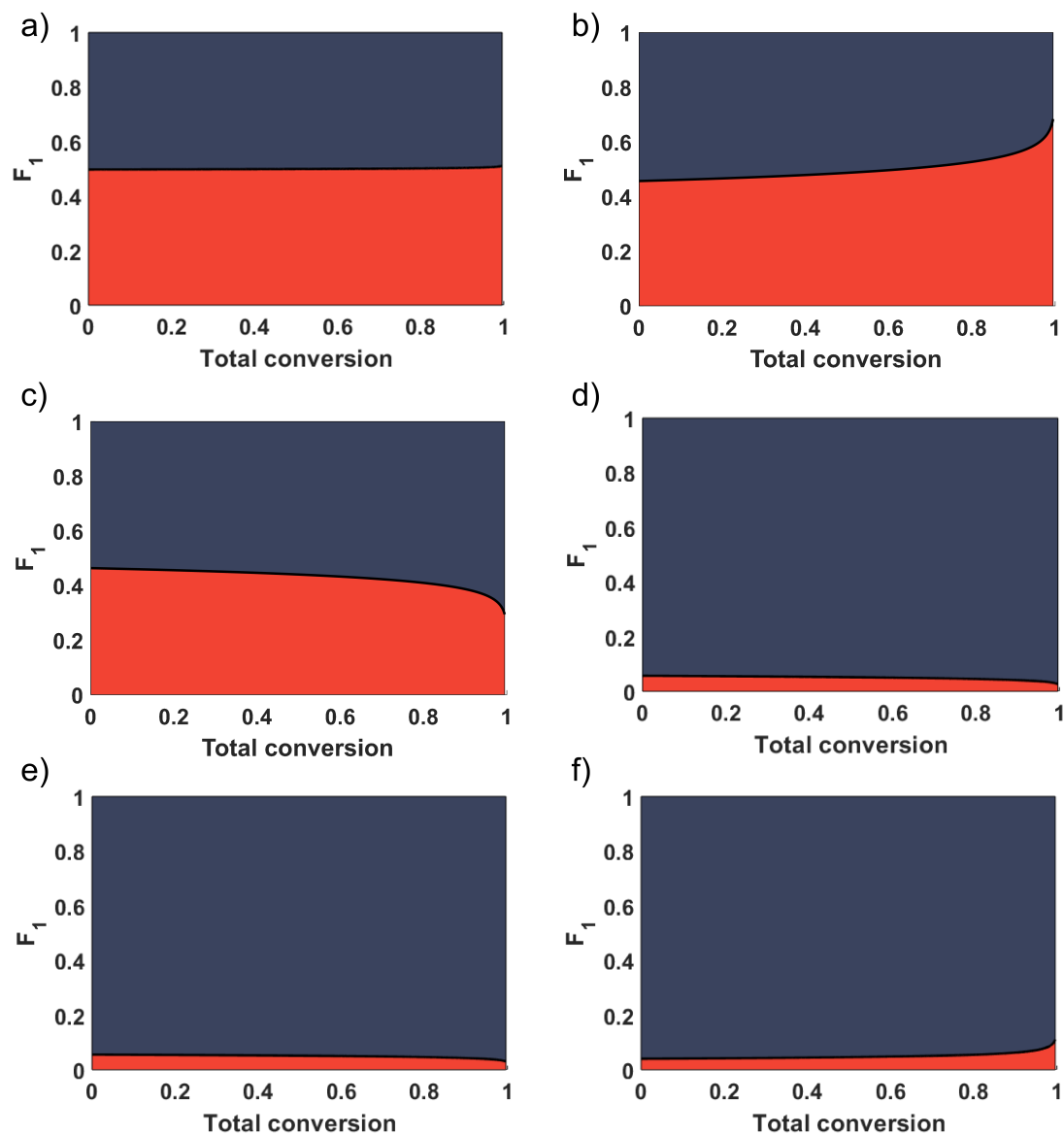
FIGURE S45   Molar based composition diagrams of M1 (blue) and MAHAA (red) of the polymers P(OEGMEMA$_9$-co-MAHAA$_9$) (**a**), P(HEMA$_{10}$-co-MAHAA$_{10}$) (**b**), P(MMA$_{12}$-co-MAHAA$_{13}$) (**c**), P(OEGMEMA$_{42}$-co-MAHAA$_2$) (**d**), P(MMA$_{76}$-co-MAHAA$_5$) (**e**) and P(HEMA$_{31}$-co-MAHAA$_2$) (**f**).
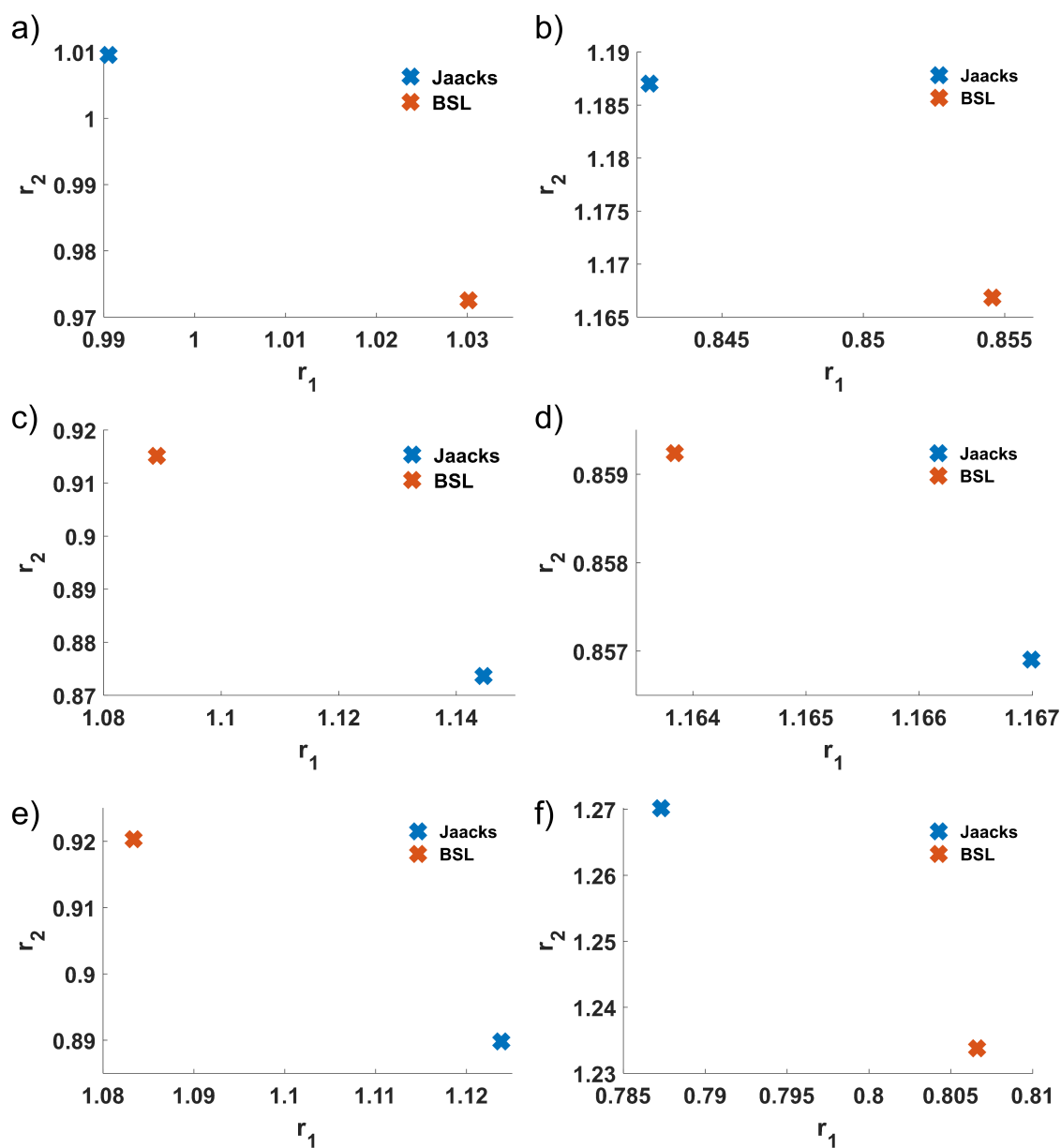
FIGURE S46 Reactivity ratios of MAHAA and M1 during the copolymerization of the corresponding monomers to $P(OEGMEMA_9\text{-}co\text{-}MAHAA_9)$ (**a**), $P(HEMA_{10}\text{-}co\text{-}MAHAA_{10})$ (**b**), $P(MMA_{12}\text{-}co\text{-}MAHAA_{13})$ (**c**), $P(OEGMEMA_{42}\text{-}co\text{-}MAHAA_2)$ (**d**), $P(MMA_{76}\text{-}co\text{-}MAHAA_5)$ (**e**) and $P(HEMA_{31}\text{-}co\text{-}MAHAA_2)$ (**f**) comparing the reactivity ratios analyzed by the Jaacks or the Beckingham-Sanoja-Lynd (BSL) method, respectively taking the total conversion versus the monomer conversion into account.

FIGURE S47 Monomer concentrations versus time P(MMA$_{76}$-*co*-MAHAA$_5$) (**a**), P(OEGMEMA$_{42}$-*co*-MAHAA$_2$) (**c**) and P(HEMA$_{31}$-*co*-MAHAA$_2$) (**e**) and the corresponding normalized plots (**b,d,f**).

REFERENCES

(1) Johann, T.; Keth, J.; Bros, M.; Frey, H. A general concept for the introduction of hydroxamic acids into polymers. *Chem. Sci.* **2019**, *10*, 7009–7022.
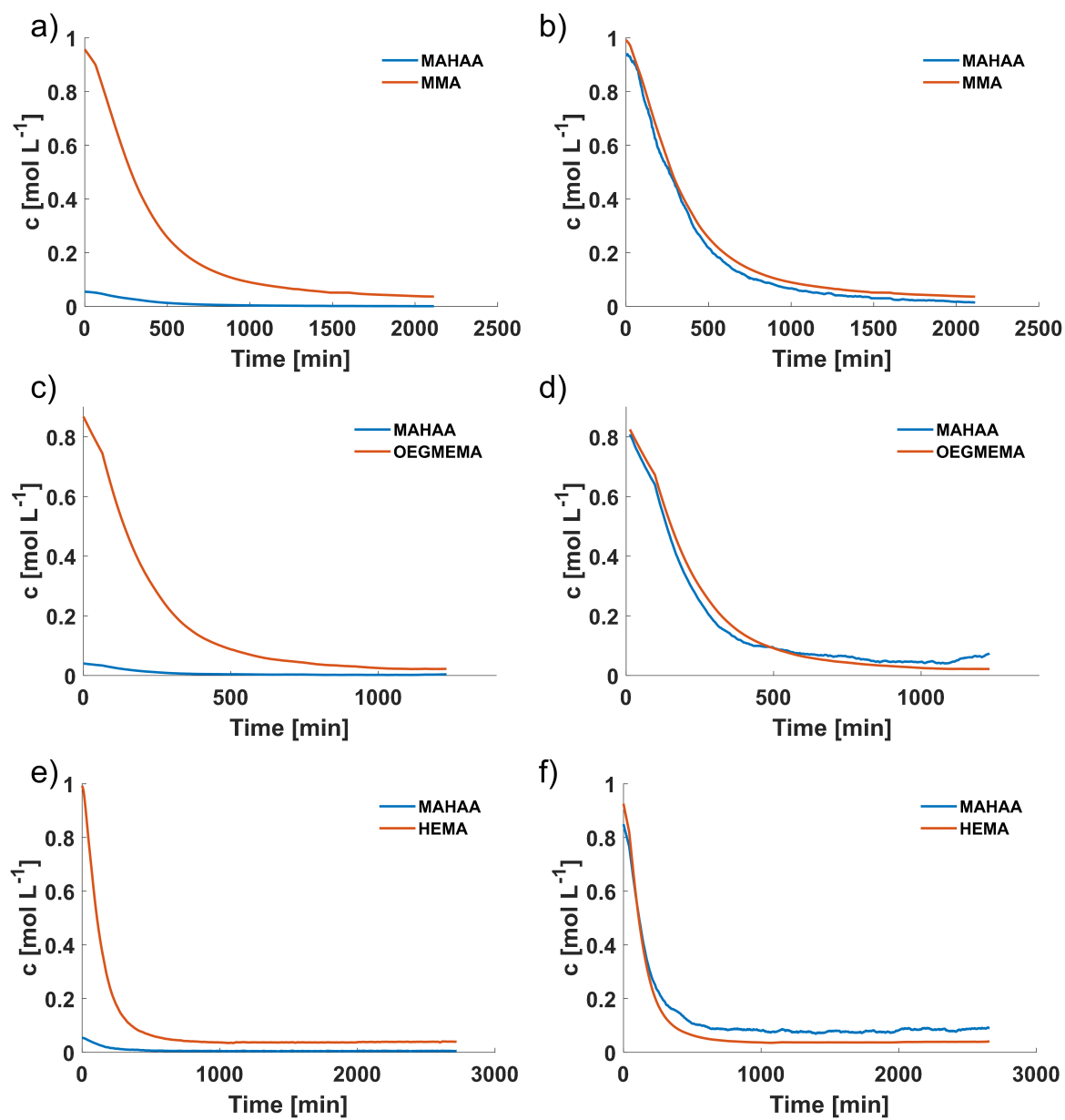
(2) Neises, B.; Steglich, W. Esterification of carboxylic acids with dicyclohexylcarbodiimide/4-dimethylaminopyridine: tert-butyl ethyl fumarate. *Org. Synth.* **1985**, *63*, 183.

(3) Hauser. C. R.; Renfrow, W. B. BENZOHYDROXAMIC ACID. *Org. Synth.* **1939**, *19*, 15.

(4) Couturier, M.; Tucker, J. L.; Proulx, C.; Boucher, G.; Dubé, P.; Andresen, B. M.; Ghosh, A. 5,5-Dimethyl-1,4,2-dioxazoles as Versatile Aprotic Hydroxamic Acid Protecting Groups. *J. Org. Chem.* **2002**, *67*, 4833–4838.

(5) Tietze, L. F.; Eicher, T. *Reaktionen und Synthesen im organisch-chemischen Praktikum und Forschungslaboratorium*; Wiley-VCH Verlag GmbH & Co. KGaA: Weinheim, FRG, 1991.

(6) Jaacks, V. A Novel Method of Determination of Reactivity Ratios in Binary and Ternary Copolymerizations. *Makromol. Chem.* **1972**, *161*, 161–172.

CHAPTER 3

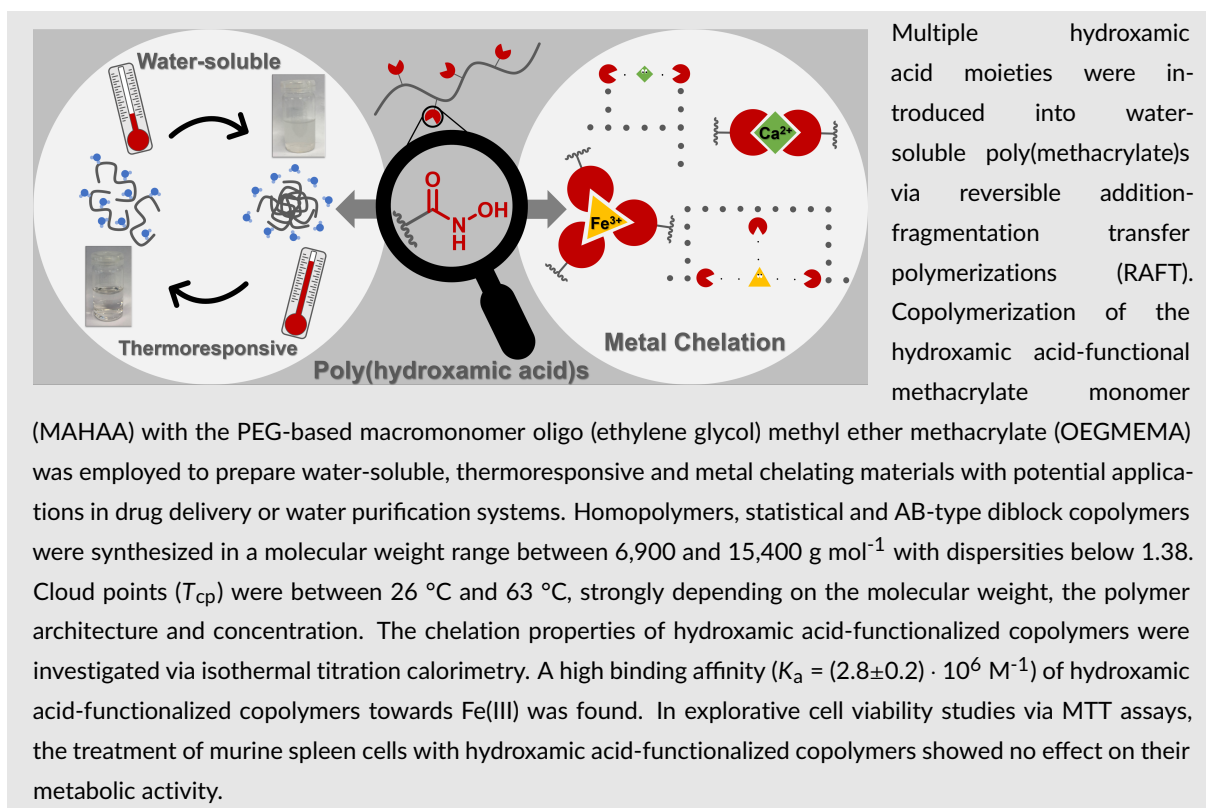WATER-SOLUBLE HYDROXAMIC
ACID-FUNCTIONALIZED POLY(METHACRYLATE)S

Copolymerization of Hydroxamic Acids with PEG-based Macromonomers: Facile Synthesis of Thermoresponsive and Metal Chelating Materials

Jennifer Keth[1], María Martínez Negro[2], Matthias Bros[3], Svenja Morsbach[2] and Holger Frey[1*]

[1]Department of Chemistry, Johannes Gutenberg University, Duesbergweg 10-14, 55128 Mainz, Germany

[2]Max Planck Institute for Polymer Research Ackermannweg 10, 55128 Mainz, Germany

[3]Department of Dermatology, University Medical Center of the Johannes Gutenberg University Mainz, Langenbeckstrasse 1, 55131 Mainz, Germany

Multiple hydroxamic acid moieties were introduced into water-soluble poly(methacrylate)s via reversible addition-fragmentation transfer polymerizations (RAFT). Copolymerization of the hydroxamic acid-functional methacrylate monomer (MAHAA) with the PEG-based macromonomer oligo (ethylene glycol) methyl ether methacrylate (OEGMEMA) was employed to prepare water-soluble, thermoresponsive and metal chelating materials with potential applications in drug delivery or water purification systems. Homopolymers, statistical and AB-type diblock copolymers were synthesized in a molecular weight range between 6,900 and 15,400 g mol^{-1} with dispersities below 1.38. Cloud points (T_{cp}) were between 26 °C and 63 °C, strongly depending on the molecular weight, the polymer architecture and concentration. The chelation properties of hydroxamic acid-functionalized copolymers were investigated via isothermal titration calorimetry. A high binding affinity (K_a = (2.8±0.2) · 10^6 M^{-1}) of hydroxamic acid-functionalized copolymers towards Fe(III) was found. In explorative cell viability studies via MTT assays, the treatment of murine spleen cells with hydroxamic acid-functionalized copolymers showed no effect on their metabolic activity.

INTRODUCTION

Polymers responding to an external stimulus are intensively investigated in the areas of nano- and bio-technology.[1–8] Thermoresponsive materials exhibiting a lower critical solution temperature (LCST) in aqueous media can be utilized for bio-active surfaces [9–11] for the selective bio-separation[12–15] and as drug delivery systems[16–21]. Temperature is utilized as a simple external trigger to switch between the soluble state below the LCST and the collapsed aggregated state above it. The most prominent thermoresponsive polymer is poly(N-isopropylacrylamide) (PNIPAM). In explorative works, Scarpa *et al.* reported in the late 1960s on the thermal phase transition behavior of PNIPAM.[22] With a lower critical solution temperature (LCST) of 32 °C in water, PNIPAM is viable for *in vivo* applications, i.e. as thermo-triggered drug releasing agent.[23] Despite its numerous advantages and versatile application fields, PNIPAM exhibits drawbacks such as an irreversible phase transition and a significant influence of the end groups on the thermal behavior especially for low molecular weight polymers.[24] To overcome these issues, various research groups focused on the synthesis of alternative thermoresponsive materials. In this context, Aoshima and coworkers[25] as well as Ishizone and coworkers[26] reported the LCST behavior of polymers containing short oligo(ethylene glycol) side chains as non-linear PEG-based macromolecules in aqueous medium.[9] The thermoresponsive properties of these polymers can be finely adjusted by the macromolecular design of the polymers, i.e. the polymer composition and the polymerization technique.[27–29] Defined phase transitions were only observed for polymers obtained by living or pseudo-living polymerization techniques due to uniform compositions.[30] Lutz *et al.* intensely investigated the thermoresponsive behavior of POEGMA and derivatives, demonstrating that the variation of the number of ethylene glycol units in the side chains is a powerful tool to control the cloud point temperatures precisely.[30] Besides the thermoresponsive properties, POEGMA possesses an excellent bio-repellency below the LCST (anti-fouling behavior) and bio-inert properties.[1,9,31] These features render POEGMA suitable for applications as bio-sensors, implants, scaffolds for tissue engineering and drug delivery devices.[1,9,30,31] Furthermore, Pispas and coworkers investigated several amphiphilic block copolymers with OEGMA as a hydrophilic block. The self-assembly to micellar structures in aqueous media enables the application as nanocarriers for the delivery of hydrophobic drugs.[32,33]

Here we describe a systematic approach to combine the thermoresponsive properties of POEGMA with the metal-chelating capability of hydroxamic acids in a single macromolecule to explore potential application fields in both materials and medical sciences. In nature, metal chelation plays an important role, and the metabolism of iron is enabled by siderophores (greek: "iron carriers") in various microorganisms. The characteristic functional groups of iron carriers can be classified mainly into two major types: i) catechols and ii) hydroxamic acids. The

excellent complexation properties of both ligands rely on the *O,O*-coordination towards metal ions that results in stable five-membered rings.[34] Despite the superior complexation properties of catechols, their facile oxidation to related quinones limits the use of these compounds in materials science significantly.

We utilized hydroxamic acid moieties that combine excellent complexation properties with long-term storage stability. Based on the seminal works of Winston *et al.* in the mid-1970s concerning the metal-chelating properties of polymers bearing hydroxamic acids [35–37], Rahman and coworkers investigated cur-rently the complexation ability of poly(hydroxamic acid) ligands for waste water treatment.[38] They demonstrated an effective removal of Cu(II), Fe(III) or Zn(II) from water samples after the treatment with poly(hydroxamic acid)s. However, poly(hydroxamic acid)s are almost exclusively synthesized via postmodification reactions of poly(acrylate) or poly(acrylamide)s with hydroxylamine, which generally do not lead to quantitative conversions or well-defined polymer structures.[39] Recently, our group reported a general procedure for the direct incorporation of hydroxamic acids into polymers via 1,4,2-dioaxzoles as suitable protecting groups to withstand the reaction conditions during radical and oxyanionic polymerizations was established. With this approach, well-defined polymer structures with control over the number and the position of hydroxamic acid functionalities were obtained.[40–42] Here we employ a 1,4,2-dioxazole protected hydroxamic acid methacrylate monomer (MAHAA) for the copolymerization with OEGMA to combine properties such as (i) aqueous solubility, (ii) metal chelation and (iii) thermoresponsiveness. Combination of these characteristics opens a variety of applications, using temperature as simple external trigger. Quantitative determination of complex stability constants with Fe(III) was performed by utilizing isothermal titration calorimetry (ITC). This analytic technique provides important information of the metal ion-hydroxamic acid interactions by monitoring the binding thermodynamics *in situ*.[39,43–45] Finally, the cell viability of murine spleen cells after the treatment with hydroxamic acid-functionalized copolymers has been investigated via MTT assays to explore their potential application in medical sciences.

RESULTS AND DISCUSSION

Polymer Synthesis

The RAFT polymerization technique was employed for the preparation of well-defined water-soluble hydroxamic acid-functionalized copolymers. To prevent possible radical-induced side reactions, oligo (ethylene glycol) methyl ether methacrylate (OEGMEMA) was utilized as hydroxyl protected derivate of OEGMA. The RAFT technique enabled the synthesis of both statistical copolymers and AB-type diblock copolymers. 2,2'-Azobis(2-methylpropionitrile) (AIBN) was applied as initiator for both statistical and block copolymers. The chain transfer agent (CTA) 2-Cyano-2-propyl benzodithioate (CPBDT) was utilized for the synthesis of statistical copolymers while P(OEGMEMA) was employed as macroCTA in the AB-type diblock copolymer synthesis. After an acidic workup under mild conditions with 0.1 M HCl at room temperature for 24 h, the hydroxamic acid moieties were released (see *Experimental section* for details, **Scheme 1**).
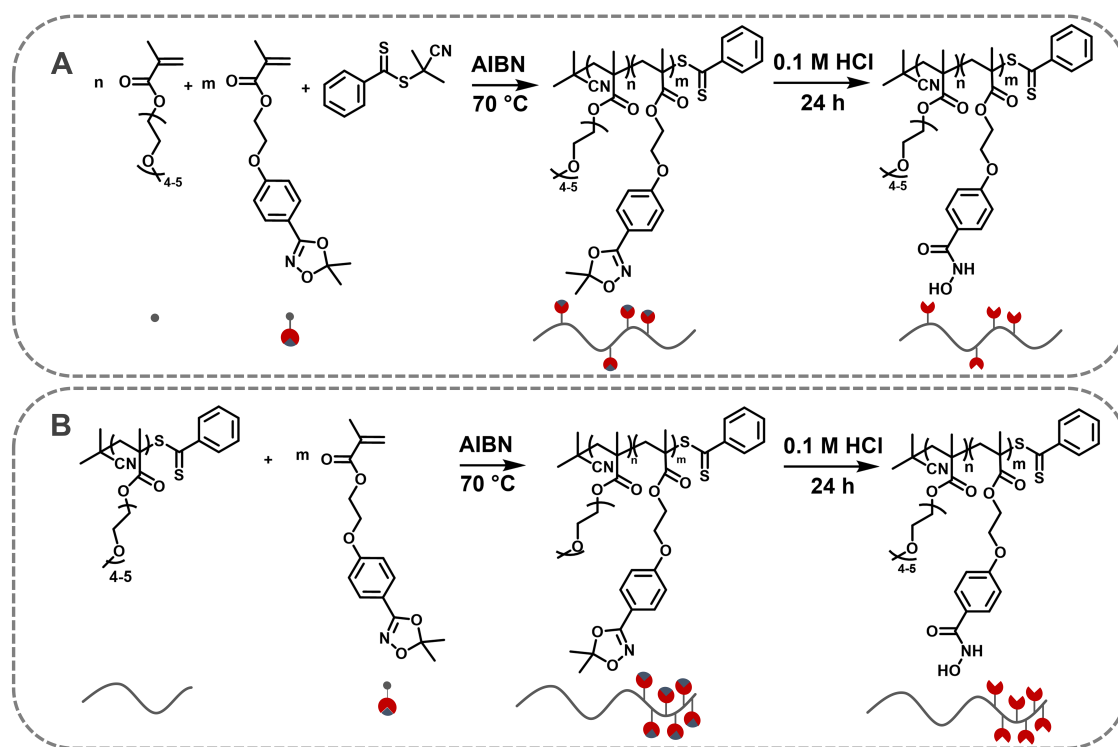
SCHEME 1 RAFT copolymerizations of OEGMEMA and MAHAA with AIBN as an initiator. The polymerizations were carried out at 70 °C for 24 h. (A) Statistical copolymerization utilizing CPBDT as CTA and (B) block copolymerization using P(OEGMEMA) as macroCTA to yield diblock copolymers. The hydroxamic acid moieties were released after an acidic workup.

The impact of heating rates, concentrations, molecular weights, polymer architectures and the amount of hydroxamic acid groups on the thermoresponsive behavior of these materials was investigated in detail (**Table 2**, **Figures S1-S7**).

Thermoresponsive Behavior

We investigated the thermoresponsive behavior of water-soluble hydroxamic acid-functionalized copolymers with respect to the amount of protected hydroxamic acid-functionalized monomer, the polymer architecture and the degree of deprotection (**Figure 1**). The cloud point temperatures T_{cp} were measured via turbidimetry (see *Experimental Section* for details) (**Figures 2** and **3**).
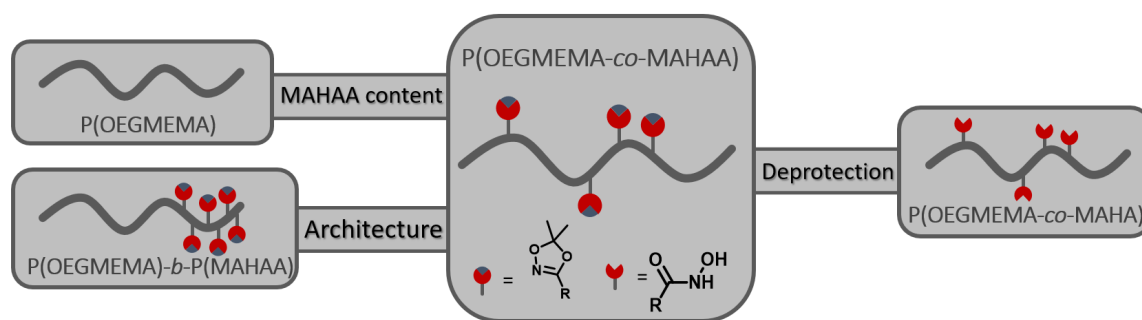
FIGURE 1 Overview of different P(OEGMEMA) based structures. Variation of MAHAA content, architecture and degree of deprotection.

MAHAA content

At low temperatures, the polymer chains are hydrated due to hydrogen bond formation between polymer and water molecules. Upon increasing the temperature, the hydrogen bonds are weakened, which finally leads to an collapse and insolubility of the polymer chains, evident from turbidity of the solution.[46] Molecular weight-dependent cloud point temperatures between 63-68 °C were observed for P(OEGMEMA) (**Figure S4**), in good agreement with literature values.[30,47–49] Copolymers that bear protected hydroxamic acid moieties, i.e. $10\%_{mol}$ of MAHAA, exhibit lower cloud point temperatures compared to P(OEGMEMA) homopolymers at similar molecular weights (**Figure 3**). These results suggest that the incorporation of apolar MAHAA units in the copolymer might lead to an interruption of the hydrogen bond formation and therefore to a weakened polymer hydration. Consequently, the copolymer solution changes from the soluble state into a collapsed aggregated state on a macroscopic scale already at lower temperatures compared to P(OEGMEMA) homopolymers.

Deprotection

We investigated the effect of free hydroxamic acid units in the copolymers on the cloud point temperature. As a result, the T_{cp} of the statistical copolymer P(OEGMEMA$_{37}$-*co*-MAHAA$_3$) was increased by more than 4 °C after the deprotection to P(OEGMEMA$_{37}$-*co*-MAHA$_3$) (**Table 1**, **Figure 2**). Furthermore, a distinct influence on the Tcp was observed for polymers with high amounts of randomly distributed MAHAA units (33%$_{mol}$) in the polymer, manifest in a decrease of the T_{cp} to 26 °C (**Figure S7**). After the deprotection, the T_{cp} increased by more than 6 °C. This may be a result of an enhanced hydration of the polymer chains for the deprotected species due to an increased hydrophilicity of the copolymer.
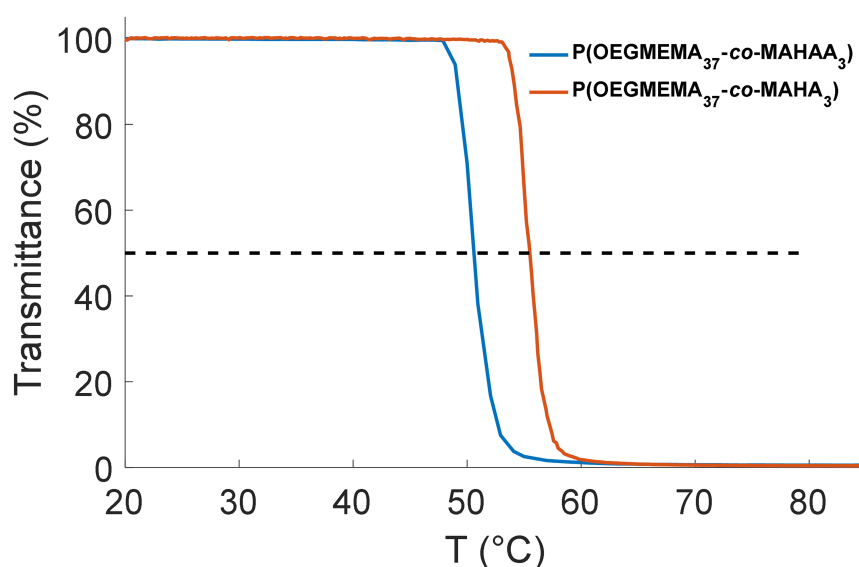
FIGURE 2 Transmittance as a function of time for the statistical copolymer P(OEGMEMA$_{37}$-*co*-MAHAA$_3$) (blue) and P(OEGMEMA$_{37}$-*co*-MAHA$_3$) (red).

Polymer Architecture

The impact of the polymer architecture on the thermoresponsive properties of hydroxamic acid-functionalized copolymers was investigated by comparing random copolymers to AB-type di-block copolymers. In our studies, we observed lower T_{cp} for copolymers that obtain MAHAA units randomly distributed in the polymer chain compared to block copolymer structures. The Tcp of the statistical copolymer P(OEGMEMA$_{23}$-*co*-MAHAA$_2$) was more than 10 °C lower than the Tcp of the block copolymer P(OEGMEMA)$_{23}$-*b*-P(MAHAA)$_3$ at similar molecular weights (**Table 1**). Consequently, randomly distributed MAHAA units may interrupt the polymer hydration to a greater extent than MAHAA units which are fixed at one end of the polymer as it is the case in block copolymers.
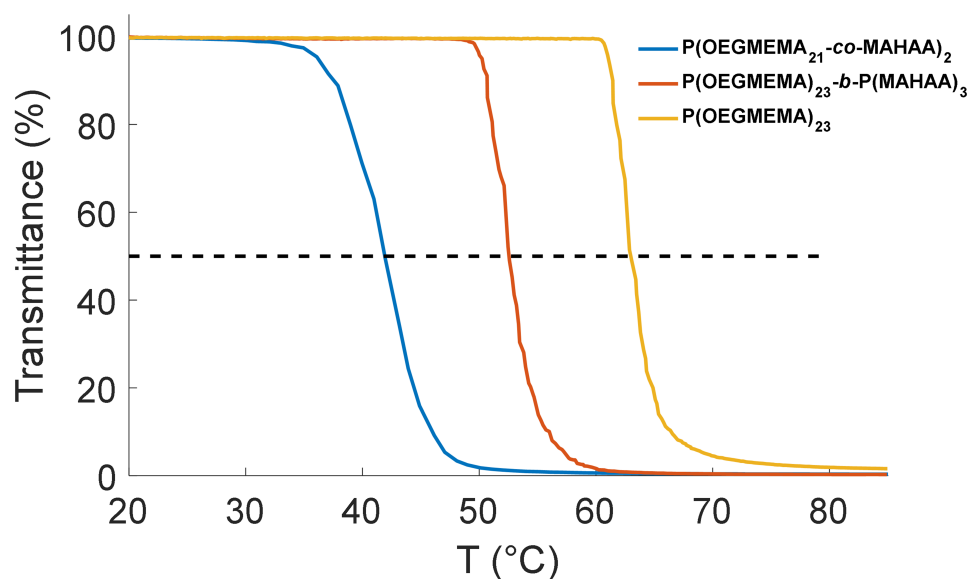
FIGURE 3 Transmittance as a function of time for the homopolymer P(OEGMEMA)$_{23}$ (yellow), the statistical copolymers P(OEGMEMA$_{23}$-co-MAHAA$_2$) (blue) and the block copolymer P(OEGMEMA)$_{23}$-b-P(MAHAA)$_3$ (red).

Summarizing, we investigated different parameters that influenced the thermoresponsiveness of the hydroxamic acid-functionalized copolymer structures. By changing the amount of MAHAA and finally its deprotected species (MAHA), the molecular weight and the polymer architecture, the cloud point temperatures were changed by more than 35 °C (**Figures S4-S7**). The processes were reversible, with a small hysteresis in the heating and cooling cycles (< 2 °C) (**Figure S8**).

TABLE 1 Overview of the properties of the synthesized homopolymer P(OEGMEMA) and the hydroxamic acid-functionalized statistical and block copolymers.

Polymer	M_n [g mol^{-1}]^a	MAHAA [%$_{mol}$]	T_{cp} [°C]
P(OEGMEMA$_{23}$-co-MAHAA$_2$)	6900	9	41.9
P(OEGMEMA)$_{23}$-b-P(MAHAA)$_3$	7900	12	52.5
P(OEGMEMA)$_{23}$	6900	0	63.0
P(OEGMEMA$_{37}$-co-MAHAA$_3$)	12000	8	50.6
P(OEGMEMA$_{37}$-co-MAHA$_3$)	11900	8	55.4

a. determined via end group analysis in ^{1}H NMR.

Isothermal Titration Calorimetry (ITC)

ITC was used to quantify the binding affinity, stoichiometry and binding enthalpy during the complex formation between Fe(III) and P(OEGMEMA$_{37}$-co-MAHA$_3$). In principle, the formation of mono, bis- and tris hydroxamato Fe(III)-complexes is possible (**Scheme 2**).[42]
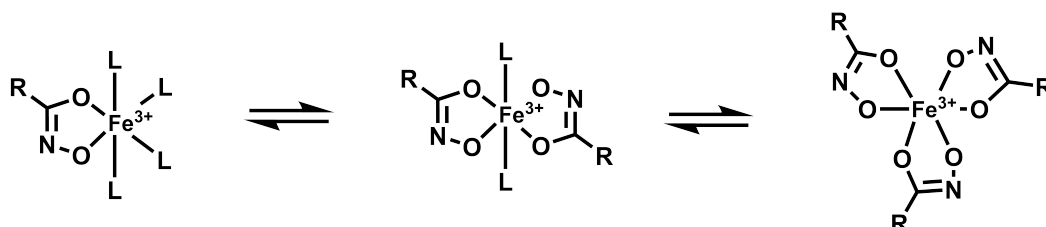
SCHEME 2 Formation of mono-, bis- and tris hydroxamato Fe(III)-complexes.

Figure 4, top shows the heat rate during a representative measurement for 0.2 mmol L^{-1} of P(OEGMEMA$_{37}$-co-MAHA$_3$) (*i.e.* 0.02 mmol L^{-1} MAHA) and $1.52 \cdot 10^{-1}$ mmol L^{-1} of FeCl$_3$ (*i.e.* 0.03 mmol L^{-1} Fe(III)). The overall heat changes during the measurement result not only from the interaction between MAHA and Fe(III) but also from the dilution of FeCl$_3$ in water, which has to be subtracted to determine the heat corresponding to the complex formation. The adsorption isotherm obtained after the corrected heat integration was fitted according to an independent binding model (**Figure 4, bottom**).
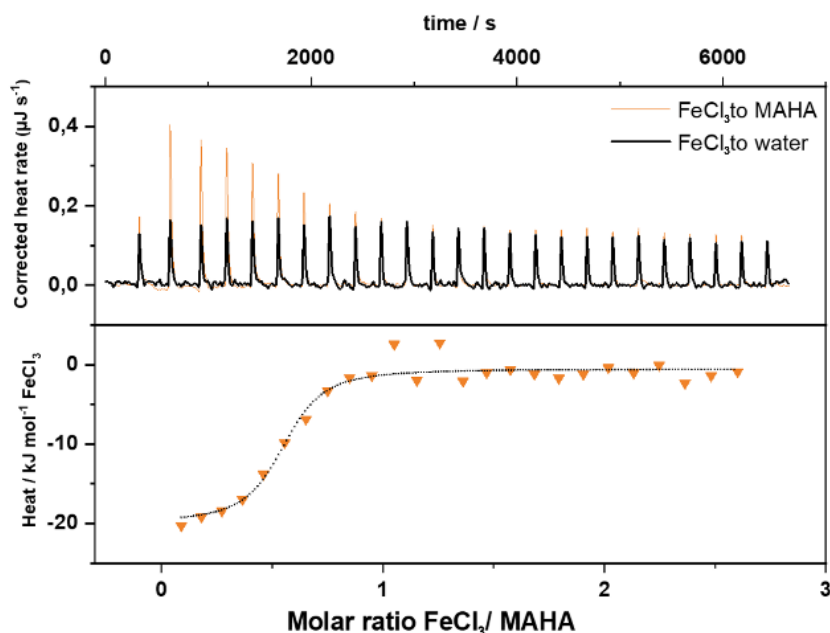
FIGURE 4 ITC data for the titration of P(OEGMEMA$_{37}$-co-MAHA$_3$) with FeCl$_3$. Titrations were carried out at 25 °C with 0.02 mmol L^{-1} P(OEGMEMA$_{37}$-co-MAHA$_3$) in the sample cell and $1.52 \cdot 10^{-1}$ mmol L^{-1} FeCl$_3$ in the syringe. Top: Corrected heat rate of the titration (orange) and corresponding dilution measurement (black). Bottom: Integrated heats from each titration step after subtraction of dilution heats together with an independent binding model fit.

TABLE 2 Experimental values obtained from ITC measurement for the reaction of P(OEGMEMA$_{37}$-*co*-MAHA$_3$) with Fe(III).

K_d [M]	K_a [M^{-1}]	ΔH [KJ mol^{-1}]	ΔS [J mol^{-1} K^{-1}]	ΔG [KJ mol^{-1}]	n [Fe/MAHA]
$(3.7\pm0.3) \cdot 10^{-7}$	$(2.8\pm0.2) \cdot 10^6$	-19.1±2.2	59.8±7.1	-36.1±0.2	0.7±0.3

From the fit based on the integrated heats, the thermodynamic parameters of interaction are obtained, *i.e.*, the association constant (K_a), the reaction enthalpy (ΔH), entropy (ΔS), Gibbs free energy (ΔG) and reaction stoichiometry (n). ΔH was determined as difference between the upper and lower plateau in the adsorption isotherm, K_a is derived from the curve's slope in the inflection point and n is the stoichiometry ratio at the inflection point (**Figure S9**). According to the reaction isotherm equation and the Gibbs-Helmholtz equation, thermodynamic parameters such as entropy ΔS and the Gibbs free energy ΔG were determined (**SI**, **Eq. 1** and **2**).[43,50]

The obtained thermodynamic values of the Fe(III)-MAHA complexation process reveal that complex formation with Fe(III) proceeds exothermically (ΔH < 0), with an increase of the overall entropy (**Table 2**). This means that complexation is both enthalpically and entropically favored. In addition, a high binding affinity of the hydroxamic acid ligands to Fe(III) was confirmed (**Table 2**). Network formation and gelation was prevented during the measurements due to high dilutions. For all titrations, only one complexation step (*i.e.* one inflection point) was observed, which yielded an average stoichiometry of $n_{\text{Fe(III)/MAHA}}$ = 0.7 ± 0.3. However, it has to be emphasized that the experiments revealed a polymer concentration dependence of the titrations (three different values of n = 0.3 ± 0.02, 0.5 ± 0.03 and 1.0 ± 0.1 obtained at three different polymer concentrations), which could suggest that the stoichiometry of the resulting metal-polymer complexes depends on the initial polymer concentration (**Figures S10-S12, Table S3**). Usually, this is not the case for titrations, but in rare cases it can be observed. Here, it might indicate a polymer conformational change during complex formation.

Iron Removal from Water

As a proof-of-principle concept, hydroxamic acid-functionalized copolymers were added to a Fe(III) chloride solution to investigate the efficiency of Fe(III) removal with time. Therefore, the copolymer solution was placed in a dialysis tube surrounded by an Fe(III) chloride solution (**Figure S13**). The dialysis tube allows Fe(III) to pass the membrane to the polymer solution while preventing the diffusion of polymer to the Fe(III) chloride solution due to the molecular weight barrier. In other words, Fe(III) is trapped inside the dialysis tube due to the complexation with the hydroxamic acid moieties. To quantify the efficiency of the removal of Fe(III) in solution, samples were taken at different times and were analyzed both via atomic absorption spectroscopy and UV-Vis spectroscopy (**Table 3**, **Figure S14**).

TABLE 3 Concentration of Fe(III) versus time after the treatment with hydroxamic acid-functionalized polymers determined by atomic absorption spectroscopy.

Time [h]	0	24	48
c [mg L^{-1}]	1.527±0.033	0.013±0.003	0.004±0.003

As a result, the water-soluble hydroxamic acid-functionalized copolymers removed Fe(III) quantitatively (>99%) after 24 h in these first proof-of-principle studies.

Cell Viability Tests.

MTT metabolic activity assays on murine spleen cells, as a common standard system, were performed to investigate the biocompatibility of P(OEGMEMA$_{37}$-co-MAHA$_3$) as Fe(III) binding agent with regard to potential therapeutic applications (**Figure 5**). The measurements were carried out in triplicate. Figure 5 shows the mean value and the standard deviation for each parameter.
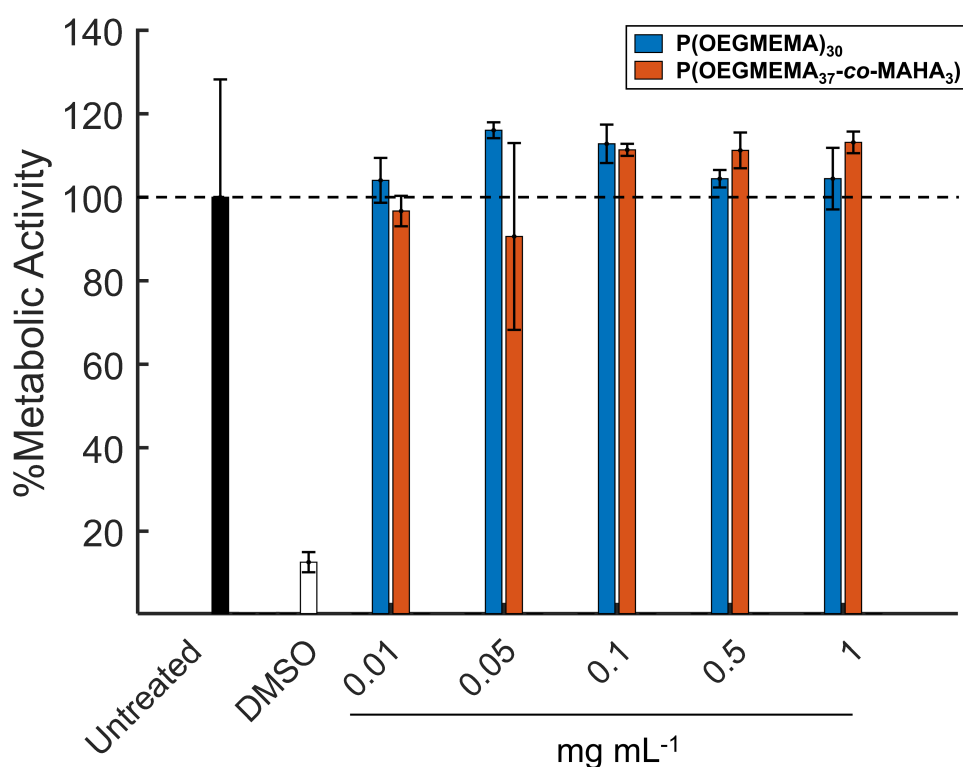
FIGURE 5 Effect of P(OEGMEMA)$_{30}$ (blue) and P(OEGMEMA$_{37}$-co-MAHA$_3$) (red) on the metabolic activity of murine spleen cells as determined via MTT assays. DMSO applied at cytotoxic concentration (10%) served as a negative control.

The homopolymer P(OEGMEMA)$_{30}$ and the hydroxamic acid-functionalized copolymer P(OEGMEMA$_{37}$-co-MAHA$_3$) showed no significant impact on the metabolic cell activity of murine spleen cells within the range of tested concentrations, evidencing low cytotoxic effects on cells *in vitro*.

CONCLUSIONS

Using RAFT copolymerization, we synthesized hydroxamic acid-functionalized P(OEGMEMA)-based copolymers with varied polymer architectures and hydroxamic acid contents of 8 to 33%$_{mol}$ in the molecular weight range from 6,900 and 15,400 g mol^{-1}. All synthesized polymers were soluble in aqueous solution and demonstrated thermoresponsive behavior, measured via turbidimetry. Copolymerization of a minor amount of the hydroxamic acid-based novel monomers changed the T_{cp} of POEGMEMA to a limited extent depending on polymer architecture and molecular weight. Upon deprotection, LCSTs increased from 50 °C to 55 °C for a fraction of 8%$_{mol}$ of hydroxamic acid-based methacrylates. Copolymers with higher hydroxamic acid contents (33%$_{mol}$) revealed LCSTs close to the physiological temperature range (> 32 °C). Furthermore, ITC studies indicated that poly(hydroxamic acid)s are efficient Fe(III) chelators in an enthalpy driven complexation reaction. In a proof-of-principle model reaction, we demonstrated the quantitative removal of Fe(III) (>99%) from water after the treatment with hydroxamic acid-functionalized copolymers after 24 h. The metabolic activity of murine spleen cells after the treatment with hydroxamic acid-functionalized copolymers was investigated via MTT assays, revealing no significant cytotoxic effects *in vitro*. Based on our findings, we conclude that water-soluble hydroxamic acid-functionalized poly(methacrylate)s possess a great potential as a biocompatible system in biomedical applications, i.e. the removal of iron in iron-metabolism related diseases.

ACKNOWLEDGEMENTS

REFERENCES

(1) Lutz, J.-F.; Hoth, A. Preparation of Ideal PEG Analogues with a Tunable Thermosensitivity by Controlled Radical Copolymerization of 2-(2-Methoxyethoxy)ethyl Methacrylate and Oligo(ethylene glycol) Methacrylate. *Macromolecules* **2006**, *39*, 893–896.

(2) Gil, E. S.; Hudson, S. M. Stimuli-reponsive polymers and their bioconjugates. *Prog. Polym. Sci.* **2004**, *29*, 1173–1222.

(3) Crespy, D.; Rossi, R. M. Temperature-responsive polymers with LCST in the physiological range and their applications in textiles. *Polym. Int.* **2007**, *56*, 1461–1468.

(4) Nath, N.; Chilkoti, A. Creating "Smart" Surfaces Using Stimuli Responsive Polymers. *Adv. Mater.* **2002**, *14*, 1243–1247.

(5) Roy, D.; Brooks, W. L. A.; Sumerlin, B. S. New directions in thermoresponsive polymers. *Chem. Soc. Rev.* **2013**, *42*, 7214–7243.

(6) Hoffman, A. S.; Stayton, P. S. Conjugates of stimuli-responsive polymers and proteins. *Prog. Polym. Sci.* **2007**, *32*, 922–932.

(7) Bordat, A.; Boissenot, T.; Nicolas, J.; Tsapis, N. Thermoresponsive polymer nanocarriers for biomedical applications. *Adv. Drug Delivery Rev.* **2019**, *138*, 167–192.

(8) Galaev, I. 'Smart' polymers and what they could do in biotechnology and medicine. *Trends Biotechnol.* **1999**, *17*, 335–340.

(9) Lutz, J.-F. Thermo-Switchable Materials Prepared Using the OEGMA-Platform. *Adv. Mater.* **2011**, *23*, 2237–2243.

(10) Hatakeyama, H.; Kikuchi, A.; Yamato, M.; Okano, T. Patterned biofunctional designs of thermoresponsive surfaces for spatiotemporally controlled cell adhesion, growth, and thermally induced detachment. *Biomaterials* **2007**, *28*, 3632–3643.

(11) da Silva, R. M. P.; Mano, J. F.; Reis, R. L. Smart thermoresponsive coatings and surfaces for tissue engineering: switching cell-material boundaries. *Trends Biotechnol.* **2007**, *25*, 577–583.

(12) Nagase, K.; Okano, T.; Kanazawa, H. Poly(*N*-isopropylacrylamide) based thermoresponsive polymer brushes for bioseparation, cellular tissue fabrication, and nano actuators. *Nano-Struct. Nano-Objects* **2018**, *16*, 9–23.

(13) Shamim, N.; Hong, L.; Hidajat, K.; Uddin, M. S. Thermosensitive polymer coated nanomagnetic particles for separation of bio-molecules. *Sep. Purif. Technol.* **2007**, *53*, 164–170.

(14) Takei, Y. G.; Aoki, T.; Sanui, K.; Ogata, N.; Okano, T.; Sakurai, Y. Temperature-responsive bioconjugates. 2. Molecular design for temperature-modulated bioseparations. *Bioconjugate Chem.* **1993**, *4*, 341–346.

(15) Nagase, K.; Kobayashi, J.; Okano, T. Temperature-responsive intelligent interfaces for biomolecular separation and cell sheet engineering. *J. R. Soc., Interface* **2009**, *6*, 293-309.

(16) Wang, D.; Huang, H.; Zhou, M.; Lu, H.; Chen, J.; Chang, Y.-T.; Gao, J.; Chai, Z.; Hu, Y. A thermoresponsive nanocarrier for mitochondria-targeted drug delivery. *Chem. Commun.* **2019**, *55*, 4051–4054.

(17) Nakayama, M.; Okano, T.; Miyazaki, T.; Kohori, F.; Sakai, K.; Yokoyama, M. Molecular design of biodegradable polymeric micelles for temperature-responsive drug release. *J. Controlled Release* **2006**, *115*, 46–56.

(18) Liu, R.; Fraylich, M.; Saunders, B. R. Thermoresponsive copolymers: from fundamental studies to applications. *Colloid Polym. Sci.* **2009**, *287*, 627–643.

(19) Las Heras Alarcon, C. de; Pennadam, S.; Alexander, C. Stimuli responsive polymers for biomedical applications. *Chem. Soc. Rev.* **2005**, *34*, 276–285.

(20) Hrubý, M.; Subr, V.; Kucka, J.; Kozempel, J.; Lebeda, O.; Sikora, A. Thermoresponsive polymers as promising new materials for local radiotherapy. *Appl. Radiat. Isot.* **2005**, *63*, 423–431.

(21) Bajpai, A. K.; Shukla, S. K.; Bhanu, S.; Kankane, S. Responsive polymers in controlled drug delivery. *Prog. Polym. Sci.* **2008**, *33*, 1088–1118.

(22) Scarpa, J. S.; Mueller, D. D.; Klotz, I. M. Slow hydrogen-deuterium exchange in a nonαhelical polyamide. *J. Am. Chem. Soc.* **1967**, *89*, 6024–6030.

(23) Schild, H. G. Poly(*N*-isopropylacrylamide): experiment, theory and application. *Prog. Polym. Sci.* **1992**, *17*, 163–249.

(24) Lutz, J.-F.; Weichenhan, K.; Akdemir, Ö.; Hoth, A. About the Phase Transitions in Aqueous Solutions of Thermoresponsive Copolymers and Hydrogels Based on 2-(2-methoxyethoxy)ethyl Methacrylate and Oligo(ethylene glycol) Methacrylate. *Macromolecules* **2007**, *40*, 2503–2508.

(25) Sugihara, S.; Hashimoto, K.; Okabe, S.; Shibayama, M.; Kanaoka, S.; Aoshima, S. Stimuli-Responsive Diblock Copolymers by Living Cationic Polymerization: Precision Synthesis and Highly Sensitive Physical Gelation. *Macromolecules* **2004**, *37*, 336–343.

(26) Han, S.; Hagiwara, M.; Ishizone, T. Synthesis of Thermally Sensitive Water-Soluble Polymethacrylates by Living Anionic Polymerizations of Oligo(ethylene glycol) Methyl Ether Methacry-lates. *Macromolecules* **2003**, *36*, 8312–8319.

(27) Ali, M. M.; Stöver, H. D. H. Well-Defined Amphiphilic Thermosensitive Copolymers Based on Poly(ethylene glycol monomethacrylate) and Methyl Methacrylate Prepared by Atom Transfer Radical Polymerization. *Macromolecules* **2004**, *37*, 5219–5227.

(28) Kitano, H.; Hirabayashi, T.; Gemmei-Ide, M.; Kyogoku, M. Effect of Macrocycles on the Temperature-Responsiveness of Poly[(methoxy diethylene glycol methacrylate)-graft-PEG]. *Macromol. Chem. Phys.* **2004**, *205*, 1651–1659.

(29) Zhang, D.; Macias, C.; Ortiz, C. Synthesis and Solubility of (Mono-) End-Functionalized Poly(2-hydroxyethyl methacrylate- g -ethylene glycol) Graft Copolymers with Varying Macromolecular Architectures. *Macromolecules* **2005**, *38*, 2530–2534.

(30) Lutz, J.-F. Polymerization of oligo(ethylene glycol) (meth)acrylates: Toward new generations of smart biocompatible materials. *J. Polym. Sci. Pol. Chem.* **2008**, *46*, 3459–3470.

(31) Lutz, J.-F.; Akdemir, O.; Hoth, A. Point by point comparison of two thermosensitive polymers exhibiting a similar LCST: is the age of poly(NIPAM) over? *J. Am. Chem. Soc.* **2006**, *128*, 13046–13047.

(32) Skandalis, A.; Pispas, S. PLMA-*b*-POEGMA amphiphilic block copolymers: Synthesis and self-assembly in aqueous media. *J. Polym. Sci. Pol. Chem.* **2017**, *55*, 155–163.

(33) Karatza, A.; Pispas, S. Poly(hydroxyl propyl methacrylate)- *b* -Poly(oligo ethylene glycol methacrylate) Thermoresponsive Block Copolymers by RAFT Polymerization. *Macromol. Chem. Phys.* **2018**, *219*, 1800060.

(34) Folkers, J. P.; Gorman, C. B.; Laibinis, P. E.; Buchholz, S.; Whitesides, G. M.; Nuzzo, R. G. Self-assembled monolayers of long-chain hydroxamic acids on the native oxides of metals. *Langmuir* **1995**, *11*, 813–824. (35) Winston, A.; Kirchner, D. Hydroxamic Acid Polymers. Effect of Structure on the Selective Chelation of Iron in Water. *Macromolecules* **1978**, *11*, 597–603.

(36) Winston, A.; McLaughlin, G. R. Hydroxamic acid polymers. II. Design of a polymeric chelating agent for iron. *J. Polym. Sci. Pol. Chem.* **1976**, *14*, 2155–2165.

(37) Winston, A.; Mazza, E. T. Hydroxamic acid polymers. *J. Polym. Sci. Pol. Chem.* **1975**, *13*, 2019–2030.

(38) Rahman, M. L.; Sarkar, S. M.; Yusoff, M. M.; Abdullah, M. H. Optical detection and efficient removal of transition metal ions from water using poly(hydroxamic acid) ligand. *Sens. Actuators, B* **2017**, *242*, 595–608.

(39) Mello, R. S.; Orth, E. S.; Loh, W.; Fiedler, H. D.; Nome, F. Polymers containing hydroxamate groups: nanoreactors for hydrolysis of phosphoryl esters. *Langmuir* **2011**, *27*, 15112–15119.

(40) Keth, J.; Johann, T.; Frey, H. Hydroxamic Acid: An Underrated Moiety? Marrying Bioinorganic Chemistry and Polymer Science. *Biomacromolecules* **2020**, *21*, 2546–2556.

(41) Johann, T.; Kemmer-Jonas, U.; Barent, R. D.; Frey, H. Multifunctional Fe(III)-Binding Polyethers from Hydroxamic Acid-Based Epoxide Monomers. *Macromolecular rapid communications* **2020**, *41*, e1900282.

(42) Johann, T.; Keth, J.; Bros, M.; Frey, H. A general concept for the introduction of hydroxamic acids into polymers. *Chem. Sci.* **2019**, *10*, 7009–7022.

(43) Prozeller, D.; Morsbach, S.; Landfester, K. Isothermal titration calorimetry as a complementary method for investigating nanoparticle-protein interactions. *Nanoscale* **2019**, *11*, 19265–19273.

(44) Parker, M. H.; Lunney, E. A.; Ortwine, D. F.; Pavlovsky, A. G.; Humblet, C.; Brouillette, C. G. Analysis of the binding of hydroxamic acid and carboxylic acid inhibitors to the stromelysin-1 (matrix metalloproteinase-3) catalytic domain by isothermal titration calorimetry.*Biochemistry* **1999**, *38*, 13592–13601.

(45) Harty, M.; Bearne, S. L. Measuring benzohydroxamate complexation with Mg^{2+}, Mn^{2+}, Co^{2+}, and Ni^{2+} using isothermal titration calorimetry. *J. Therm. Anal. Calorim.* **2016**, *123*, 2573–2582.

(46) Zhang, Q.; Weber, C.; Schubert, U. S.; Hoogenboom, R. Thermoresponsive polymers with lower critical solution temperature: from fundamental aspects and measuring techniques to recommended turbidimetry conditions. *Mater. Horiz.* **2017**, *4*, 109–116.

(47) Ishizone, T.; Seki, A.; Hagiwara, M.; Han, S.; Yokoyama, H.; Oyane, A.; Deffieux, A.; Carlotti, S. Anionic Polymerizations of Oligo(ethylene glycol) Alkyl Ether Methacrylates: Effect of Side Chain Length and ω-Alkyl Group of Side Chain on Cloud Point in Water. *Macromolecules* **2008**, *41*, 2963–2967.

(48) Maeda, Y.; Kubota, T.; Yamauchi, H.; Nakaji, T.; Kitano, H. Hydration changes of poly(2-(2-methoxyethoxy)ethyl methacrylate) during thermosensitive phase separation in water. *Langmuir* **2007**, *23*, 11259–11265.

(49) Porsch, C.; Hansson, S.; Nordgren, N.; Malmström, E. Thermo-responsive cellulose-based architectures: tailoring LCST using poly(ethylene glycol) methacrylates. *Polym. Chem.* **2011**, *2*, 1114.

(50) Garcia-Valls, R.; Hatton, T. A. Metal ion complexation with lignin derivatives. *Chem. Eng. J.* **2003**, *94*, 99–105.

SUPPORTING INFORMATION

Materials

All reagents were used without further purification, unless otherwise stated. All chemicals and solvents were purchased from Abcr, Acros, Aldrich, Fisher Scientific, Fluka, Riedel-de-Haën or Roth. Deuterated solvents were purchased from Deutero GmbH. If not mentioned the compounds were used as received.

Instrumentation

NMR analysis. ^{1}H NMR spectra at 300 MHz and ^{13}C NMR spectra at 75 MHz were recorded on a Bruker Avance III HD 300 (5 mm BBFO-Head with z-gradient) at 23 °C. ^{1}H NMR spectra at 400 MHz and ^{13}C NMR spectra at 100 MHz were recorded on a Bruker Avance III HD 400 (5 mm BBFO-Smartprobe with z-gradient) at 23 °C. All NMR spectra were referenced to the residual proton signals of the deuterated solvent.

Size exclusion chromatography (SEC). SEC was performed in DMF (1 mL/min, 50 °C) containing 1 g/L lithium bromide as additive. An Agilent 1100 series SEC system including a HEMA 300/100/40 Å column cascade, an UV (254 nm) and a RI detector was used. Furthermore, SEC was performed in THF (1 mL/min, 20 °C) containing 1 g/L lithium bromide as additive. A MZ-gel SD plus column, an UV (254 nm) and a RI detector was used. Calibration was carried out using P(MMA) standards provided by Polymer Standard Service (PSS).

Cloud point temperature measurements. Cloud points were determined with a JASCO V-630 spectrophotometer with a light source fixed at 600 nm. The samples were prepared in deionized water at a concentration of 2.5 mg mL^{-1}. The cloud point temperature was determined at 50 % of the initial transmittance.

Isothermal titration calorimetry. The calorimetric measurements were performed using a NanoITC Low Volume (TA Instruments, Eschborn, Germany) with an effective cell volume of 170 µL. In an experiment 50 µL of an $FeCl_3$ solution (0.152 mM) were titrated to a suspension of MAHA (0.02 mM) in water. The experimental temperature was kept constant at 25 °C. Additionally the same amount of $FeCl_3$ solution was titrated into pure water to determine the heat of dilution for reference. The number and injected volume of the titration steps were the same for all measurements (25 x 2 µL). The spacing between injections was set to 300 s. The measure-

ments were carried out by triplicate, showing the mean value together the standard deviation for each parameter. Nano Analyze Data Analysis software from TA Instruments was used for the data evaluation of the ITC measurements (Software version 2.5.0) from TA instruments.

Metabolic activity. Murine spleen cells (10^7/mL) were seeded in wells (each 100 μL) of 96 well cell culture plates. Afterwards, polymer formulations and DMSO at cytotoxic concentration (10 %) were applied as indicated. One day later, metabolic activity was assayed using chromogenic MTT assay reagent as recommended by the manufacturer (Promega, Madison, WI).

EXPERIMENTAL SECTION

RAFT copolymerization of OEGMEMA and MAHAA (P(OEGMEMA-*co*-MAHAA)).
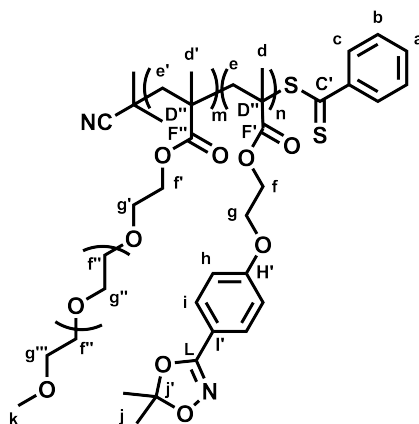
In a 10 mL Schlenk tube 1200 mg (4.00 mmol, 45eq) OEGMEMA, 135.7 mg (0.44 mmol, 5eq) MAHAA, 19.67 mg (0.09 mmol, 1eq) CPBDT and 0.73 mg (0.01 mmol, 0.1eq) AIBN were dissolved in 2.2 mL dioxane. After three freeze pump thaw cycles the mixture was stirred for 24 h at 70 °C. After precipitation in ice cold diethylether (45 mL, -20 °C), the product was recovered by centrifugation (4500 RPM, 10 minutes).

^{1}H NMR (300 MHz, CDCl$_3$): δ [ppm] = 7.81 (*s*, ArC^{2,6}*H*, c), 7.66 (*AA'BB'*, ArC^{3,5}*H*, i), 7.49 (*s*, ArC^4*H*, a), 7.32 (*s*, ArC^{3,5}*H*, b), 6.92 (*AA'BB'*, ArC^{2,6}*H*, h), 4.35-4.17 (*s*, Ar-O-C*H$_2$*-CH$_2$, f+g), 4.17-3.97 (*s*, O-C*H$_2$*, f'), 3.67-3.56 (*s*, O-C*H$_2$*-CH$_2$-O, g'+f"+g"), 3.56-3.50 (*s*, O-C*H$_2$*, g'"), 3.40-3.34 (*s*, O-C*H$_3$*, k), 2.14-1.69 (*m*, C-C*H$_2$*, e+e'), 1.64 (*s*, *H$_3$*C-CO$_2$-C*H$_3$*, j), 1.13-0.72 (*m*, C-C*H$_3$*, d+d').

^{13}C NMR (75 MHz, CDCl$_3$): δ [ppm] = 177.15 (*C*=O, F'+F"), 176.33 (*C*=O, F'+F"), 174.45 (*C*=O, F'+F"), 128.41 (Ar*C*^{3,5}, I), 114.64 (H$_3$*C*-CO$_2$-CH$_3$, J'), 71.90 (*s*, O-*C*H$_2$, G'"), 70.55 (*s*, O-*C*H$_2$-CH$_2$-O, F"+G"), 68.47 (O-*C*H$_2$-CH$_2$-O, G'), 63.86 (O-*C*H$_2$, F'), 59.02 (O-*C*H$_3$, K), 54.09 (*C*H$_2$, E+E'), 44.76 (*C*, D"), 24.83 (H$_3$*C*-CO$_2$-CH$_3$, J), 18.30 (C-*C*H$_3$, (D+D')$_a$), 16.32 (C-*C*H$_3$, (D+D')$_{syn}$).

Deprotection of P(OEGMEMA-*co*-MAHAA).

492 mg of the polymer were dissolved in 10 mL methanol and 10 mL of a 0.1 M HCl solution. The mixture was stirred for 24 h. The solution was quenched in 75 mL DCM. The Aqueous layer was extracted with 50 mL DCM for three times. The organic layer was dried over Na$_2$SO$_4$. The solvent was removed via rotary evaporation.
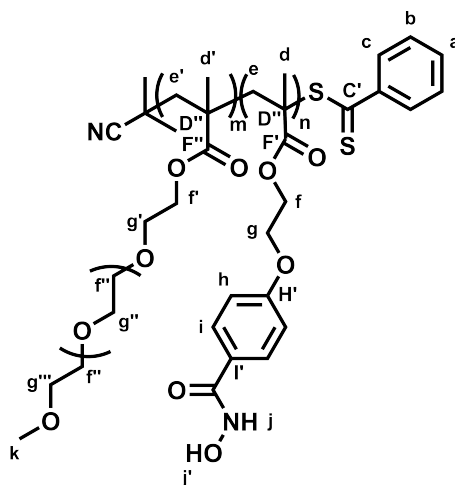
^{1}H NMR (300 MHz, DMSO-d_6): δ [ppm] = 11.06 (s, NH, j), 8.91 (s, OH, j'), 7.80 (s, ArC^{2,6}H, c), 7.72 (AA'BB', ArC^{3,5}, i), 7.63 (s, ArC^4H, a), 7.45 (s, ArC^{3,5}, b), 6.95 (AA'BB', ArC^{2,6}H, h), 4.41-4.16 (m, O-CH_2-CH_2-O, f+g), 4.13-3.82 (s, O-CH_2, f'), 3.70-3.56 (s, O-CH$_2$-CH$_2$, g'), 3.54-3.48 (s, O-CH$_2$-CH$_2$-O, f"+g"), 3.45-3.36 (s, O-CH_2, g'''), 3.28-3.14 (s, O-CH_3, k), 2.06-1.65 (m, C-CH_2, e+e'), 1.61, 1.06-0.51 (m, C-CH_3, d+d').

^{13}C NMR (75 MHz, DMSO-d_6): δ [ppm] = 177.21 (C=O, F'+F"), 176.42 (C=O, F'+F"), 129.04 (ArC^{3,5}, B), 126.63 (ArC^{2,6}, C), 125.62 (ArC^4, I'), 114.47 (ArC^{2,6}, H), 71.76 (O-CH$_2$, G'''), 70.28 (O-CH$_2$-CH$_2$-O, F"+G"), 68.27 (O-CH$_2$-CH$_2$-O, G'), 64.19 (O-CH$_2$, F'), 58.52 (O-CH$_3$, K), 55.37 (CH$_2$, E+E'), 44.54 (C, D"), 18.45 (C-CH$_3$, (D+D')$_a$), 16.63 (C-CH$_3$, (D+D')$_{syn}$).

IR-ATR $\tilde{v}$ [cm^{-1}] = 3248 (O-H, N-H), 2882 (CH$_3$), 2251 (CN), 1725 (C=O), 1606 (C=C), 1248 (C-O-C), 846 (C-H$_{Ar}$).

Sample preparation for ITC measurements.

200 mg of the deprotected polymer sample were dialyzed against Milli-Q water (MWCO = 1000 g mol^{-1}) for 24 h.

DETERMINATION OF CLOUD POINT TEMPERATURES.

Effect of the concentration.

We investigated polymer concentrations ranging from 0.5 mg mL^{-1} to 10 mg mL^{-1} to find the optimal conditions for the cloud point temperature (T_{cp}) measurements. The polymer concentration of 2.5 mg mL^{-1} revealed the sharpest thermo-induced collapse transition and was therefore used as concentration for all the following measurements (**Figure S1**). The concentration of the solution influences the cloud point temperature remarkably. Higher concentrations result in a decrease of the T_{cp}. Comparing 0.5 mg mL^{-1} with 10 mg mL^{-1}, we determined a change in the T_{cp} from more than 6 °C (**Table S1**). With concentrations higher than 5 mg mL^{-1}, we observed a reduction in the optical transmittance due to the coloring of the sample.
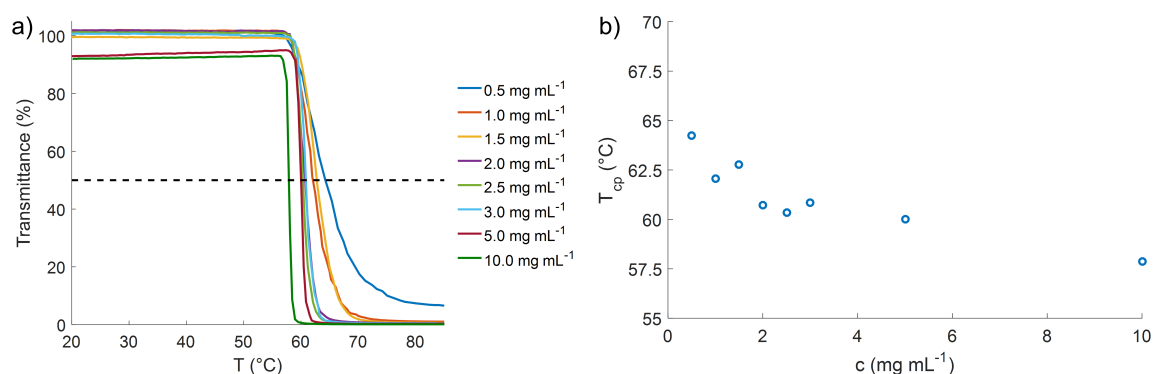
FIGURE S1 Transmittance versus temperature curves for **a)** (P(OEGMEMA$_{44}$-co-MAHAA$_3$) solution with varied concentrations. The dashed line illustrates the 50% transmittance region that was used to determine the T_{cp}.
b) Overview of different cloud point temperatures plotted versus the concentration.

TABLE S1 Experimental and interpolated cloud point temperatures for (P(OEGMEMA$_{44}$-co-MAHAA$_3$) with varied concentrations.

c [mg mL^{-1}]	$T_{cp}{}^{a}$ [°C]	$T_{cp}{}^{b}$ [°C]	Transmittance^{b} [%]
0.5	64.3	64.3	50.0
1.0	62.1	62.0	51.2
1.5	62.8	62.8	48.5
2.0	60.7	60.7	51.7
2.5	60.3	60.4	46.5
3.0	60.9	60.9	49.2
5.0	60.0	60.1	47.5
10	57.9	58.1	32.3

a. T_{cp} was interpolated at 50% of the inital transmittance. **b.** T_{cp} as a data point to the corresponding transmittance^{b}.

Effect of the heating rate.

The impact of the heating rate on the T_{cp} was investigated by screening 1, 3, 5, 8 and 10 °C min^{-1} using 0.5 mg mL^{-1} and 2.5 mg mL^{-1} as concentrations (**Figure S2**). We observed no significant deviations in the T_{cp} (<1 °C) for the different heating rates at 2.5 mg mL^{-1}. For a polymer concentration of 0.5 mg mL^{-1}, we observed a considerable effect of the heating rate on the cloud point temperatures (>3 °C) (**Table S2**). Thus, we used polymer concentrations of 2.5 mg mL^{-1} for further investigations.
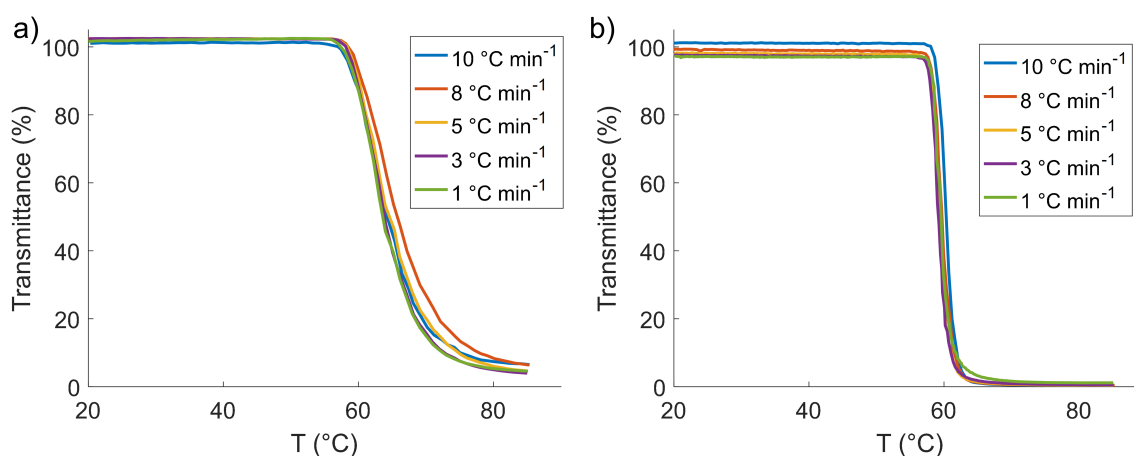
FIGURE S2 Transmittance versus temperature curves for a (P(OEGMEMA$_{44}$-co-MAHAA$_3$) solution with varied heating rates in a concentration of **a)** 0.5 mg mL^{-1} and **b)** 2.5 mg mL^{-1}.

TABLE S2 Experimental and interpolated cloud point temperatures for (P(OEGMEMA$_{44}$-co-MAHAA$_3$) with a concentration of 0.5 mg mL^{-1} respectively 2.5 mg mL^{-1} at varied heating rates.

c [mg mL^{-1}]	Heating rate [°C min^{-1}]	$T_{cp}{}^a$ [°C]	$T_{cp}{}^b$ [°C]	Transmittance[b] [%]
0.5	1	63.6	64.0	45.8
0.5	3	63.9	64.0	47.9
0.5	5	64.6	65.3	46.2
0.5	8	65.8	66.2	47.3
0.5	10	64.3	64.3	50.0
2.5	1	59.6	59.6	45.8
2.5	3	59.2	59.3	47.7
2.5	5	59.3	59.3	49.6
2.5	8	59.7	59.6	52.7
2.5	10	60.3	60.4	46.5

a. T_{cp} was interpolated at 50% of the inital transmittance. **b.** T_{cp} as a data point to the corresponding transmittance[b].

The effect of the heating rate has been shown for two different concentrations. At both concentrations, the cloud point temperature increases with the heating rate (**Figure S3**).
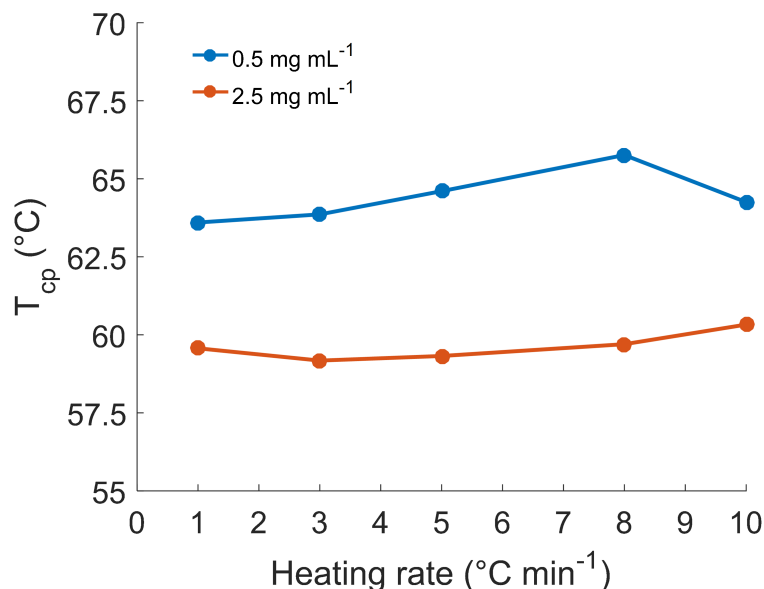
FIGURE S3   Cloud point temperatures in dependence on the heating rate for P(OEGMEMA$_{44}$-*co*-MAHAA$_3$) solutions with concentrations of 0.5 mg mL^{-1} (**blue**) and 2.5 mg mL^{-1} (**red**), respectively.

Effect of the molecular weight.

We investigated the influence of the molecular weight on the cloud point temperature by comparing the homopolymers P(OEGMEMA)$_{17}$, P(OEGMEMA)$_{20}$ and P(OEGMEMA)$_{29}$. The cloud point temperatures increased from 49.7 °C to 67.5 °C with decreasing molecular weights (**Figures S4a** and **S5**). This observation suggests that the longer polymer chains facilitate the formation of inter- and intramolecular aggregation at lower temperatures.[1] In literature, several cloud point temperatures of P(OEGMEMA) were reported. The T_{cp} were in a range between 64 °C and 68 °C and depends besides the molecular weight also strongly on the polymer concentration, the heating rate, the wavelength of the incident light, the cuvette type and the stirring process.[2–6]
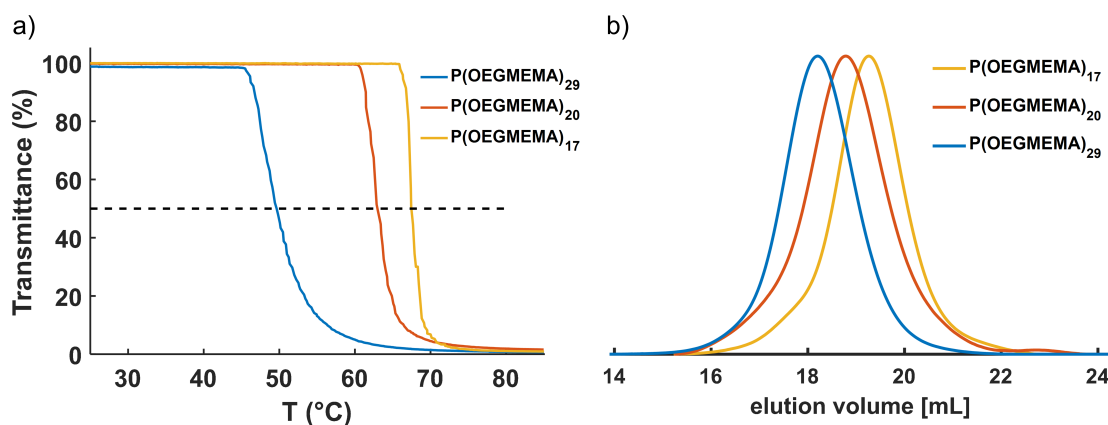
FIGURE S4 **a)** Transmittance as a function of temperature for the homopolymers P(OEGMEMA)$_{29}$ (**blue**) and P(OEGMEMA)$_{20}$ (**red**) and P(OEGMEMA)$_{17}$ (**yellow**). The solutions were prepared with a concentration of 2.5 mg mL^{-1}, all measurements were carried out using a heating rate of 1 °C min^{-1}. **b)** Corresponding SEC traces of the homopolymers (DMF as solvent, PMMA calibration, RI detector) are shown.

Figure S5 shows the linear correlation between the cloud point temperature and the molecular weight of various P(OEGMEMA) samples. A linear fit was used (y = -0.005171x + 94.52) for illustration. Based on this linear fit and as a first estimation, cloud point temperatures may be predicted according to their molecular weight (**Eq.1**).

$$T_{cp} = 94.52 \,°\mathrm{C} - 0.005171 \frac{\mathrm{mol}}{\mathrm{g}} \cdot M_n \,(\mathrm{P(OEGMEMA)}) \tag{1}$$
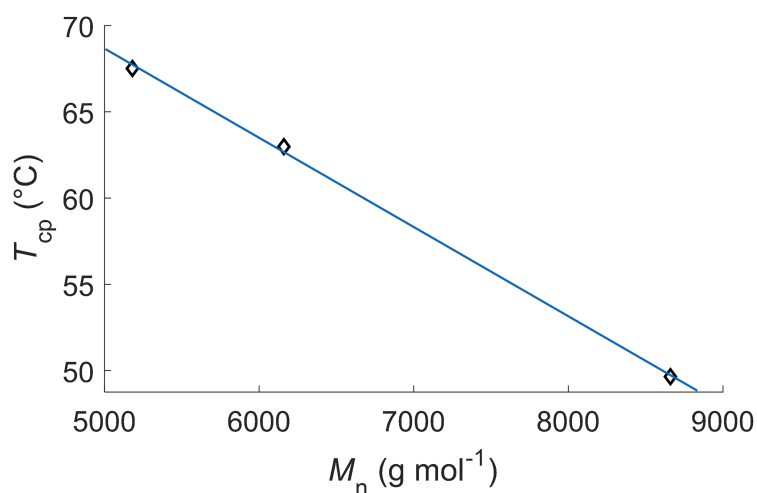
FIGURE S5 Cloud point temperatures as a function of the molecular weight. A linear fit was used (y = -0.005171x + 94.52).

Effect of the MAHAA content.

We investigate the effect of different polymer compositions by varying the MAHAA content in P(OEGMEMA-*co*-MAHAA) polymers with similar molecular weights (**Figure S6b**). With an increase of the MAHAA content from 10 to 33%$_{mol}$, we observed a significant decrease in the T_{cp} of the copolymer from 47.9 °C to 25.9 °C. Due to the hydrogen bond formation of the hydrophilic OEGMEMA, the polymer is in a single phase state (*i.e.* hydrated). The incorporation of MAHAA interrupts the polymer hydration that leads to a collapsed aggregated state which is achieved at lower temperatures, visible with the turbidity of the solution.
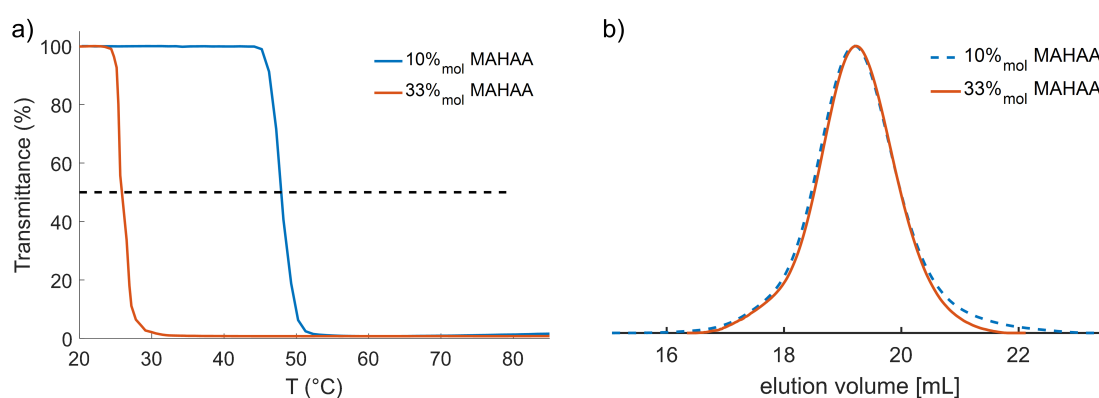
FIGURE S6 **a)** Transmittance as a function of temperature for the copolymers containing 10 (blue) and 33%$_{mol}$ MAHAA (red) respectively. The solutions were prepared with a concentration of 2.5 mg mL^{-1}, both measurements were carried out using a heating rate of 10 °C min^{-1}. The dashed line illustrates the 50% transmittance region that was used to determine the T_{cp}. **b)** Corresponding SEC traces of the copolymers (DMF as solvent, PMMA calibration, RI detector) are shown.

Effect of deprotection.

We studied the effect of deprotection on the cloud point temperature for hydroxamic acid-functionalized copolymers. The cloud point temperatures for P(OEGMEMA$_{33}$-*co*-MAHAA$_{18}$) and the deprotected specie P(OEGMEMA$_{33}$-*co*-MAHAA$_{18}$) were determined (**Figure S7**). By removing the protecting group, the cloud point temperature increased from 25.9 °C to 32.5 °C. While the hydrophilicity of the copolymer increases with the degree of deprotection, the hydration of the polymer chains is enhanced which leads to higher cloud point temperatures.
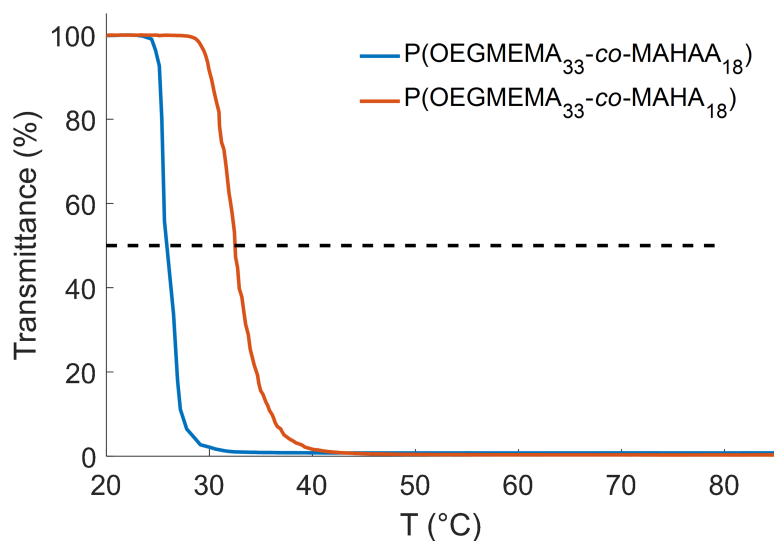
FIGURE S7 Transmittance as a function of temperature for the copolymers P(OEGMEMA$_{33}$-*co*-MAHAA$_{18}$) (blue) and the corresponding deprotected copolymer P(OEGMEMA$_{33}$-*co*-MAHAA$_{18}$) (red) respectively. The solutions were prepared with a concentration of 2.5 mg mL^{-1}, both measurements were carried out using a heating rate of 10 °C min^{-1}. The dashed line illustrates the 50% transmittance region that was used to determine the T_{cp}.

Hysteresis behavior.

The polymer solutions were heated with a constant heating rate of 1 °C min^{-1}. The optical transmittance was followed during the heating and cooling processes. At 50% of the initial transmittance, we defined the cloud point temperature (dashed line in **Figure S8**). By comparing the heating and cooling curves, we observed only small changes in the cloud point temperature (<2 °C).
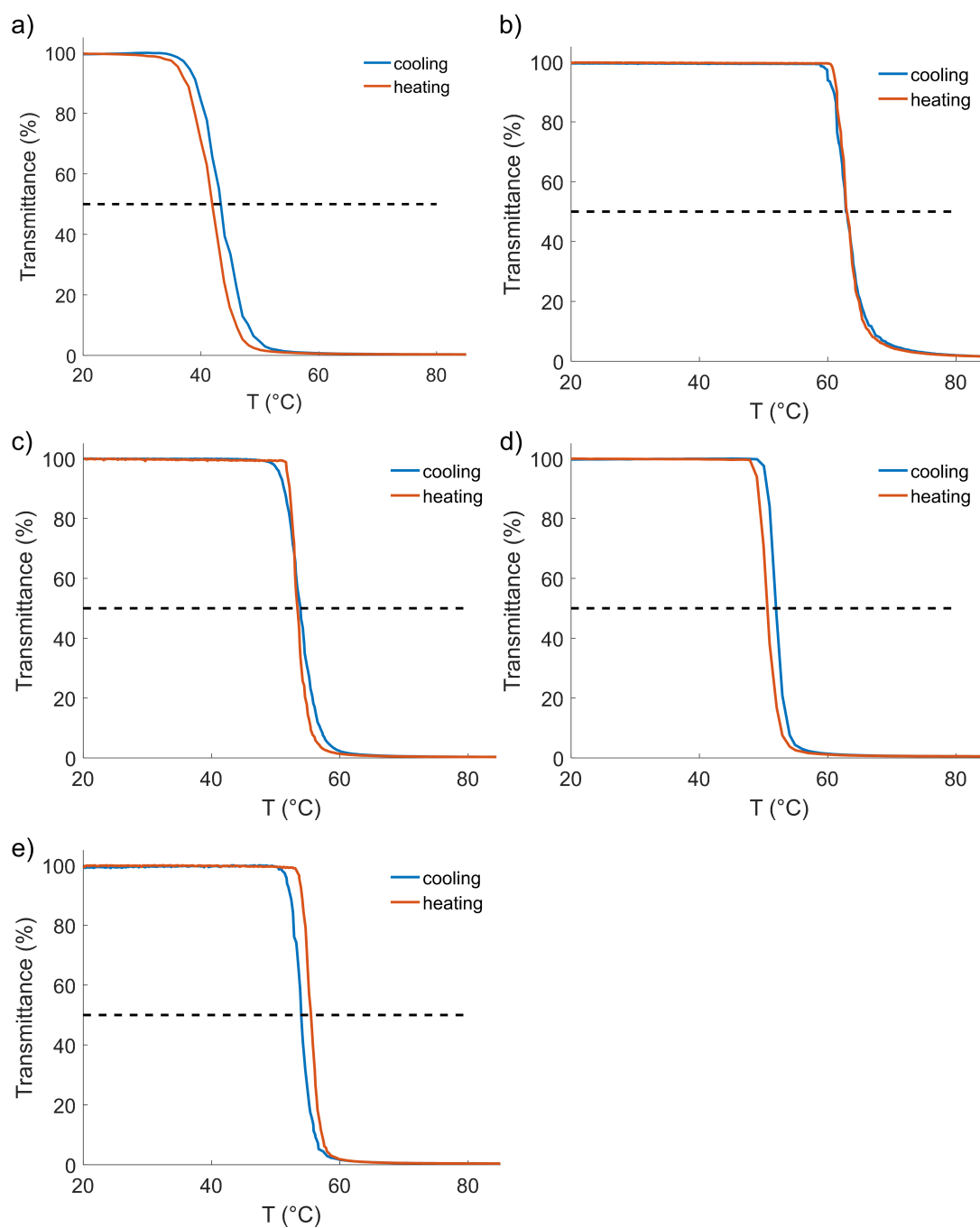
FIGURE S8   Transmittance versus temperature curves for **a)** (P(OEGMEMA$_{21}$-*co*-MAHAA$_2$), **b** P(OEGMEMA)$_{23}$, **c)** P(OEGMEMA)$_{23}$-*b*-P(MAHAA)$_3$, **d)** (P(OEGMEMA$_{37}$-*co*-MAHAA$_3$) and **e)** (P(OEGMEMA$_{37}$-*co*-MAHA$_3$) during heating and cooling processes.

ISOTHERMAL TITRATION CALORIMETRY.

Isothermal titration calorimetry gives access to thermodynamic parameters such as enthalpy ΔH, entropy ΔS and the Gibbs free energy ΔG. The titrations were carried out at 25 °C. The association constant K_a was determined from the curve's slope at its inflection point and the stoichiometry n is determined as inflection point of the curve (**Figure S9**). The Gibbs energy was calculated using **Eq. 2**. The enthalpy ΔH is the difference between the two plateaus illustrated with dashed lines (**Figure S9**). With the Gibbs-Helmholtz equation, the entropy ΔS was determined (**Eq. 3**).[7,8] Different P(OEGMEMA$_{37}$-co-MAHA$_3$) concentration $1 \cdot 10^{-5}$, $2 \cdot 10^{-5}$ and $3 \cdot 10^{-5}$ M were measured, and each concentration was carried out in triplicate (**Figures S10-S12**).

$$\Delta G = -\mathrm{R}T \cdot \ln K_a \qquad (2)$$

$$\Delta G = \Delta H - T\Delta S \qquad (3)$$
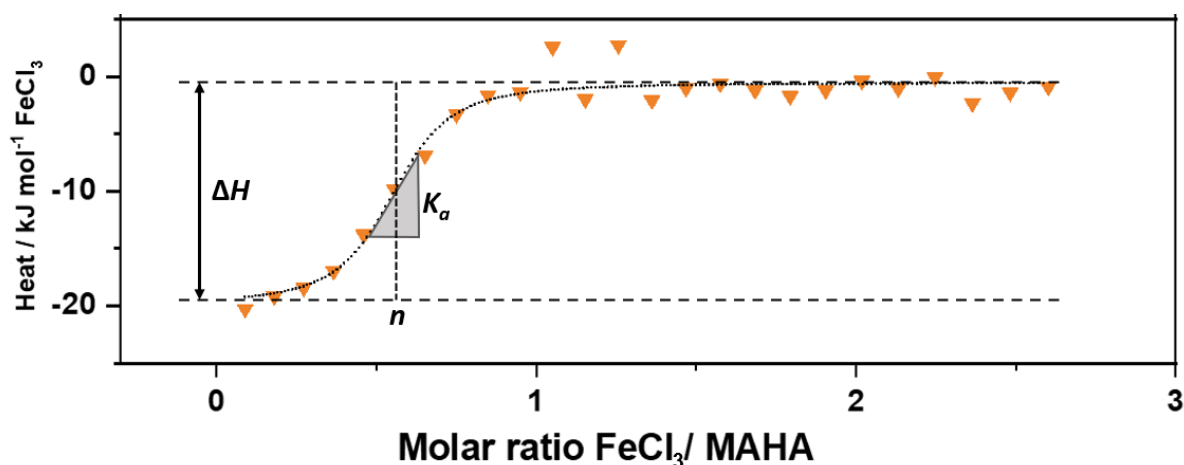
FIGURE S9 ITC data from the measurement of P(OEGMEMA$_{37}$-co-MAHA$_3$) titrated with Fe^{3+}.
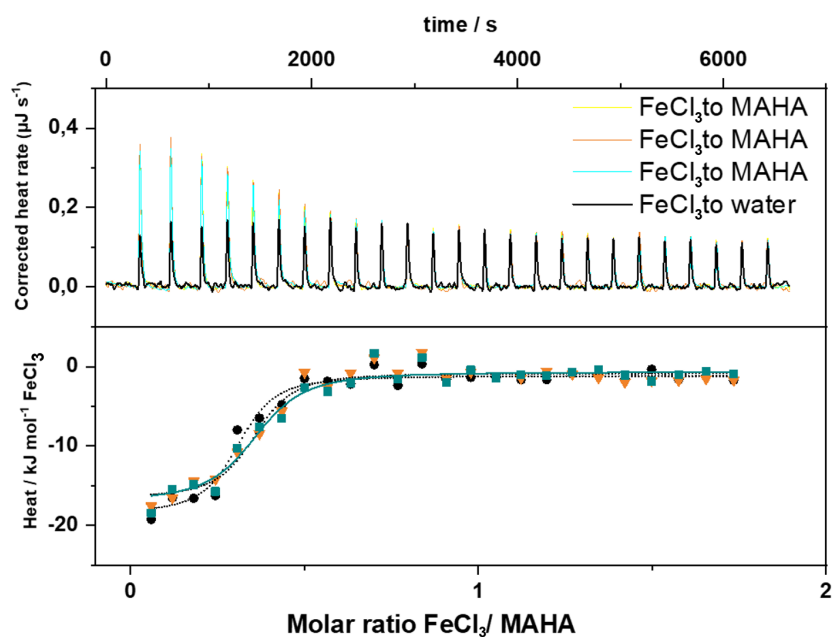
FIGURE S10 Adsorption isotherms of a P(OEGMEMA$_{37}$-*co*-MAHA$_3$) solution with a concentration of $3 \cdot 10^{-5}$ M titrated with FeCl$_3$ together with the corresponding independent binding fits carried out in triplicate. The stoichiometry found was $n_{FeCl3/MAHA}$ = 0.3 ± 0.02.
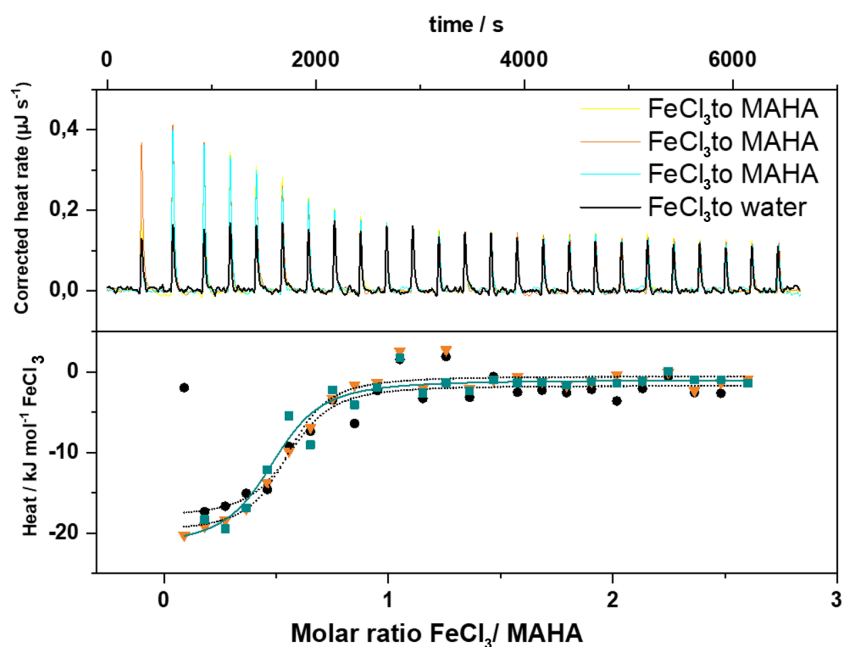
FIGURE S11 Adsorption isotherms of a P(OEGMEMA$_{37}$-*co*-MAHA$_3$) solution with a concentration of $2 \cdot 10^{-5}$ M titrated with FeCl$_3$ together with the corresponding independent binding fits carried out in triplicate. The stoichiometry found was $n_{FeCl3/MAHA}$ = 0.5 ± 0.03.
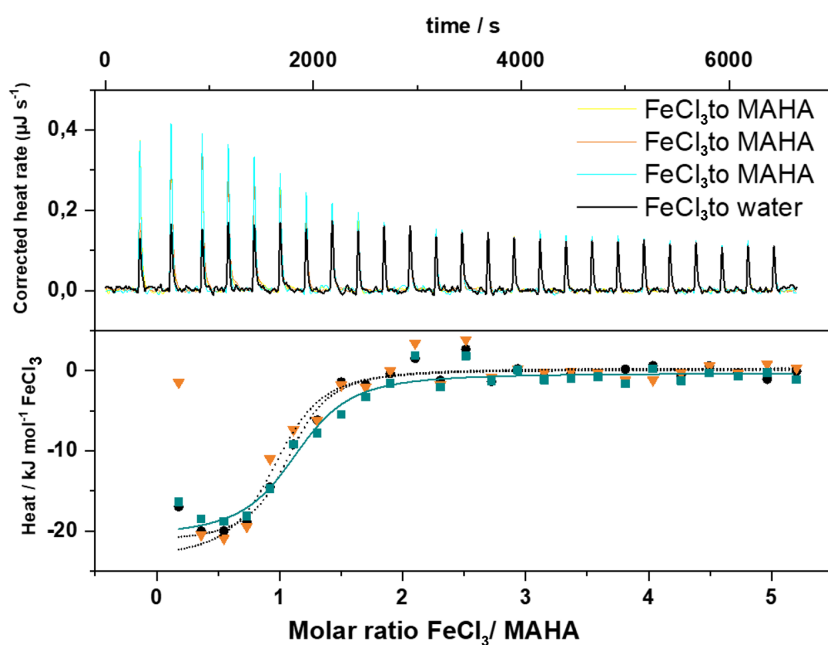
FIGURE S12 Adsorption isotherms of a P(OEGMEMA$_{37}$-*co*-MAHA$_3$) solution with a concentration of $1 \cdot 10^{-5}$ M titrated with FeCl$_3$ together with the corresponding independent binding fits carried out in triplicate. The stoichiometry found was $n_{\text{FeCl3/MAHA}}$ = 1.0 ± 0.1.

TABLE S3 Experimental values obtained from ITC measurement for the reaction of P(OEGMEMA$_{37}$-*co*-MAHA$_3$) with Fe(III) at different concentrations.

K_d [M]	K_a [M^{-1}]	ΔH [KJ mol^{-1}]	ΔS [J mol^{-1} K^{-1}]	ΔG [KJ mol^{-1}]	n [Fe/MAHA]	c [mol L^{-1}]
$(3.3\pm0.7) \cdot 10^{-7}$	$(3.1\pm0.6) \cdot 10^6$	-16.5±0.6	68.8±2.8	-37.0±0.5	0.3±0.02	$3 \cdot 10^{-5}$
$(3.9\pm0.9) \cdot 10^{-7}$	$(2.6\pm0.6) \cdot 10^6$	-18.8±1.8	59.7±7.4	-36.6±0.5	0.5±0.03	$2 \cdot 10^{-5}$
$(3.8\pm0.8) \cdot 10^{-7}$	$(2.8\pm0.6) \cdot 10^6$	-22.0±1.3	49.4±5.0	-36.6±0.6	1.0±0.1	$1 \cdot 10^{-5}$

Iron removal from water.

To quantify the iron concentration after the treatment with hydroxamic acid-functionalized polymers, samples were taken at different times and analyzed by AAS (**Figure S13b**) and UV-Vis spectroscopy (**Figures S14a** and **b**).

a)

b)
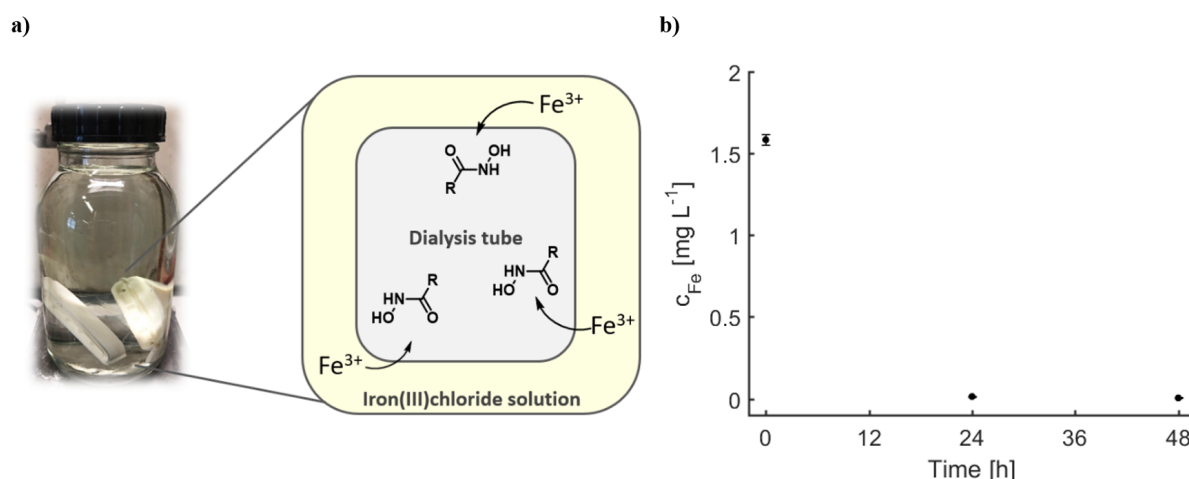
FIGURE S13 **a)** Schematic drawing of the experimental setup: Hydroxamic acid-functionalized polymer containing dialysis tube surrounded by an Fe(III) chloride solution. **b)** Time dependent reduction of Fe(III) ions after the treatment with P(OEGMEMA$_{32}$-*co*-MAHA$_{20}$). Concentrations were determined via atomic absorption spectroscopy.

Furthermore, UV-Vis spectroscopy was utilized as a second method to quantify the Fe(III) concentration. Ascorbic acid was used to reduce Fe(III) to Fe(II). After the addition of ferrozine, the complexation reaction was followed via UV-Vis spectroscopy due to a strong absorption of the ferrozine-iron complex at 562 nm (**Figure S14a**). According to the calibration concentration of 1.4 mg L^{-1}, the concentrations of the different samples were determined and plotted against the time (**Figure S14b**).

a)

b)
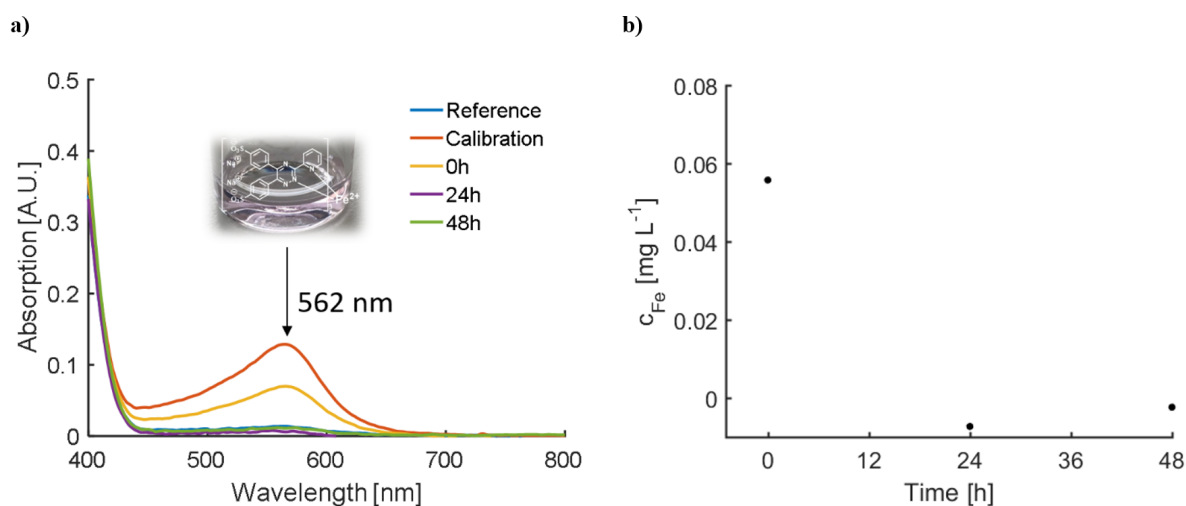
FIGURE S14 **a)** Absorption changes of different Fe(II)-ferrozine complexes depending on their concentration. **b)** Time dependent reduction of Fe(II). Complete removal of iron after 24 h detected.

With both methods, a complete iron removal after 24 h was shown (**Table S4**).

TABLE S4 Overview of the iron concentration after the treatment with hydroxamic acid-functionalized polymers determined by AAS and UV-Vis spectroscopy.

Time [h]	0	24	48
c [mg L^{-1}][a]	1.527 ± 0.033	0.013 ± 0.003	0.004 ± 0.003
c [mg L^{-1}][b]	0.6070	-0.0798	-0.0259

a. determined by AAS, **b.** determined by UV-Vis spectroscopy.

CHARACTERIZATION.
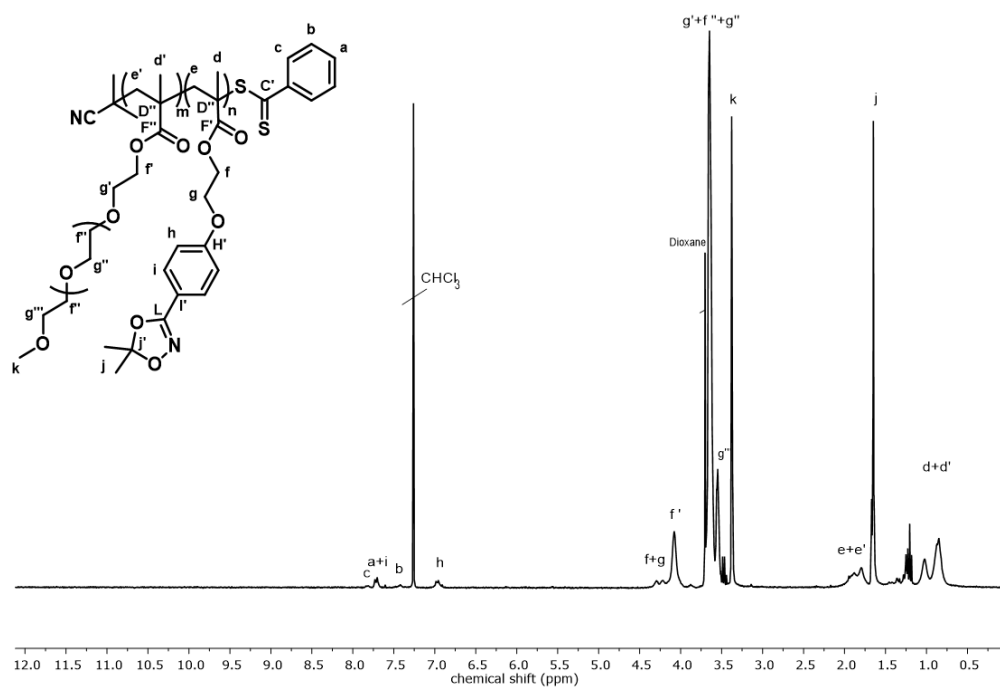
FIGURE S15 ^{1}H NMR spectrum of P(OEGMEMA-*co*-MAHAA) (300 MHz, CDCl$_3$).
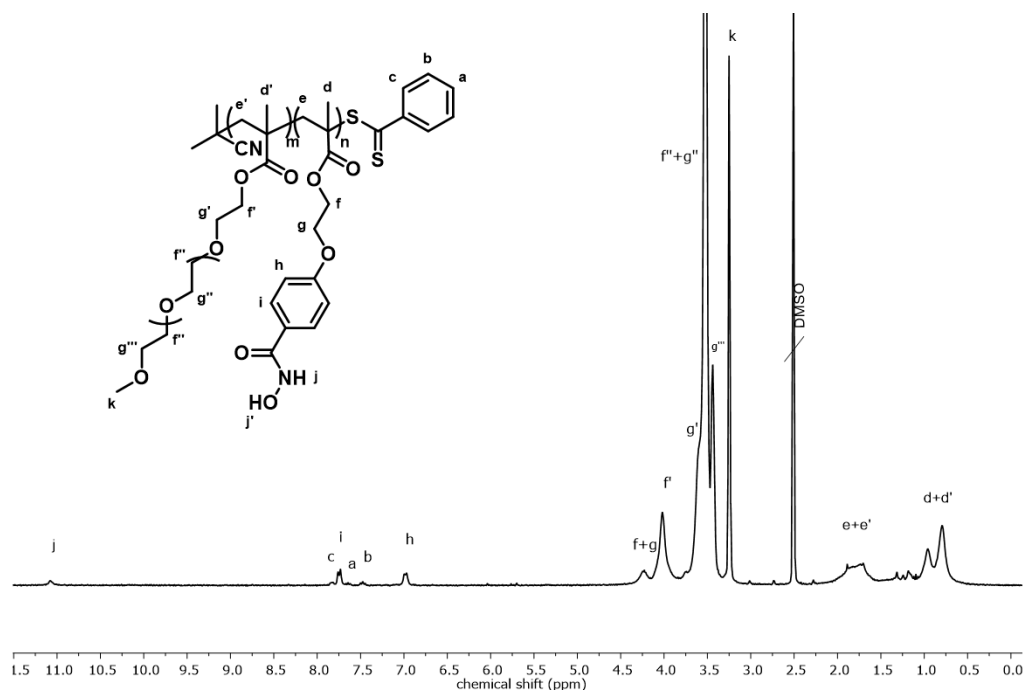
FIGURE S16 ^{1}H NMR spectrum of P(OEGMEMA-*co*-MAHA) (300 MHz, DMSO-d_6).
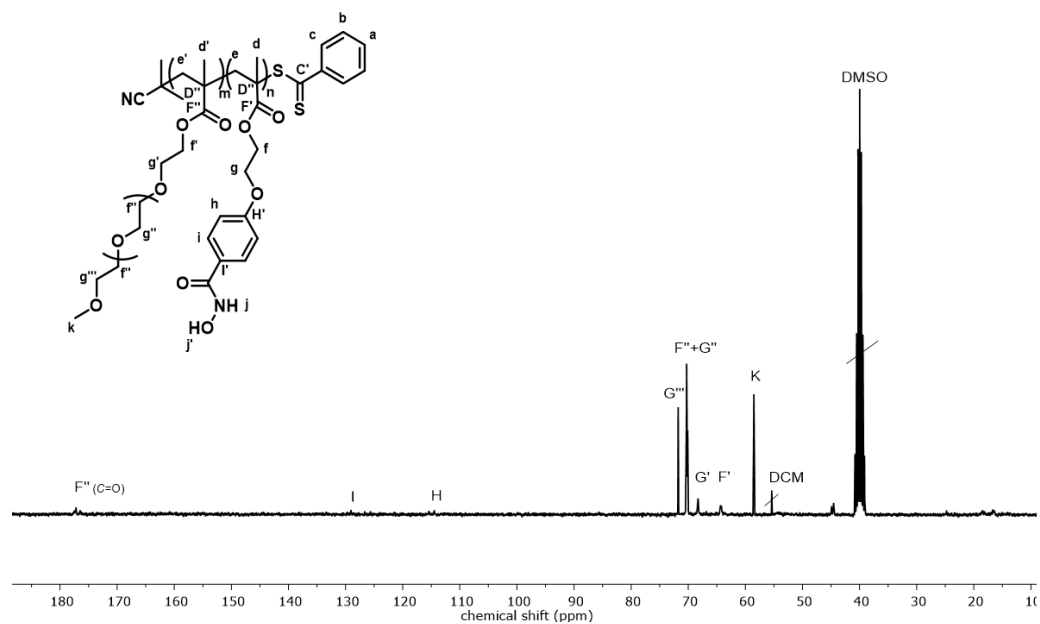
FIGURE S17 ^{13}C NMR spectrum of P(OEGMEMA-*co*-MAHA) (75 MHz, DMSO-d_6).
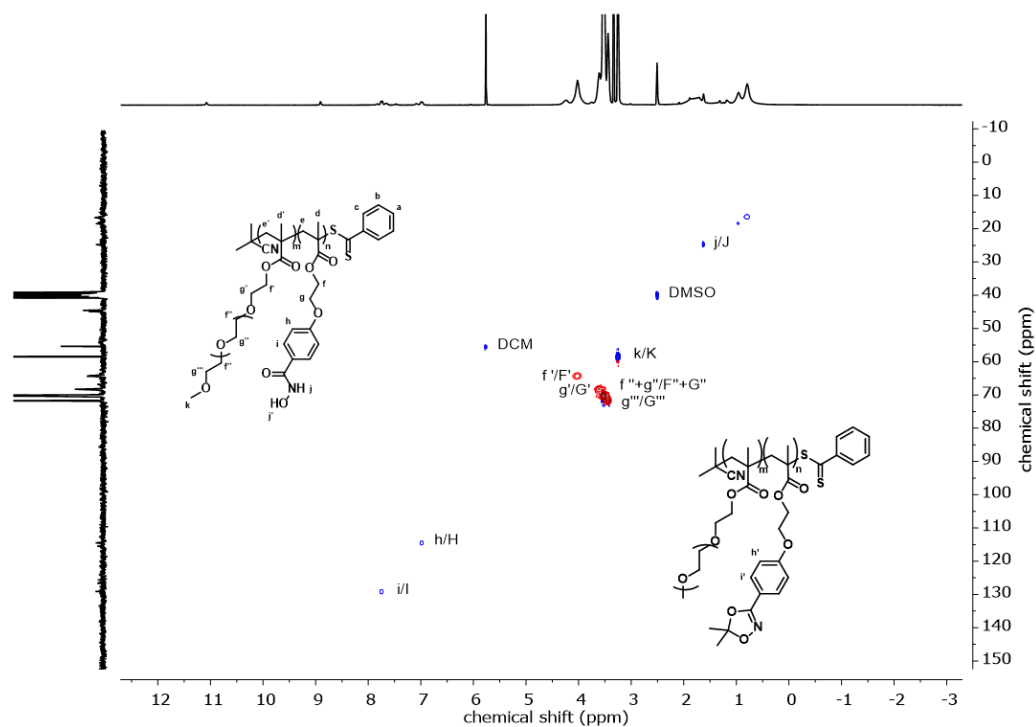
FIGURE S18 ^{1}H-^{13}C HSQC NMR spectrum of P(OEGMEMA-*co*-MAHA) (300 MHz, 75 MHz, DMSO-d_6).
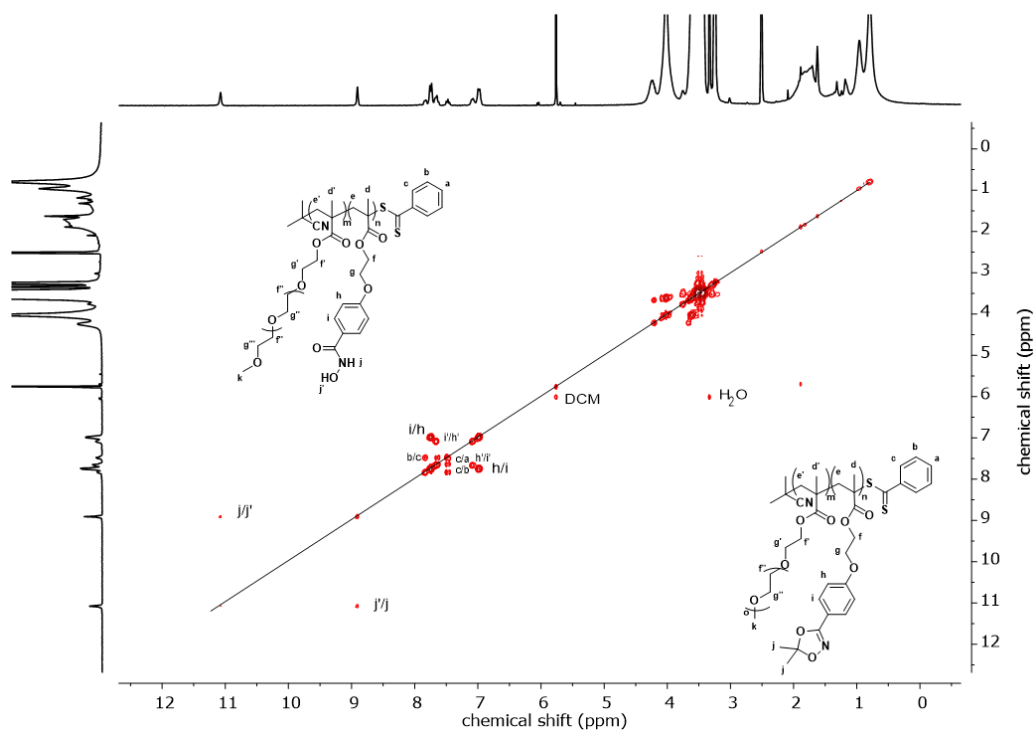
FIGURE S19 ^{1}H-^{13}C HMBC NMR spectrum of P(OEGMEMA-*co*-MAHA) (300 MHz, 75 MHz, DMSO-d_6).
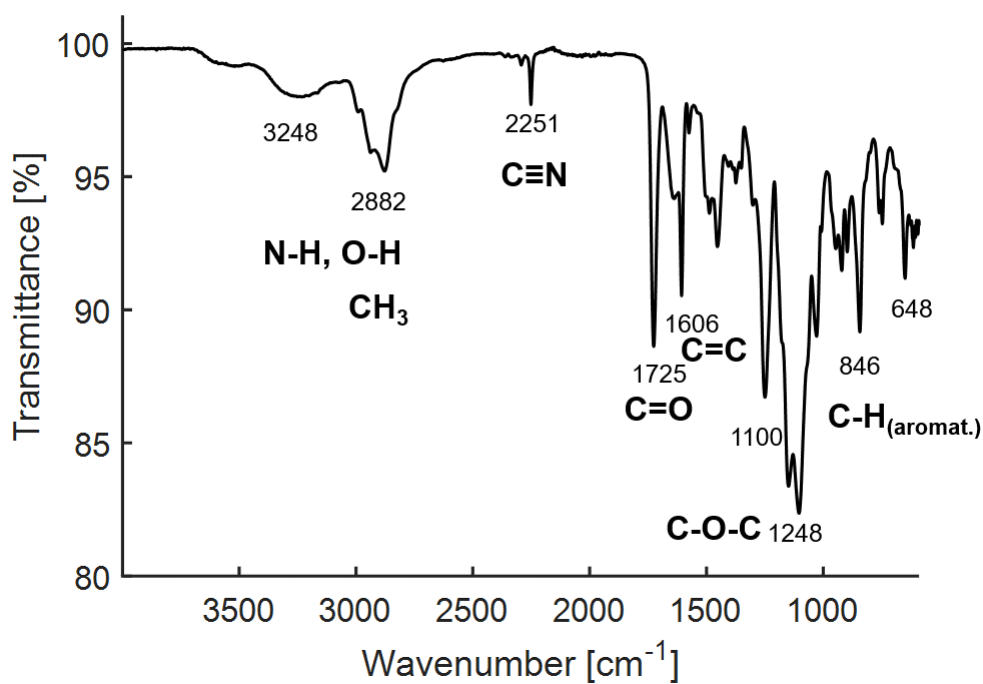
FIGURE S20   FT-ATR-IR spectrum of P(OEGMEMA-co-MAHA).
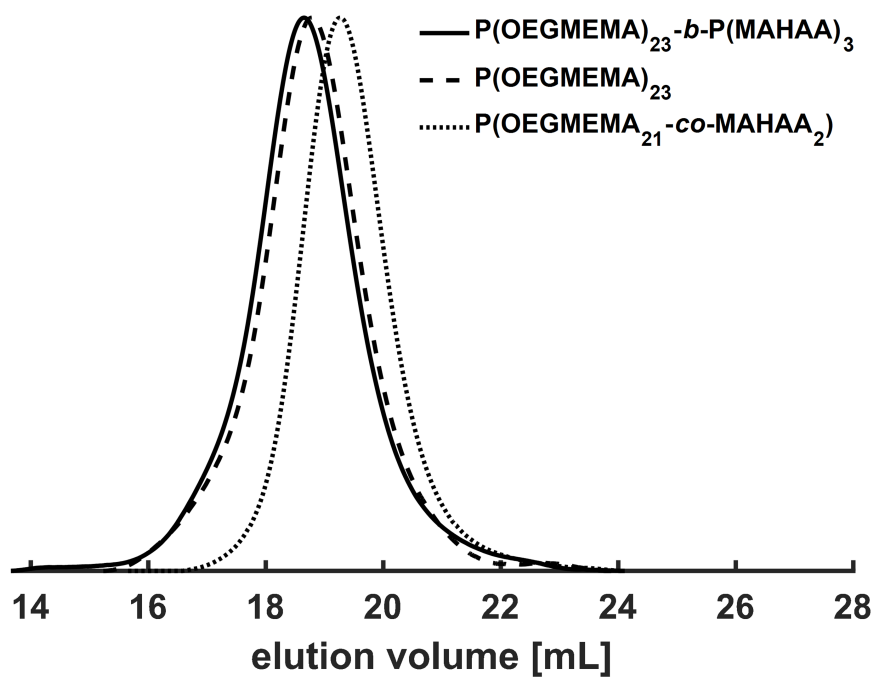
FIGURE S21 SEC traces of P(OEGMEMA)$_{23}$, P(OEGMEMA$_{23}$-co-(MAHAA$_2$)) and P(OEGMEMA)$_{23}$-b-P(MAHAA)$_3$) (DMF as solvent, PMMA calibration, RI detector).

REFERENCES.

(1) Han, S.; Hagiwara, M.; Ishizone, T. Synthesis of Thermally Sensitive Water-Soluble Polymethacrylates by Living Anionic Polymerizations of Oligo(ethylene glycol) Methyl Ether Methacrylates. *Macromolecules* **2003**, *36*, 8312–8319.

(2) Maeda, Y.; Kubota, T.; Yamauchi, H.; Nakaji, T.; Kitano, H. Hydration changes of poly(2-(2-methoxyethoxy)ethyl methacrylate) during thermosensitive phase separation in water. *Langmuir* **2007**, *23*, 11259–11265.

(3) Ishizone, T.; Seki, A.; Hagiwara, M.; Han, S.; Yokoyama, H.; Oyane, A.; Deffieux, A.; Carlotti, S. Anionic Polymerizations of Oligo(ethylene glycol) Alkyl Ether Methacrylates: Effect of Side Chain Length and ω-Alkyl Group of Side Chain on Cloud Point in Water. *Macromolecules* **2008**, *41*, 2963–2967.

(4) Lutz, J.-F. Polymerization of oligo(ethylene glycol) (meth)acrylates: Toward new generations of smart biocompatible materials. *J. Polym. Sci. Pol. Chem.* **2008**, *46*, 3459–3470.

(5) Porsch, C.; Hansson, S.; Nordgren, N.; Malmström, E. Thermo-responsive cellulose-based architectures: tailoring LCST using poly(ethylene glycol) methacrylates. *Polym. Chem.* **2011**, *2*, 1114.

(6) Zhang, Q.; Weber, C.; Schubert, U. S.; Hoogenboom, R. Thermoresponsive polymers with lower critical solution temperature: from fundamental aspects and measuring techniques to recommended turbidimetry conditions. *Mater. Horiz.* **2017**, *4*, 109–116.

CHAPTER 4

POLYMERIC NANOPARTICLES FOR SPION ENCAPSULATION

Multifunctional SPION-encapsulating Polymeric Nanoparticles: Hydroxamic Acids as Metal Chelating Motifs

Jennifer Keth [‡][1],   **Michael Patrick Klak** [‡][2],   **Matthias Bros**[3],   **Peter Langguth**[2*] **and   Holger Frey**[1*]

[1]Department of Chemistry, Johannes Gutenberg-University, Duesbergweg 10-14, 55128 Mainz, Germany

[2]Institute of Pharmacy, Johannes Gutenberg University, Staudingerweg 5, 55099 Mainz, Germany

[3]Department of Dermatology, University Medical Center of the Johannes Gutenberg University Mainz, Langenbeckstrasse 1, 55131 Mainz, Germany

[‡]Equally contributing authors.
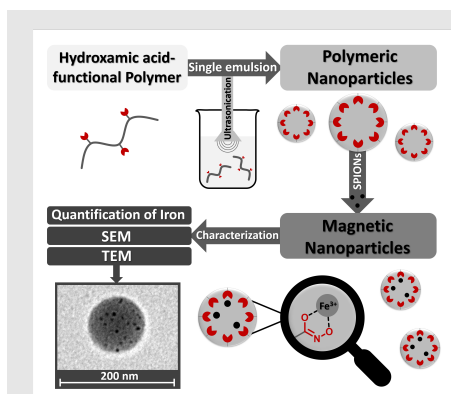
The introduction of superparamagnetic iron nanoparticles (SPION) into polymeric nanoparticles has enabled new theranostic possibilities for drug targeting using external magnets. To build on that concept and to reduce current limitations, hydroxamic acids (HA) were incorporated into biocompatible poly(methyl methacrylate)s as effective iron chelators to enhance iron loading efficiency via increased SPION uptake. Low molecular weight polymers (5,000 g mol^{-1}) with varied hydroxamic acid contents were developed to study the effect of metal complexation on the iron loading efficiency. The emulsion solvent diffusion evaporation method was applied to transfer hydroxamic acid-functionalized poly(methyl methacrylate)s into polymeric nanoparticles with diameters of $\approx$ 200 nm. The hydroxamic acids demonstrated to enhance iron loading into polymeric nanoparticles by 5% already at low hydroxamic acid amounts of 5%$_{mol}$, compared to non-functional polymeric nanoparticles consisting of PMMA. Therefore, the concept of introducing hydroxamic acids for metal complexation offers a platform to enhance the efficiency of iron loading into the polymeric nanoparticles. Due to higher SPION loadings into the polymeric nanoparticles, the efficiency of magnetic targeting, hyperthermia or their use as theranostic contrast agents may be improved by using the same amount of carrier.

INTRODUCTION

Cancer has been estimated by the WHO to be the first or second leading cause of death in 91 countries.[1] A widely known concept in cancer treatment are nanoparticle-based drug delivery systems. Especially, superparamagnetic iron oxide nanoparticles (SPIONs) were investigated in this context due to their versatile properties, i.e. the enhanced permeability and retention (EPR) effect or targeting through magnets, antigens or ultrasound.[2] SPIONs are particles comprising magnetite (Fe_3O_4) in a size < 20 nm. This leads to a single magnetic domain, which results in superparamagnetic behavior. Therefore, these particles only show magnetic characteristics if they are under the influence of an external magnetic field.[3] Hence, SPIONs are very promising materials with regard to applications in nanomedicine.[4] Especially in cancer treatment, these magnetic nanoparticular systems find interest as novel formulations.[5] One application is the widely use of SPIONs as theranostic agents for magnetic resonance imaging (MRI) and to increase local temperatures through external magnetic fields.[6] For instance, a licensed formulation (Nanotherm®) for the hyperthermic treatment of glioblastoma received approval in 2011 in Germany and all member states of the European Union.[4]

It is a common method to incorporate magnetic nanoparticles into biodegradable polymeric nanoparticles, i.e. based on poly(lactic-*co*-glycolic acid) (PLGA), to enable drug loading, targeting and stabilization of the nanoparticles.[7] These polymeric nanoparticles are used as agents for the hyperthermic denaturation of cancer tissues.[8] As nanoparticular systems, they can be used in combination with cytostatic drugs in theranostic applications as potential negative contrast agents for MRI.[9] Further, their surfaces can be conjugated with ligands for cancer imaging. To that end, prior works demonstrated the linkage of Herceptin® (HER) or the human transferrin receptor-binding peptide T7 to PLGA.[10,11] With another attempt, the saturation of nanoparticles loaded with cytostatic drugs was significantly increased through magnetic targeting by positioning a strong magnetic field over a certain spot of interest.[12] Additionally, magnetic polymeric nanoparticles were used for the magnetic induced release of drugs from nanospheres through inductive heating of the nanosphere shell (**Scheme 1**).[13,14]

Previous publications have shown that the magnetization of magnetic polymer nanoparticles correlates with the amount of incorporated iron.[15] Therefore, the quantity of iron inside the particles seems to be crucial for the efficiency of those systems. For the use of polymeric magnetic nanoparticles as MRI contrast agents, the correlation of higher iron content and better T2 (spin-spin) relaxation rate was already shown.[11]
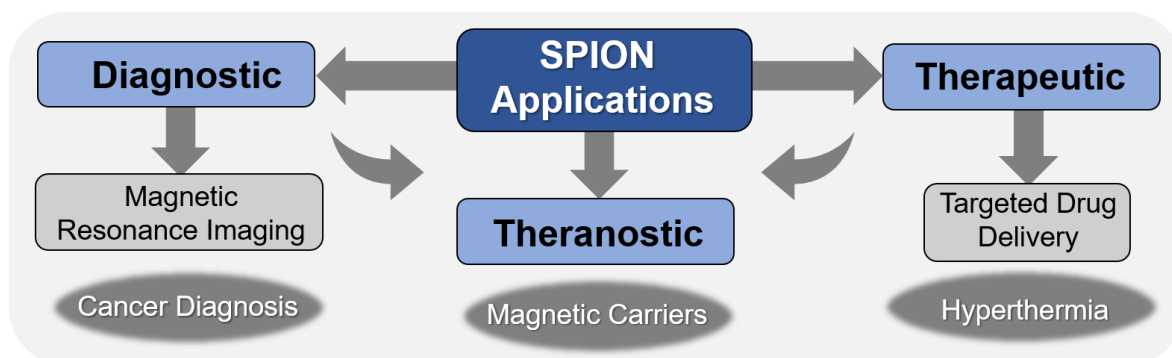
SCHEME 1   Diagnostic and therapeutic applications of SPIONs.[14]

To enhance the iron loading efficiency of the particles, we introduced a metal chelating motif in the polymer side chain. Known from nature, we utilized hydroxamic acids as metal complexing agents. As a major class of Fe(III) complexing groups in "siderophores" (greek: "iron carriers"), hydroxamic acids enhance the bioavailability of Fe(III) in various organisms.[16] Their outstanding complexation properties rely on their chemical structure, that enables the O,O-coordination as bidentate ligands to form stable five-membered rings with various metal ions, i.e. very prominent complexes are formed with Fe(III) ions.[17] The complex stability is approximately 7 orders of magnitude higher compared to carboxylic acids that form only four-membered rings with metal ions.[18] Mono-, bis- and tris-hydroxamic acid complexes are known.[19] Due to the formation of highly stable complexes with Fe(III), hydroxamic acids are known to play a crucial role in the iron metabolism of various organisms.[20]

First reports about polymeric hydroxamic acids date back to 1942.[24] Since then, many approaches have been made to introduce hydroxamic acids into macromolecules. In the 1970's, Winston *et al.* thoroughly investigated the complexation behavior of hydroxamic acid-functionalized polymers by the systematic variation of polymer backbone and chain flexibility and contributed herewith fundamentally to a better understanding of poly(hydroxamic acid)s as metal chelating motifs.[25,26] Most of the reported approaches rely on post-polymerization modifications of polyacryl-derivatives with hydroxylamine that are mainly used until today for the introduction of hydroxamic acids into polymers.[25,27] Unfortunately, most post-modification reactions are commonly not quantitatively as shown for the conversion of poly(acrylamide)s to hydroxamic acids by Nome *et al.*.[28] The direct incorporation of hydroxamic acids into poly(ether)s has already been established in our group via oxyanionic polymerizations. In these previous works, the development of a 1,4,2-dioxazole group as a suitable protecting group is reported that withstand the reaction conditions during the polymerization.[18,29,30] In radical polymerizations, the direct incorporation of the hydroxamic acid functionalities is a challenging procedure

as radical transfer between the active chain end and the functional group of the monomer might occur in radical polymerizations.

To overcome this issue, we used a broad applicable hydroxamic acid-functionalized methacrylate monomer (MAHAA) for the introduction of hydroxamic acid moieties into methacrylic polymer structures that possesses a 1,4,2-dioxazole protecting group to withstand any attack during polymerization.[31] After an acidic cleavage under mild conditions, the hydroxamic acid moieties can be released. Polymeric nanoparticles were synthesized via the solvent diffusion evaporation method. The presence of hydroxamic acids as iron receptor sites in the polymeric nanoparticles may enhance the efficiency of cancer treatment due to an enhanced polymer to iron oxide ratio, without the loss of a uniform distribution of SPIONs in the polymeric nanoparticles.

RESULTS AND DISCUSSION

Functional PMMA Nanoparticles for SPION Encapsulation

First reports in the mid-1970s highlighted the importance of PMMA in biomedical application fields. In these early works, PMMA was used as adjuvant for vaccines to enhance the antibody responses due to a polymer induced virus encapsulation. In addition, an increased protection against infections was found compared to classical adjuvants.[31,32] Furthermore, PMMA is utilized as prosthetic material in dental and mandibular corrections due to its low toxicity and biocompatible properties.[31,33] Another advantage of PMMA besides its biocompatibility is the preparation from low cost and easy available reagents that enable scale-up approaches. Due to these versatile properties, PMMA was chosen as a potential carrier for SPIONs. The copolymerization of MMA with MAHAA, a hydroxamic acid-functionalized monomer, was employed to introduce multiple metal chelating functionalities in the polymer backbone to improve the SPION-encapsulation efficiency. The polymerizing group of MAHAA was designed to have a structural analogy to MMA that should facilitate the reaction conditions in a RAFT polymerization for obtaining random copolymers.

Polymer Synthesis

The controlled copolymerization of hydroxamic acids and other comonomers, such as methyl methacrylate (MMA) is a powerful tool to introduce multiple functionalities in a single macromolecule. The polarity of the copolymer was precisely adjusted by the balance between hydrophilic hydroxamic acids and hydrophobic MMA to fulfill the requirements of the emulsion solvent diffusion evaporation method for the synthesis of nanoparticles, i.e. the solubility of the

polymer in ethyl acetate. Due to a similar chemical surrounding of the polymerizing double bond, both monomers were known to incorporate randomly among the polymer backbone.

The polymers were synthesized with constant molecular weights but varying amounts of randomly distributed hydroxamic acids to study the effect of metal chelation in detail (**Figure S12**). In our studies, PMMA was compared to hydroxamic acid-functionalized copolymer structures containing 5%$_{mol}$ or 10%$_{mol}$ respectively at constant molecular weights (**Table 1**).

TABLE 1 Overview of the synthesized polymers.

Polymer	M_n target [g mol^{-1}]	M_n[a] [g mol^{-1}]	M_n[b] [g mol^{-1}]	Đ[b]	HA [%$_{mol}$]
P(MMA)$_{49}$	5500	5620	4930	1.10	0
P(MMA$_{41}$-co-MAHAA$_2$)	5500	5300	4830	1.10	5
P(MMA$_{37}$-co-MAHAA$_4$)	5400	4340	4920	1.10	10

a. Determined via ^{1}H NMR end group analysis. **b.** Determined via SEC (THF, PMMA calibration, RI detector).

A molar ratio of 10:1 between CTA and AIBN was chosen to reduce the impact of AIBN-induced chain growth. However, deviations between theoretical molecular weight and the molecular weights determined by NMR and SEC analysis might be a result of the partial monomer consumption through AIBN.

Nanoparticle Synthesis

The synthesis of polymeric nanoparticles was employed to enable drug loading, targeting and to enhance the stability of the loaded SPIONs. The synthesized SPIONs were analyzed by vibrating sample magnetometer (VSM) measurements that confirmed the superparamagnetic behavior of the particles (**Figure S14**). In addition, the characteristic lattice fringes of the synthesized nanoparticles can be clearly seen in high-resolution transmission electron microscopy (HR-TEM) images (**Figure S15**). The synthesis of polymeric nanoparticles was employed to enable the encapsulation of SPIONs and to enhance their stability (see *Experimental section* for details). After the encapsulation of SPIONs into the polymeric nanoparticles, DLS, SEM, TEM and STEM measurements were carried out to characterize the obtained polymeric MNPs.

Morphological Characterization

DLS was used both to investigate the mean size and the size distribution of the magnetic nanoparticles. For all nanoparticles a particle size of around 220 nm was obtained resulting in a comparable surface to volume ratio for all samples (**Table 2**, **Figure S16**). Hereby, the particles match

the size range, which is crucial for the so-called enhanced permeability and retention (EPR) effect. In other works, it was demonstrated that the accumulation of particles in tumor tissues was enhanced if the particles were in the size range between 50 and 500 nm.[34]

TABLE 2 Average size (by number) and PDI of PMMA MNPs with varying hydroxamic acid amounts.

PMMA MNP	Average Size [nm]	PDI
0% HA	211.6±12.1	0.116±0.055
5% HA	235.0±5.2	0.137±0.040
10% HA	209.8±3.0	0.149±0.032

Scanning electron microscopy was carried out to investigate the size and morphology of the particles. For a direct comparison of the structure-property correlation between the nanoparticles with varying hydroxamic acid amounts, it was mandatory to produce nanoparticles with similar size and shape. In our studies, it was shown that the nanoparticles exhibit a spherical shape with similar sizes around 100-200 nm and size distributions (**Figure 1**). These findings are in line with DLS measurements revealing average particles sizes of 210-235 nm with narrow polydispersities (**Table 2**, **Figure S16**). Furthermore, the surface of the nanoparticles showed no agglomerations through melting.
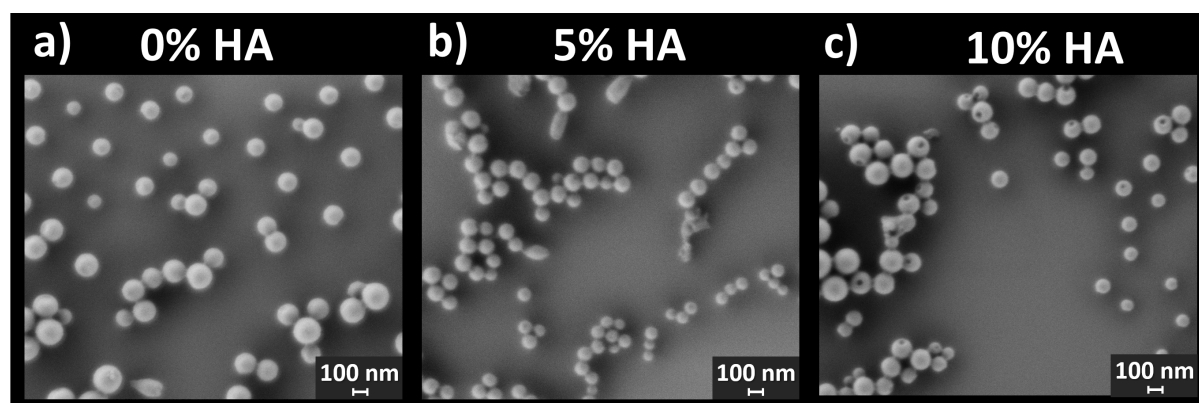
FIGURE 1 SEM images of SPION encapsulating PMMA nanoparticles containing a) 0% b) 5% and c) 10% of hydroxamic acid.

Transmission electron microscopy was applied to investigate the incorporation and the distribution of the iron nanoparticles within the polymeric nanoparticles. The measurements revealed that hydroxamic acid-functionalized polymeric nanoparticles enhanced the incorporation and the uniform distribution of SPIONs (black spheres) within the polymeric shell (**Figure 2**). The non-functional PMMA nanoparticles (**Figure 2a**) led to an agglomeration of SPIONs at one spot, whereas the presence of hydroxamic acids led mainly to a homogeneous distribution of the iron

nanoparticles (**Figure 2b**, **Figure 2c**). Therefore, hydroxamic acids demonstrate to enhance the homogeneous uptake of SPIONs into the polymeric nanoparticles while preventing the formation of agglomerates on the particle surface.
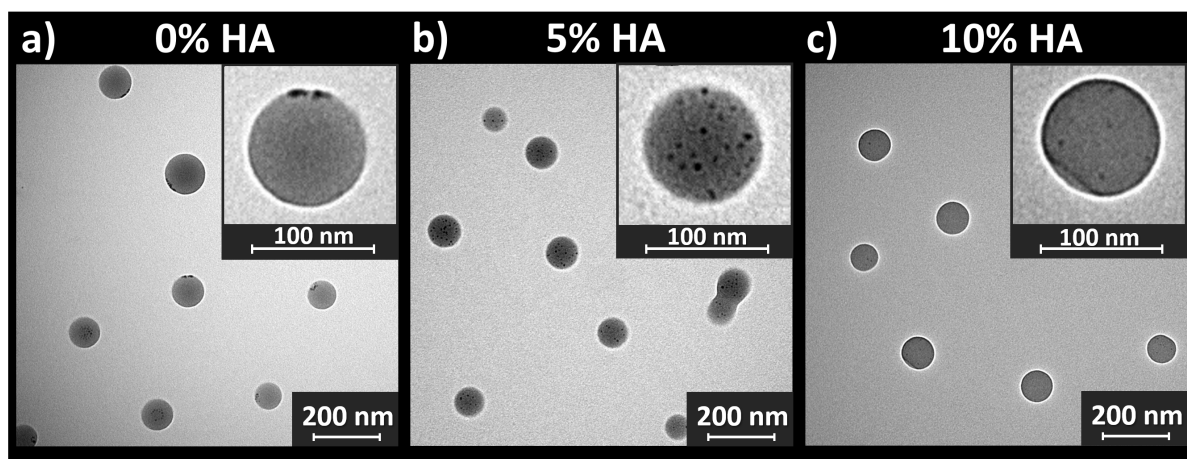
FIGURE 2   TEM images of SPION encapsulating PMMA nanoparticles containing a) 0% b) 5% and c) 10% of hydroxamic acid.

Additionally, STEM images visualized the homogeneous distribution of the iron nanoparticles (white spheres) in the inside of the polymeric nanoparticles (**Figure 3**). The images are in line with TEM measurements revealing an iron agglomeration for non-functional PMMA nanoparticles (**Figure 3a**) and a homogeneous distribution of SPIONs for the hydroxamic acid-functionalized nanoparticles (**Figure 3b**, **Figure 3c**).
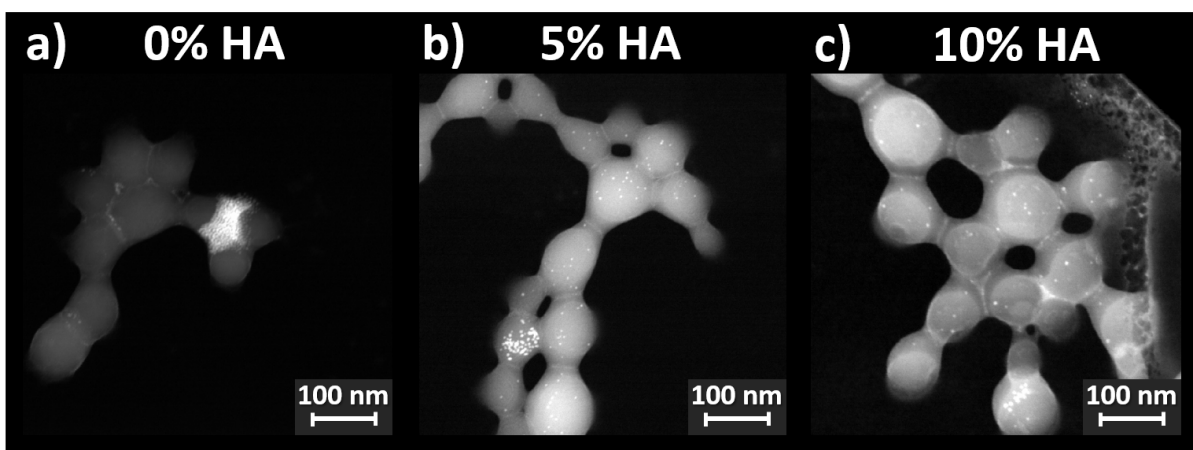
FIGURE 3   STEM images visualizing the distribution of iron nanoparticles (white spheres) in PMMA nanoparticles bearing a) 0% b) 5% and c) 10% of hydroxamic acid moieties.

These findings can be explained by the multiple iron binding receptor sites that are introduced through the incorporation of hydroxamic acid moieties inside the polymeric nanoparticles.

Quantitative Iron Determination

The SPION loaded polymeric nanoparticles were hydrolyzed with nitric acid to analyze the quantitative amount of iron encapsulated by the polymeric nanoparticles (see *Experimental section* for details). We utilized the complexation reaction between Fe(II) as central ion and ferrozine as ligand that was followed via UV-Vis spectroscopy due to a strong absorption band of the ferrozine-iron complex at 562 nm. This enabled us to quantify the iron concentration of the unknown sample by utilizing an iron standard solution as reference measurement (**Figure S17**, **Figure S18**, see *Supporting Information* for details on calculations). Beforehand, the Fe(III) species were reduced to Fe(II) with ascorbic acid to enable a quantitative analysis via the ferrozine method. In multiple UV-Vis measurements, it was shown that the incorporation of hydroxamic acids as metal chelating motifs in the polymer structure enhances the iron loading efficiency of the polymer nanoparticles remarkably (**Figure 4**).
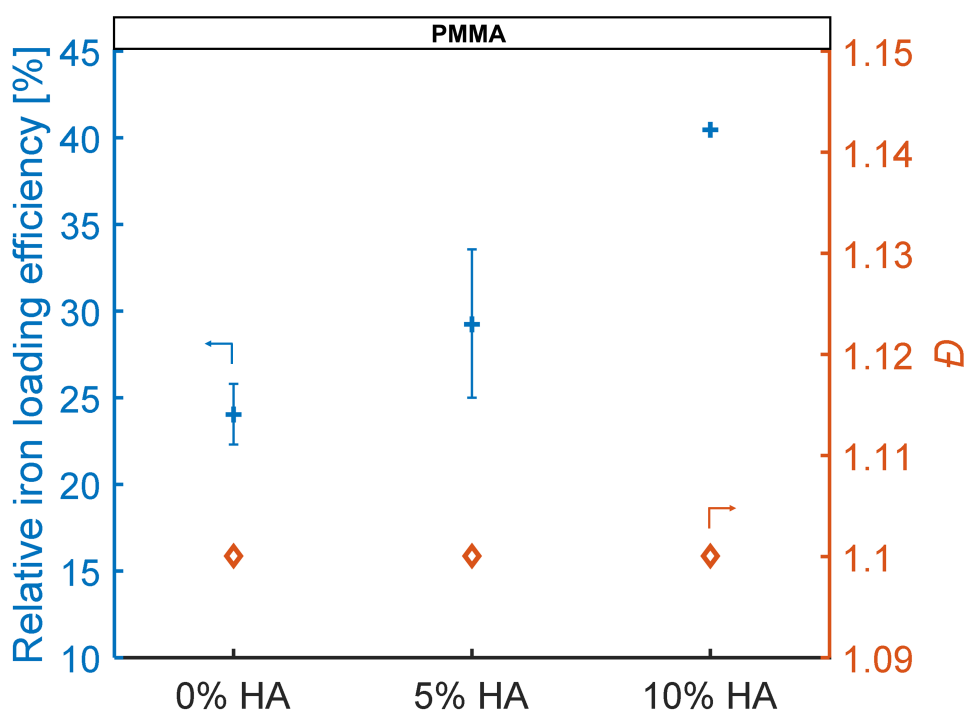
FIGURE 4 Iron loading efficiency of polymeric nanoparticles based on PMMA with varying hydroxamic acid (HA) amounts (blue crosses). The molecular weights of the polymers were illustrated as orange diamonds.

Polymeric nanoparticles bearing only 5%$_{mol}$ of HA increased the SPION encapsulation by 5% compared to non-functional PMMA nanoparticles. In total, the iron uptake of the polymeric nanoparticles was increased from 24% for non-functional PMMA to 40% for hydroxamic acid-

functionalized PMMA bearing 10%$_{mol}$ of metal chelating moieties, randomly distributed along the polymer chains. This is an improvement of inclusion by a factor of 1.2 and 1.6 for 5%$_{mol}$ and 10%$_{mol}$ respectively. The enhanced SPION encapsulation of hydroxamic acid-functionalized polymeric nanoparticles might be explained by the strong interactions between Fe(III) and hydroxamic acids as O,O-bidentate ligands. As a result of the numerous iron receptor sites within the hydroxamic acid-functionalized polymeric nanoparticles, the MNP are embedded into the polymeric nanoparticles (i) with a higher tendency and (ii) in a uniformly distributed manner (**Figure 2**). The prevention of an uneven distribution of SPIONs, especially the agglomeration of many SPIONs in a few particles and no SPIONs in the majority of the polymeric nanoparticles is favored as it would lead to an increased loss of carriers as empty particles are not responding to external magnetic fields.[15]

Our results demonstrate the high potential of hydroxamic acids as metal chelators to increase both the SPION encapsulation capability and their even distribution into polymeric nanoparticles. Furthermore, we compared these results to well-established polymer nanoparticle systems consisting of PLGA under the same MNP synthesis reaction conditions. As a first result, the PLGA nanoparticles showed lower SPION encapsulation capabilities compared to non-functional and functional PMMA nanoparticles (**Figure S19**). The molecular weights of the corresponding polymers as starting materials for the nanoparticle synthesis were on the same order of magnitude proven via SEC measurements (**Figure S12**, **Figure S13**) but the polydispersity differs strongly between the commercially available PLGA and the synthesized PMMA due to different polymerization techniques (**Figure S19**) which may have an impact on the SPION encapsulation capability. Thus, a direct comparison between these two systems is strongly limited. The results with respect to the quantitative iron uptake of PLGA nanoparticles should therefore only be utilized as a vague estimation. However, we rather want to highlight the hydroxamic acid-induced enhanced SPION encapsulation of PMMA based nanoparticles.

Cell Viability Tests

MTT metabolic activity assays on murine spleen cells were performed to investigate the biocompatibility of hydroxamic acid-functionalized magnetic nanoparticle structures with regard to potential therapeutic applications. The measurements were carried out in triplicate, and data show the mean value and the standard deviation for each tested concentrations (**Figure 5**).
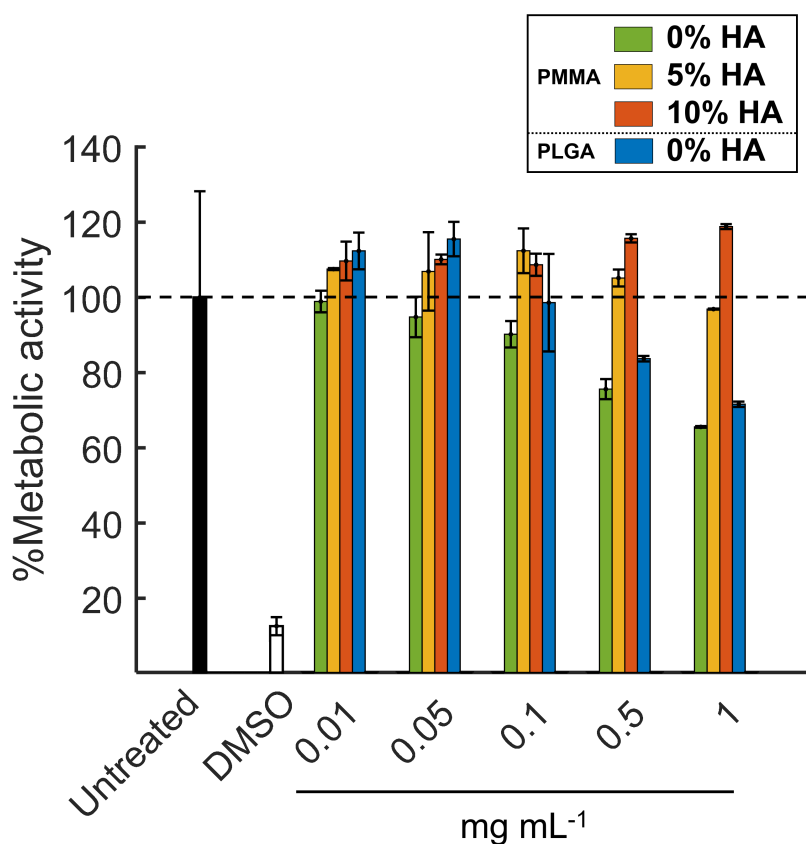
FIGURE 5 Effect of magnetic nanoparticles with varied hydroxamic acid contents (0, 5 and 10%$_{mol}$) on the metabolic activity of murine spleen cells as determined via MTT assays. DMSO applied at cytotoxic concentration (10%) served as a negative control.

As a result, the hydroxamic acid-functionalized magnetic nanoparticles (MNP) showed no significant impact on the cell viability within the range of tested concentrations, revealing low cytotoxic effects on cells in vitro. Only in the case of non-functionalized magnetic nanoparticles consisting of PMMA and PLGA respectively, a considerable decrease of the metabolic activity was observed, suggesting an increased toxicity compared to the hydroxamic acid-functionalized analogues.

Furthermore, fluorescence activated cell sorting measurements were carried out to investigate the cell-type specific accumulation of magnetic nanoparticles (MNP). After the labeling with curcumin, the samples were characterized with respect to their accumulation behavior in murine splenic leukocyte populations, comprising neutrophils, B cells, dendritic cells and macrophages (**Figures S21-28**). As a result, the MNPs were accumulated in neutrophils and macrophages but no significant accumulation in B cells and dendritic cells was observed (**Table S2**). The viability of all cells (>95%) after the treatment with MNPs was proven via fixable viability dye (FVD) labeled measurements (**Figure S20**).

CONCLUSIONS

The introduction of randomly distributed hydroxamic acid moieties as effective iron receptors within polymeric nanoparticle systems has been demonstrated to represent a powerful tool to enhance both the SPION encapsulation capability and to improve the distribution of MNP inside the polymeric nanoparticles. Both effects may contribute to an improved response of the carriers upon application of an external magnetic field. As a consequence, a reduced dosage of the nanocarriers may be applied, while retaining the same efficiencies as known for non-functional compounds. For this purpose, functional PMMAs were prepared with varying hydroxamic acid amounts via controlled radical polymerization techniques. The emulsion solvent diffusion evaporation method demonstrated to be a powerful technique to prepare well-defined spherical nanoparticles that were treated with SPIONSs. TEM and SEM showed an enhanced SPION encapsulation efficiency as well as a homogenous distribution of SPIONs for the hydroxamic acid-functionalized nanoparticles compared to non-functional PMMA nanoparticles. Additionally, the quantitative determination of iron via UV-Vis spectroscopy confirmed the enhanced uptake of iron for the hydroxamic acid-functionalized species. In addition, the hydroxamic acid-functionalized PMMA MNPs were studied with respect to their further use in medical applications via cell viabilities tests. All synthesized functional and non-functional MNPs showed no significant decrease in the metabolic activity of murine spleen cells.

ACKNOWLEDGEMENTS

EXPERIMENTAL SECTION

Synthesis of PMMA (1a) In a 10 mL Schlenk tube 500.00 mg (4.994 mmol, 1 eq) MMA, 11.07 mg (0.050 mmol, 0.01 eq) 2-Cyano-2-propyl benzodithioate (CPBDT) and 0.41 mg (0.005 mmol, 0.001 eq) 2,2'-Azobis(2-methylpropionitrile) (AIBN) were dissolved in 1.5 mL dioxane. After three freeze pump thaw cycles, the mixture was stirred for 24 h at 70 °C. After precipitation in ice cold methanol (45 mL, -20 °C), the product was recovered by centrifugation (4500 RPM, 10 minutes).

^{1}H NMR (300 MHz, CDCl$_3$): δ [ppm] = 7.87 (d, J = 7.4 Hz, 2H, ArC^{2,6}H), 7.52 (t, J = 7.4 Hz, 1H, ArC^4H), 7.36 (t, J = 7.7 Hz, 2H, ArC^{3,5}H), 3.63-3.54 (s, O-CH_3), 2.10-1.70 (m, C-CH_2), 1.16-0.73 (m, C-CH_3).

^{13}C NMR (75 MHz, CDCl$_3$): δ [ppm] = 178.17 (C=O), 177.87 (C=O), 177.03 (C=O), 144.90, 132.56 (ArC^4), 128.39 (Ar$C^{3,5}$), 126.74 (Ar$C^{2,6}$), 125.55, 125.07, 54.43 (CH$_2$), 52.91, 51.88 (O-CH$_3$), 44.91 (quaternary C), 30.34, 18.75 (C-CH$_3$), 16.37 (C-CH$_3$).

IR-ATR $\tilde{v}$ [cm^{-1}] = 2959 (CH$_3$), 1725 (C=O), 1434 (CH), 1260 (CH), 1144 (CH), 1016 (CH), 799 (CH$_{aromat.}$).

Synthesis of P(MMA-*co*-MAHAA) (1b) In a 10 mL Schlenk tube 400.00 mg (3.995 mmol, 47.5 eq) MMA, 64.2 mg (0.210 mmol, 2.5 eq) MAHAA, 18.62 mg (0.084 mmol, 1 eq) 2-Cyano-2-propyl benzodithioate (CPBDT) and 0.69 mg (0.008 mmol, 0.10 eq) 2,2'-Azobis(2-methylpropionitrile) (AIBN) were dissolved in 1.4 mL dioxane. After three freeze pump thaw cycles, the mixture was stirred for 24 h at 70 °C. After precipitation in ice cold methanol (45 mL, -20 °C), the product was recovered by centrifugation (4500 RPM, 10 minutes). The same procedure was applied with a ratio of 40.5:4.5:1:0.1 for MMA:MAHAA:CPBDT:AIBN to yield copolymers with 10%$_{mol}$ HA.

^{1}H NMR (300 MHz, CDCl$_3$): δ [ppm] = 7.88 (d, J = 8.2 Hz, ArC^{2,6}H), 7.72 (AA'BB', ArC^{3,5}H), 7.52 (t, J = 7.3 Hz, ArC^4H), 7.36 (t, J = 7.6 Hz, ArC^{3,5}H), 6.95 (AA'BB', ArC^{2,6}H), 4.32 (s, Ar-O-CH_2-CH_2), 4.23 (s, Ar-O-CH_2), 3.59 (s, O-CH_3), 2.03-1.81 (m, C-CH_2), 1.68 (s, H_3C-CO$_2$-CH_3), 1.02-0.84 (m, C-CH_3).

^{13}C NMR (75 MHz, CDCl$_3$): δ [ppm] = 178.20 (C=O), 177.90 (C=O), 177.08 (C=O), 160.87 (ArC^4), 158.13 (OC=N), 128.55 (Ar$C^{3,5}$), 128.43 (Ar$C^{3,5}$), 126.79 (Ar$C^{2,6}$), 116.56 (ArC-O), 115.30 (H_3C-CO$_2$-CH$_3$), 114.76 (Ar$C^{2,6}$), 65.47 (Ar-O-CH$_2$), 63.24 (Ar-O-CH$_2$-CH$_2$), 54.47 (CH$_2$), 51.92 (O-CH$_3$), 44.98 (quaternary C), 24.93 ($H_3$$C$-CO$_2$-CH$_3$), 18.79 (C-CH$_3$), 16.56 (C-CH$_3$).

IR-ATR $\tilde{v}$ [cm^{-1}] = 2956 (CH$_3$), 2250 (C≡N), 1732 (C=O), 1452 (C=C), 1255 (C-O-C), 1118 (C-O-C), 906 (C-H$_{aromat.}$), 726 (C-H$_{aromat.}$).

Deprotection of 1b to P(MMA-*co*-MAHA) (1c)   In a 50 mL round-bottom flask, 216 mg of *DL*-campher sulfonic acid (CSA) were dissolved in 4 mL methanol. 208 mg of **1b** were dissolved in 12 mL acetonitrile and were added to the flask. The mixture was stirred for 24 h at rt. The product was purified by dialysis (MWCO: 1000 g mol^{-1}) in 24 h from methanol.

^{1}H NMR (300 MHz, CDCl$_3$): δ [ppm] = 11.09 (s, N*H*), 10.07 (s, O*H*), 7.85 (d, *J* = 7.7 Hz, ArC^{2,6}*H*), 7.74 (AA'BB', ArC^{3,5}*H*), 7.65 (t, *J* = 7.7 Hz, ArC^4*H*), 7.48 (t, *J* = 7.5 Hz, ArC^{3,5}*H*), 6.99 (AA'BB', ArC^{2,6}*H*), 4.48-4.11 (s, Ar-O-C*H$_2$*-C*H$_2$*), 3.77-3.35 (s, O-C*H$_3$*), 2.07-1.55 (m, C-C*H$_2$*), 1.07 – 0.44 (m, C-C*H$_3$*).

^{13}C NMR (75 MHz, CDCl$_3$): δ [ppm] = 177.61 (*C*=O), 176.64 (*C*=O), 144.62 (*C*=S), 129.25 (Ar*C^{3,5}*), 129.12 (Ar*C^{3,5}*), 126.73 (Ar*C^{2,6}*), 125.71 (Ar*C^4*), 114.56 (Ar*C^{2,6}*), 54.09 (*C*H$_2$), 52.22 (O-*C*H$_3$), 44.34 (quaternary *C*), 18.92 (*C*-CH$_3$), 16.59 (*C*-CH$_3$).

IR-ATR $\tilde{v}$ [cm^{-1}] = 2997 (O-H, N-H), 2949 (CH$_3$), 1725 (C=O), 1433 (C=C), 1238 (C-O-C), 1149 (C-O-C), 989(C-HAr), 841 (C-H$_{aromat.}$), 750 (C-H$_{aromat.}$).

Synthesis of superparamagnetic nanoparticles (SPIONs)   SPIONs were made by the specifications described by Sun *et al.*.[35] 706.3 mg (2 mmol, 1 eq) Iron(III) acetylacetonate were dispersed in a solution of 2.58 g (10 mmol, 5 eq) of 1,2-hexadecanediole, 1.69 g (6 mmol, 3 eq) of oleic acid and 1.60 g (6 mmol, 3 eq) of oleylamine in 20 mL benzyl ether. First, the reaction vessel was heated to 140-150 °C for 30 minutes under reduced pressure and nitrogen atmosphere to remove oxygen and water. The dispersion was then heated to 200 °C for 2 hours and to 300 °C for one additional hour under constant stirring and nitrogen atmosphere. After cooling to room temperature, the sample was precipitated in ethanol and centrifuged 3 times with 10,000 g for 10 min by a Heraeus Multifuge X1R, with a Fiberlite F15-8 x 50cy rotor (Thermo Fisher Scientific, Waltham, MA, USA). In the first and second centrifugation step, the supernatant was removed and replaced by fresh ethanol. For the last step, the pellet was dispersed in 10 mL chloroform, 50 µL oleic acid and 50 µL oleylamine. For further purification, the product was centrifuged with 20,000 g for 10 min and the supernatant was collected.

Preparation of magnetic polymer nanoparticles   Magnetic polymer nanoparticles were prepared in a modified procedure according to literature via the emulsion solvent diffusion evaporation method.[36] 10 mg of the polymer were dissolved in 1 mL of ethyl acetate and 1 mg of SPIONs distributed in chloroform were added. This suspension was pipetted in a 2 % solution of polyvinyl alcohol and stirred for 1 h. Afterwards, the suspension was homogenized by an ultrasonic staff for 1 minute. The nanoparticles were washed 4 times by centrifugation at 10,000 g for 20 min with MilliQ water.

Hydrolysis of the nanoparticles   1.9 mg of the SPION-functionalized nanoparticles were dissolved in 2 mL nitric acid ($50\%_{vol}$) and stirred at room temperature for 20 h.

Metabolic activity   Murine spleen cells (10^7/mL) were seeded in wells (each 100 µL) of 96 well cell culture plates. Afterwards, nanoparticle formulations and DMSO at cytotoxic concentration (10%) were applied as indicated. One day later, metabolic activity was assayed using chromogenic MTT assay reagent as recommended by the manufacturer (Promega, Madison, WI).

Nanoparticle Binding   Binding of curcumin-labelled PMMA nanoparticles to leukocyte populations was assessed by flow cytometry. Bone marrow (BM) was flushed from the tibiae and femurs of C57BL/6 mice using a syringe, and BM cells were resuspended in IMDM medium, containing 5% fetal bovine serum (FBS), 2 mM L-glutamine, 100 U mL^{-1} penicillin, 100 µg mL^{-1} streptomycin (all from Sigma-Aldrich, Deisenhofen, Germany), and 50 µM β-mercaptoethanol (Roth, Karlsruhe, Germany). Aliquots of BM cells ($2 \cdot 10^6$/mL) were supplemented with 100 ng m^{-1} recombinant murine GM-CSF (R&D Systems, Wiesbaden, Germany) as a survival factor for neutrophils, transferred into FACS tubes (500 µL) and were incubated with the different nanoparticles. Neutrophils were identified as Ly6G-positive cells. Another aliquot of BM cells was supplemented with 10 ng mL^{-1} recombinant murine GM-CSF, and cells were seeded in 12 well suspension cell culture plates ($2 \cdot 10^5$/mL) to promote parallel differentiaton of BM progenitor cells towards macrophages and dendritic cells. After one week, BM cultures (1 mL/well) were incubated with nanoparticles. Dendritic cells were identified as CD11c-positive and macrophages as CD11c-negative cells, respectively. For assessment of nanoparticle binding to B cells, spleens were retrieved from C57BL/6 mice, and erythrocytes were lysed using a hypotonic lysis buffer. Spleen cells were resuspended in IMDM culture medium ($4 \cdot 10^6$/mL). Spleen cells were transferred into FACS tubes (500 µL), and the different nanoparticle formulations were applied. B cells were identified as CD19-positive cells. After over-night incubation with the accoding nanoparticles formulations, cells were washed (PBS, 2 mM EDTA, 2 % fetal bovine serum), and Fcγ receptors were blocked by applying anti-CD16/32 antibody to preevent unspecific binding of subsequently applied cell type-specific antibodies. Then, samples were incubated with cell type-characterizing antibodies (see above), each labeled with phycoerythrin. Afterwards, viability was assessed by incubation with fixable viability dye (FVD), labeled with eFl780 as recommended by the manufacturer (Thermo Fisher, Waltham, MA). All antibodies were purchased from BioLegend (San Diego, CA) or Thermo Fisher. Samples were fixed (FACS buffer including 0.7% paraformaldehyde), and analysed using an Attune Nxt flow cytometer.

REFERENCES

(1) F. Bray, J. Ferlay, I. Soerjomataram, R. L. Siegel, L. A. Torre, A. Jemal, *Ca-Cancer J. Clin.* **2018**, *68*, 394.

(2) a) Y. Xin, M. Yin, L. Zhao, F. Meng, L. Luo, *Cancer Biol. Med.* **2017**, *14*, 228; b) A. Wicki, D. Witzigmann, V. Balasubramanian, J. Huwyler, *J. Controlled Release* **2015**, *200*, 138.

(3) J. Dulińska-Litewka, A. Łazarczyk, P. Hałubiec, O. Szafrański, K. Karnas, A. Karewicz, *Materials* **2019**, *12*, 617.

(4) O. L. Gobbo, K. Sjaastad, M. W. Radomski, Y. Volkov, A. Prina-Mello, *Theranostics* **2015**, *5*, 1249.

(5) H. Zhang, X. L. Liu, Y. F. Zhang, F. Gao, G. L. Li, Y. He, M. L. Peng, H. M. Fan, *Sci. China Life Sci.* **2018**, *61*, 400.

(6) K. Ulbrich, K. Holá, V. Šubr, A. Bakandritsos, J. Tuček, R. Zbořil, *Chem. Rev.* **2016**, *116*, 5338.

(7) M. K. Lima-Tenório, E. A. G. Pineda, N. M. Ahmad, H. Fessi, A. Elaissari, *Int. J. Pharm.* **2015**, *493*, 313.

(8) Y. Chen, L. Jiang, R. Wang, M. Lu, Q. Zhang, Y. Zhou, Z. Wang, G. Lu, P. Liang, H. Ran, H. Chen, Y. Zheng, *Adv. Mater.* **2014**, *26*, 7468.

(9) N. Schleich, P. Sibret, P. Danhier, B. Ucakar, S. Laurent, R. N. Muller, C. Jérôme, B. Gallez, V. Préat, F. Danhier, *Int. J. Pharm.* **2013**, *447*, 94.

(10) a) J. Yang, C.-H. Lee, J. Park, S. Seo, E.-K. Lim, Y. J. Song, J.-S. Suh, H.-G. Yoon, Y.-M. Huh, S. Haam, *J. Mater. Chem.* **2007**, *17*, 2695; b) S.-J. Lee, H.-J. Kim, Y.-M. Huh, I. W. Kim, J. H. Jeong, J.-C. Kim, J.-D. Kim, *J. Nanosci. Nanotechnol.* **2018**, *18*, 1542.

(11) Y. Cui, M. Zhang, F. Zeng, H. Jin, Q. Xu, Y. Huang, *ACS Appl. Mater. Interfaces* **2016**, *8*, 32159.

(12) a) C. Alexiou, R. Tietze, E. Schreiber, R. Jurgons, H. Richter, L. Trahms, H. Rahn, S. Odenbach, S. Lyer, *J. Magn. Magn. Mater.* **2011**, *323*, 1404; b) N. Schleich, C. Po, D. Jacobs, B. Ucakar, B. Gallez, F. Danhier, V. Préat, *J. Controlled Release* **2014**, *194*, 82.

(13) a) K. Fang, L. Song, Z. Gu, F. Yang, Y. Zhang, N. Gu, Colloids and surfaces. B, Biointerfaces **2015**, 136, 712; b) W.-L. Chiang, C.-J. Ke, Z.-X. Liao, S.-Y. Chen, F.-R. Chen, C.-Y. Tsai, Y. Xia, H.-W. Sung, *Small* **2012**, *8*, 3584.

(14) M. Mahmoudi, S. Sant, B. Wang, S. Laurent, T. Sen, *Adv. Drug Delivery Rev.* **2011**, *63*, 24.

(15) R. A. Wassel, B. Grady, R. D. Kopke, K. J. Dormer, *Colloids Surf., A* **2007**, *292*, 125.

(16) J. B. Neilands, *Science* **1967**, *156*, 1443.

(17) J. P. Folkers, C. B. Gorman, P. E. Laibinis, S. Buchholz, G. M. Whitesides, R. G. Nuzzo, *Langmuir* **1995**, *11*, 813.

(18) J. Keth, T. Johann, H. Frey, *Biomacromolecules* **2020**, *21*, 2546.

(19) G. Schwarzenbach, K. Schwarzenbach, *Helv. Chim. Acta* **1963**, *46*, 1390.

(20) M. J. Miller, *Chem. Rev.* **1989**, *89*, 1563.

(21) Z. D. Liu, R. C. Hider, *Coord. Chem. Rev.* **2002**, *232*, 151.

(22) World Health Organization, Model List of Essential Medicines, http://www.who.int/medicines/publications/essentialmedicines/en/, accessed: January, **2016**.

(23) a) S. Abbina, U. Abbasi, A. Gill, K. Wong, M. T. Kalathottukaren, J. N. Kizhakkedathu, *ACS Cent. Sci.* **2019**, 5, 917; b) J. L. Hamilton, M. I. Ul-Haq, A. L. Creagh, C. A. Haynes, J. N. Kizhakkedathu, *Macromol. Biosci.* **2017**, *17*, 1600244; c) N. A. A. Rossi, I. Mustafa, J. K. Jackson, H. M. Burt, S. A. Horte, M. D. Scott, J. N. Kizhakkedathu, *Biomaterials* **2009**, *30*, 638; d) M. Imran ul-haq, J. L. Hamilton, B. F. L. Lai, R. A. Shenoi, S. Horte, I. Constantinescu, H. A. Leitch, J. N. Kizhakkedathu, *ACS Nano* **2013**, *7*, 10704.

(24) D. D. Coffman, US2402604 A,**1946**.

(25) A. Winston, E. T. Mazza, *J. Polym. Sci. Pol. Chem.* **1975**, *13*, 2019.

(26) a) A. Winston, G. R. McLaughlin, *J. Polym. Sci. Pol. Chem.* **1976**, *14*, 2155; b) A. Winston, D. Kirchner, *Macro-*

molecules **1978**, *11*, 597; c) Varaprasad, D. V. P. R., J. Rosthauser, A. Winston, *J. Polym. Sci. Pol. Chem.* **1984**, *22*, 2131.

(27) a) Y.K. Agrawal, H. Kaur, S.K. Menon, *React. Funct. Polym.* **1999**, *39*, 155; b) M. L. Rahman, S. M. Sarkar, M. M. Yusoff, M. H. Abdullah, *Sens. Actuators, B* **2017**, *242*, 595.

(28) R. S. Mello, E. S. Orth, W. Loh, H. D. Fiedler, F. Nome, *Langmuir* **2011**, *27*, 15112.

(29) T. Johann, J. Keth, M. Bros, H. Frey, *Chem. Sci.* **2019**, *10*, 7009–7022.

(30) T. Johann; U. Kemmer-Jonas; R. D. Barent; H. Frey, *Macromolecular rapid communications* **2020**, *41*, e1900282.

(31) A. Bettencourt, A. J. Almeida, *J. Microencapsulation* **2012**, *29*, 353.

(32) J. Kreuter in *Vaccine Adjuvants* (Ed.: D. T. O'Hagan), Humana Press, New Jersey, **2000**, 105–119.

(33) P. E. Feuser, P. C. Gaspar, E. Ricci-Júnior, M. C. S. d. Silva, M. Nele, C. Sayer, P. H. H. de Araújo, *Macromol. Symp.* **2014**, *343*, 65.

(34) V. Torchilin, *Adv. Drug Delivery Rev.* **2011**, *63*, 131.

(35) S. Sun, H. Zeng, D. B. Robinson, S. Raoux, P. M. Rice, S. X. Wang, G. Li, *J. Am. Chem. Soc.* **2004**, *126*, 273.

(36) C. Shi, C. Thum, Q. Zhang, W. Tu, B. Pelaz, W. J. Parak, Y. Zhang, M. Schneider, *J. Controlled Release* **2016**, *237*, 50.

SUPPORTING INFORMATION

Materials

All reagents were used without further purification, unless otherwise stated. All chemicals and solvents were purchased from Abcr, Acros, Aldrich, Fisher Scientific, Fluka, Riedel-de-Haën or Roth. Deuterated solvents were purchased from Deutero GmbH. If not mentioned, the compounds were used as received. Prior to use, MMA was passed through a neutral aluminium oxide column to remove the stabilizer. The hydroxamic acid-functionalized comonomer MAHAA was synthesized according to the procedure described in previous works.

Instrumentation

NMR analysis ^{1}H NMR spectra at 300 MHz and ^{13}C NMR spectra at 75 MHz were recorded on a Bruker Avance III HD 300 (5 mm BBFO-Head with z-gradient) at 23 °C. ^{1}H NMR spectra at 400 MHz and ^{13}C NMR spectra at 100 MHz were recorded on a Bruker Avance III HD 400 (5 mm BBFO-Smartprobe with z-gradient) at 23 °C. All NMR spectra were referenced to the residual proton signals of the deuterated solvent.

Size exclusion chromatography (SEC)   SEC was performed in DMF (1 mL/min, 50 °C) containing 1 g/L lithium bromide as additive. An Agilent 1100 series SEC system including a HEMA 300/100/40 Å column cascade, an UV (254 nm) and a RI detector was used. Furthermore, SEC was performed in THF (1 mL/min, 20 °C) containing 1 g/L lithium bromide as additive. A MZ-gel SD plus column, an UV (254 nm) and a RI detector was used. Calibration was carried out using P(MMA) standards provided by Polymer Standard Service (PSS).

Infrared spectroscopy   FT-IR spectra were recorded using a Nicolet iS10 FT-IR spectrometer (Thermo Fisher Scientific).

Vibrating sample magnetometer (VSM)   The magnetic properties of the SPIONS were confirmed with a Vibrating Sample Magnetometer (VSM) Model 7300 (Lake Shore Cryotronics Inc., Westerville, OH, USA). A certain volume of the suspension with a known concentration was pipetted on a Teflon holder. The sample was analyzed under a maximum field strength of 600 kA/m.

High-resolution transmission electron microscopy (HR-TEM)   High resolution TEM experiments were carried out on a FEI Tecnai F20 operated at 200 kV.

Transmission electron microscopy (TEM) The shape and the distribution of iron inside the polymeric nanoparticles was determined with a Tecnai 12 transmission electron microscope (TEM) at an accelerating voltage of 120 kV.

Scanning electron microscopy (SEM) SEM images were made for additional morphology and size investigations with two different kinds of scanning electron microscopes, Hitachi SU8000 (HHT, Krefeld) and Leo 1530 GEMINI (ZEISS, Oberkochen).

Scanning transmission electron microscopy (STEM) Dark field STEM images were taken on a FEI Tecnai F20 operated at 200 kV.

Dynamic light scattering The nanoparticle size was measured by dynamic light scattering with a Malvern Nano ZS (Malvern Instruments Ltd., Worcesterhire, United Kingdom). The suspension was diluted 1 to 10 in MilliQ water. Particle sizes were obtained as the Z average size in (nm). Each polymer particle type was produced three times. and was one Datapoint. Every datapoint is an average of 36 measurements.

UV-Vis spectroscopy UV-Vis spectra were recorded at 25 °C using a JASCO V-630 spectrophotometer with a light source fixed at 600 nm. The nanoparticle dispersion was hydrolyzed prior to use for iron quantification. 100 μL of the hydrolyzed sample were added to 500 μL of acetate buffer mixed with ascorbic acid for reduction of Fe(III) to Fe(II). Spectra were recorded after the addition of 20 μL ferrozine.

Polymer characterization

NMR spectra

FIGURE S1 ^{1}H NMR spectrum of MAHAA (300 MHz, CDCl$_3$).

FIGURE S2 ^{1}H NMR spectrum of P(MMA-*co*-MAHAA) (300 MHz, CDCl$_3$).

FIGURE S3 ^{13}C NMR spectrum of P(MMA-*co*-MAHAA) (75 MHz, CDCl$_3$).

FIGURE S4 ^{1}H-^{13} HSQC NMR spectrum of P(MMA-*co*-MAHAA) (300 MHz, 75 MHz, CDCl$_3$).

FIGURE S5 ^{1}H-^{13} HMBC NMR spectrum of P(MMA-*co*-MAHAA) (300 MHz, 75 MHz, CDCl$_3$).

FIGURE S6 ^{1}H NMR spectrum of P(MMA-*co*-MAHA) (300 MHz, CDCl$_3$).

FIGURE S7 ^{13}C NMR spectrum of P(MMA-*co*-MAHA) (75 MHz, DMSO-d_6).

FIGURE S8 ^{1}H-^{13} HSQC NMR spectrum of P(MMA-*co*-MAHAA) (300 MHz, 75 MHz, DMSO-d_6).

FIGURE S9 ^{1}H NMR spectra overlay of P(MMA-*co*-MAHAA) before (top) and after (bottom) deprotection (300 MHz, CDCl$_3$). Corresponding signals of the methyl groups of the protection functionality are shown in blue.

Infrared spectra

FIGURE S10   FT-ATR-IR spectrum of P(MMA-*co*-MAHAA) (**1a**).

FIGURE S11   FT-ATR-IR spectrum of P(MMA-*co*-MAHA) (**1b**).

Size exclusion chromatography measurements

— 0% HA (M_n: 4530 g/mol; Đ: 1.12)
– – 5% HA (M_n: 4930 g/mol; Đ: 1.10)
······· 10% HA (M_n: 4960 g/mol; Đ: 1.12)

— 0% HA (M_n: 4930 g/mol; Đ: 1.10)
– – 5% HA (M_n: 4830 g/mol; Đ: 1.10)
······· 10% HA (M_n: 4920 g/mol; Đ: 1.10)

FIGURE S12 SEC traces of PMMA and P(MMA-*co*-MAHAA) copolymers with varying amounts of hydroxamic acids (HA) (THF, PMMA calibration, UV detector (left), RI detector (right)).

— 0% HA (M_n: 5050 g/mol; Đ: 1.82)

FIGURE S13 SEC trace of PLGA (THF, PMMA calibration, RI detector).

SPION characterization

VSM measurements

Vibrating sample magnetometer measurements were carried out to investigate the magnetic properties of the iron nanoparticles. We observed no significant remanence of the hysteresis curve, indicating that the nanoparticles were superparamagnetic (**Figure S13**). Saturation magnetization was measured at a value of 21.59 A m^2 kg^{-1} with the Langevin fit. Deviations from literature values (typically between 50 and 60 A m^2 kg^{-1}) may arise due to high amounts of oleic acid which resulted in a strong overestimation of the nanoparticle mass.

FIGURE S14 Magnetization behavior of SPIONs at different magnetic field strength measured with a vibrating sample magnetometer.

HR-TEM measurements

FIGURE S15   HR-TEM image of the synthesized SPIONs revealing a lattice fringe pattern.

Nanoparticle characterization

DLS measurements

FIGURE S16 Dynamic light scattering measurements showing the hydrodynamic mean diameter (by number) of PMMA nanoparticles with a) 0%$_{mol}$ HA, b) 5%$_{mol}$ HA and c) 10%$_{mol}$ HA respectively after the attachment of SPIONs.

Quantitative Iron Determination

The absorption maxima at 562 nm were utilized to calculate the iron concentration of the hydrolyzed nanoparticles solutions (**Figure S17**).

FIGURE S17 Overlay of the absolute absorption bands of the hydrolyzed PLGA (a), PMMA (b) and P(MMA-*co*-MAHA) (c,d) nanoparticle dispersions in an acetate buffer after the addition of ferrozine for the determination of Fe(II) measured by UV-Vis spectroscopy. Ascorbic acid was utilized to reduce the Fe(III) species to Fe(II) before the analysis. A reference measurement was carried out by using a standard Fe(II)-solution with a concentration of 1.4 mg L^{-1} (black line).

To quantify the exact iron concentration of the unknown samples, we measured a standard Fe(II) solution with a known concentration of 1.4 mg L^{-1}. As an example, the spectra of a standard iron solution and a 5%$_{mol}$ HA sample were plotted (**Figure S17**).

FIGURE S18 UV-Vis spectra of a reference iron(II) solution with a known concentration of 1.4 mg L^{-1} and a hydrolyzed nanoparticle solution containing 5%$_{mol}$ of hydroxamic acid after the reduction of Fe(III) to Fe(II) with ascorbic acid and the addition of ferrozine as complexing agent. The absorption maxima at 562 nm were utilized to calculate the concentration of Fe(II).

By using Equation **1** and **2**, we were able to calculate the iron concentration of the unknown samples (**Table S1**). The measured extinction values are defined as E_{CAL} (iron standard solution) and E_S (sample). ΔE_{SB} describes the difference between the measured extinction for the sample (E_S) and a blank measurement (E_B).

$$\Delta E_{SB} = E_S - E_B = 0.3426 - 0.01485 = 0.3278 \tag{1}$$

$$c(\text{Fe}) = \Delta E_{SB} \cdot \frac{1.4 \text{ mg L}^{-1}}{E_{CAL}} = 0.3278 \cdot \frac{1.4 \text{ mg L}^{-1}}{0.1343} = 3.4166 \text{ mg L}^{-1} \tag{2}$$
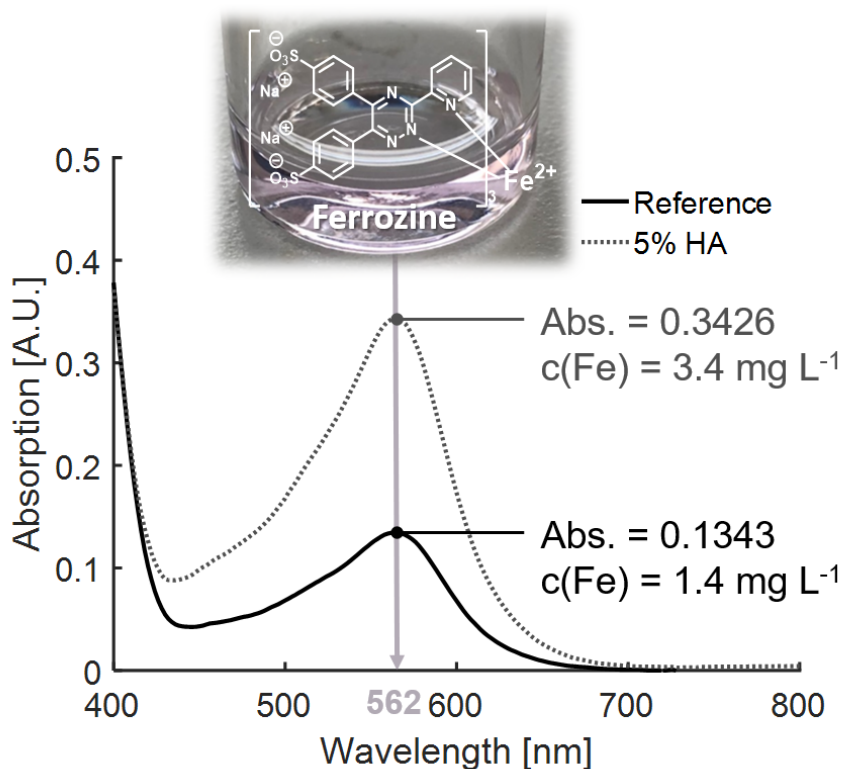
TABLE S1 Overview of the absolute and relative iron uptake of PLGA, PMMA and P(MMA-*co*-MAHA) with varying hydroxamic acid contents.

Polymer	$c(Fe)_{theo.}$ [mg L^{-1}]	$c(Fe)$ [mg L^{-1}][a]	SPION loading [%]	Average SPION loading [%]
PLGA - 0% HA	7.3568	1.2738	17.31	16.61 ± 1.90
	7.8370	1.0851	13.85	
	10.1604	1.8464	18.17	
	13.9037	2.379	17.11	
P(MMA)$_{49}$ - 0% HA	11.6279	3.0269	26.03	24.05 ±1.75
	13.7421	3.2185	23.42	
	13.8224	3.1385	22.71	
P(MMA$_{41}$-*co*-MAHA$_2$) - 5% HA	9.5137	2.4461	25.71	29.28 ± 4.28
	10.0423	3.4166	34.02	
	10.2205	2.8735	28.11	
P(MMA$_{37}$-*co*-MAHA$_4$) - 10% HA	6.4551	2.6107	40.44	40.44

a. Determined via UV-Vis measurements referred to an iron standard solution with a concentration of 1.4 mg L^{-1}.
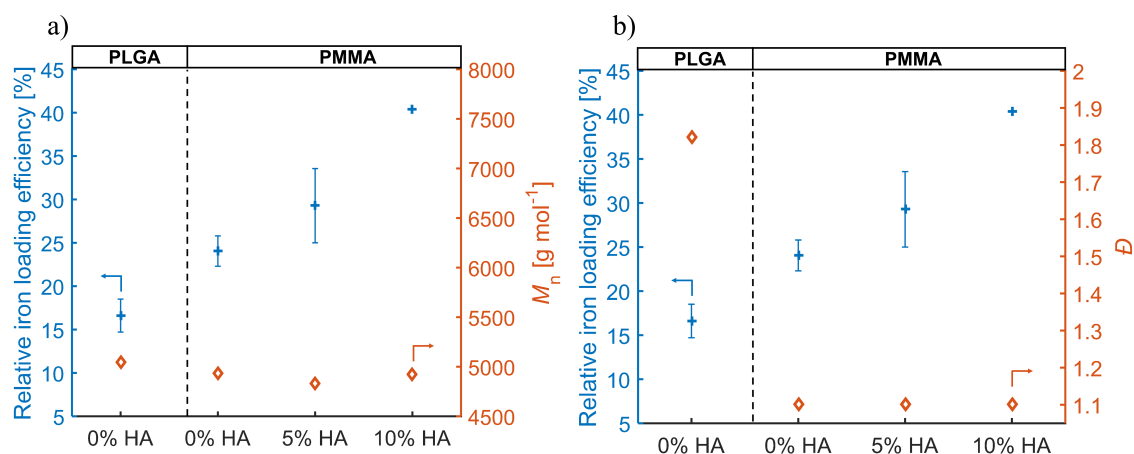
FIGURE S19 a) Relative iron loading efficiency of PLGA and PMMA nanoparticles with varying hydroxamic acid contents related to a) the molecular weight (M_n) and b) the dispersity (Đ) of the polymers.

Engagement of MNP by leukocytes.

Fluorescence activated cell sorting measurements were carried out to investigate the cell populations after treatment with curcumin-labelled polymeric nanoparticles on myeloid cells. Ly6G was utilized as a neutrophil-specific selective antibody to investigate the accumulation of MNPs in bone marrow neutrophils; whereas CD19 was applied to investigate the accumulation in splenic B cells. CD11 positive cells were utilized to identify bone marrow-derived dendritic cells and CD11c negative cells of the BMDC culture constitute macrophages. As a result, we observed a strong accumulation of polymeric nanoparticles in neutrophiles proven via a 54-fold increased mean fluorescence intensity (MFI) compared to the untreated reference sample. A strong accumulation was also observed in macrophages that was quantified as a 36-fold increase in the MFI. Rather moderate engagement was observed for dendritic cells (5-fold), but no considerable interaction with B cells (2-fold). (**Table S2**). All cell types demonstrated an excellent viability proven via the attachment of a fixable viability dye (FVD) (**Figure S19**).
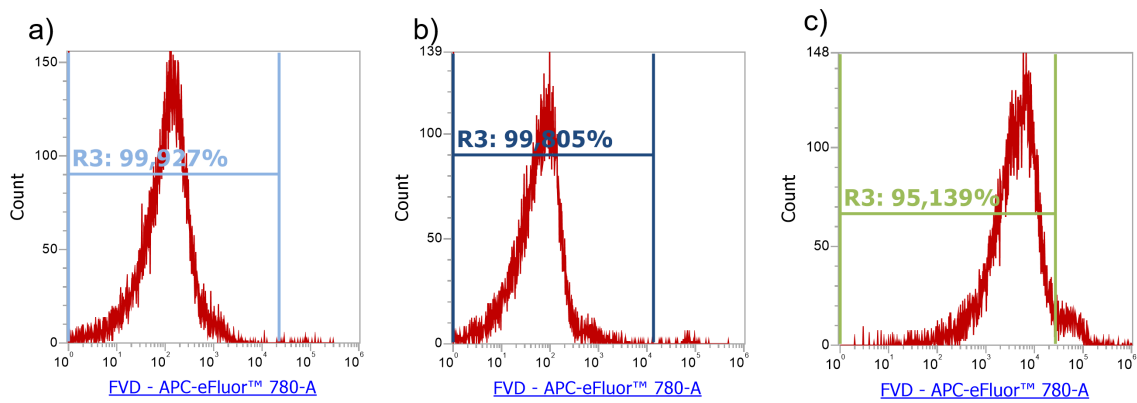
FIGURE S20 Fixable viability dye-labelled bone marrow neutrophils (a), splenic B cells (b), and bone marrow-derived dendritic cells and macrophages (c). The frequencies of viable (FVD-negative) cells are indicated.

TABLE S2 Mean fluorescence intensity (MFI) of the various tested leukocyte populations after over-night incubation with curcumin-labelled PMMA nanoparticles with varied hydroxamic acid amounts at different concentrations.

Concentration	SPION attached	HA [%$_{mol}$]	MFI (Neutrophils)	MFI (B cells)	MFI (Dendritic cells)	MFI (Macrophages)
		Untreated	1634	347	5690	1446
5%$_{vol}$	No	0	14913	378	9055	4623
	No	5	38799	510	18193	23124
	Yes	0	49278	685	16985	15767
	Yes	5	21676	400	14275	11540
50%$_{vol}$	No	0	24004	395	9698	7046
	No	5	89742	631	28004	52107
	Yes	0	57823	831	22813	25076
	Yes	5	59480	648	14596	14500
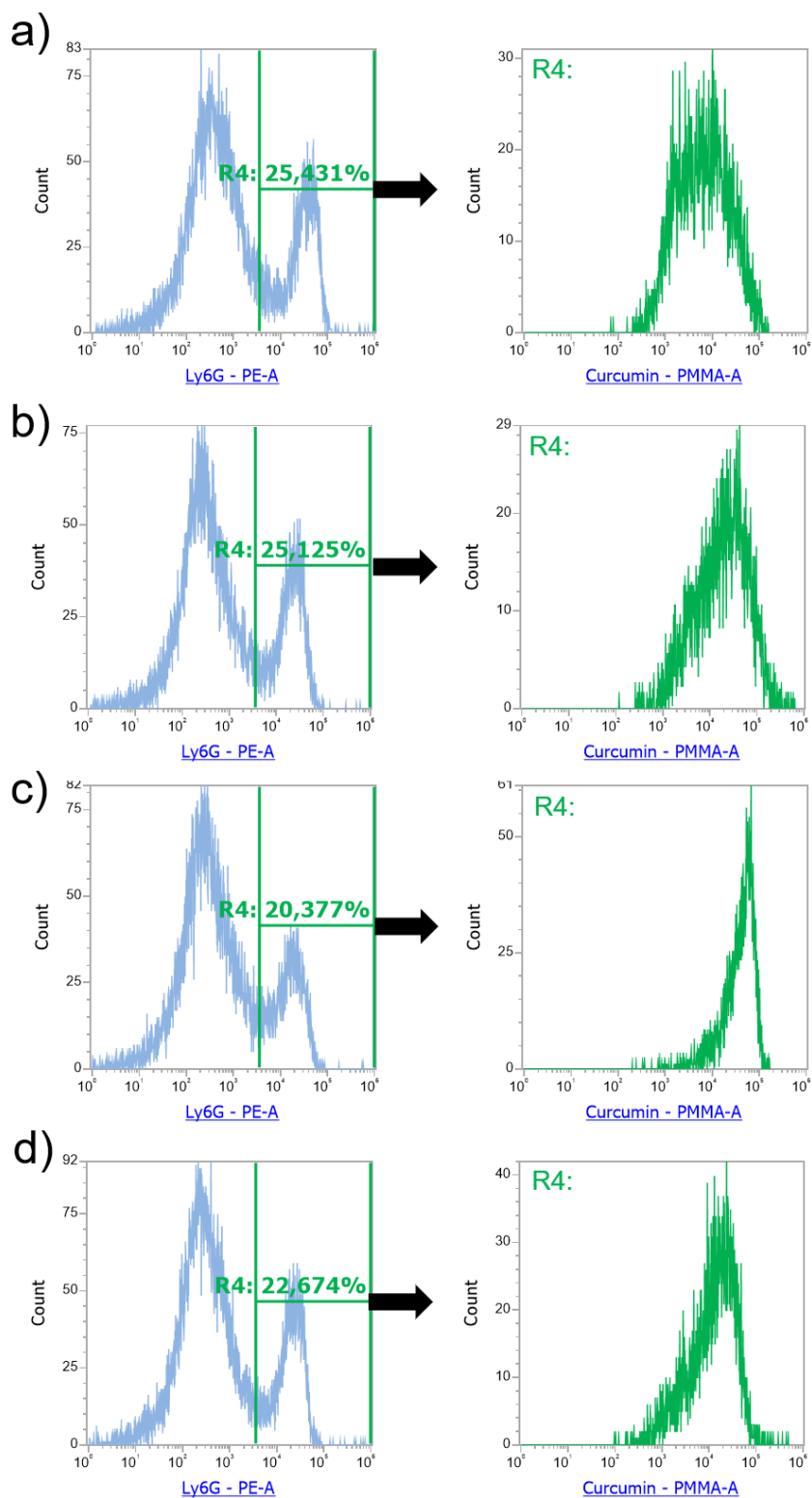
FIGURE S21 Fluorescence activated cell sorting of bone marrow Ly6G$^+$ neutrophils (left panel; frequencies indicated) after over-night incubation with curcumin-labelled PMMA nanoparticles (right panel; curcumin intensities) with varying hydroxamic acid contents before (a,b) and after (c,d) SPION attachment with a concentration of 5%$_{vol}$. a),c) PMMA nanoparticles (NP) with 0%$_{mol}$ HA, b),d) PMMA NP with 5%$_{mol}$ HA.
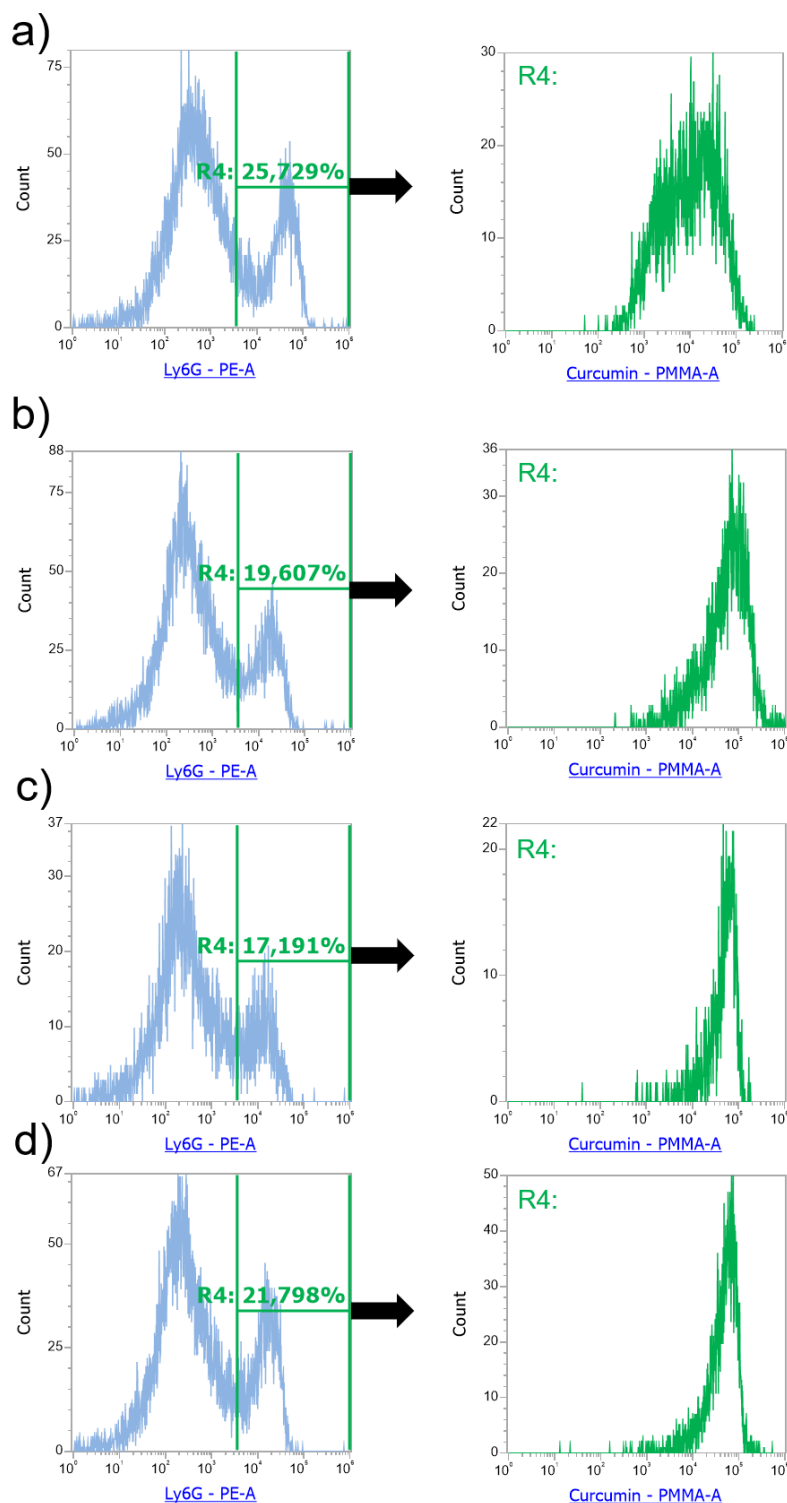
FIGURE S22 Fluorescence activated cell sorting of bone marrow Ly6G$^+$ neutrophils (left panel; frequencies indicated) after over-night incubation with curcumin-labelled PMMA nanoparticles (right panel; curcumin intensities) with varying hydroxamic acid contents before (a,b) and after (c,d) SPION attachment with a concentration of 50%$_{vol}$. a),c) PMMA nanoparticles (NP) with 0%$_{mol}$ HA, b),d) PMMA NP with 5%$_{mol}$ HA.
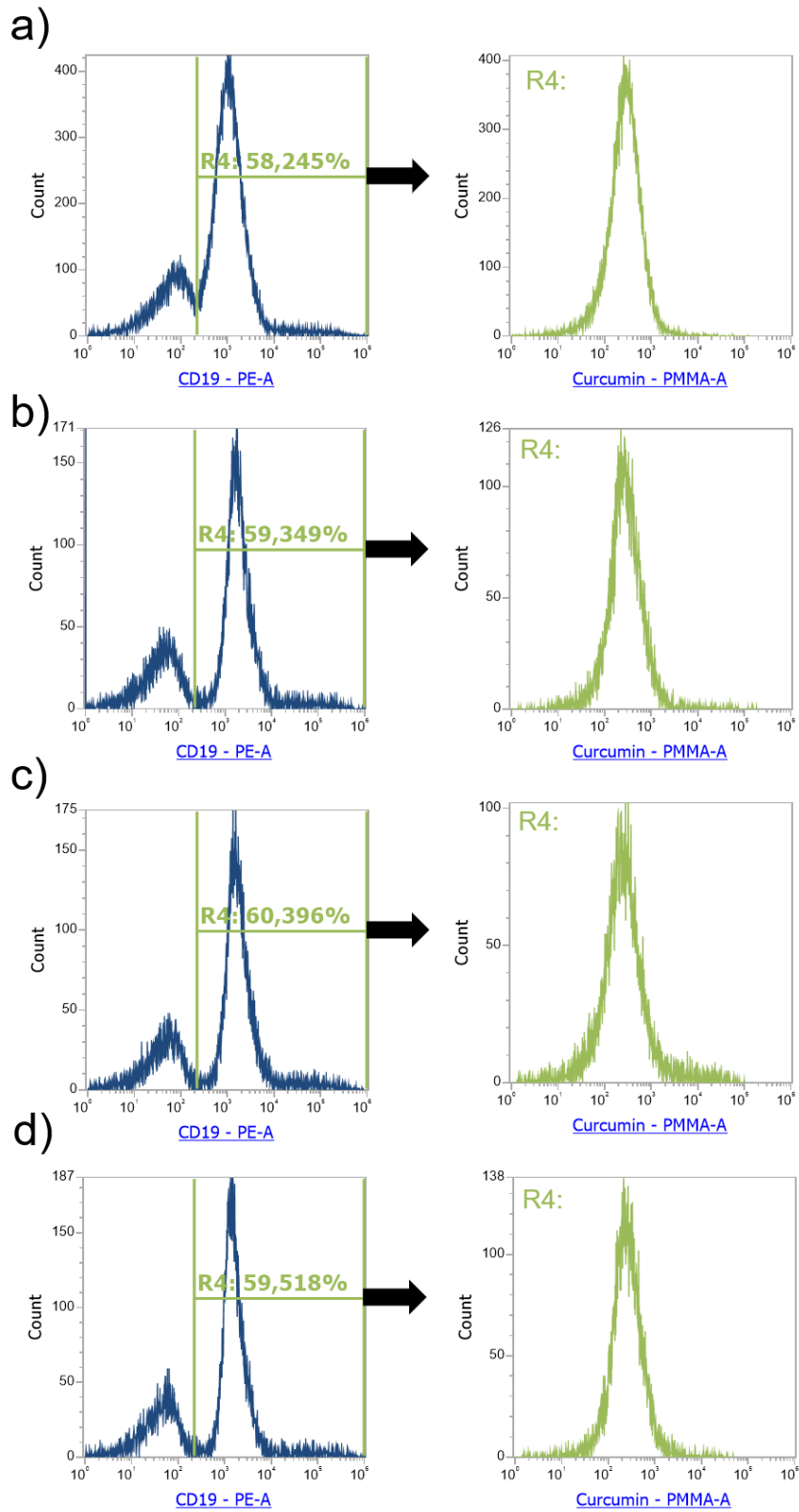
FIGURE S23 Fluorescence activated cell sorting of splenic CD19$^+$ B cells (left panel; frequencies indicated) after over-night incubation with curcumin-labelled PMMA nanoparticles (right panel; curcumin intensities) with varying hydroxamic acid contents before (a,b) and after (c,d) SPION attachment with a concentration of 5%$_{vol}$. a),c) PMMA nanoparticles (NP) with 0%$_{mol}$ HA, b),d) PMMA NP with 5%$_{mol}$ HA.
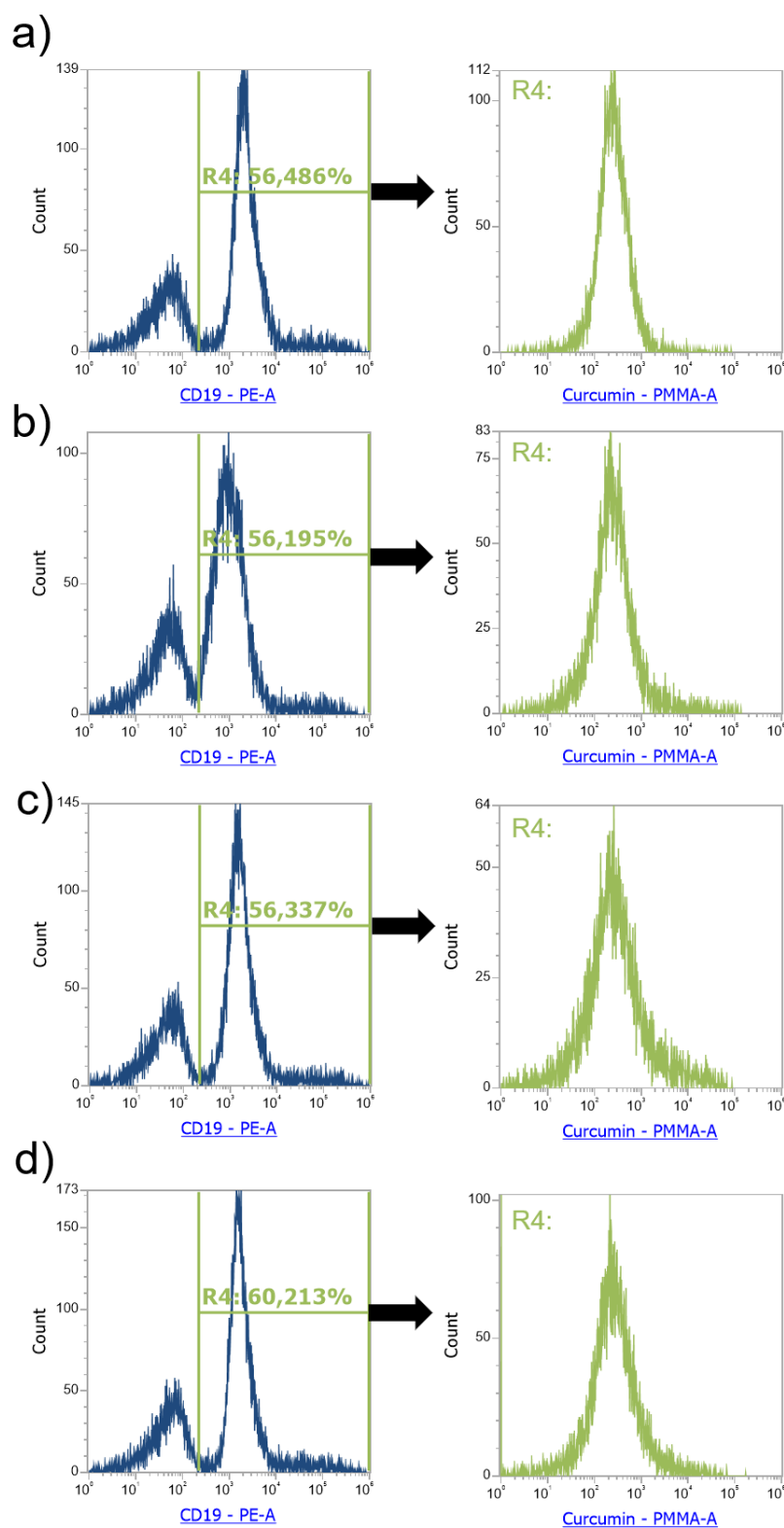
FIGURE S24 Fluorescence activated cell sorting of splenic CD19$^+$ B cells (left panel; frequencies indicated) after over-night incubation with curcumin-labelled PMMA nanoparticles (right panel; curcumin intensities) with varying hydroxamic acid contents before (a,b) and after (c,d) SPION attachment with a concentration of 50%$_{vol}$. a),c) PMMA nanoparticles (NP) with 0%$_{mol}$ HA, b),d) PMMA NP with 5%$_{mol}$ HA. CD19 was utilized as selective antibody.
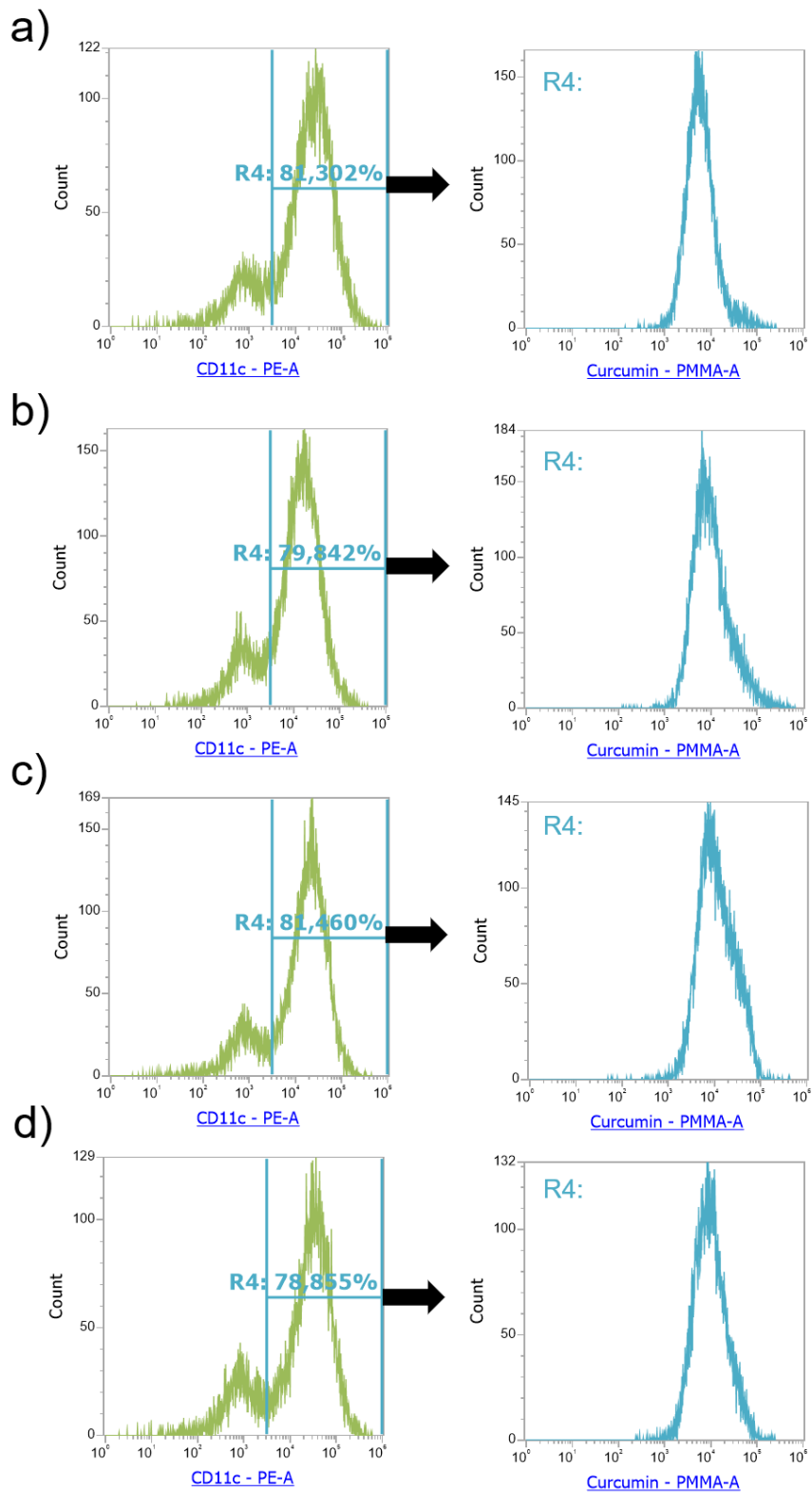
FIGURE S25 Fluorescence activated cell sorting of bone marrow-derived CD11c^{+} dendritic cells (left panel; frequencies indicated) after over-night incubation with curcumin-labelled PMMA nanoparticles (right panel; curcumin intensities) with varying hydroxamic acid contents before (a,b) and after (c,d) SPION attachment with a concentration of 5%$_{vol}$. a),c) PMMA nanoparticles (NP) with 0%$_{mol}$ HA, b),d) PMMA NP with 5%$_{mol}$ HA. CD11 was utilized as selective antibody.
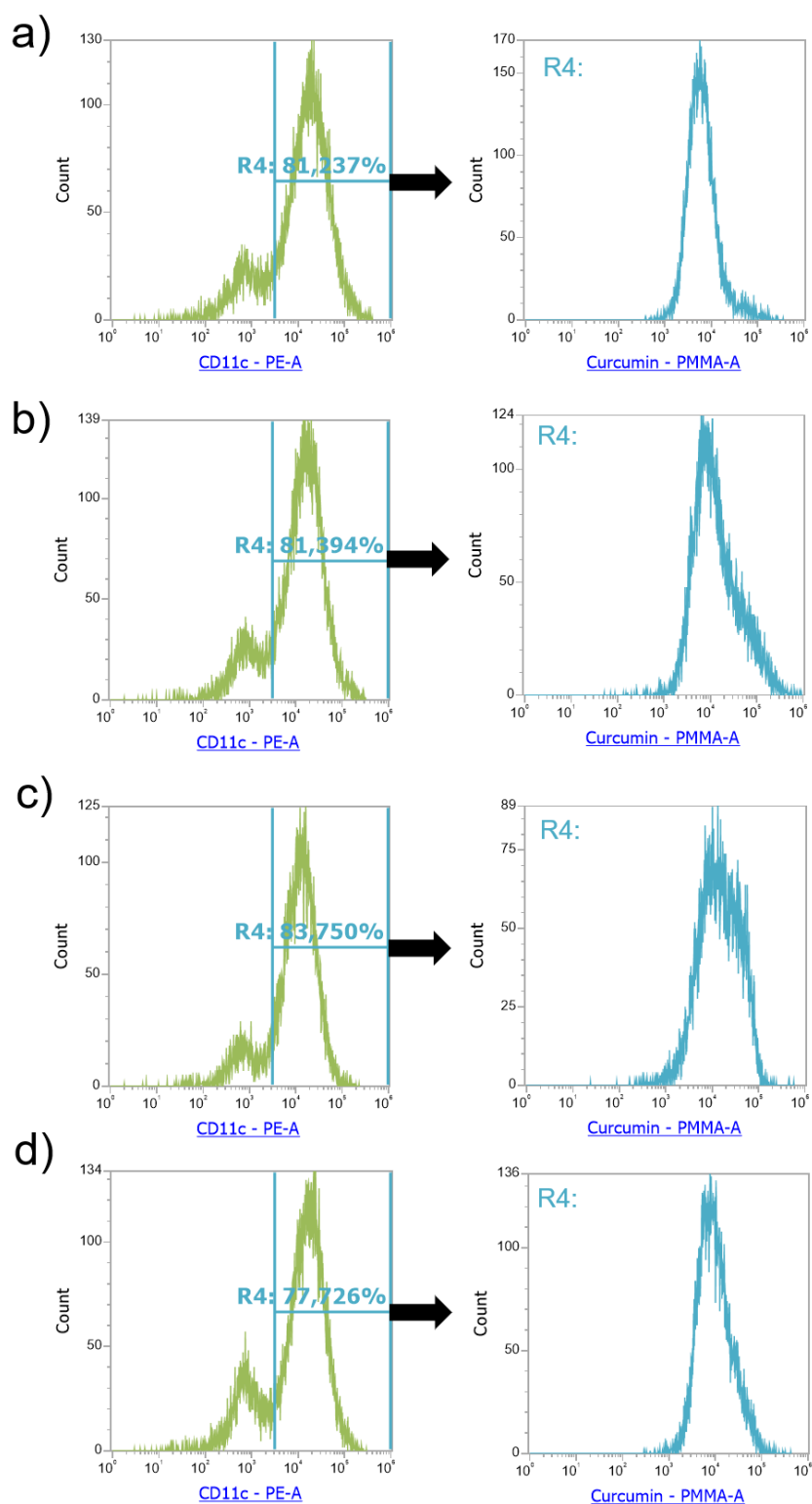
FIGURE S26 Fluorescence activated cell sorting of bone marrow-derived CD11c$^+$ dendritic cells (left panel; frequencies indicated) after over-night incubation with curcumin-labelled PMMA nanoparticles (right panel; curcumin intensities) with varying hydroxamic acid contents before (a,b) and after (c,d) SPION attachment with a concentration of 50%$_{vol}$. a),c) PMMA nanoparticles (NP) with 0%$_{mol}$ HA, b),d) PMMA NP with 5%$_{mol}$ HA. CD11 was utilized as selective antibody.
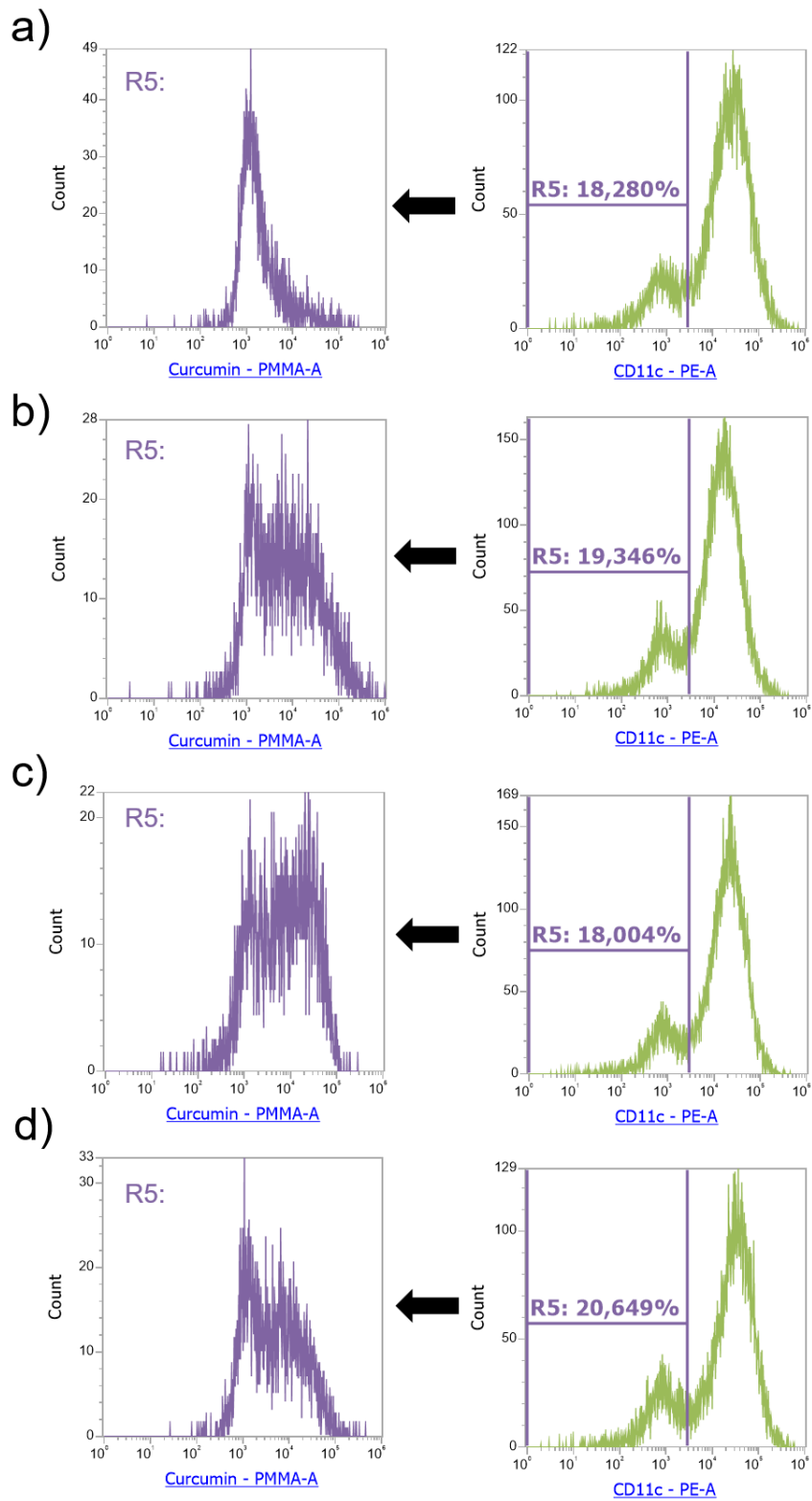
FIGURE S27 Fluorescence activated cell sorting of bone marrow-derived macrophages (CD11b$^+$CD11c$^-$) (right panel; frequencies indicated) after over-night incubation with curcumin-labelled PMMA nanoparticles (left panel; curcumin intensities) with varying hydroxamic acid contents before (a,b) and after (c,d) SPION attachment with a concentration of 5%$_{vol}$. a),c) PMMA nanoparticles (NP) with 0%$_{mol}$ HA, b),d) PMMA NP with 5%$_{mol}$ HA. CD11 was utilized as selective antibody.
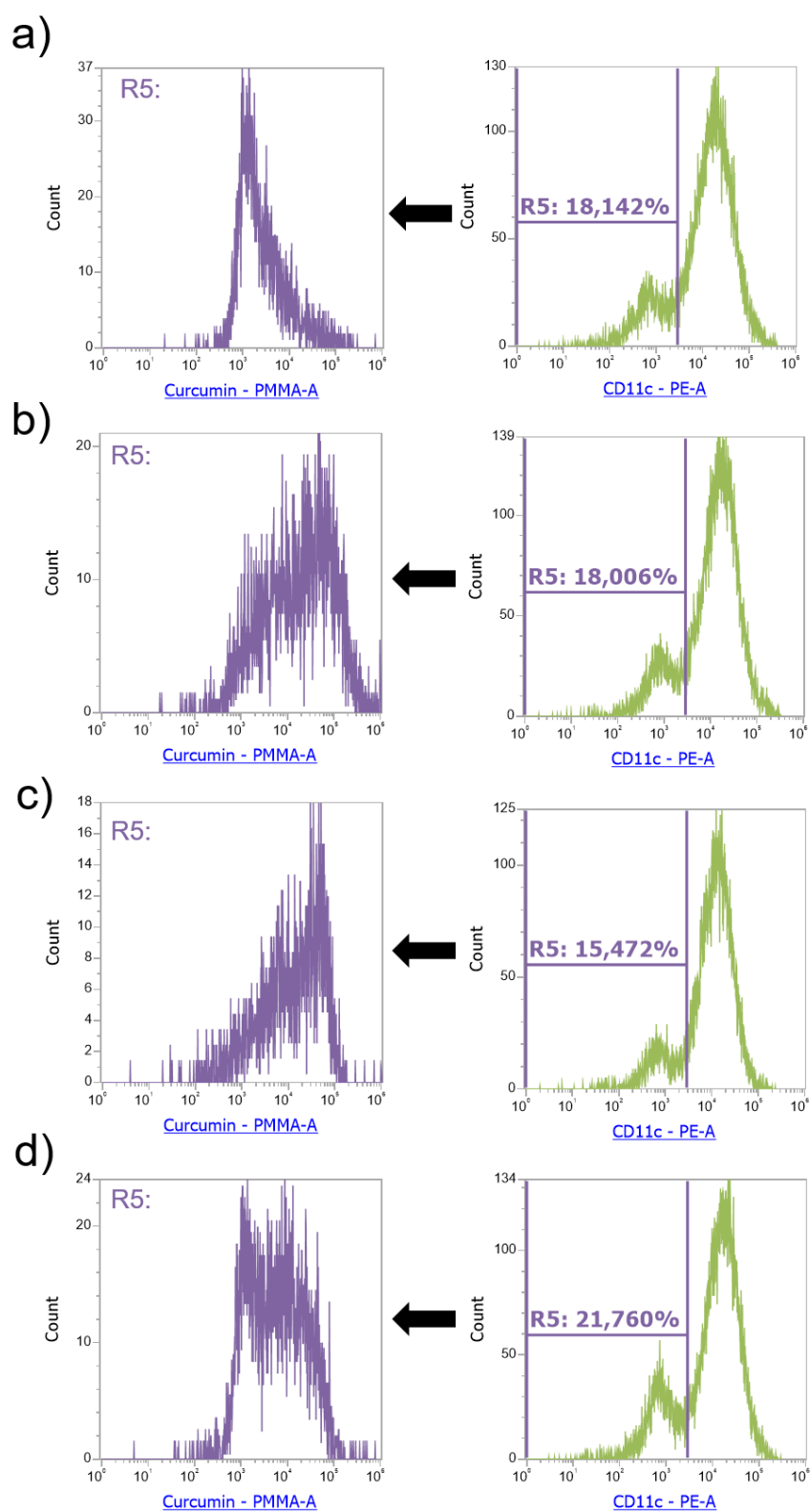
FIGURE S28 Fluorescence activated cell sorting of bone marrow-derived macrophages (CD11b$^+$CD11c$^-$) (right panel; frequencies indicated) after over-night incubation with curcumin-labelled PMMA nanoparticles (left panel; curcumin intensities) with varying hydroxamic acid contents before (a,b) and after (c,d) SPION attachment with a concentration of 50%$_{vol}$. a),c) PMMA nanoparticles (NP) with 0%$_{mol}$ HA, b),d) PMMA NP with 5%$_{mol}$ HA. CD11 was utilized as selective antibody.

APPENDIX

INTRODUCTION OF HYDROXAMIC ACIDS INTO
POLYMERS

APPENDIX

A general concept for the introduction of hydroxamic acids into polymers

Tobias Johann[1], Jennifer Keth[1], Matthias Bros[2] and Holger Frey[1,*]

[1]Institute of Organic Chemistry, Johannes Gutenberg University, Duesbergweg 10-14, 55128 Mainz, Germany
[2]Department of Dermatology, University Medical Center of the Johannes Gutenberg University Mainz, Langenbeckstrasse 1, 55131 Mainz, Germany

This work is closely connected to the investigations on hydroxamic acid-functionalized poly(methacrylate)s as metal chelators presented in Chapter 2. The author of this thesis contributed to this work by the synthesis of the methacrylate-based hydroxamic acid monomer MAHAA and its polymerization via controlled radical polymerization techniques.

Chemical Science

Check for updates

A general concept for the introduction of hydroxamic acids into polymers†

Tobias Johann,[a] Jennifer Keth,[a] Matthias Bros[b] and Holger Frey [ID] *[a]

Hydroxamic acids (HA) form stable complexes with a large variety of metal-ions, affording hydroxamates with high complexation constants. Hydroxamic acid moieties play a crucial role in the natural iron metabolism. In this work, 1,4,2-dioxazoles linked to a hydroxyl group are introduced as key compounds for the installation of hydroxamic acids at synthetic polymers in well-defined positions. A general synthetic scheme is developed that gives access to a series of novel functional key building blocks that can be universally used to obtain hydroxamic acid-based monomers and polymers, for instance as protected HA-functional initiators or for the synthesis of a variety of novel HA-based monomers, such as epoxides or methacrylates. To demonstrate the excellent stability of the dioxazole-protected hydroxamic acids, direct incorporation of the dioxazole-protected hydroxamic acids into polyethers is demonstrated *via* oxyanionic polymerization. Convenient subsequent deprotection is feasible under mild acidic conditions. α-Functional HA-polyethers, *i.e.* poly ethylene glycol, polypropylene glycol and polyglycerol based on ethylene oxide, propylene oxide and ethoxy ethyl glycidyl ether, respectively are prepared with low dispersities (<1.2) in the molecular weight range of 1000 to 8500 g mol^{-1}. Water-soluble hydroxamic acid functional poly(ethylene glycol) (HA-PEG) is explored for a variety of biomedical applications and surface coating. Complexation of Fe(III) ions, coating of various metal surfaces, enabling *e.g.*, solubilization of FeO$_x$ nanoparticles by HA-PEGs, are presented. No impact of the polyether chain on the chelation properties was observed, while significantly lower anti-proliferative effects were observed than for deferoxamine. HA-PEGs show the same complexation behavior as their low molecular weight counterparts. Hydroxamic acid functional polymers are proposed as an oxidatively stable alternative to the highly established catechol-based systems.

Introduction

In the last two decades, biomimetic materials with chelating and interface-adhesive moieties, such as catechols or their derivatives, have been investigated intensely.[1,2] Particularly catechol-bearing polymers that mimic mussel-foot proteins containing dopamine have attracted broad interest, as their outstanding adhesive properties enable strong interaction with almost every surface.[1,3,4] Numerous applications like self-healing hydrogels, surface coatings for anti-fouling purposes or the formation of supramolecular networks, especially by combination of chelating moieties with polymers, have been demonstrated.[5] In two of our previous works we focused on the direct incorporation of catechols into polyethers *via* anionic polymerization. Polymers bearing a single catechol moiety were used for the stabilization of MnO nanoparticles in solution. *Via* a tailored catechol epoxide monomer, multiple units were introduced along the polyether backbone enabling gelation upon iron(III) addition.[6] However, most catechols are unstable under aqueous conditions and are known to crosslink *via* oxidative coupling. This irreversible reaction leads to highly toxic Michael systems. Even though no Michael adduct of amines and the quinone structure was found in studies of Deming *et al.*, the quinone structures lead to cross-linked materials, impeding the reversibility of the formed complexes.[4] Nevertheless, catechols are ubiquitous in nature as one of two moieties to form so called siderophores (greek: "iron carrier"). The second prominent class of siderophores relies on hydroxamic acids. These *N*-hydroxylated amides are capable of forming stable complexes with a large variety of metal-ions, affording hydroxamates with complexation constants in the range of $\log K = 28$ for tris-complexes to $\log K = 20$ for bis-complexes.[7,8] Their binding affinity to metals is generally 7 magnitudes higher compared to carboxylic acids due to the formation of a five membered ring.[9] In nature this class of siderophores is essential to solubilize water-insoluble iron oxide, thus increasing the bioavailability of this key element.[10]

[a]Institute of Organic Chemistry, Johannes Gutenberg University, Duesbergweg 10-14, 55128 Mainz, Germany. E-mail: hfrey@uni-mainz.de

[b]Department of Dermatology, University Medical Center of the Johannes Gutenberg University Mainz, Langenbeckstrasse 1, 55131 Mainz, Germany

† Electronic supplementary information (ESI) available: NMR, IR, SEC, LCST and mass spectroscopy characterization, cell toxicity and proliferation assay data. See DOI: 10.1039/c9sc02557j

More than 42 different metal-hydroxamate complexes including (but not limited to) Fe(III), Mn(II), Zn(II), Cu(II) and Ni(II) are currently known.[7,8,11] In contrast to catechols, hydroxamic acids are stable under physiological conditions and neither undergo oxidation nor crosslinking. They show similar pK_s-values in the range of 7–9.[12]

While there are only few studies on hydroxamic acids in the field of synthetic polymers, they are well established in the therapy of iron overload diseases or as potent inhibitors for histone deacetylases that are mostly associated with cancer development.[13] Early efforts to combine hydroxamic acids with polymers were patented in 1942 by Du Pont.[14] First systematic studies were reported by Winston et al. in the late 1970s. In these works, poly(hydroxamic acids) were synthesized by polymer modification reaction of poly(methacrylate)-based active esters with hydroxylamine derivatives.[15,16]

A variety of applications was proposed for polymers containing hydroxamic acids. Due to their strong complexation of metal-ions the most prominent application is their use as ion-exchange resins or for waste-water treatment.[17–19] In other works, poly(hydroxamic acid)s were used for the separation of rare earth metals.[17,19] Furthermore, application of poly(-hydroxamic acid)s as starting material for peptide synthesis and as resin-bound acryl transfer reagent was reported.[20] We emphasize that in all published reports the hydroxamic acid containing polymers were synthesized via polymer modification (post-polymerization) of carbonyl compounds, such as esters or amides with hydroxylamine. However, this approach inevitably leads to limited conversion due to the harsh reaction conditions, which is an obstacle for many applications, particularly for medical purposes.[21] Nome and coworkers showed that the conversion of polyamides to hydroxamic acids by reaction with hydroxylamine leads to an alternating copolymer with both carboxylic and hydroxamic acids due to neighboring effects.[22] In recent works Kizhakkedathu et al. reported conjugates of hyperbranched polyethers with deferoxamine (DFO, Desferal), a biologically produced tris-hydroxamic acid used for the therapy of iron overload diseases.[23] These modified polyethers improved the plasma half time of deferoxamine 500-fold. This enhancement in pharmacokinetic properties impressively demonstrates the potential of hydroxamic acid functional polyethers. Besides the medical use of hydroxamic acids for the therapy of iron overload diseases, structures analogous to biological siderophores like desferrichrome containing multiple hydroxamic acids have been investigated as potent Zr(IV) chelators for PET imaging.[24] Radical polymerization of hydroxamic acid functional methacrylates was shown to proceed with incomplete conversion due to radical transfer to the hydroxamic acid moiety.[25] Hence, the attachment of hydroxamic acids to synthetic polymer architectures via polymer modification or direct radical polymerization represents a challenge, and new strategies based on HA-based building blocks are required.

In this work we describe a systematic approach for the introduction of hydroxamic acids to polymers via tailored hydroxyl functional 1,4,2-dioxazoles. The concept presented can be applied to different classes of monomers and initiators that are amenable to both radical and anionic polymerization. Polymers from epoxide and methacrylate based monomers utilizing the 1,4,2-dioxazole group to introduce multiple hydroxamic acids along the polymer backbone are currently in progress and will reported in forthcoming works. At the example of the harsh conditions of the anionic ring opening polymerization, we demonstrate in the second part of this work the introduction of precisely one hydroxamic acid end group in polyethers, in particular in poly(ethylene glycol), aiming at a narrow molecular weight distribution for medical application, combined with a well-defined polymer structure, enabling investigation of the structure-related properties of hydroxamic acid functional polyethers. We aim at combining the chelating properties of hydroxamic acids with PEG as the current "gold standard" of biocompatible, water-soluble polymers.[26] Based on this work we propose hydroxamic acids as an oxidation-stable alternative to catechols in the field of materials science.

Results and discussion

A. Molecular construction kit for hydroxamic acid synthons based on 1,4,2-dioxazole protected functional structures

For the introduction of hydroxamic acids to polymers we initially screened various polymer modification approaches. Typically hydroxamic acids are introduced at the end of a synthetic sequence, e.g. at a polymer structure by reaction with hydroxylamine or its protected derivatives, leading to incomplete functionalization with many side products. This strategy also lacks general applicability.[22,27] Hence, for the introduction of hydroxamic acids into polymers, we decided to avoid post-polymerization processes with hydroxylamine as a common option for functionalization, as they are restricted to a particular polymer system and thus limit the universal character for further applications. To establish functional groups at well-defined sites during chain-growth polymerization either (i) functional initiators (ii) functional monomers or (iii) functional termination reagents can be employed. Protected hydroxyl functional hydroxamic acids were developed for this approach, featuring both a protected hydroxamic acid to ensure stability during polymerization and a hydroxyl group for further transformation or use as initiators or monomers.

The hydroxyl moiety can be conveniently transformed to methacrylate monomers and epoxide monomers (Scheme 2), for instance glycidyl ethers. Additionally, the hydroxyl group can directly be used in anionic ring opening polymerization (AROP) as an initiator for epoxide or lactide polymerization, thus creating a platform for both radical as well as anionic polymerization (Scheme 1). In this work we place the focus on the use of hydroxyl functional initiators for AROP of common epoxides (EO, PO, glycidyl ethers) to combine the hydroxamic acids with medically relevant polymers. Multifunctional polyethers from hydroxamic acid functional epoxides, as well as methacrylate based HA copolymers are currently in progress and will be reported in forthcoming works.

Selection and optimization process of the protected hydroxamic acid initiator. Based on the abovementioned prerequisites, we focused on (i) the selection of suitable
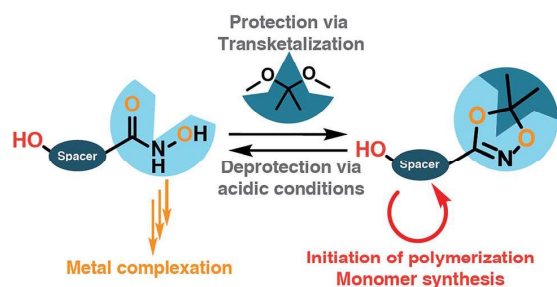
Scheme 1 General concept for the introduction of hydroxamic acids at polymers: the hydroxamic acid is protected in the 1,4,2-dioxazole group *via* transketalization. The remaining free hydroxyl group can be used as a starting point either for monomer synthesis (methacrylates, epoxides) or as an initiator for anionic ring opening polymerization. After acidic treatment the 1,4,2-dioxazole group is cleaved to release the free hydroxamic acid for metal complexation.

functional hydroxamic acids and (ii) the optimization of protection and deprotection procedures to ensure stability of the hydroxamic acid during the polymerization process, while maintaining the capability of mild and facile deprotection and release of the functional moiety.

Choice of suitable hydroxyl functional hydroxamic acids. No compound containing a hydroxyl group combined with a hydroxamic acid, except for salicylhydroxamic acid and N,4-dihydroxybenzamide (Scheme 2, compound **2a**), is currently commercially available. Salicylhydroxamic acid is not suitable
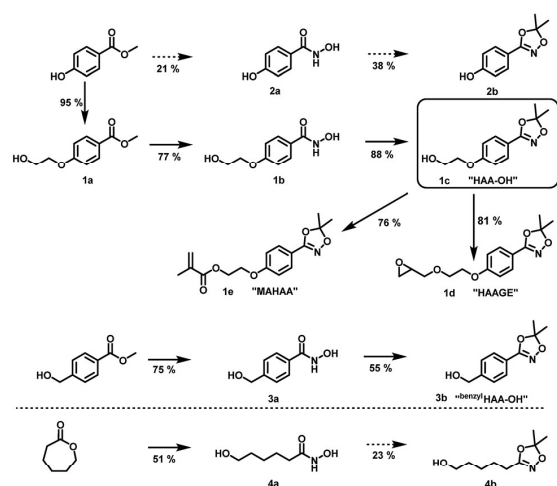
Scheme 2 Preparation of hydroxyl functional hydroxamic acids, their corresponding protected 1,4,2-dioxazole form and further trans-formation to monomers (**1d**, **1e**) developed in this work. See ESI Scheme S1† for additional reactions with C_3 and C_4 aliphatic spacers. Conditions for the preparation of hydroxamic acids (**1b**, **2b**, **3a**, **4a**): NH$_2$OH/KOH/MeOH or water, RT; conditions for the preparation of 1,4,2-dioxazoles: 2,2-dimethoxy propane or 2,2-diethoxy propane, CSA, DCM, RT. For detailed synthesis description see experimental section.

for facile conversion to 1,4,2-dioxazoles due to the close proximity of the hydroxyl group in *ortho* position to the hydroxamic acid moiety, prohibiting the synthesis *via* scalable processes.[28] Hence, N,4-dihydroxybenzamide (**2a**) was chosen as a first candidate for the preparation of the desired initiators. Even though N,4-dihydroxybenzamide (**2a**) is available at specialized chemical distributors, albeit its high price impedes larger scale synthesis of the 1,4,2-dioxazole. The preparation of **2a** is known in literature, but typically multistep syntheses or costly protected hydroxylamine derivatives are employed.[29]

To maintain a scalable process, we focused on preparation methods for hydroxamic acids based on esters and hydroxylamine, due to the absence of protecting group chemistry, excellent commercial availability and the preparation in one step. Hence, *para*-methyl paraben was chosen as a starting material for the synthesis of **2a** *via* nucleophilic cleavage of the ester bond by hydroxylamine (See ESI Fig. S5a–f† for NMR and IR characterization data). Unfortunately, all attempts to synthesize the corresponding hydroxamic acid led to low yields with many side products and thus troublesome purification. This is attributed to the deprotonation of the phenolic hydroxyl group, leading to a delocalized negative charge within the aromatic system. Hence, nucleophilic attack by hydroxylamine to form the hydroxamic acid is highly obstructed. To overcome this issue, we introduced an ethylene glycol C_2 spacer, which enabled facile synthesis of the hydroxyl functional hydroxamic acid ("HA-OH", **1b**) in high yields (77%) (ESI Fig. S3a–f†). Aiming at a reduction of the necessary synthetic effort, the aromatic hydroxamic acid ("^{benzyl}HA-OH", **2a**) was also prepared from the commercially available ester precursor (ESI Fig. S7a–e†). Additionally lactones were explored for the preparation of aliphatic derivatives (**4a**, see ESI Scheme S1† for further details), since naturally occurring hydroxamic acid-based siderophores are typically aliphatic structures.[10] The preparation of hydroxamic acids from lactones is known in literature.[30] The conversion of caprolactone to N,6-dihydroxyhexanamide (**4a**) (ESI Fig. S9a–f†) and valerolactone to N,5-dihydroxypentanamide (Scheme S1† compound **5**) proceeded smoothly in moderate yields, but all attempts to convert butyrolactone to N,4-dihydroxybutanamide led to complex mixtures requiring excessive purification efforts. In summary, the aromatic hydroxamic acids **1b** and **3a**, as well the aliphatic hydroxamic acids **4a** and **5** fulfilled the necessary requirements for facile and large-scale synthesis and were subsequently used for conversion to 1,4,2-dioxazoles.

Optimization of the protection and deprotection reaction. The anionic ring opening polymerization of epoxides employs both strong nucleophilic as well as harsh basic conditions. Therefore, any carbonyl compound and protic groups have to be protected. The 1,4,2-dioxazole group was chosen as a suitable protection group, as it can be expected to withstand the harsh conditions of AROP. Besides its inert character against strongly basic conditions, the 1,4,2-dioxazole group has been reported to be stable against other nucleophiles, such as EtMgBr, oxidation with KMnO$_4$ or reduction by NaBH$_4$. In this context, the four hydroxamic acid derivatives **1b**, **2a**, **3a** and **4a** were converted to the corresponding 1,4,2-dioxazoles (Scheme 2). This 1,4,2-dioxazole group can be viewed as the acetonide derivative of
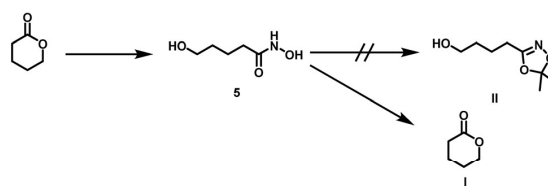
a tautomeric form of **1b** and is therefore designated "hydroxamic acid acetonide" (HAA). As reported in a different context by Couturier *et al.*[31] and Geffken and Fröböse,[32] the transketalization of hydroxamic acids is unfortunately not straightforward. Varying amounts of side products, depending on the substituent adjacent to the hydroxamic acid, is formed during the reaction. In this side reaction *O*-acyl acetone oxime (see Scheme 3I for an exemplary structure) is formed, which readily reacts with nucleophiles such as alcohols to form esters. The amount of side product is significantly higher for aliphatic hydroxamic acids (8 : 1 dioxazole : side product) compared to aromatic derivatives (25–30 : 1 dioxazole : side product).[31] For evaluation purposes, all three aromatic hydroxamic acids (**1b**, **2a** and **3a**) were converted to the corresponding 1,4,2-dioxazoles. As expected, the side reaction occurred in only negligible amounts (ESI Fig. S4a–f, S6a–e and S8a–e†).

Surprisingly, the reaction starting from the aliphatic hydroxamic acid **4a** proceeded to form mainly caprolactone by intramolecular ring closure of the *O*-acyl acetone oxime side product (Scheme 2, see Fig. S10† for ¹H NMR of 1,4,2-dioxazole, after purification still some caprolactone is left due to troublesome separation). Hence, intramolecular attack of the hydroxyl group appears to enhance the side reaction, limiting the overall yield (<23%) of the desired aliphatic 1,4,2-dioxazole derivative. Attempts to prepare 4-(5,5-dimethyl-1,4,2-dioxazol-3-yl)butan-1-ol from valerolactone *via* the hydroxamic acid **5** completely failed and led to this side reaction exclusively (Scheme 4). Considering the synthetic effort and low yields, the aliphatic (**4b**) as well aromatic (**2b**) protected hydroxamic acid were not further used for any polymerization. These findings suggest that a rigid spacer like the aromatic ring is beneficial for the preparation of hydroxyl functional 1,4,2-dioxazoles *via* transketalization.

Suitable hydroxamic acid initiators for the oxyanionic polymerization have to be both aprotic and base-stable and must possess one hydroxyl group that can be used to form the corresponding alkoxide-initiator salt for the anionic ring opening polymerization. Both aromatic protected hydroxamic acids (**1c** "HAA-OH", **3b** "ᵇᵉⁿᶻʸˡHAA-OH") fulfil these requirements for AROP and have been successfully used for the preparation of functional polyethers (see below). For the different polymer molecular weight series, **1c** was selected due to methyl paraben being a cheap and widely commercially available starting material. We emphasize that this synthetic route employs only inexpensive and commercially available chemicals, permitting
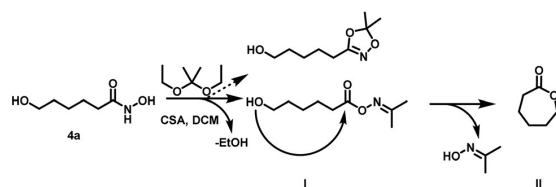
Scheme 4 Side reaction during transketalization of **5** leading to valerolactone (**I**) *via* formation of *O*-acyl acetone oxime, subsequent intramolecular ring closure.

scale-up to 20 g with 64% overall yield. We have to emphasize that although the aliphatic initiator **4b** was not used in this work for further polymerization, aliphatic hydroxamic acids can be installed in polyethers *via* this approach. Additionally, to further demonstrate the wide applicability of this approach HAA-OH (**1b**) was used as a starting material for the preparation of an 1,4,2-dioxazol bearing glycidyl ether (**1d**) and a methacrylate derivative (**1e**). The hydroxamic acid acetonide glycidyl ether (HAAGE) was synthesized in high yields (81%) from **1b** *via* phase transfer catalysis in a one-step reaction (See ESI Fig. S11† for NMR analysis). Methacrylate hydroxamic acid acetonide (MAHAA) (**1e**) was obtained *via* Steglich esterification of **1b** with methacrylic acid (See ESI Fig. S12† for NMR analysis). Polymers based on both monomers are currently in progress and will be reported in a forthcoming work. To sum up, hydroxyl-functional 1,4,2-dioxazoles represent the key structure for the preparation of monomers and polymers.

B. Polymer synthesis: hydroxamic acid functional polyethers

α-Functional polyethers were prepared from the two selected functional initiators **1c**, **3b** to introduce one terminal hydroxamic acid (HA) moiety. Although this limits the binding capacity for metal ions, the use of a single complexing moiety inherently prevents crosslinking *via* metal chelation, thus providing water-soluble complexes in case of PEG. This requirement is essential to avoid aggregation of coated nanoparticles or gelation.

Scheme 3 Side reaction during transketalization of **4a** leading to caprolactone (**II**) *via* formation of *O*-acyl acetone oxime (**I**) and subsequent intramolecular ring closure.
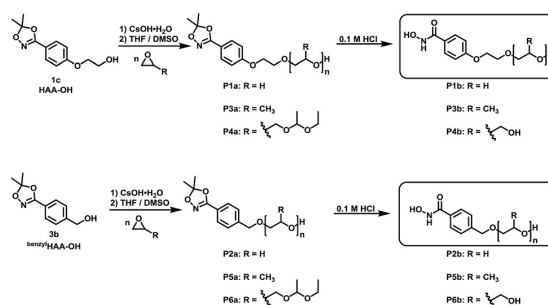
Scheme 5 Synthesis of HAA based polyethers (HAA–PEG, HAA–PPO, HAA–PEEGE) and subsequent cleavage of the protecting group to release the free hydroxamic acid functional polyethers (HA–PEG, HA–PPO, HA-*lin*PG).

HAA-poly(ethylene glycol)s (HAA-PEGs) **P1a**, **P2a** with molecular weights in the range of 1000 to 8500 g mol^{-1} were prepared *via* AROP of ethylene oxide (Scheme 5, Table 1) in THF/DMSO. The preparation of polyethylene glycol based polymers was chosen as PEG represents the gold standard polymer for biomedical application. Also polymers based on propylene oxide (PO) **P3a**, **P5a** and ethoxy ethyl glycidyl ether (EEGE) **P4a**, **P6a** have been prepared to broaden the scope of materials and to demonstrate general application of **1c**. Polypropylene oxide (PPO) was chosen as a hydrophobic polyether counterpart to PEG. PPO exhibits a lower critical solution temperature (LCST), enabling temperature dependent aqueous solubility below 20 °C (for PPO$_{50}$).[26,33] One downside of linear polyethers is their limited number of functional groups. In the case of functional initiated polyethers like in this work, only the terminal OH group can be addressed for further functionalization of the polymers. To overcome this issue, poly(ethoxy ethyl glycidyl ether) (PEEGE) polymers were prepared. EEGE is an acetal-protected glycidol monomer. These hydrophobic PEEGE polymers can easily be converted (by acidic treatment) to hydrophilic linear polyglycerol (*lin*PG), which exhibits one hydroxyl group per repeating unit, enabling access to multi-functional polyethers.[33]

In all cases full conversion was achieved within 24 h reaction time. All HAA-PEG, HAA-PPO and HAA-PEEGE polymers exhibit monomodal molecular weight distributions with narrow dispersities below 1.20 (Fig. 1, Table 1, ESI Fig. S1†). The degree of polymerization was kept low (10–20) for both the PPO and PEEGE polymers to limit this side reaction. Higher degrees of polymerization are possible, based on these proof-of-principle studies and further optimization. Purification of the polymers was performed *via* partitioning between water and DCM to obtain the salt-free, pure polymers in good yields (73–94%).

For all polymerizations conducted good agreement of target molecular weights with molecular weights determined *via* NMR end group analysis can be confirmed. Slight differences are accounted to the normalization of the integrals to the initiator, leading to uncertainties in the determination of approx. ±250 g
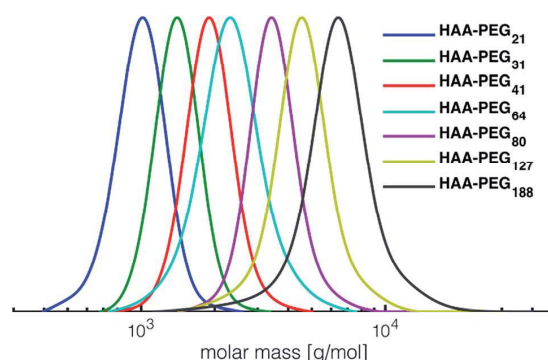
Fig. 1 SEC traces of the prepared HAA-PEGs (DMF, PEG-calibration). HA-PEGs after deprotection strongly interact with SEC column material and hence cannot be analyzed *via* SEC. See Fig. S1† for SEC traces of PPO and PEEGE as well benzylHAA-OH initiated polymers.

mol^{-1}. The discrepancy between SEC and NMR molecular weight can be explained by the PEG standards used for calibration. Similar underestimation of molecular weights *via* SEC have been reported for both PPO as well PEEGE polymers.[33] In case of PEEGE slight broadening of the molecular weight distribution can be detected. This is attributed to the high polymerization temperature of EEGE (80 °C), increasing known side reactions such as proton abstraction and elimination, leading to overall broadening of the molecular weight distribution.[34]

^{1}H NMR analysis confirms (ESI Fig. S13–S18†) the successful initiation of the polymers from either HAA-OH or benzylHAA-OH respectively. This can further be verified by the excellent overlap of UV and RI signal in SEC measurements (not shown). The thermo-responsive behaviour of HAA-PPO$_{21}$ was investigated in deionized water. As expected, a cloud point at 12.9 °C was observable (ESI Fig. S2†), at which the aqueous solution turned turbid and HAA-PPO$_{21}$ precipitated. In summary, both hydroxyl-functional protected hydroxamic acids have been proven to be

Table 1 Overview of the prepared protected hydroxamic acid functional polyethers

Polymer	M_n target [g mol^{-1}]	M_n (NMR)^a [g mol^{-1}]	M_n (SEC)^b [g mol^{-1}]	$Đ^b$
HAA-PEG$_{21}$	990	1160	960	1.06
HAA-PEG$_{31}$	1470	1600	1370	1.05
HAA-PEG$_{41}$	1950	2040	1850	1.06
HAA-PEG$_{64}$	3010	3050	2210	1.11
HAA-PEG$_{80}$	3800	3760	3380	1.06
HAA-PEG$_{127}$	6180	5830	4360	1.09
HAA-PEG$_{188}$	8080	8520	6010	1.13
benzylHAA-PEG$_{41}$	2200	2010	1250	1.09
benzylHAA-PEG$_{75}$	4220	3510	1810	1.07
HAA-PPO$_{21}$	1400	1460	1360	1.06
benzylHAA-PPO$_{21}$	1370	1430	1310	1.07
HAA-PEEGE$_7$	1700	1410	860	1.22
HAA-PEEGE$_{26}$	4470	4180	1790	1.14
benzylHAA-PEEGE$_6$	1670	1080	880	1.20

^{a} Determined *via* end group analysis in NMR. ^{b} DMF SEC, PEG standard.

a viable initiator for the polymerization of various epoxide monomers, leading to water-soluble hydrophilic PEG, thermoresponsive PPO or multi-functional PEEGE polymers bearing a terminal hydroxamic acid unit.

Cleavage of the protecting group and release of the free hydroxamic acid moiety. In an optimized procedure, cleavage of the protecting group was achieved by simple treatment of the HAA-PEGs with 0.1 molar HCl. These acidic conditions lead to degradation of the dioxazole structure, thus liberating the free hydroxamic functional PEG (HA-PEG, **P1b**) in quantitative yields. Compared to the reported deprotection scheme of Couturier *et al.* this greatly reduces the necessary effort by omitting the usage of ion-exchange resins.[31] Successful cleavage of the acetal protecting group can both be confirmed *via* ^{1}H NMR (Fig. 2, ESI Fig. S13b†) and mass spectra (Fig. 3). No signal of the dioxazole methyl group was detected in the product. Furthermore, both signals of the labile NH and OH-protons are observed at 11.06 and 8.90 ppm (^{1}H NMR) in DMSO-d_6. The polyether backbone remained unaltered.

ESI mass spectra reveal only the desired HAA-PEG and HA-PEG species, respectively. Comparing both polymers, a distinct shift of 40 g mol^{-1}, corresponding to cleavage of the protecting group, can be seen. Each spectrum shows only the distribution of the polymers with 44.05 g mol^{-1} per repeating unit. No sub-distribution can be detected (see ESI Fig. S19 and S20† for full spectra).

Both protecting groups employed in the synthesis of HAA-PEEGE (**P6a**) are acetals. Hence, the cleavage of both protecting groups can be achieved simultaneously *via* acidic treatment. Due to the hydrophobicity of PEEGE the cleavage is very slow in aqueous media. For improved reaction kinetics, the cleavage was performed in isopropanol solution with DOWEX 10WX8 acidic ion exchange resin, leading to HA-*lin*PG (**P6b**) (Scheme 6).

Full cleavage of the protecting groups is confirmed *via* ^{1}H NMR spectroscopy (Fig. 4). After treatment with DOWEX10WX8 in isopropanol all acetal signals of PEEGE (Fig. 4 yellow) as well the methyl signals of the 1,4,2-dioxazole group at 1.6 ppm (Fig. 4 green) have vanished. The free hydroxamic acid can be confirmed *via* the NH-signal appearing at 11 ppm (Fig. 4 blue, top). In conclusion, the 1,4,2-dioxazole group can be

Fig. 3 ESI-mass spectra of HAA-PEG$_{31}$ (bottom) and HA-PEG$_{31}$ (top).

simultaneously cleaved with other protecting groups reacting under the same acidic conditions, like acetals without interference leading to multi-functional *lin*PG bearing one hydroxamic acid (Scheme 6). Considering the high stability of the 1,4,2-dioxazole group under basic conditions, orthogonal protecting group chemistry should also be possible for selective release of the functional moieties.

Chelation characterization and demonstration of the applicability of hydroxamic acid functional PEG

Chelation properties. Fundamental chelation properties of the HA-PEGs were investigated, relying on UV-Vis spectroscopy of the highly colored iron(III) complexes. As already reported by Winston *et al.*[16], at low iron(III) concentration the tris(hydroxamato)iron(III) complex is favored. When increasing the iron(III) to HA-PEG ([Fe]/[HA-PEG]) ratio the tris-complex is consecutively cleaved to form bis- and finally mono(hydroxamato) iron(III) complexes (Scheme 7). Simultaneously, the color changes from the red tris-complex ($\lambda_{max} = 500$ nm) to the purple mono-complex ($\lambda_{max} = 550$ nm) (Fig. 5, ESI Fig. S21). This distinct shift cannot be detected in case of chelating trishydroxamic acids such as deferoxamine due to their highly favored formation of tris-complexes.[16]

This behavior can also be verified by a steep increase in absorbance in the course of iron(III) chloride addition, until

Fig. 2 ^{1}H NMR analysis of HAA-PEG (bottom) and HA-PEG (top) after cleavage of the protecting group.

Scheme 6 Reaction scheme for cleavage of the protecting group in HAA-PEEGE releasing both the hydroxyl groups as well as the hydroxamic acid moiety.
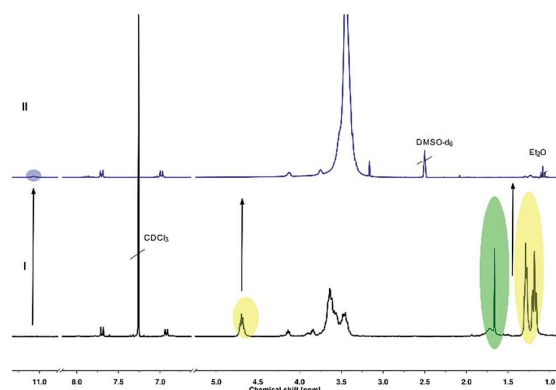
Fig. 4 Stacked ^{1}H NMR spectra of HAA-PEEGE$_7$ (**I**) before cleavage of the protecting groups and (**II**, top) HA-*lin*PG$_7$ as the reaction product.
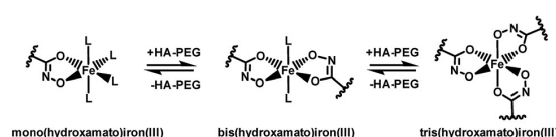
Scheme 7 Equilibria of the formation of mono-, bis-, or tris(PEG-hydroxamato)iron(III) complexes.
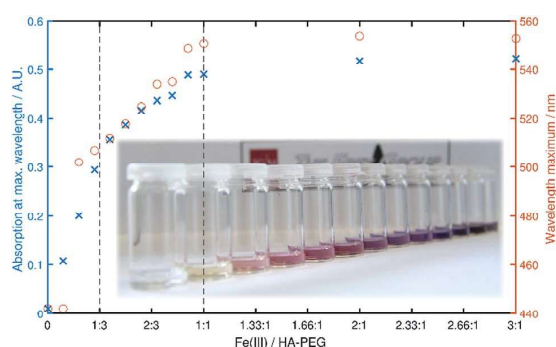
Fig. 5 Maximum absorbance (blue) and λ_{max} (red) in dependency of the [Fe]/[HA-PEG$_{188}$] ratio. The vertical lines denote a ratio of 1 : 3 (tris complex) and 1 : 1 (mono complex) respectively.

a ratio of 1 : 3 ([Fe]/[HA-PEG]) is achieved. With further addition of iron(III) the absorbance increases until equimolarity is obtained. At this ratio all hydroxamic acid moieties are saturated as mono-complexes, and thus no increase in absorbance can be induced by further addition of iron(III). This behavior suggests that there is no influence of the polymer chain on the chelation behavior of the hydroxamic acid end group connected to the polyether backbone. Hence, the chelation properties of HA-PEGs are comparable to low molecular weight hydroxamic acids and are not altered due to the conjugation with PEG.

Nanoparticle and surface modification. Besides binding of low molecular iron, the coating of macroscopic surfaces or metal oxide nanoparticles is another prominent application of polymeric chelators.[1] As a proof of principle for the coating of surfaces with HA-PEGs, solubilization of iron oxide nanoparticles (FeO$_x$-NP) in water as well as enhancement of the hydrophilicity of different metal surfaces were demonstrated (ESI Fig. S22 and S23†). In all cases, the hydrophilicity of the surfaces increased due to coating with HA-PEGs. By coating FeO$_x$-NP with HA-PEGs with a molecular weight of 1000, 3800 and 8500 g mol^{-1} the NP diameter was systematically increased from 20 nm for the oleate-coated NP up to 50 nm in case of HA-PEG with a molecular weight of 8500 g mol^{-1}. Control experiments with non-functionalized PEG resulted only in minor changes in size within the error range of the uncoated NP distribution (Fig. 6, see Table S1†).

After coating, the initially water-insoluble NPs were freely soluble in water or methanol (ESI Fig. S21†). TEM images prepared from water show the coated, non-agglomerated NPs (Fig. 7). As expected, no differences in size or distribution in comparison to the NP prior to coating can be detected.

Cell toxicity and proliferation assays. First, biocompatibility tests were performed using primary human blood cells to explore applicability of the polymers for the transport of Fe(III) or other metal ions in medicine. In all cases HA-PEG as well as their protected counterpart HAA-PEG showed no significant impact on the metabolic cell activity within the range of tested concentrations, thus low to no toxicity can be expected (ESI Fig. S24 and S26†). To further investigate the shielding effect of the PEG chain, T-Cell proliferation studies were performed.

Commercially available hydroxamic acid-based drugs like deferoxamine mesylate (Desferal, Novartis) are known to strongly inhibit T-cell proliferation.[35] In contrast HAA-PEG, as well as HA-PEG with a MW of 8500 g mol^{-1} did not significantly influence the proliferation of T-cells, while the low molecular weight HA **1b** showed dose-dependent inhibition of the proliferation (Fig. 8, ESI Fig. S25†).
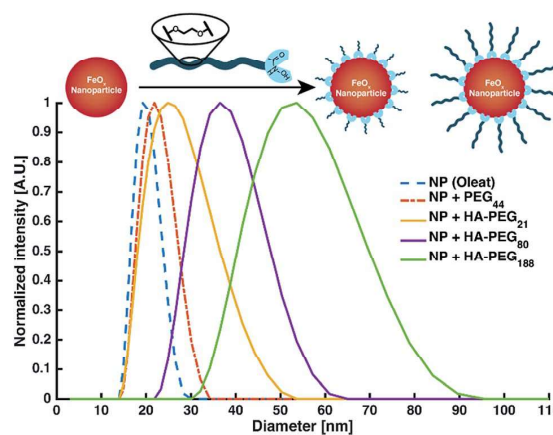
Fig. 6 Intensity distribution of the FeO$_x$ nanoparticles by DLS.
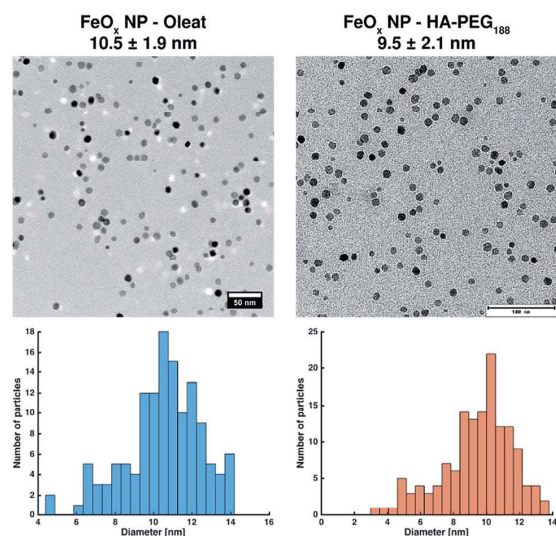
Fig. 7 TEM image of non-modified (oleate coated) FeO_x nanoparticles (left, blue histogram, prepared from hexane) and FeO_x nanoparticles after coating with HA-PEG$_{188}$ (right, red histogram, obtained from aqueous solution).
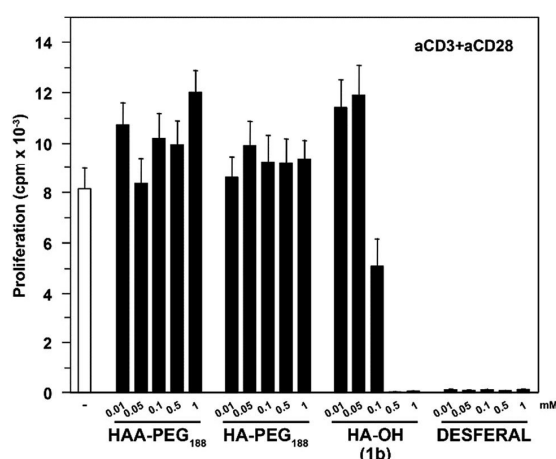
Fig. 8 T-Cell proliferation assay. Human PBMC (4 donors) were stimulated with aCD3 and aCD28 antibodies to induce T-cell proliferation in the presence of different test compounds.

Conclusions

1,4,2-Dioxazoles with an adjacent hydroxyl group have been demonstrated to represent key structures for the direct introduction of hydroxamic acids into polymers. These structures permit to install hydroxamic acids at synthetic polymers in a well-defined manner at the α-position. A general synthetic scheme was developed that gives access to a large variety of novel functional key building blocks that can be universally used to obtain hydroxamic acid-based monomers and polymers, for instance as protected HA-functional initiators or for the synthesis of a variety of novel HA-based monomers, exemplified by epoxides and methacrylates in this work.

Relying on these novel synthons, hydroxamic acid functional polyethers based on ethylene oxide, propylene oxide and ethoxy ethyl glycidyl ether, respectively, were prepared to show the general applicability of this approach, even under the harsh conditions of the AROP. After mild acidic treatment of the resulting polyethers, the free hydroxamic acid can be recovered. Consequently, hydroxyl-functional 1,4,2-dioxazoles are broadly applicable for the initiation of AROP or for preparation of HA-based monomers by modification of the hydroxyl group with polymerizable structures.

The HA-initiated polyethers were studied both with respect to their future use in materials science and for medical purposes, for instance in the treatment of diseases related to the iron metabolism. No measureable difference in terms of chelation properties of the hydroxamic acid functional polyethers was detected, compared to low molecular weight hydroxamic acids, while anti-proliferative effects of low molecular weight hydroxamic acid therapeutics like deferoxamine were highly reduced. The complexation of Fe(III) ions, the coating of various metal surfaces as well as FeO_x nanoparticles confirm outstanding chelation properties. From these proof-of-principle studies and the basic synthons established in this work, a vast variety of typical applications known for other polymeric chelators, such as catechol-bearing or terpyridine-bearing polymers become viable. The combination of hydroxamic acids with polymers is a promising alternative to catechols with their low oxidative stability. Hydroxamic acid based polyethers offer promise for iron-depletion therapies, for medical purposes related to metal ion transport in general as well as in materials science and for surface coating.

Based on the general concept for protected hydroxamic acids introduced in this work, a variety of novel monomers based on acrylates, methacrylates and epoxides has been prepared and polymerized. These structures and their use for both material science and medicine will be reported in due course.

Experimental section

Materials

Unless otherwise stated, all reagents were used without further purification. All chemicals and solvents were purchased from Acros, Aldrich, Fisher Scientific, Fluka, Riedel-de-Haën or Roth. Deuterated solvents were purchased from Deutero GmbH. THF was dried *via* distillation over sodium/benzophenone. DMSO was dried using molecular sieve 4 Å. Hydrophobic FeO_x nanoparticles coated with oleic acid were provided by Jan Hilgert (Group of Prof. Tremel, University of Mainz).

Abbreviations

Ethyl acetate (EA), petrol ether (PE), dichloromethane (DCM), tetrahydrofuran (THF), dimethyl sulfoxide (DMSO), ethylene

oxide (EO), camphor sulfonic acid (CSA), methanol (MeOH), correlation spectroscopy (COSY), heteronuclear single-quantum correlation spectroscopy (HSQC), heteronuclear multiple-bond correlation spectroscopy (HMBC).

Characterization techniques

NMR analysis. ^{1}H NMR spectra at 300 MHz and ^{13}C spectra at 75 MHz were recorded on a Bruker Avance III HD 300 (5 mm BBFO-Head with z-gradient) at 23 °C. ^{1}H NMR spectra at 400 MHz and ^{13}C spectra at 100 MHz were recorded on a Bruker Avance III HD 400 (5 mm BBFO-Smartprobe with z-gradient) at 23 °C. The spectra are referenced internally to residual proton signal of the deuterated solvent. In the rare case of no detectable residual proton signal in 2D measurements, the spectra are referenced to compound signals from 1D spectra. All signals are assigned according to IUPAC nomenclature guidelines. For better clarity, the 2D spectra are annotated using lowercase letters for proton signals and capital letters for carbon signals.

Size exclusion chromatography. SEC chromatography was performed in DMF (1 mL min^{-1}, 50 °C) containing 1g L^{-1} lithium bromide as an additive, using an Agilent 1100 series SEC system including a HEMA 300/100/40 Å column cascade, a UV (254 nm) and RI detector. Calibration was carried out using poly(ethylene oxide) (PEO) standards provided by Polymer Standard Service (PSS).

Mass spectrometry. Polymer mass spectra were recorded on an Agilent 6545 QTOF mass spectrometer in electron spray ionization (ESI) mode. Sample concentration was 1 mg mL^{-1} in methanol. Mass spectra of low molecular weight compounds were recorded using a Finnigan MAT 95 mass spectrometer in field desorption (FD) mode.

Ultraviolet-Visible spectroscopy. UV-Vis spectra were recorded on a JASCO V-630 spectrophotometer in the range of 230 nm to 800 nm with 1 nm data interval. Scan speed was set to 400 nm min^{-1}. All samples were prepared in methanol.

Dynamic light scattering. DLS measurements were performed on a Zetasizer Nano ZS (Malvern Instruments) at an angle of 173° and a wavelength of 633 nm at 25 °C. Three measurements were performed per sample. All DLS measurements were performed in DCM.

Infrared spectroscopy. FT-IR spectra were recorded using a Nicolet iS10 FT-IR spectrometer (Thermo Fisher Scientific) in the range of 500 to 3500 cm^{-1}.

Lower critical solution temperature measurements. Cloud points were determined in deionized water at a concentration of 2.5 mg mL^{-1} and observed by optical transmittance of a laser beam (670 nm). The measurement was recorded in a Tepper turbidimeter TP1. Heating rate was 1 K min^{-1}. For determination of the LCST the temperature at 50% of initial transmittance was used.

Contact angle measurements. Contact angle measurements were performed after cleaning the appropriate metal slide in acetone by sonification for 1 h. Then each slide was put into either solution of PEG$_{44}$ as a reference or HA-PEG$_{188}$ (each 10 mg mL^{-1} in DCM) overnight at room temperature. The slides were removed from the solution, dried under air and rinsed with MilliQ-water to remove non-adhered polymer. The contact angle measurement was performed using the sessile drop method by applying one drop of MilliQ water on the surface and determining the apparent angle between liquid and solid phase. Every measurement was performed five times.

Transmission electron microscopy. TEM images were recorded with a FEI Tecnai 12 microscope equipped with a LaB$_6$ cathode (120 kV acceleration voltage, nominal magnification: 68 000; nominal underfocus: 0.5–1.5 mm). For sample preparation, carbon grids for TEM applications were negatively glow discharged at 25 mA for 30 s in an Emitech K100X glow discharge system. A droplet of the sample (5 µl) was placed on the grid and incubated for 30 s. The grid was dried with Whatman filter paper no. 4 by side-blotting.

Metabolic activity. Potential cytotoxic effects of the various agents on peripheral blood mononuclear cells (PBMC) were monitored by assaying their metabolic activity. For this, PBMC were isolated from blood donations of healthy volunteers by density gradient centrifugation using Ficoll as recommended by the manufacturer (Sigma-Aldrich, Deisenhofen, Germany). PBMC (10^7/mL) were seeded into wells of 96 well cluster plates (100 µl per well), and agents were applied to triplicates at the concentrations indicated. Samples left untreated or incubated with DMSO at cytotoxic dose (10%) were included as controls. On the next day, MTT substrate was applied as recommended by the manufacturer (Promega, Madison, WI). MTT reagent is reduced by mitochondrial dehydrogenases to a purple formazan product. Absorbance was measured at 570 nm using a EMax Plus microplate reader (Molecular Devices, San José, CA).

Proliferation assays. To assess effects of the different agents on the proliferative capacity of T cells, PBMC (10^6/mL) were seeded into wells of 96 well cluster plates (100 µl per well). To induce polyclonal T cell proliferation, wells were precoated with mouse anti-human CD3 antibody (1 µg mL^{-1}; clone HIT3a), and mouse anti-human CD28 antibody (1 µg mL^{-1}; clone CD28.2) was added to PBMC prior to seeding (both antibodies from Biolegend, San Diego, CA). In parallel settings, T cells were stimulated using phytohemagglutinin (PHA) isolated from *Phaseolus vulgaris* (Sigma-Aldrich) at a final concentration of 5 µg mL^{-1}. PBMC left unstimulated served as internal controls. The different agents were applied to triplicates at the concentrations indicated. T cell proliferation was assayed as genomic incorporation of ^{3}H-thymidine (0.5 µCi per well) added on day 3 of culture. On the next day, cells were harvested onto glass fiber filters. Retained radioactivity was detected using a ß counter (1205 Betaplate, LKB Wallac, Turcu, Finnland).

Synthesis procedures of hydroxamic acids and 1,4,2-dioxazoles

Synthesis of the hydroxamic acid functional initiator (HAA-OH) employed as an initiator for polymerization and HAA monomer derivatives (1a–1e).
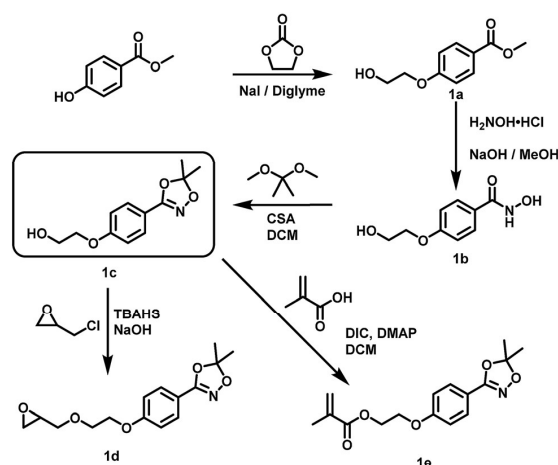
(1a) Methyl 4-(2-hydroxyethoxy)benzoate. (**1a**) was prepared in a modified procedure described elsewhere.[36] A 250 mL flask equipped with a condenser and gas bubbler was charged with 76.07 g (0.500 mol, 1.00 eq.) methyl 4-hydroxybenzoate, 46.25 g (0.525 mol, 1.05 eq.) ethylene carbonate, 7.50 g (0.050 mol, 0.10 eq.) NaI and 100 mL diglyme and heated under vigorous stirring for 16 h at 140 °C oil bath temperature. Finally, the temperature was increased to 160 °C for two hours. The solution was cooled to room temperature and the solvent were removed until dryness *in vacuo*. The residue was dissolved in 300 mL EA and washed with 50 mL water, 50 mL saturated NaHCO$_3$ and 50 mL brine and dried using Na$_2$SO$_4$. After evaporation of the solvent 93.6 g (0.477 mol, 95%) of methyl 4-(2-hydroxyethoxy)benzoate were obtained.

^{1}H NMR (300 MHz, CDCl$_3$) δ [ppm] = 7.99 (AA'BB', 2H, *HC*^{2,6}), 6.93 (AA'BB', 2H, *HC*^{3,5}), 4.17 (t, J = 4.1 Hz, 2H, *CH$_2$*–O–Ar), 3.99 (t, J = 4.1 Hz, 2H, HO–*CH$_2$*–), 3.88 (s, 3H, *CH$_3$*).

^{13}C NMR (75 MHz, CDCl$_3$) δ [ppm] = 166.92 Ar–*C*=O, 162.48 *C*^{4}, 131.78 *C*^{2,6}, 123.13 *C*^{3,5}, 114.24 *C*^{1}, 69.45 Ar–O–*C*, 61.42 HO–*C*, 52.06 *C*H3.

(1b) N-hydroxy-4-(2-hydroxyethoxy)benzamide. (**1b**) was prepared in a modified procedure based on the work of Hauser and Renfrow.[37] 42.9 g (0.62 mol, 2.00 eq.) H$_2$NOH·HCl were dissolved in 240 mL methanol and neutralized by addition of a solution of 52.1 g (0.93 mol, 3.00 eq.) KOH in 140 mL methanol. After cooling in an ice-bath for 5 min the solution was filtered to remove precipitated KCl. To this solution 60.6 g (0.31 mol, 1.00 eq.) methyl 4-(2-hydroxyethoxy)benzoate (**1a**) were added in one step, and the solution was stirred until homogenous. After standing for 24 h at room temperature, the basic solution was acidified with 2 M HCl to pH 4 and all solvents were removed until dryness *in vacuo*. The residue was transferred into a soxhlet apparatus and extracted using THF (1000 mL) overnight. After cooling at −20 °C and vacuum filtration 47.5 g (0.24 mol 77%) N-hydroxy-4-(2-hydroxyethoxy)benzamide (**1b**) were obtained as a colourless solid.

^{1}H NMR (300 MHz, DMSO-d_6) δ [ppm] = 11.06 (s, 1H, N*H*), 8.90 (s, 1H, NH–O*H*), 7.71 (AA'BB', 2H, *HC*^{2,6}), 6.98 (AA'BB', 2H,

HC^{3,5}), 4.89 (t, J = 5.5 Hz, 1H, *HO*–CH$_2$), 4.03 (t, J = 4.9 HZ, 2H, *CH$_2$*–O–Ar), 3.72 (dt, J = 5.5, 4.9 Hz, 2H, HO–*CH$_2$*–).

^{13}C NMR (75 MHz, DMSO-d_6) δ [ppm] = 164.02 *C*≡O, 160.95 *C*^{4}, 128.62 *C*^{2,6}, 124.82 *C*^{1}, 123.13 *C*^{3,5}, 69.70 Ar–O–*C*, 59.48 HO–*C*.

IR-ATR ν [cm^{-1}] = 3279 m, 2947 w, 2750 m br, 1638 m, 1606 *vs.* (C=O), 1564 s, 1503 s, 1445 m, 1413 m, 1378 m, 1335 w, 1304 m, 1253 *vs.* (C–O), 1185 m, 1162 m, 1115 w, 1088 s, 1050 s, 1031 m, 1010 m, 919 m, 894 *vs.*, 847 *vs.*, 817 m.

R_f (EA : PE = 2 : 1) = 0.05.

Elemental analysis. Found C: 53.68, H: 6.09, N: 6.66 – calculated 54.82, H: 5.62, N: 7.10.

FD-MS (m/z) = 197.2532 (100%), 198.2448 (8.1%).

(1c) 2-(4-(5,5-dimethyl-1,4,2-dioxazol-3-yl)phenoxy)ethan-1-ol. (**1c**) was prepared in a modified procedure based on the work of Couturier *et al.*[31] 19.72 g (0.10 mol, 1.00 eq.) N-hydroxy-4-(2-hydroxyethoxy)benzamide (**1b**) were suspended in 2000 mL DCM in a dry 3 L flask. To this suspension 31.25 g (0.30 mol, 3.00 eq.) 2,2-dimethoxypropane and 23.23 g (0.10 mol, 1.00 eq.) camphor sulfonic acid were added. The suspension was vigorously stirred for 15 h and then neutralized by addition of 250 mL 4 M aqueous NaOH solution. After stirring over night the organic layer was separated and washed twice with 100 mL 2 M NaOH, dried using Na$_2$SO$_4$ and evaporated to dryness *in vacuo*. The pure product was obtained by column chromatography (SiO$_2$, EA : PE = 1 : 1 as eluent). Yield: 20.89 g (0.088 mol, 88%) as colourless liquid that solidified at −20 °C.

^{1}H NMR (300 MHz, DMSO-d_6) δ [ppm] = 7.64 (AA'BB', 2H, *HC*^{3,5}), 6.94 (AA'BB', 2H, *HC*^{2,6}) 4.12 (t, J = 5.2 Hz, 2H, Ar–O–*CH$_2$*–), 3.98 (t, J = 5.2 Hz, 2H, HO–*CH$_2$*–), 1.66 (s, 6H, *CH$_3$*).

^{13}C NMR (75 MHz, DMSO-d_6) δ [ppm] = 161.12 *C*^{1}, 158.21 *C*=N, 128.58 *C*^{3,5}, 116.50 *C*^{4}, 115.34 *C*(CH$_3$)$_2$, 114.71 *C*^{2,6}, 69.45 Ar–O–*CH$_2$*–, 61.43 HO–*CH$_2$*–, 24.97 *C*H$_3$.

IR-ATR ν [cm^{-1}] = 3396 vw br (OH), 2935 vw, 1710 vw, 1606 m (C=N), 1514 m, 1454 w, 1423 m, 1363 m, 1306 m, 1251 *vs.*, 1215 s, 1166 s, 1115 m, 1078 s, 1044 m, 1010 m, 978 m, 945 w, 916 m, 884 m, 836 s, 816 m, 771 m.

R_f (EA : PE = 1 : 1) = 0.38.

FD-MS (m/z) = 237.2485 (100%), 238.2470 (11.5%), 239.2456 (1.2%).

(1d) 5,5-dimethyl-3-(4-(2-(oxiran-2-ylmethoxy)ethoxy)phenyl)-1,4,2-dioxazole. A 250 mL three-necked flask equipped with a dropping funnel, thermometer and mechanical stirrer was charged with 56 mL 50% (w/w) aqueous NaOH solution, 35.0 mL (0.45 mol, 5.3 eq.) epichlorhydrin and 1.18 g (3.5 mmol, 0.04 eq.) tetrabutylammonium hydrogen sulfate (TBAHS). 20.0 g (84.3 mol, 1.0 eq.) 2-(4-(5,5-dimethyl-1,4,2-dioxazol-3-yl) phenoxy) ethan-1-ol were added within 30 minutes while cooling in an ice bath. After addition, the ice bath was removed and the suspension stirred vigorously overnight. After complete conversion of the alcohol was verified *via* TLC the reaction was quenched by addition of 100 mL of an ice-water mixture. The organic phase was separated, and the aqueous phase was extracted three times each with 60 mL dichloromethane. The combined organic phase was washed with brine until a pH of 8 was obtained, then dried using Na$_2$SO$_4$, filtered and all solvents

Edge Article   Chemical Science

were removed *in vacuo*. After column chromatography (SiO$_2$, eluent: PE : EA = 4 : 1) 20.0 g (68.2 mmol, 81%) 5,5-dimethyl-3-(4-[2-(oxiran-2-ylmethoxy)ethoxy]phenyl)-1,4,2-dioxazole were obtained as a colourless liquid.

^{1}H NMR (400 MHz, DMSO-d_6) δ = 7.68–7.59 (AA′BB′, 2H, $HC^{3,5}$), 7.11–7.02 (AA′BB′, 2H, $HC^{2,6}$), 4.21–4.14 (m, 2H, Ar–O–CH$_2$–CH$_2$–), 3.85–3.72 (m, 3H, Ar–O–CH$_2$–CH$_2$, epoxide-CH$_2$–O), 3.35–3.27 (m, 1H, epoxide-CH$_2$–O), 3.15–3.09 (m, CH), 2.73 (dd, J = 5.1, 4.2 Hz, 1H, CH$_2$ in epoxide), 2.56 (dd, J = 5.1, 2.7 Hz, 1H, CH$_2$ in epoxide), 1.61 (s, 6H, acetonide CH$_3$).

(1e) 2-(4-(5,5-dimethyl-1,4,2-dioxazol-3-yl)phenoxy)ethyl methacrylate. In a 50 mL Schlenk flask 6.06 g (0.026 mol, 1.10 eq.) 2-(4-(5,5-dimethyl-1,4,2-dioxazol-3-yl)phenoxy)ethan-1-ol, 2.00 g (0.023 mol, 1.00 eq.) methacrylic acid and 0.23 g (1.9 mmol, 0.08 eq.) 4-dimethylaminopyridine (DMAP) were dissolved in 15 mL dichloromethane. Under ice cooling it was added 3.23 g (0.026 mol, 1.10 eq.) N,N′-diisopropylcarbodiimide (DIC) within 5 minutes. After stirring for 15 minutes under ice cooling, the mixture was stirred for 5 h at rt. The mixture was filtered through a frit, and the filtrate was washed twice with 100 mL of a saturated sodium hydrogen carbonate solution. The organic phase was dried over MgSO$_4$ and the solvent was removed under reduced pressure. The solid was purified by column chromatography in a solvent mixture of PE : EA (6 : 1). Methacrylate hydroxamic acid acetonide (MAHAA, **1e**) was obtained in yields of 5.35 g (0.018 mol, 76%).

^{1}H NMR (300 MHz, CDCl$_3$): δ [ppm] = 7.73 (AA′BB′, 2H, $HC^{3,5}$), 6.93 (AA′BB′, 2H, $HC^{2,6}$), 6.15 (s, 1H, HC=C), 5.60 (s, 1H, HC=C), 4.51 (m, 2H, MA–O–CH$_2$–), 4.26 (m, 2H, Ar–O–CH$_2$), 1.96 (s, 3H, CH$_3$–C=C), 1.67 (s, 6H, acetonide CH$_3$).

Synthesis of phenolic hydroxamic acid functional initiator not employed for polymerization (2a–2b).
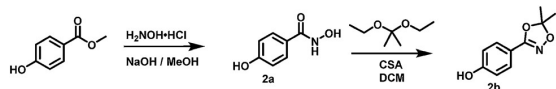
(2a) N,4-dihydroxybenzamide. (**2a**) was prepared in a modified procedure based on the work of Jeanrenaud *et al.*[38] A 250 mL round bottom flask was charged with 3.80 g (25 mmol, 1 eq.) methyl paraben and 3.47 g (50 mmol, 2 eq.) H$_2$NOH·HCl in 87.5 mL water. To this suspension 3.5 g (88 mmol, 3.5 eq.) NaOH as a 2 M solution was added. After 4 hours of stirring at room temperature the solution was acidified using 110 mL 1 M HCl and cooled overnight at 4 °C. Unreacted reagents were filtered off and the residue reduced *in vacuo* to few mL residual volume. The residual aqueous phase was extracted four times with 50 mL EA each. The combined organic phase was dried using Na$_2$SO$_4$ and freed from any solvents *in vacuo*. The crude product was purified using column chromatography (SiO$_2$, PE : EA = 1 : 1 as starting eluent, increasing elution strength gradually up to EA : MeOH 19 : 1). Yield 820 mg (5.4 mmol, 21%) of N,4-dihydroxybenzamide (**2a**) as a colourless solid.

^{1}H NMR (300 MHz, DMSO-d_6) δ [ppm] = 10.97 (s, 1H, NH), 9.96 (s, 1H, Ar–OH), 8.84 (s, 1H, NH–OH), 7.62 (AA′BB′, 2H, $HC^{2,6}$), 6.78 (AA′BB′, 2H, $HC^{3,5}$)

^{13}C NMR (75 MHz, DMSO-d_6) δ [ppm] = 164.48 (C=O), 160.12 C^1, 128.81 C^{2,6}, 123.40 C^4, 114.98 C^{3,5}.

IR-ATR ν [cm^{-1}] = 3314 m, 3191 m, br, 2923 w, 1606 s (C=O), 1570 s, 1534 m, 1493 m, 1457 m, 1457 m, 1350 m, 1316 m, 1263 s, 1128 *vs.* (C–O), 1177 m, 1157 *vs.*, 1028 m, 971 m, 893 s, 848 *vs.*, 768 s.

R_f (EA : PE = 2 : 1) = 0.09.

Mp: 146 °C.

(2b) 4-(5,5-dimethyl-1,4,2-dioxazol-3-yl)phenol. (**2b**) was prepared in a modified procedure based on the work of Couturier *et al.*[31] A dried 100 mL Schlenk flask was charged with 337 mg (2.2 mmol, 1 eq.) N,4-dihydroxybenzamide (**2b**) and dried with 4 mL benzene under high vacuum. The solid residue was suspended in 50 mL of dry DCM (dried over P$_2$O$_5$, followed by distillation) and 872 mg (6.6 mmol, 3 eq.) 2,2-diethoxypropane were added. To this suspension 511 mg (2.2 mmol, 1 eq.) camphor sulfonic acid was added at once under argon atmosphere. After 105 minutes of stirring at room temperature the reaction was quenched by the addition of 10 mL saturated NaHCO$_3$ solution. The mixture was stirred over night at room temperature and then the organic phase separated. The aqueous phase was extracted three times with 50 mL ether, and the combined organic phase dried using Na$_2$SO$_4$. After evaporation of all solvents *in vacuo* the residue was dissolved in THF and diethyl ether (to a final ratio of 1 : 1) was added. 4-(5,5-dimethyl-1,4,2-dioxazol-3-yl)phenol (**2b**) crystallized after days as colourless needles. Yield: 160 mg (0.8 mmol, 38%).

^{1}H NMR (300 MHz, DMSO-d_6) δ [ppm] = 7.65 (AA′BB′, 2H, $HC^{3,5}$), 6.89 (AA′BB′, 2H, $HC^{2,6}$), 1.68 (s, 6H, CH$_3$).

^{13}C NMR (75 MHz, DMSO-d_6) δ [ppm] = 159.27 C^1, 158.75 (C=N), 128.90 C^{3,5}, 115.94 C^{2,6}, 115.58 CCH$_3$, 115.24 C^4, 24.90 CH$_3$.

R_f (EA) = 0.92.

Synthesis of benzylic hydroxamic acid functional initiator (^{benzyl}HAA-OH) not employed for polymerization (3a–3b)

(3a) N-hydroxy-4-(hydroxymethyl)benzamide. The synthesis was carried out in a modified procedure based on the work of Hauser and Renfrow analogous to the synthesis of (**1b**).[37] Starting from 14.95 g (0.09 mol, 1 eq.) methyl 4-(hydroxymethyl)benzoate 11.28 g (0.068 mol, 75%) of N-hydroxy-4-(hydroxymethyl)benzamide (**3a**) were obtained as a colourless solid.

^{1}H NMR (400 MHz, DMSO-d_6) δ [ppm] = 11.08 (s, 1H, NH), 8.98 (s, 1H, NH–OH), 7.77–7.64 (AA′BB′, 2H, $HC^{2,4}$), 7.46–7.30 (AA′BB′, 2H, $HC^{3,5}$), 5.28 (t, J = 5.7 Hz, 1H, HO–CH$_2$), 4.53 (d, J = 5.7 Hz, 2H, CH$_2$).

^{13}C NMR (100 MHz, DMSO-d_6) δ [ppm] = 164.54 C=O, 145.83 C^4, 131.10 C^1, 126.70 C^{2,4}, 126.10 C^{3,5}, 62.4S4 CH$_2$.

(3b) (4-(5,5-dimethyl-1,4,2-dioxazol-3-yl)phenyl)methanol. The synthesis was carried out in a modified procedure based on the work of Couturier *et al.* analogous to the synthesis of **1c**.[31] Starting from 5.03 g (0.03 mol, 1 eq.) N-hydroxy-4-(hydroxymethyl)benzamide 3.43 g (0.016 mol, 55%) (4-(5,5-dimethyl-1,4,2-dioxazol-3-yl)phenyl)methanol (**3b**) was obtained as a colourless liquid which solidified after one week at −20 °C.

^{1}H NMR (400 MHz, DMSO-d_6) δ [ppm] = 7.72–7.59 (AA'BB', 2H, $HC^{3,5}$), 7.50–7.39 (AA'BB', 2H, $HC^{2,4}$), 5.36 (t, J = 5.7 Hz, 1H, CH$_2$OH), 4.56 (d, J = 5.7 Hz, 2H, CH_2), 1.63 (s, 6H, CH_3).

^{13}C NMR (100 MHz, DMSO-d_6) δ [ppm] = 157.49 C=N, 146.58 C^1, 126.68 C^{2,4}, 126.11 C^{3,5}, 115.36 C(CH$_3$)$_2$, 62.36 CH$_2$, 24.41 CH$_3$.

R_f (EA : PE = 1 : 4) = 0.35.

Synthesis of aliphatic hydroxamic acid functional initiator not employed for polymerization (4a–4b).
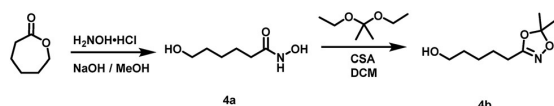
(4a) N,6-dihydroxyhexanamide. The synthesis was carried out in an modified procedure of Hauser and Renfrow.[37] A 250 mL round bottom flask was charged with 17.12 g (150 mmol, 1.00 eq.) freshly distilled ε-caprolactone. In a separated flask 11.47 g (165 mmol, 1.1 eq.) H$_2$NOH·HCl is dissolved in 65 mL methanol and neutralized with a solution of 12.62 g (225 mmol, 1.5 eq.) KOH in 32 mL methanol under shaking and cooling in a water bath. After 15 minutes the solution was filtered from precipitated KCl and added to the round bottom flask containing the caprolactone and stirred for 90 minutes. After the reaction had proceeded, the solution was acidified using conc. HCl to pH 4 and reduced under vacuum until most of the product solidified. The residue was recrystallized twice from THF (approx. 200 mL). 11.24 g (76 mmol, 51%) *N*,6-dihydroxyhexanamide (**4a**) were recovered after crystallization for 72 h at −20 °C as a colourless solid.

^{1}H NMR (300 MHz, DMSO-d_6) δ [ppm] = 10.37 (s, 0.9H, NH), 9.72 s (s, 0.1H, NH), 9.03 (s, 0.1H, NH–OH), 8.68 (s, 0.9H, NH–OH), 4.37 (s, 1H, CH$_2$–OH), 3.35 (t, J = 6.4 Hz, 2H, C$^6H_2$), 1.93 (t, J = 7.5 Hz, 2H, C$^2H_2$), 1.52–1.42 (m, 2H, C$^3H_2$), 1.42–1.32 (m, 2H, C$^5H_2$), 1.30–1.16 (m, 2H, C$^4H_2$).

^{13}C NMR (75 MHz, DMSO-d_6) δ [ppm] = 169.25 C^1, 60.67 C^6, 32.42 C^2, 32.30 C^5, 25.23 C^4, 25.16 C^3.

IR-ATR ν [cm^{-1}] = 3311 m, 3205 m, 3029 m, 2932 m, 2858 m br, 1616 *vs.* (C=O), 1544 m, 1449 m, 1466 m, 1362 m, 1274 m, 1116 m, 1078 m, 1055 *vs.*, 1012 *vs.*, 977 *vs.*, 785 m.

R_f (EA : MeOH = 9 : 1) = 0.42.

Mp: 84 °C.

(4b) 5-(5,5-dimethyl-1,4,2-dioxazol-3-yl)pentan-1-ol. The synthesis of **4b** was carried out analogous to the preparation of **1** on a scale of 4.27 g (29 mmol) *N*,6-dihydroxyhexanamide (**4a**). Purification was performed *via* column chromatography (SiO$_2$, EA : PE = 1 : 1 as eluent). Yield: 1.25 g (7 mmol, 23%) 5-(5,5-dimethyl-1,4,2-dioxazol-3-yl)pentan-1-ol (**4b**) as a colourless liquid.

^{1}H NMR (300 MHz, CDCl$_3$) δ [ppm] = 3.64 (t, J = 6.3 Hz, 2H, C$^1H_2$), 2.31 (t, J = 7.3 Hz, C$^5H_2$), 1.76 (s, 1H, OH), 1.69–1.56 (m, 4H, C$^2H_2$, C$^4H_2$), 1.55 (s, 6H, CH_3), 1.50–1.39 (m, 2H, C$^3H_2$).

^{13}C NMR (75 MHz, CDCl$_3$) δ [ppm] = 160.39 C=N, 114.54 C(CH$_3$)$_2$, 62.65 C^1, 32.26 C^2, 25.22 C^3, 25.18 C^4, 24.91 CH$_3$, 23.95 C^5.

R_f (EA : PE = 1 : 1) = 0.46.

Polymerization procedures

Synthesis of HAA-polyether (P1a–P6a) and deprotection to obtain the free hydroxamic acid functional polyether (P1b–P6b).
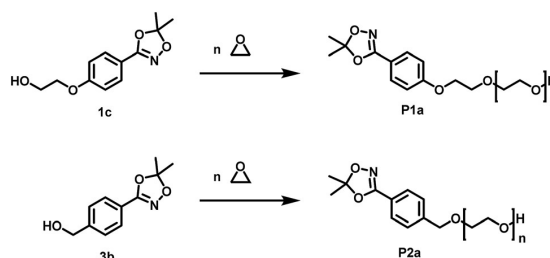
(P1a/P2a) synthesis of HAA-PEG and ^{benzyl}HAA-PEG. Preparation in example of HAA-OH as initiator. In a typical procedure, 2-(4-(5,5-dimethyl-1,4,2-dioxazol-3-yl)phenoxy)ethan-1-ol (1 eq.) (**1d**) was deprotonated by 90 mol% cesium hydroxide monohydrate in 10 mL benzene in a 100 mL Schlenk flask. After stirring for 60 minutes at 50 °C under vacuum the solvents were removed with high vacuum (10^{-3} mbar) and subsequently the flask was heated to 60 °C overnight under high vacuum. The formed alkoxide salt was dissolved in 15 mL dry THF and 2 mL dry DMSO. EO was first distilled in the cold into a graduated ampoule and subsequently into the reaction flask containing the dissolved initiator. The mixture was heated to 50 °C and stirred for 2 days. Afterwards, 1 mL methanol was added to quench the reaction. Except for high boiling DMSO all residual solvents were removed *in vacuo*. The residue was diluted with 40 mL DCM and washed three times with 10 mL water. The organic phase was separated and dried using Na$_2$SO$_4$. The volume was reduced *in vacuo* to approx. 5 mL and the polymer precipitated in cold diethyl ether (45 mL, −20 °C, recovery through centrifugation at 4500 RPM for 10 minutes). Yields: 73–94%.

^{1}H NMR (400 MHz, DMSO-d_6) δ [ppm] = 7.63 (AA'BB', 2H, ArC$^{3,5}H$), 7.06 (AA'BB', 2H, ArC$^{2,6}H$), 4.56 (t, J = 5.5 Hz, 1H, terminal OH), 4.19–4.11 (m, 2H, Ar-O-CH_2-), 3.79–3.71 (m, 2H, Ar-O-CH$_2$-CH_2-O-), 3.71–3.28 (m, polyether backbone), 1.61 (s, 6H, CH_3).

(P1b/P2b) removal of the acetal protecting group of HAA-PEG (2a) to form HA-PEG.
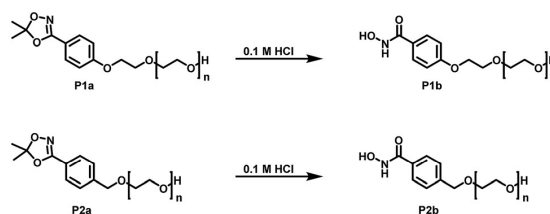
Preparation in example of HAA-PEG (**P1a**). In a typical procedure, 500 mg HAA-PEG (**P1a**) were dissolved in 20 mL 0.1 M HCl and shaken for 24 h. The polymer was recovered by adding 40 mL DCM and partitioning between the organic and

aqueous phase. The organic phase was separated and dried over Na_2SO_4 and reduced *in vacuo* to a volume of approx. 5 mL. After precipitation in ice cold diethyl ether (45 mL, −20 °C, recovery using centrifugation at 4500 RPM for 10 minutes), HA-PEG (**P1b**) was obtained in near quantitative (>98%) yields.

^{1}H NMR (400 MHz, DMSO-d_6) δ [ppm] = 11.06 (s, 1H, N*H*), 8.90 (s, 1H, NH–O*H*), 7.72 (AA'BB', 2H, ArC[2,6]*H*), 6.99 (AA'BB', 2H, ArC[3,5]*H*), 4.57 (t, *J* = 5.5 Hz, 1H, terminal O*H*), 4.19–4.08 (m, 2H, Ar–O–C*H₂*–), 3.79–3.72 (m, 2H, Ar–O–CH₂–C*H₂*–O–), 3.73–3.37 (m, polyether backbone).

(P3a, P4a, P5a, P6a) synthesis of HAA-PPO, HAA-PEEGE, [benzyl]*HAA-PPO,* [benzyl]*HAA-PEEGE.* Preparation example of HAA-PPO with HAA-OH as an initiator. In a typical procedure 2-(4-(5,5-dimethyl-1,4,2-dioxazol-3-yl)phenoxy)ethan-1-ol (1 eq.) (**1d**) was deprotonated by 90 mol% cesium hydroxide monohydrate in 10 mL in a 25 mL Schlenk flask. After stirring for 60 minutes at 50 °C under vacuum the solvents were removed with high vacuum (10^{-3} mbar) and subsequently the flask heated to 60 °C overnight under high vacuum. 1 mL dry propylene oxide (dried *via* cryo-distillation over CaH_2) were added to the formed alkoxide using a syringe and the polymerization was performed at 40 °C under vacuum overnight. Subsequently, 1 mL methanol was added to quench the reaction and the polymer was dissolved in 40 mL DCM and washed three times with 10 mL. The organic phase was separated, dried using Na_2SO_4 and all solvents were evaporated *in vacuo*. Typical yield: 78-95% as highly viscous amorphous polymer.

Preparation of PEEGE polymers was carried out analogously.

^{1}H NMR (300 MHz, CDCl₃) δ [ppm] = 7.70 (AA'BB', 2H, ArC[3,5]*H*), 6.94 (AA'BB', 2H, ArC[2,6]*H*), 4.19–4.11 (m, 2H, Ar–O–C*H₂*–), 4.16 (m, 2H, Ar–O–CH₂–C*H₂*–O–), 3.85 (m, 2H, Ar–O–CH₂–C*H₂*–O–), 3.69–3.28 (m, polyether backbone), 1.66 (s, 6H, C(C*H₃*)₂), 1.34-1.08 (m, propylene oxide C*H₃*).

(P6b) cleavage of the protection groups of HAA-PEEGE to obtain HA-linPG (linear polyglycerol). 50 mg of HAA-PEEGE (**P6a**) were dissolved in 10 mL isopropanol and 200 mg DOWEX 50WX8 acidic ion exchange resin were added. The mixture was shaken for 2 days and filtered afterwards. The resin was washed with 5 mL isopropanol and 5 mL methanol, and the combined organic phases were evaporated *in vacuo* to obtain 41 mg (81%) of HA-*lin*PG (**P6b**) as yellowish amorphous polymer.

Cleavage of the protecting group of **P3a**, **P4a** and **P5a** was carried out analogous.

^{1}H NMR (300 MHz, DMSO-d_6) δ [ppm] = 11.07 (s, 1H, N*H*), 7.70 (AA'BB', 2H, ArC[2,6]*H*), 6.99 (AA'BB', 2H, ArC[3,5]*H*), 4.19–4.04 (m, 2H, Ar–O–C*H₂*–), 3.72–3.13 (m, polyether backbone).

Nanoparticle modification

Coating of FeO$_x$ nanoparticles with HA-PEG. In a typical procedure, 10 mg HA-PEG (**P1b**) were dissolved in 5 mL DCM. 3 mg oleate-coated FeO$_x$ nanoparticles were dissolved in DCM as well and added slowly to the polymer solution. The suspension was shaken overnight and precipitated in ice-cold diethyl ether (15 mL, −20 °C, recovery through centrifugation at 4500 RPM for 15 minutes). After redissolving in DCM the magnetic nanoparticles were washed by concentrating the nanoparticles

with a strong neodymium magnet at the bottom of a flask and subsequent decantation of the supernatant. For DLS measurements the nanoparticles were redissolved in DCM and sterile filtered. For TEM measurement water was used for redissolving instead.

Conflicts of interest

There are no conflicts to declare.

Acknowledgements

Notes and references

1 E. Faure, C. Falentin-Daudré, C. Jérôme, J. Lyskawa, D. Fournier, P. Woisel and C. Detrembleur, *Prog. Polym. Sci.*, 2013, **38**, 236.

2 (*a*) E. J. Werner, J. Kozhukh, M. Botta, E. G. Moore, S. Avedano, S. Aime and K. N. Raymond, *Inorg. Chem.*, 2009, **48**, 277; (*b*) S. M. Cohen, B. O'Sulliva and K. N. Raymond, *Inorg. Chem.*, 2000, **39**, 4339; (*c*) J. Xu, T. M. Corneillie, E. G. Moore, G.-L. Law, N. G. Butlin and K. N. Raymond, *J. Am. Chem. Soc.*, 2011, **133**, 19900.

3 N. Patil, C. Jérôme and C. Detrembleur, *Prog. Polym. Sci.*, 2018, **82**, 34.

4 M. Yu, J. Hwang and T. J. Deming, *J. Am. Chem. Soc.*, 1999, **121**, 5825.

5 (*a*) B. P. Lee, J. L. Dalsin and P. B. Messersmith, *Biomacromolecules*, 2002, **3**, 1038; (*b*) B. P. Lee, P. B. Messersmith, J. N. Israelachvili and J. H. Waite, *Annu. Rev. Mater. Res.*, 2011, **41**, 99; (*c*) T. Gillich, E. M. Benetti, E. Rakhmatullina, R. Konradi, W. Li, A. Zhang, A. D. Schlüter and M. Textor, *J. Am. Chem. Soc.*, 2011, **133**, 10940; (*d*) N. Holten-Andersen, M. J. Harrington, H. Birkedal, B. P. Lee, P. B. Messersmith, K. Y. C. Lee and J. H. Waite, *Proc. Natl. Acad. Sci. U. S. A.*, 2011, **108**, 2651; (*e*) U. S. Schubert and C. Eschbaumer, *Angew. Chem., Int. Ed. Engl.*, 2002, **41**, 2892; (*f*) P. R. Andres and U. S. Schubert, *Adv. Mater.*, 2004, **16**, 1043.

6 (*a*) K. Niederer, C. Schüll, D. Leibig, T. Johann and H. Frey, *Macromolecules*, 2016, **49**, 1655; (*b*) V. S. Wilms, H. Bauer, C. Tonhauser, A.-M. Schilmann, M.-C. Müller, M. Tremel and H. Frey, *Biomacromolecules*, 2013, **14**, 193.

7 G. Schwarzenbach and K. Schwarzenbach, *Helv. Chim. Acta*, 1963, **46**, 1390.

8 Y. K. Agrawal and S. G. Tandon, *J. Inorg. Nucl. Chem.*, 1972, **34**, 1291.

9 J. P. Folkers, C. B. Gorman, P. E. Laibinis, S. Buchholz, G. M. Whitesides and R. G. Nuzzo, *Langmuir*, 1995, **11**, 813.

10 J. B. Neilands, *Science*, 1967, **156**, 1443.

11 (a) R. Codd, *Coord. Chem. Rev.*, 2008, **252**, 1387; (b) B. Kurzak, H. Kozłowski and E. Farkas, *Coord. Chem. Rev.*, 1992, **114**, 169.

12 L. Bauer and O. Exner, *Angew. Chem., Int. Ed. Engl.*, 1974, **13**, 376.

13 (a) A. Vannini, C. Volpari, G. Filocamo, E. C. Casavola, M. Brunetti, D. Renzoni, P. Chakravarty, C. Paolini, R. de Francesco, P. Gallinari, C. Steinkühler and S. Di Marco, *Proc. Natl. Acad. Sci. U. S. A.*, 2004, **101**, 15064; (b) C. J. Marmion, D. Griffith and K. B. Nolan, *Eur. J. Inorg. Chem.*, 2004, **2004**, 3003.

14 US2402604A, 1946.

15 (a) J. W. Rosthauser and A. Winston, *Macromolecules*, 1981, **14**, 538; (b) A. Winston and D. Kirchner, *Macromolecules*, 1978, **11**, 597; (c) A. Winston and G. R. McLaughlin, *J. Polym. Sci., Polym. Chem. Ed.*, 1976, **14**, 2155; (d) D. V. P. R. Varaprasad, J. W. Rosthauser and A. Winston, *J. Polym. Sci., Polym. Chem. Ed.*, 1984, **22**, 2131.

16 A. Winston and E. T. Mazza, *J. Polym. Sci., Polym. Chem. Ed.*, 1975, **13**, 2019.

17 Y. K. Agrawal, H. Kaur and S. K. Menon, *React. Funct. Polym.*, 1999, **39**, 155.

18 T. Hirotsu, S. Katoh, K. Sugasaka, M. Sakuragi, K. Ichimura, Y. Suda, M. Fujishima, Y. Abe and T. Misonoo, *J. Polym. Sci., Polym. Chem. Ed.*, 1986, **24**, 1953.

19 F. A. Alakhras, K. A. Dari and M. S. Mubarak, *J. Appl. Polym. Sci.*, 2005, **97**, 691.

20 (a) P. N. Sophiamma and K. Sreekumar, *React. Funct. Polym.*, 1997, **35**, 169; (b) M. Narita, T. Teramoto and M. Okawara, *Bull. Chem. Soc. Jpn.*, 1972, **45**, 3149.

21 (a) W. Kern and R. C. Schulz, *Angew. Chem.*, 1957, **69**, 153; (b) A. Domb, E. Cravalho and R. Langer, *J. Polym. Sci., Polym. Chem. Ed.*, 1988, **26**, 2623.

22 R. S. Mello, E. S. Orth, W. Loh, H. D. Fiedler and F. Nome, *Langmuir*, 2011, **27**, 15112.

23 (a) M. Imran ul-haq, J. L. Hamilton, B. F. L. Lai, R. A. Shenoi, S. A. Horte, I. Constantinescu, H. A. Leitch and J. N. Kizhakkedathu, *ACS Nano*, 2013, **7**, 10704; (b) J. L. Hamilton and J. N. Kizhakkedathu, *Molecular and Cellular Therapies*, 2015, **3**, 3; (c) N. A. A. Rossi, I. Mustafa, J. K. Jackson, H. M. Burt, S. A. Horte, M. D. Scott and J. N. Kizhakkedathu, *Biomaterials*, 2009, **30**, 638.

24 C. J. Adams, J. J. Wilson and E. Boros, *Mol. Pharmaceutics*, 2017, **14**, 2831.

25 G. M. Iskander, H. M. Kapfenstein, T. P. Davis and D. E. Wiley, *J. Appl. Polym. Sci.*, 2000, **78**, 751.

26 J. Herzberger, K. Niederer, H. Pohlit, J. Seiwert, M. Worm, F. R. Wurm and H. Frey, *Chem. Rev.*, 2016, **116**, 2170.

27 S. R. Sandler and W. Karo, *Organic functional group preparations*, Acad. Press, Orlando, 1989, vol. 12.

28 D. Geffken and J. Froböse, *J. Prakt. Chem.*, 1994, **336**, 550.

29 (a) J. Lim, Y. Song, J.-H. Jang, C.-H. Jeong, S. Lee, B. Park and Y. H. Seo, *Arch. Pharmacal Res.*, 2018, **41**, 967; (b) E. Orlowska, A. Roller, H. Wiesinger, M. Pignitter, F. Jirsa, R. Krachler, W. Kandioller and B. K. Keppler, *RSC Adv.*, 2016, **6**, 40238; (c) B. M. R. Liénard, L. E. Horsfall, M. Galleni, J.-M. Frère and C. J. Schofield, *Bioorg. Med. Chem. Lett.*, 2007, **17**, 964.

30 D. Cerniauskaite, J. Rousseau, A. Sackus, P. Rollin and A. Tatibouët, *Eur. J. Org. Chem.*, 2011, **2011**, 2293.

31 M. Couturier, J. L. Tucker, C. Proulx, G. Boucher, P. Dubé, B. M. Andresen and A. Ghosh, *J. Org. Chem.*, 2002, **67**, 4833.

32 D. Geffken and J. Froböse, *J. Prakt. Chem.*, 1993, **335**, 555.

33 M. Schömer and H. Frey, *Macromolecules*, 2012, **45**, 3039.

34 (a) M. Hans, H. Keul and M. Moeller, *Polymer*, 2009, **50**, 1103; (b) A. Thomas, S. S. Müller and H. Frey, *Biomacromolecules*, 2014, **15**, 1935.

35 B. E. Bierer and D. G. Nathan, *Blood*, 1990, **76**, 2052.

36 T. Yoshino, S. Inaba and Y. Ishido, *Bull. Chem. Soc. Jpn.*, 1973, **46**, 553.

37 C. R. Hauser and W. B. Renfrow Jr, *Org. Synth.*, 1939, **19**, 15.

38 A. Jeanrenaud, *Ber. Dtsch. Chem. Ges.*, 1889, **22**, 1270.

Supporting Information

A general concept for the introduction of hydroxamic acids into polymers

Tobias Johann,[a] Jennifer Keth,[a] Matthias Bros[b] and Holger Frey[*,a]

[a] Institute of Organic Chemistry, Johannes Gutenberg University, Duesbergweg 10-14, 55124 Mainz, Germany.
[b] Department of Dermatology, University Medical Center of the Johannes Gutenberg University Mainz, Langenbeckstrasse 1, 55131 Mainz, Germany

Table of contents

Optimization of protected hydroxamic acids with aliphatic spacers

Scheme S1. Overview over the synthesis attempts to yield protected hydroxamic acids with C_4 and C_3 aliphatic spacers.

SEC and LCST Polymer characterization
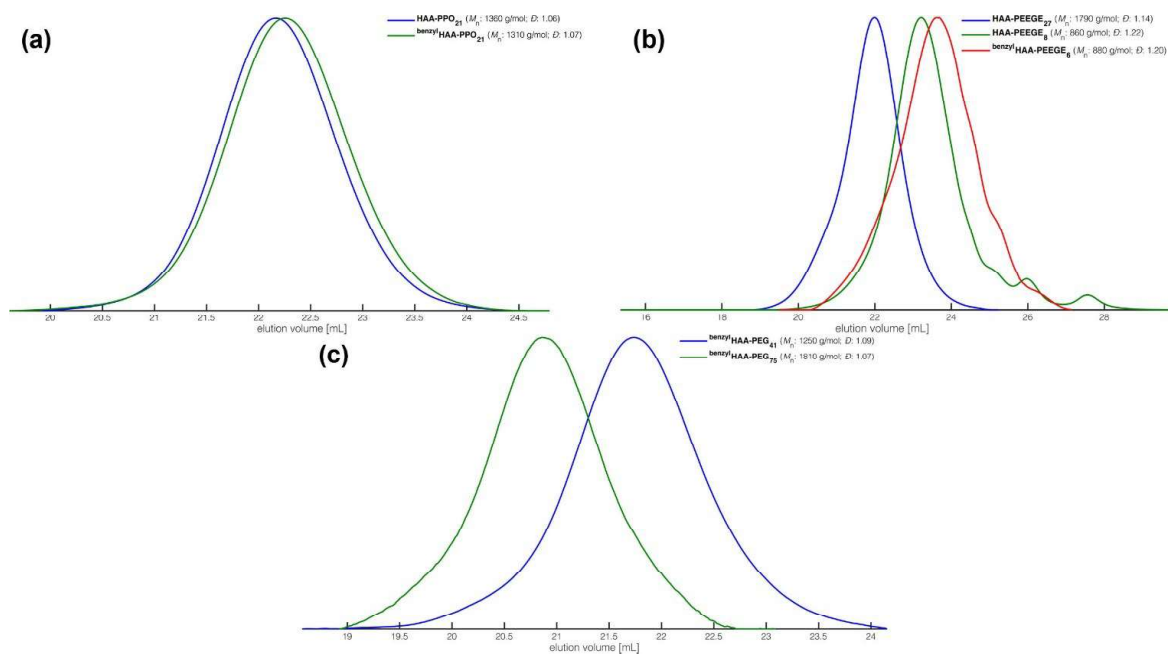
Figure S1. (a) SEC traces of PPO polymers. (b) SEC traces of PEEGE polymer. (c) benzylHAA-PEG polymers.
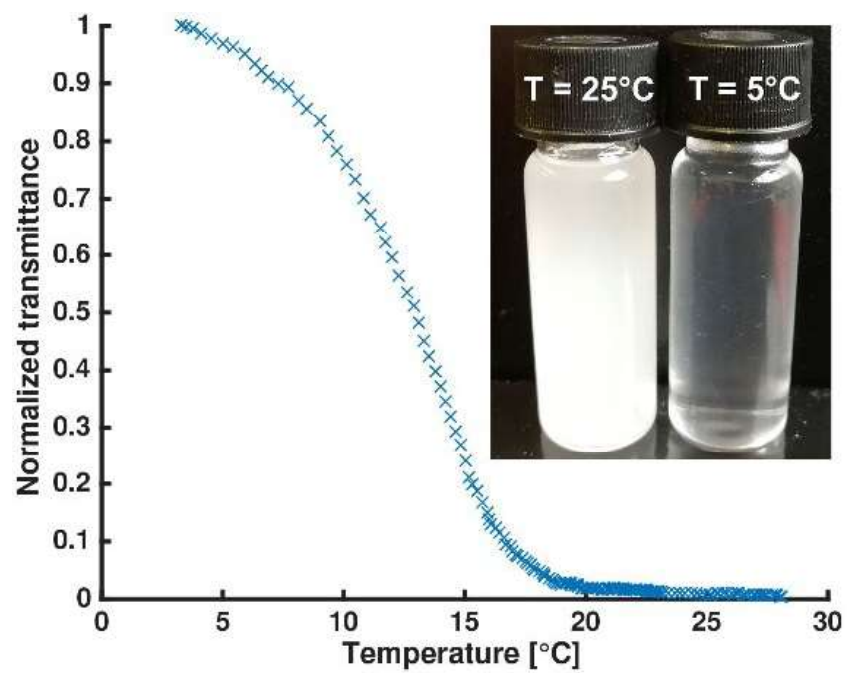
Figure S2. Cloud point measurement of HAA-PPO$_{21}$ in deionized water. Turbidity rapidly increased between 10 and 15 °C with 50 % of original transmittance at 12.9°C.

NMR and IR Characterization

Characterization of *N*-hydroxy-4-(2-hydroxyethoxy)benzamide (1b) "HA-OH"
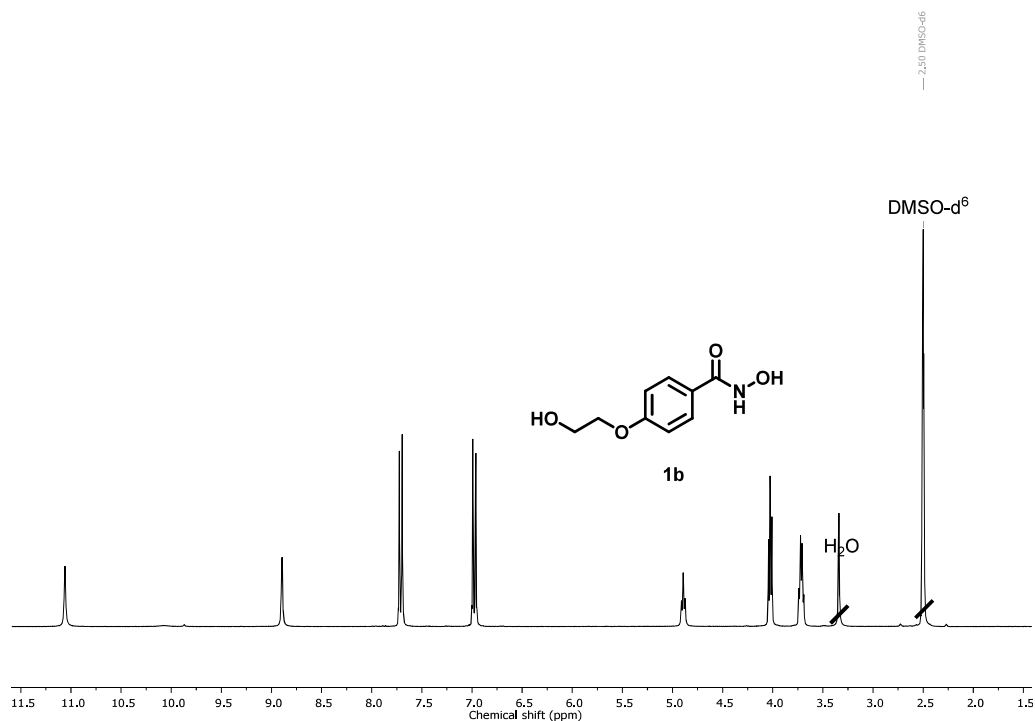
Figure S3a. ¹H NMR spectrum (300 MHz, DMSO-d_6) of *N*-hydroxy-4-(2-hydroxyethoxy)benzamide **(1b)**. See synthesis procedure for detailed assignment of the signals.
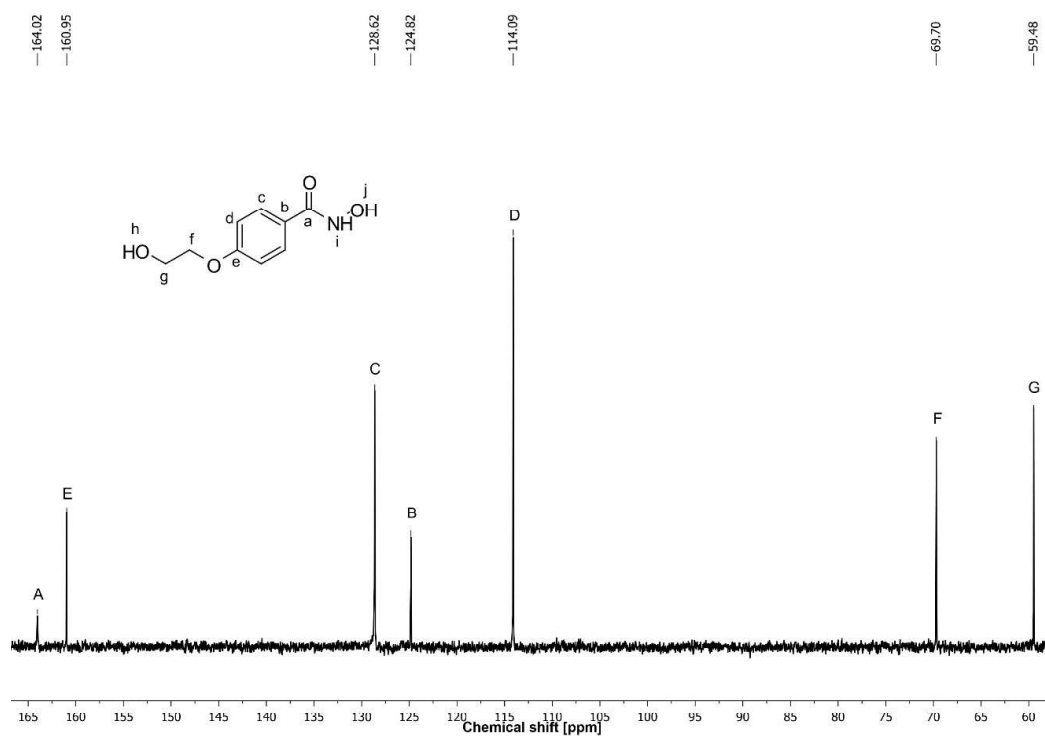
Figure S3b. ¹³C NMR spectrum (75 MHz, DMSO-d_6) of *N*-hydroxy-4-(2-hydroxyethoxy)benzamide **(1b)**.
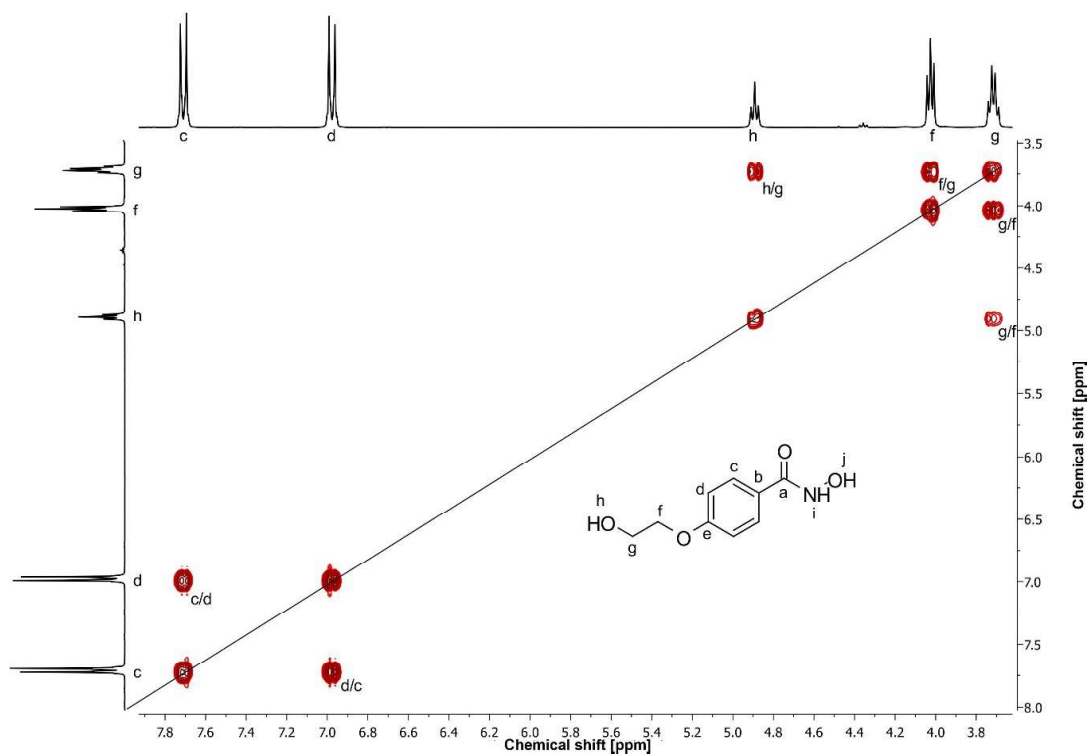
Figure S3c. ^{1}H-^{1}H COSY NMR spectrum (300 MHz, DMSO-d_6) of *N*-hydroxy-4-(2-hydroxyethoxy)benzamide **(1b)**.
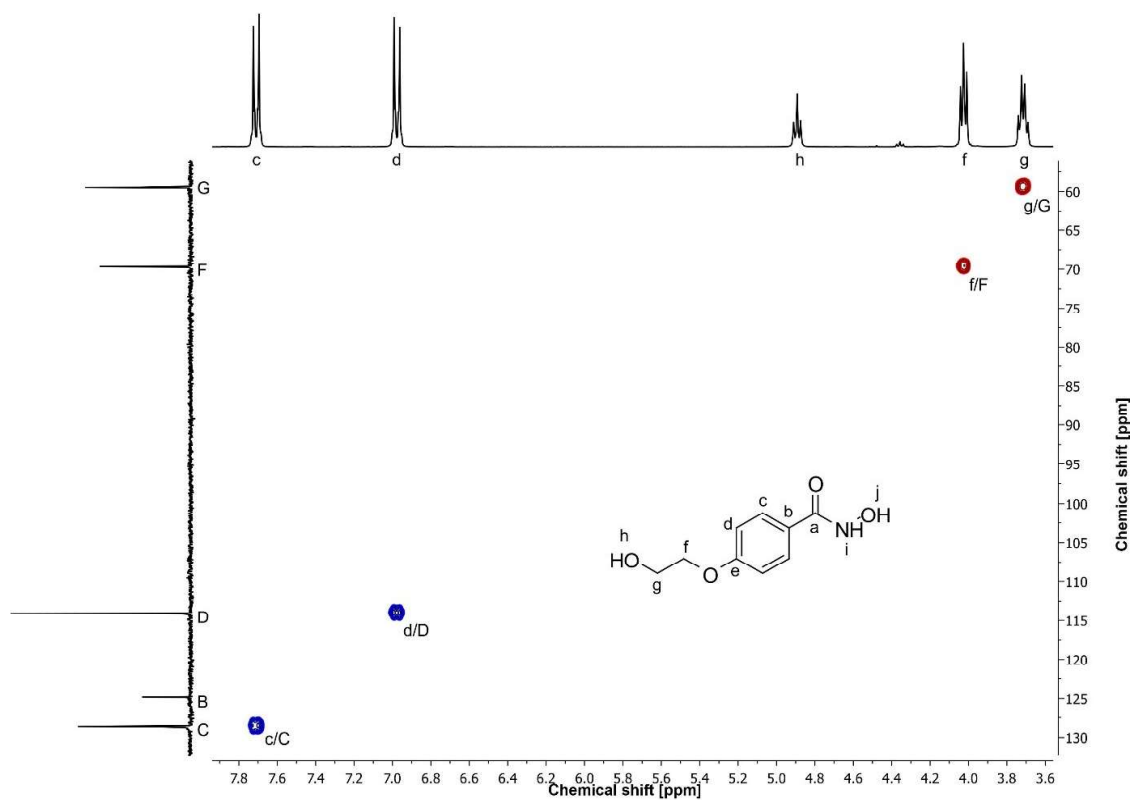
Figure S3d. ^{1}H-^{13}C HSQC NMR spectrum (300 MHz / 75 MHz, DMSO-d_6) of *N*-hydroxy-4-(2-hydroxyethoxy)benzamide **(1b)**.

Figure S3e. ^{1}H-^{13}C HMBC NMR spectrum (300 MHz / 75 MHz, DMSO-d_6) of *N*-hydroxy-4-(2-hydroxyethoxy)benzamide **(1b)**.

Figure S3f. FT-ATR-IR spectrum of *N*-hydroxy-4-(2-hydroxyethoxy)benzamide **(1b)**.
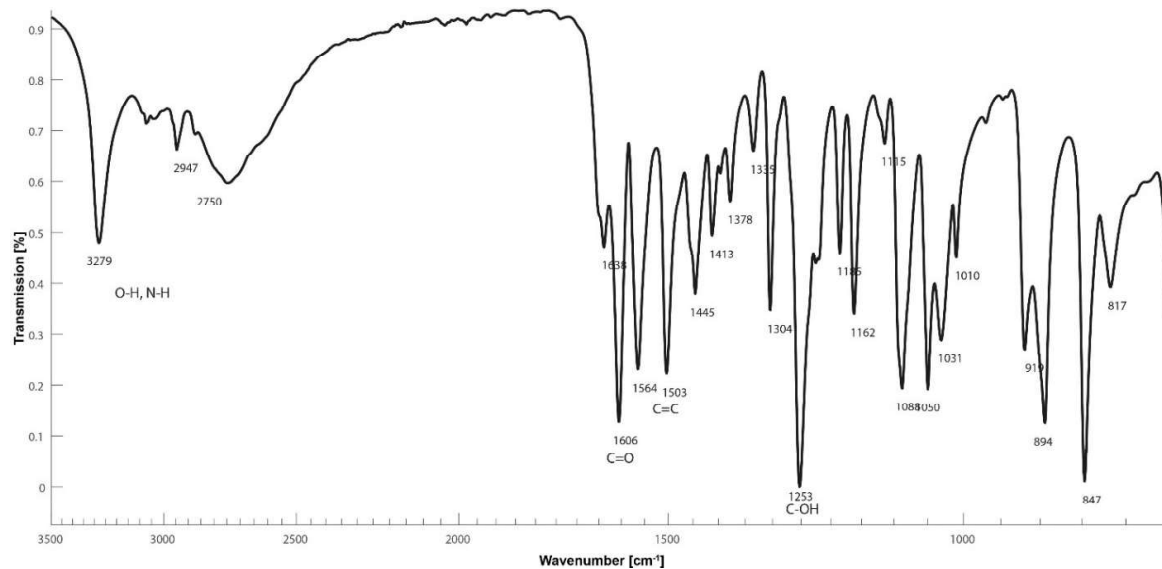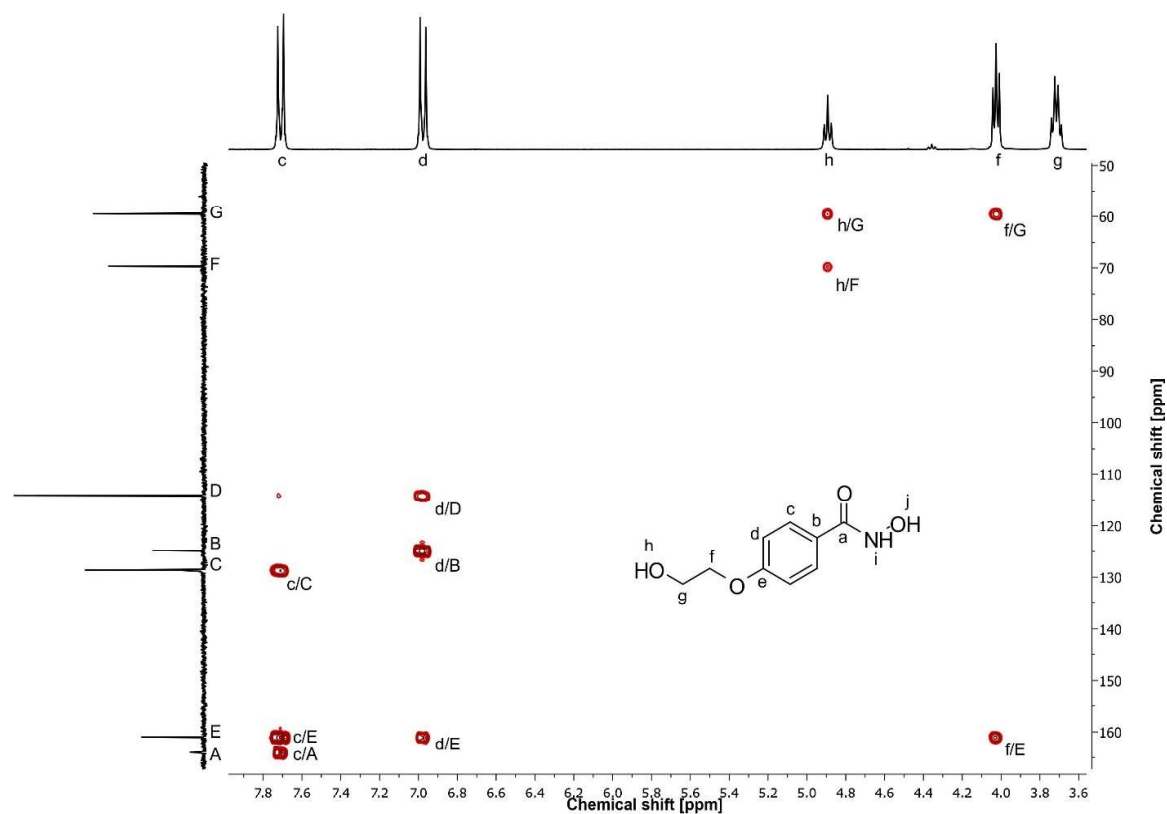
Characterization of 2-(4-(5,5-dimethyl-1,4,2-dioxazol-3-yl)phenoxy)ethan-1-ol (1c) "HAA-OH"
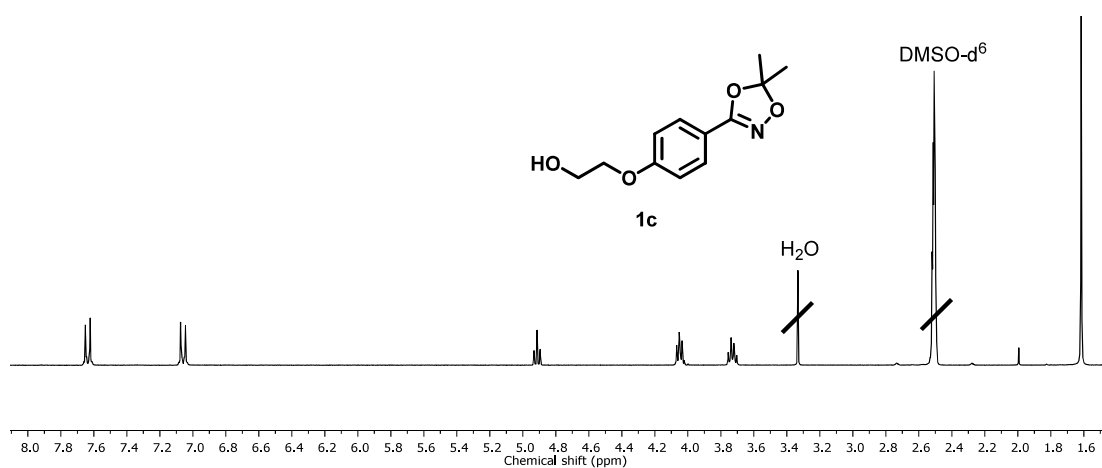
Figure S4a. ^{1}H NMR spectrum (300 MHz, DMSO-d_6) of 2-(4-(5,5-dimethyl-1,4,2-dioxazol-3-yl)phenoxy)ethan-1-ol **(1c)**. See synthesis procedure for detailed assignment of the signals.
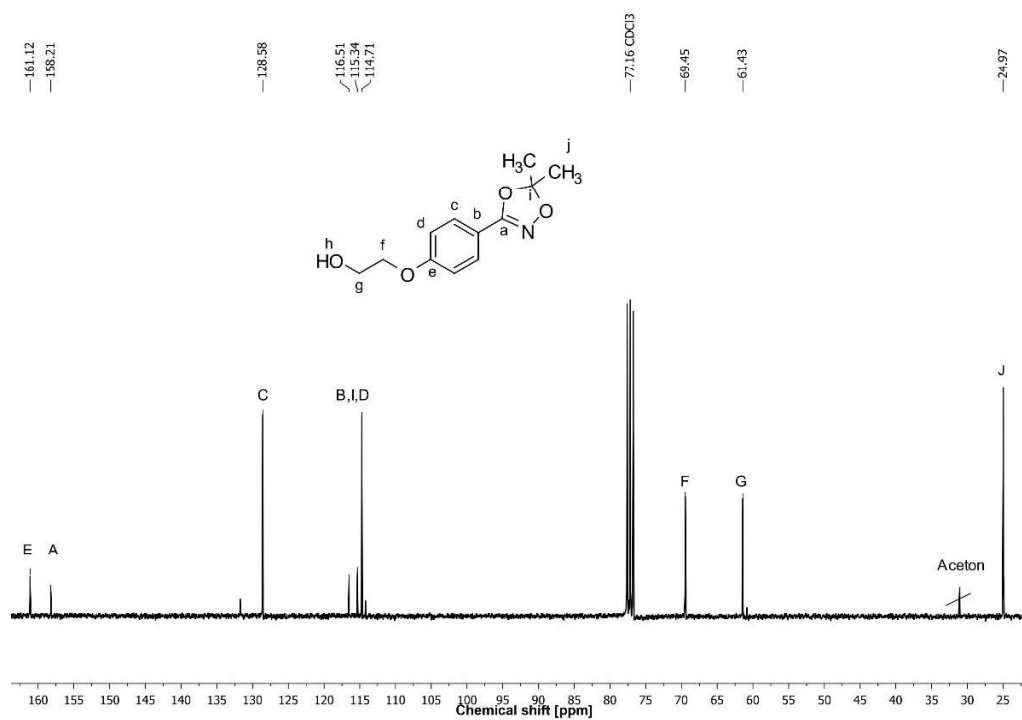
Figure S4b. ^{13}C NMR spetrcum (75 MHz, DMSO-d_6) of 2-(4-(5,5-dimethyl-1,4,2-dioxazol-3-yl)phenoxy)ethan-1-ol **(1c)** prior to purification via column chromatography.
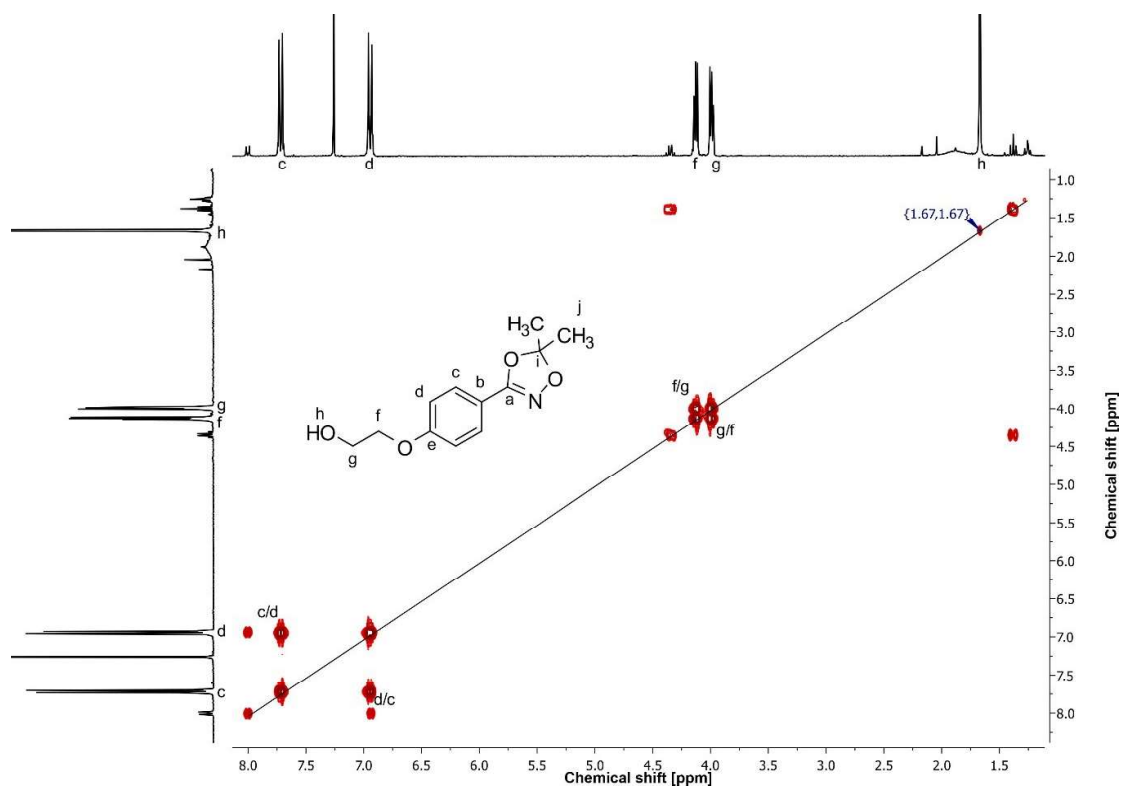
Figure S4c. ^{1}H-^{1}H COSY NMR spetrum (300 MHz, DMSO-d_6) of 2-(4-(5,5-dimethyl-1,4,2-dioxazol-3-yl)phenoxy)ethan-1-ol **(1c)** prior to purification via column chromatography.
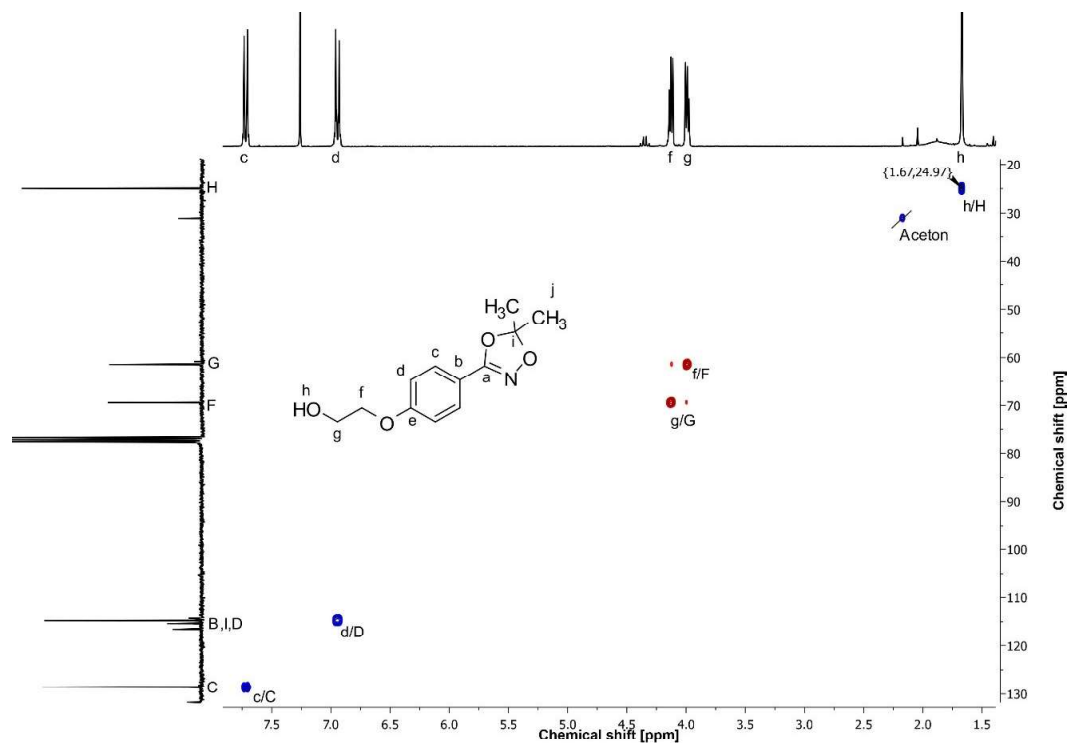
Figure S4d. ^{1}H-^{13}C HSQC NMR spectrum (300 MHz / 75 MHz, DMSO-d_6) of 2-(4-(5,5-dimethyl-1,4,2-dioxazol-3-yl)phenoxy)ethan-1-ol **(1c)** prior to purification via column chromatography.
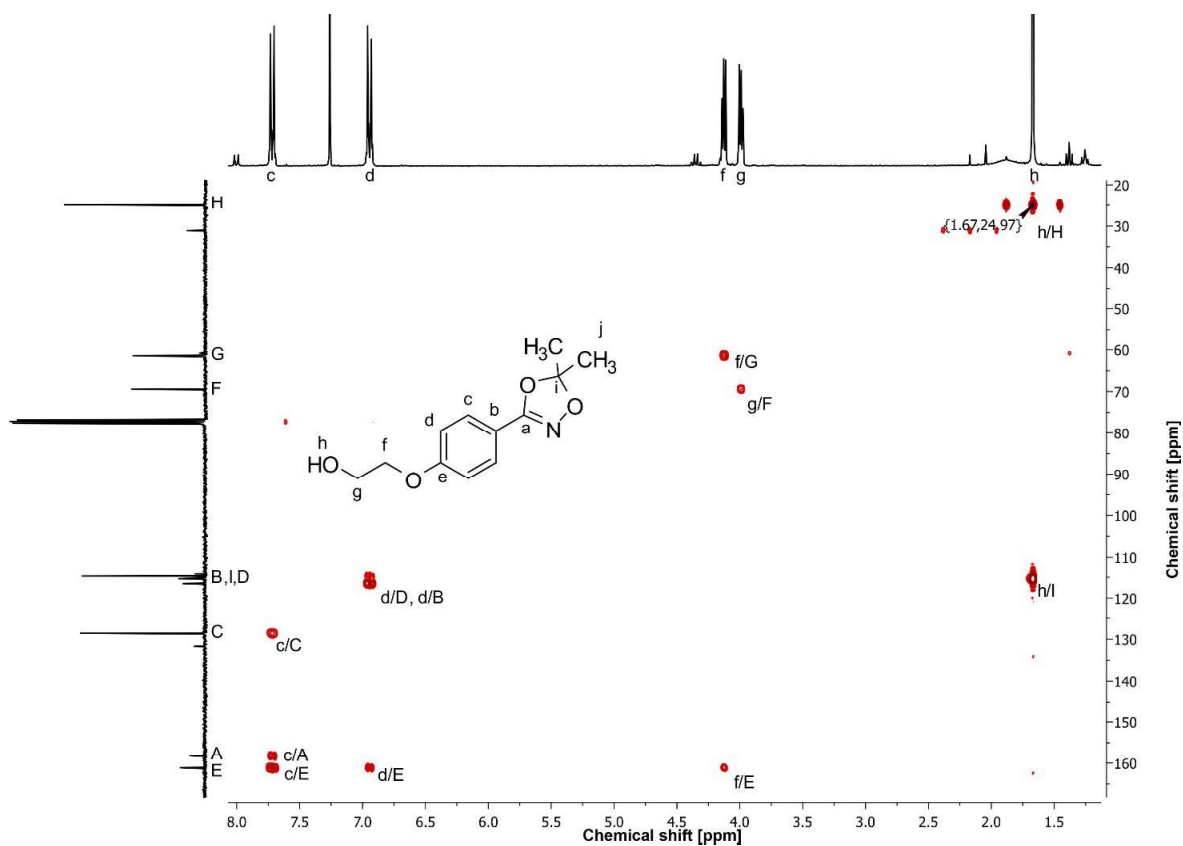
Figure S4e. ^{1}H-^{13}C HMBC NMR spectrum (300 MHz / 75 MHz, DMSO-d_6) of 2-(4-(5,5-dimethyl-1,4,2-dioxazol-3-yl)phenoxy)ethan-1-ol **(1c)** prior to purification via column chromatography.
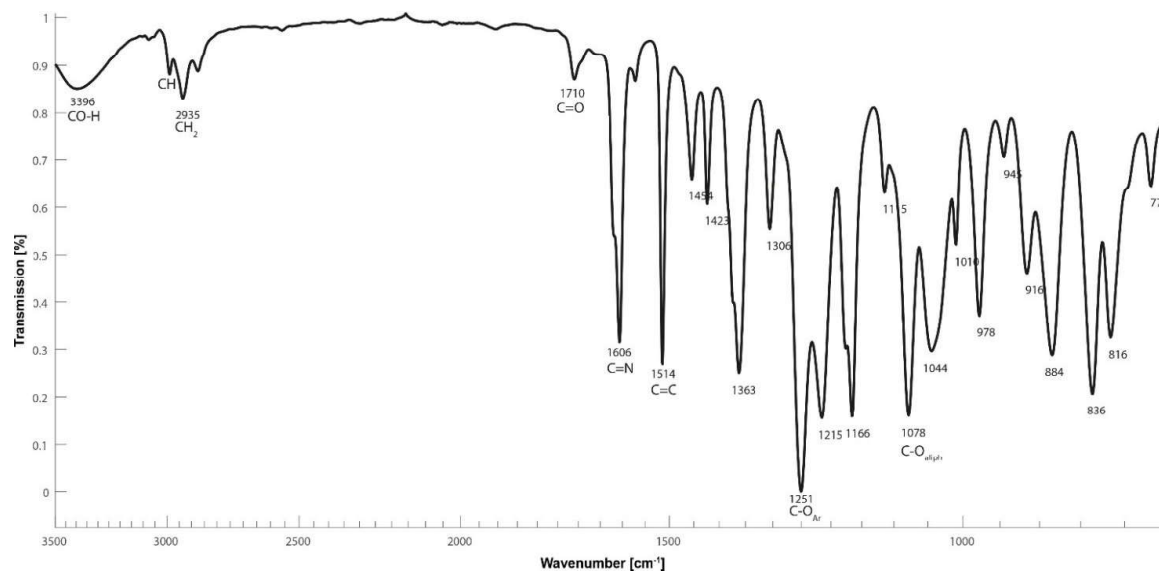
Figure S4f. FT-ATR-IR spectrum of 2-(4-(5,5-dimethyl-1,4,2-dioxazol-3-yl)phenoxy)ethan-1-ol **(1c)** prior to purification via column chromatography.

Characterization of *N*,4-dihydroxybenzamide (2a)
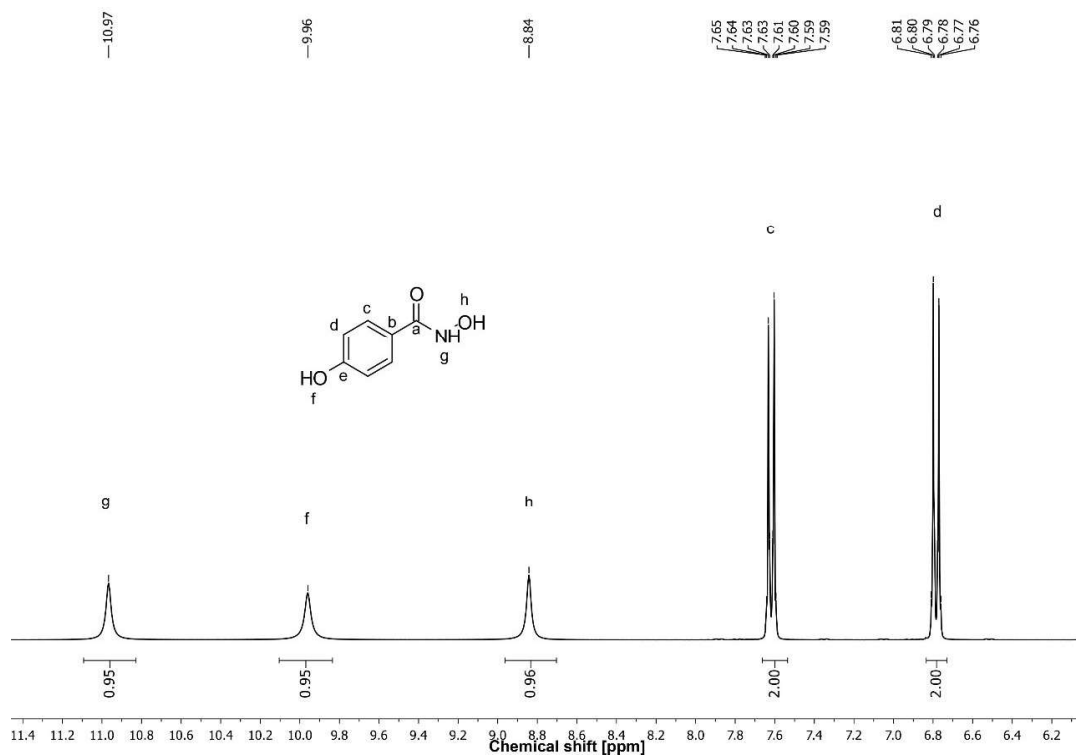
Figure S5a. ¹H NMR spectrum (300 MHz, DMSO-*d*₆) of *N*,4-dihydroxybenzamide **(2a)**.
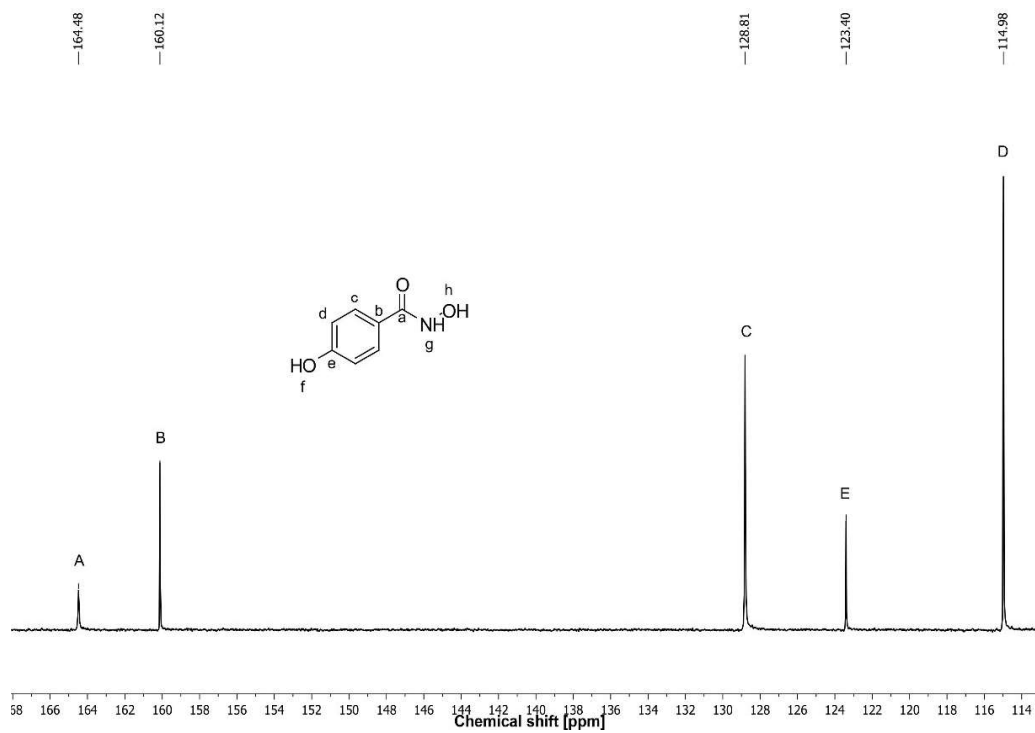
Figure S5b. ¹³C NMR spectrum (75 MHz, DMSO-*d*₆) of *N*,4-dihydroxybenzamide **(2a)**.
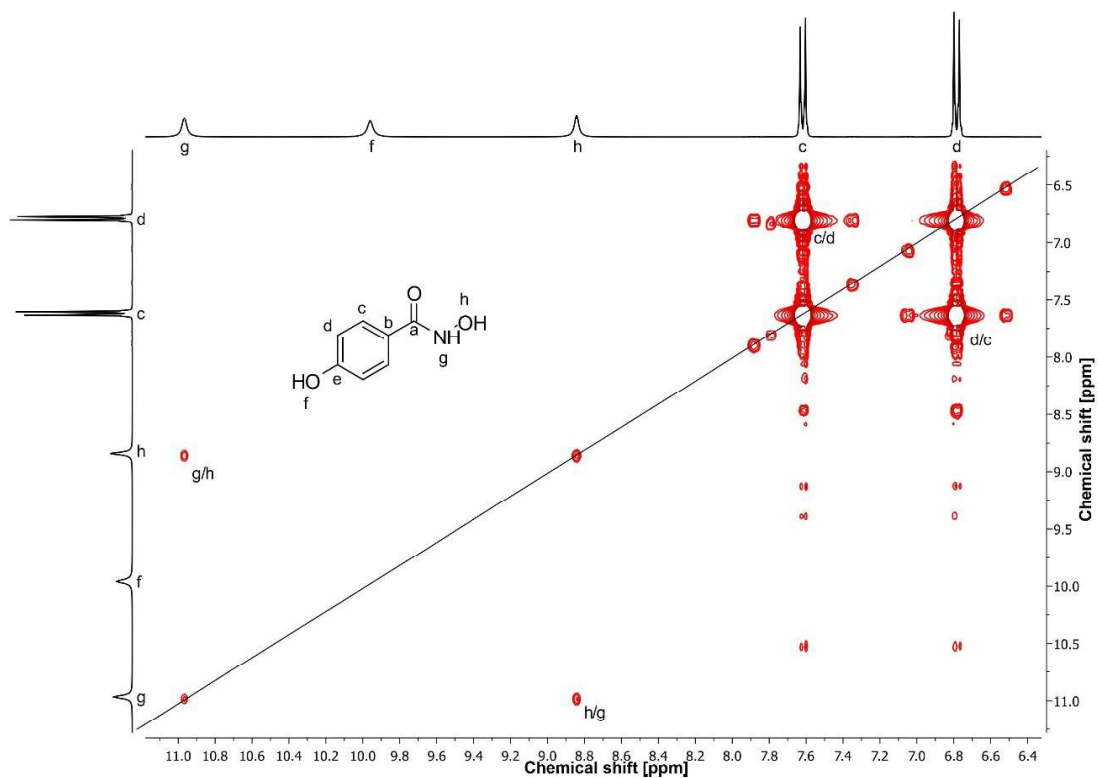
Figure S5c. ^1H-^1H COSY NMR spectrum (300 MHz, DMSO-d_6) of N,4-dihydroxybenzamide **(2a)**.
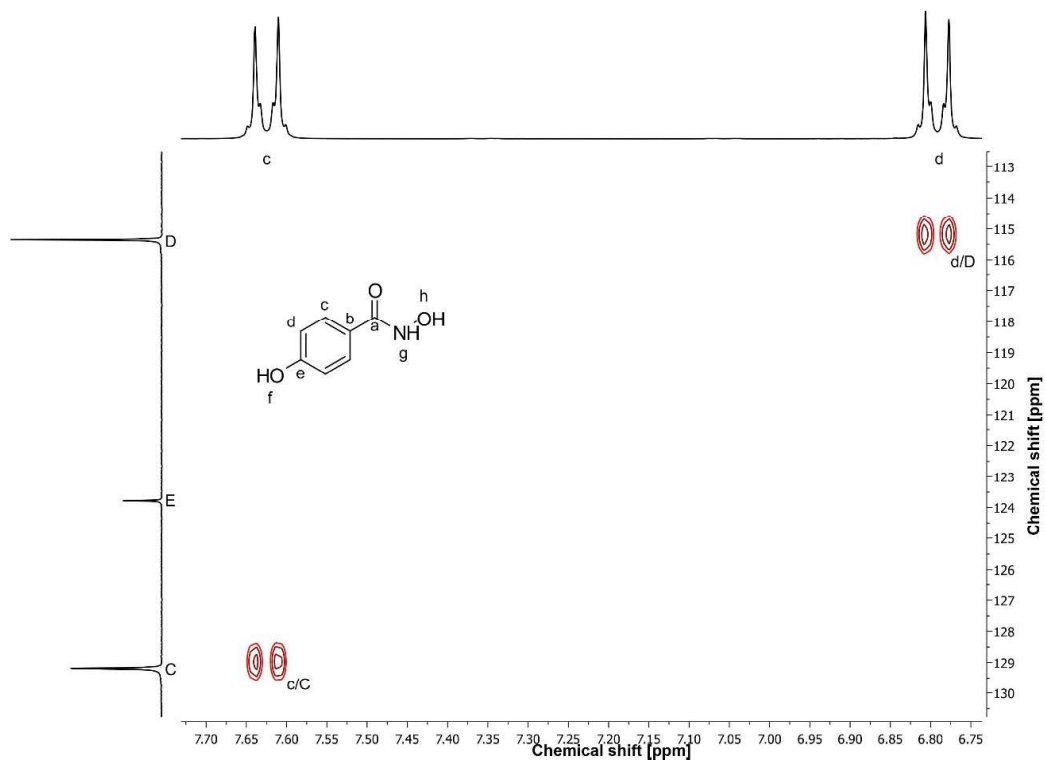
Figure S5d. ^1H-^{13}C HSQC NMR spectrum (300 MHz / 75 MHz, DMSO-d_6) of N,4-dihydroxybenzamide **(2a)**.
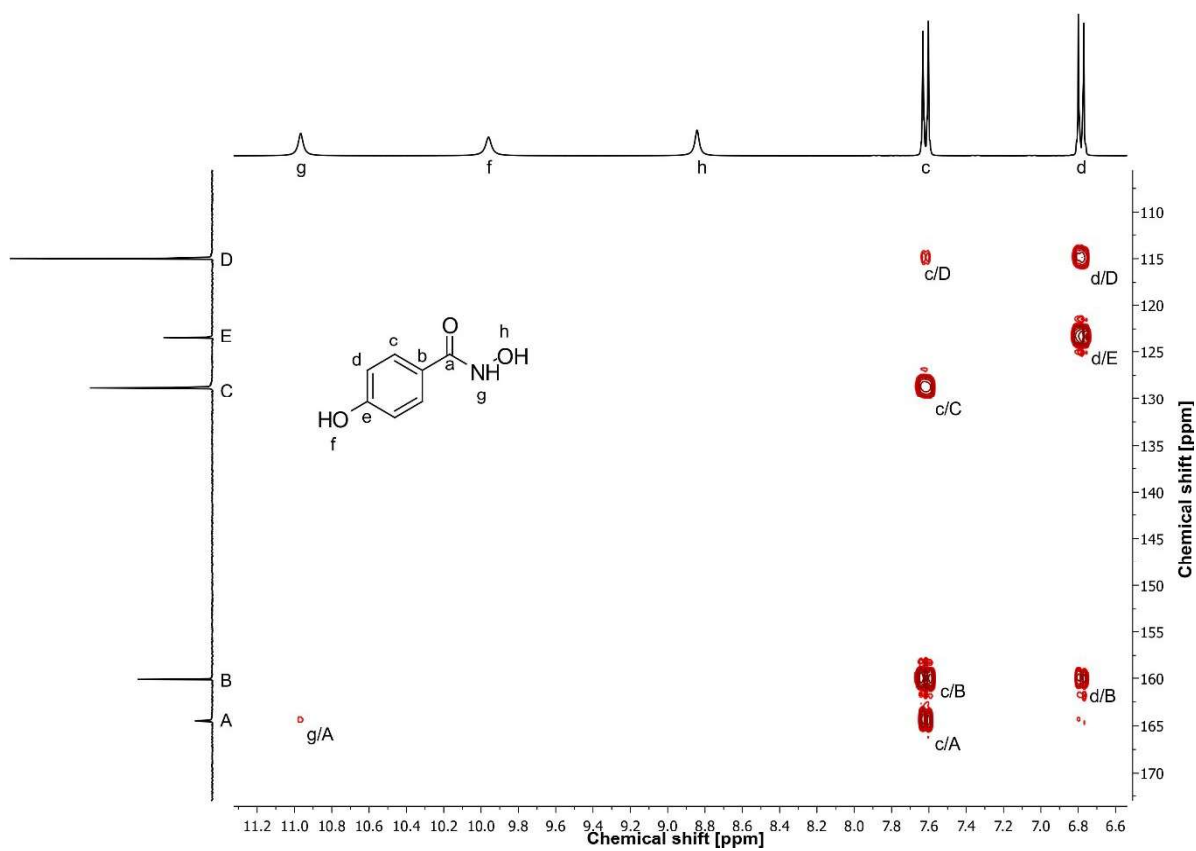
Figure S5e. ^{1}H-^{13}C HMBC NMR spectrum (300 MHz / 75 MHz, DMSO-d_6) of N,4-dihydroxybenzamide **(2a)**.
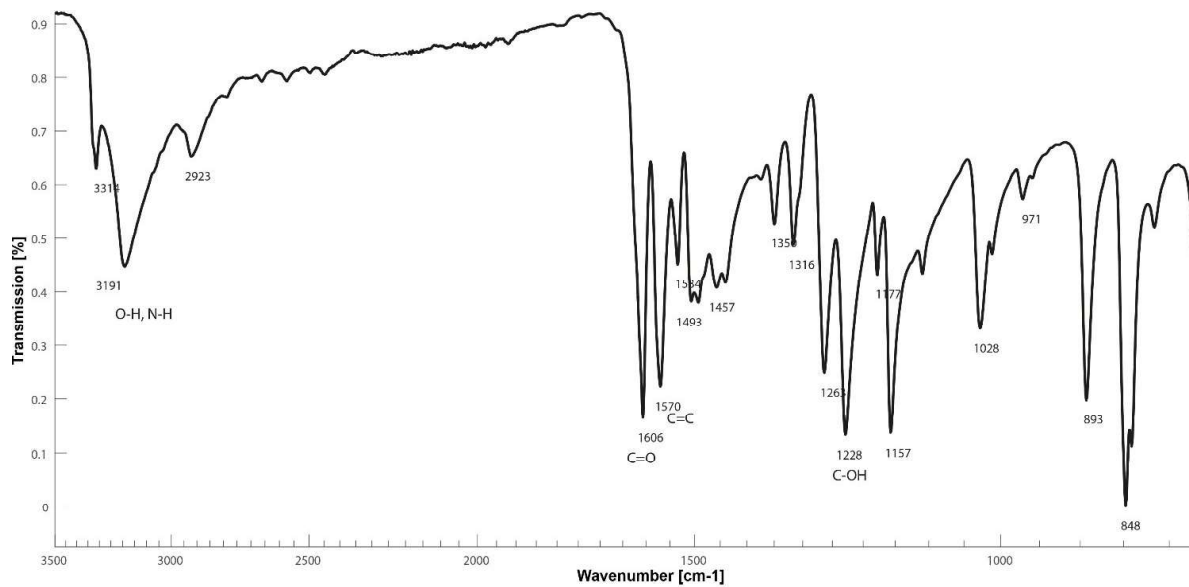
Figure S5f. FT-ATR-IR spectrum of N,4-dihydroxybenzamide **(2a)**.

Characterization of 4-(5,5-dimethyl-1,4,2-dioxazol-3-yl)phenol (2b)
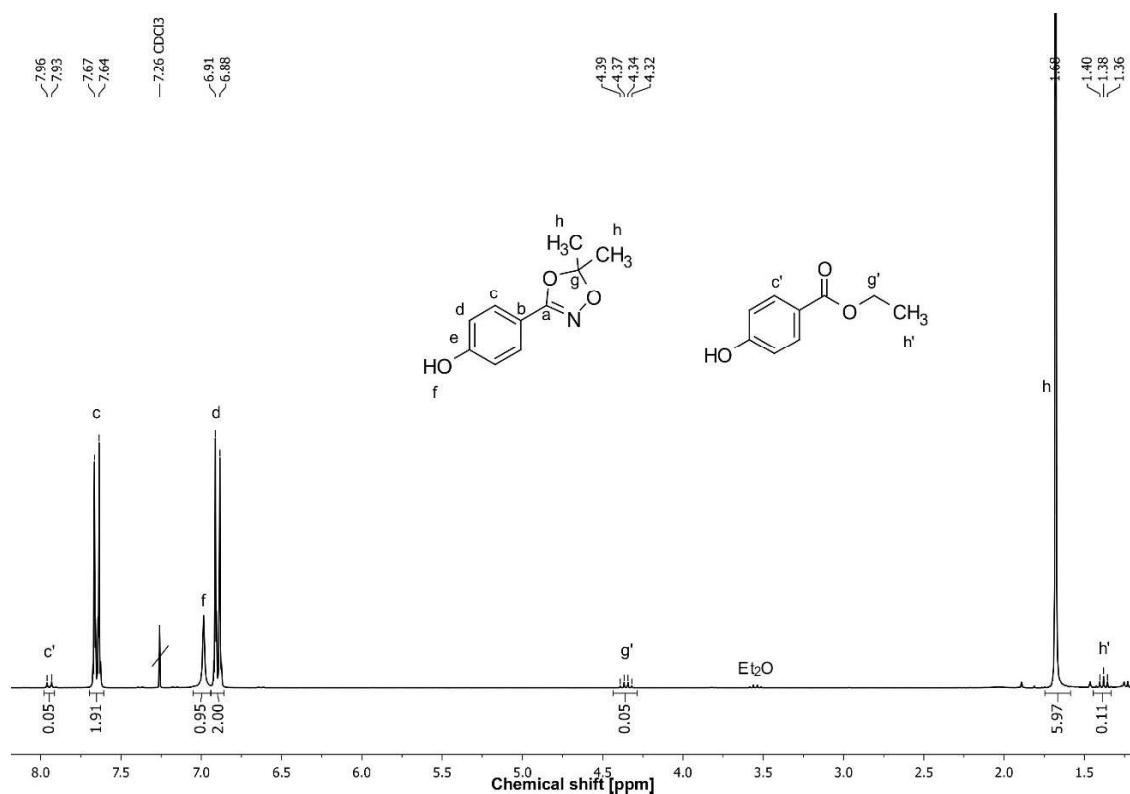
Figure S6a. ^{1}H NMR spectrum (300 MHz, DMSO-d_6) of 4-(5,5-dimethyl-1,4,2-dioxazol-3-yl)phenol **(2b)**. The ethyl ester residue originates from the side reaction during transketalization.
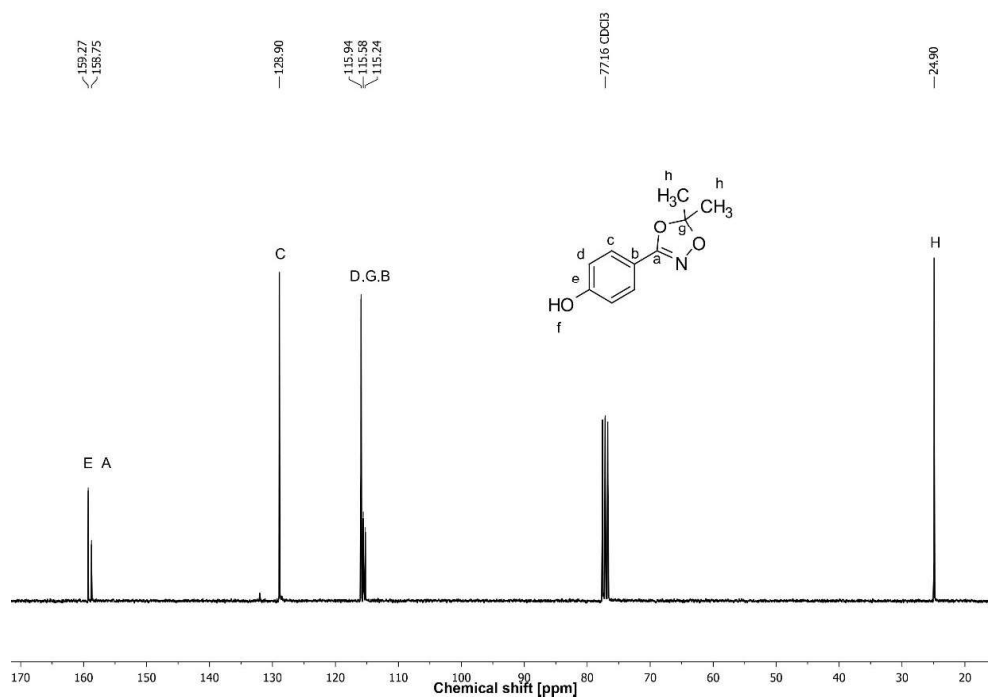
Figure S6b. ^{13}C NMR spectrum (75 MHz, DMSO-d_6) of 4-(5,5-dimethyl-1,4,2-dioxazol-3-yl)phenol **(2b)**.
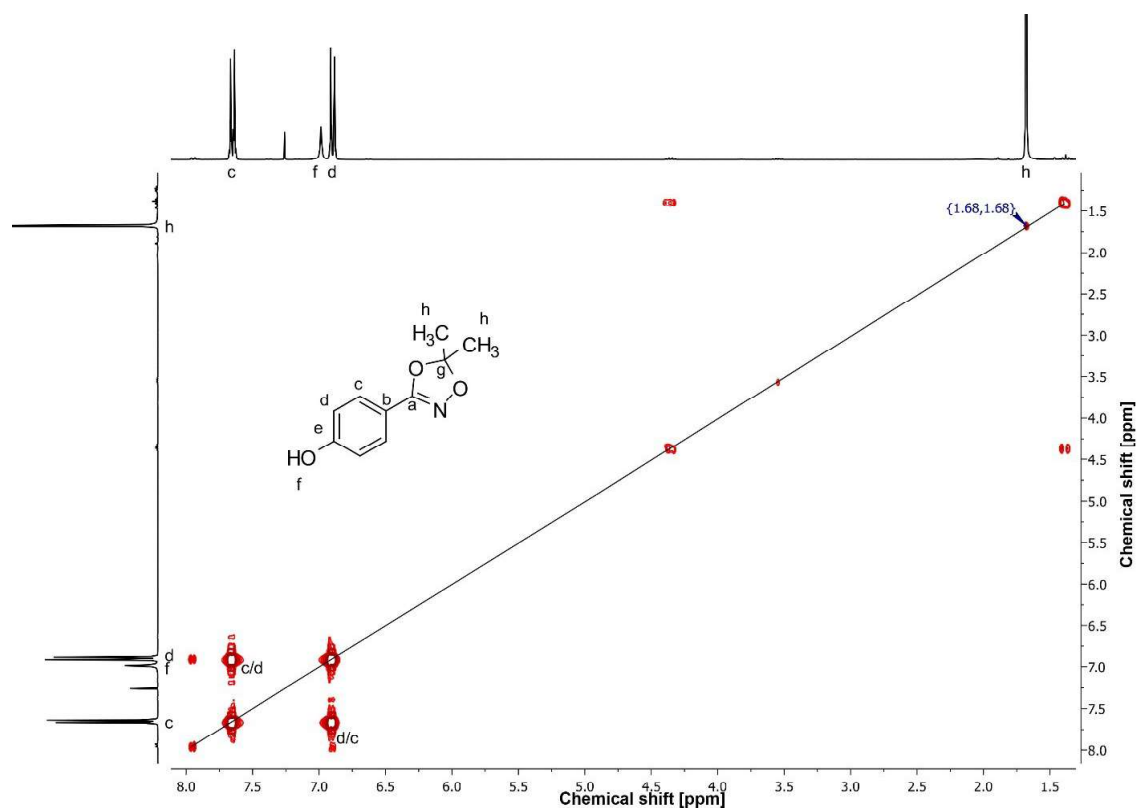
Figure S6c. ^{1}H-^{1}H COSY NMR spectrum (300 MHz, DMSO-d_6) of 4-(5,5-dimethyl-1,4,2-dioxazol-3-yl)phenol **(2b).**
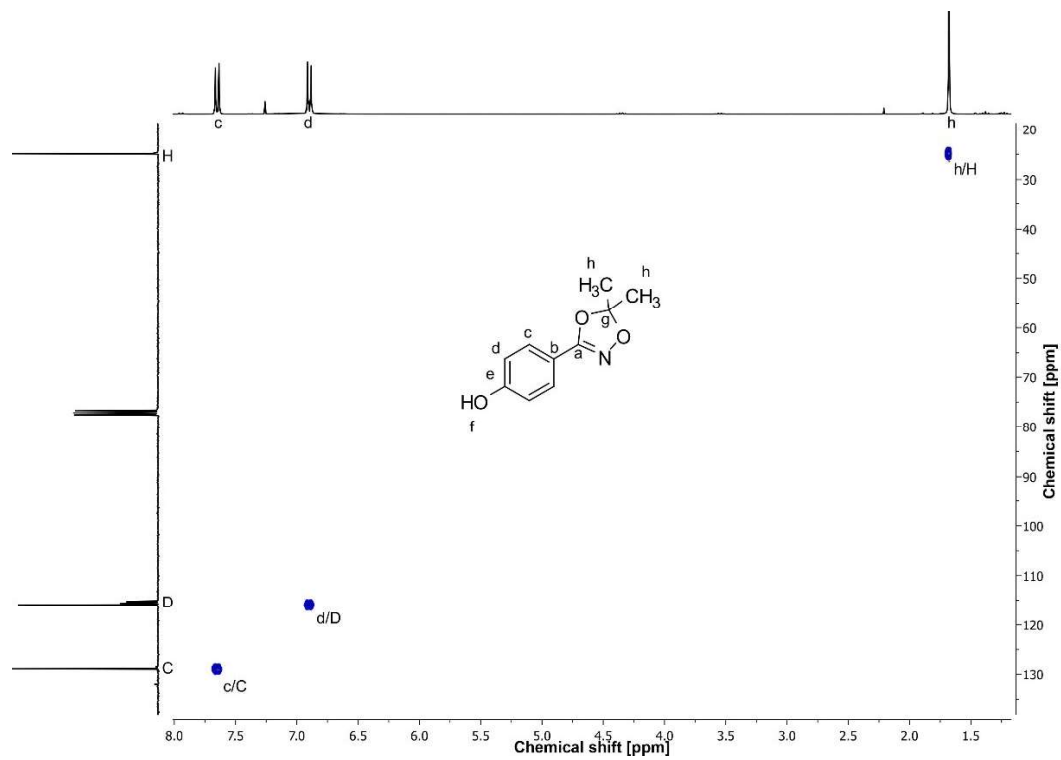
Figure S6d. ^{1}H-^{13}C HSQC NMR spectrum (300 MHz / 75 MHz, DMSO-d_6) of 4-(5,5-dimethyl-1,4,2-dioxazol-3-yl)phenol **(2b).**
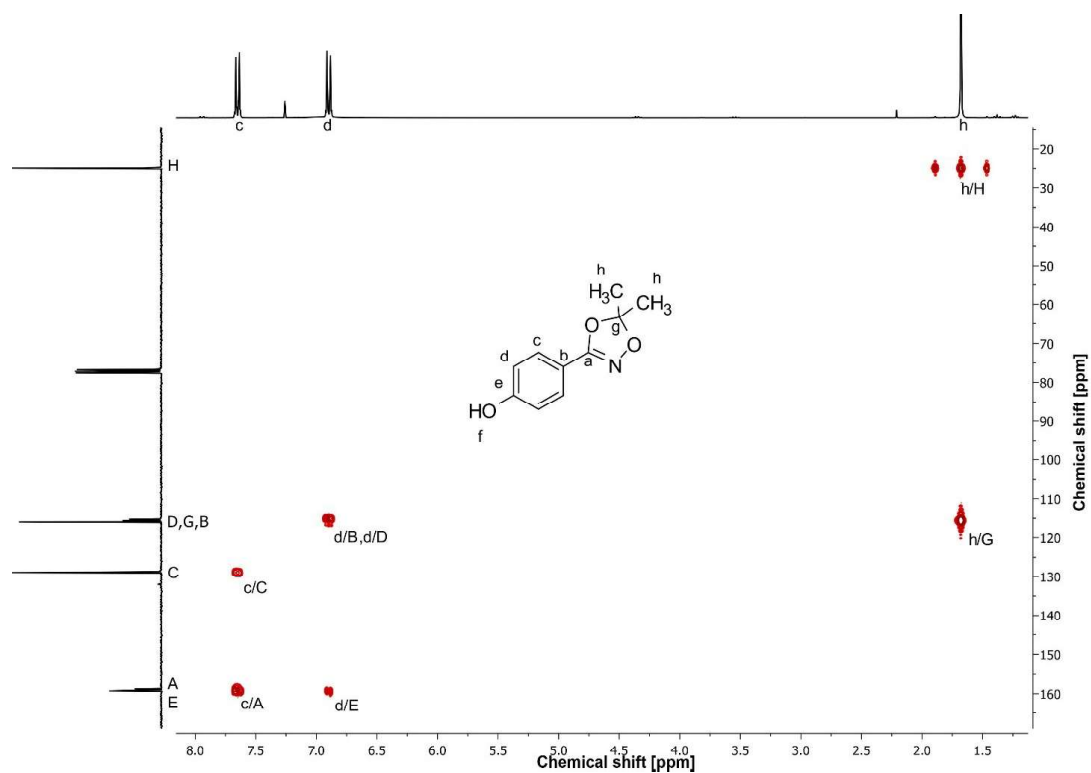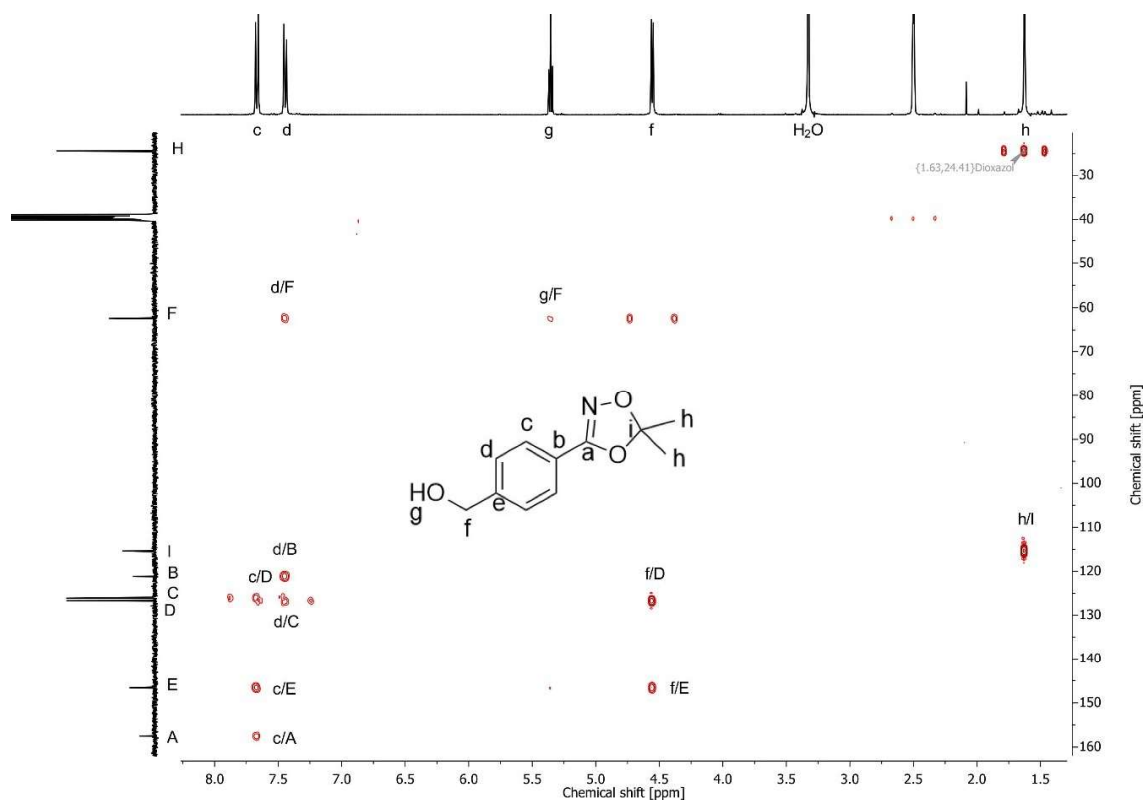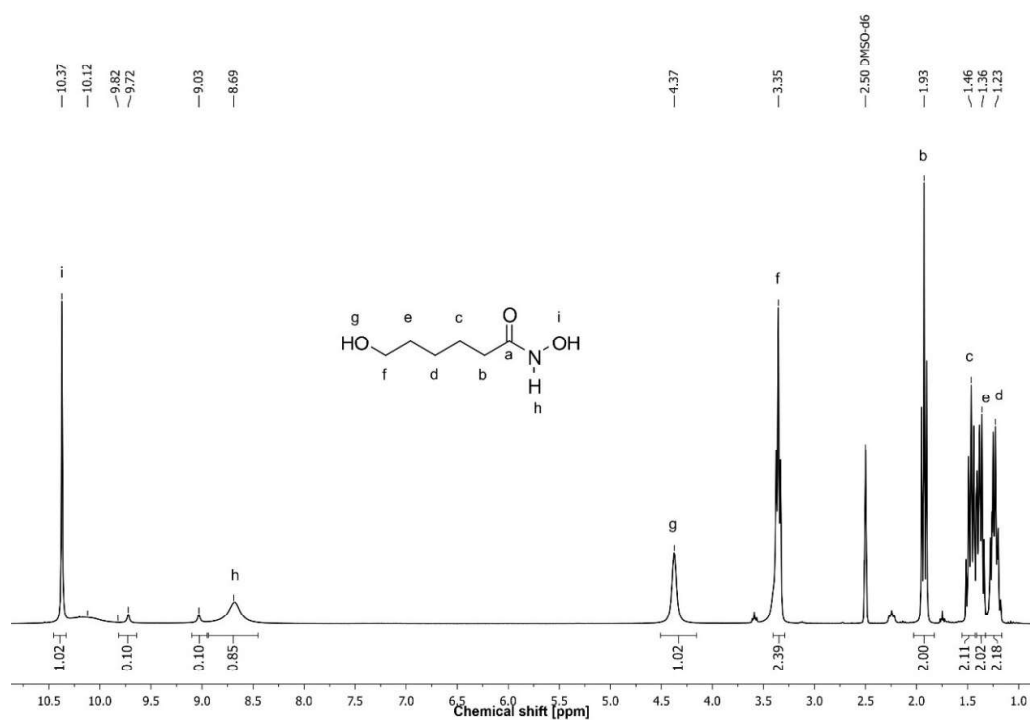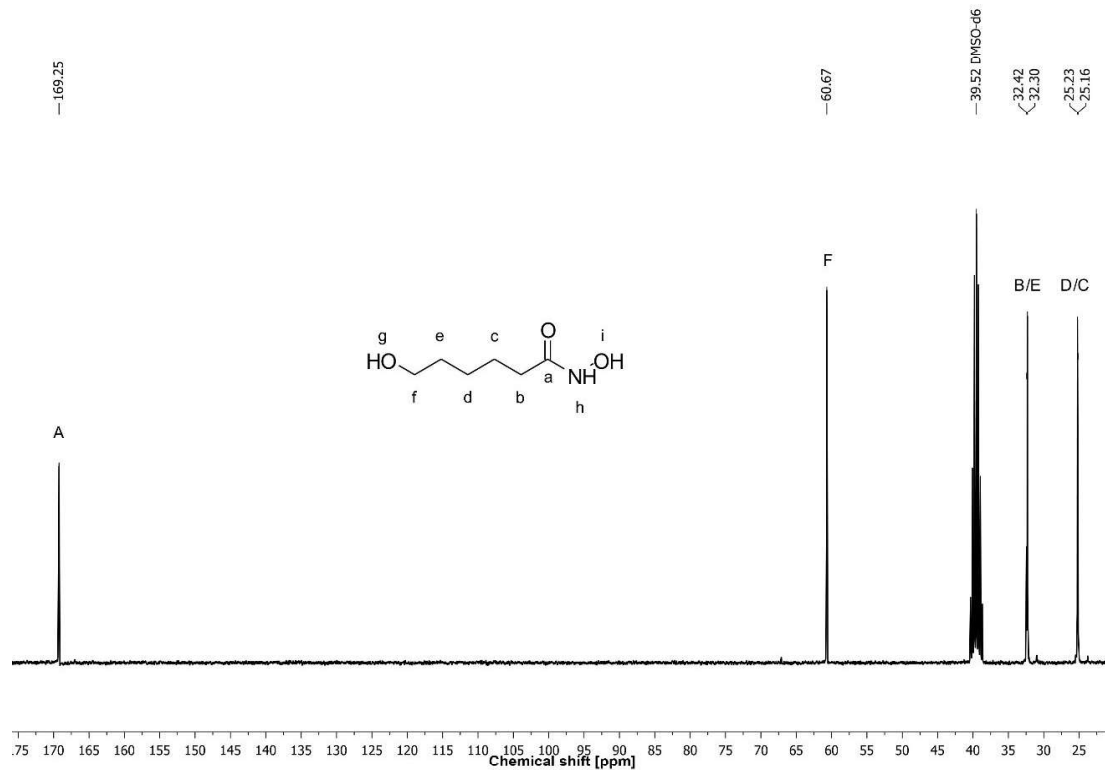
Figure S6e. ^{1}H-^{13}C HMBC NMR spectrum (300 MHz / 75 MHz, DMSO-d_6) of 4-(5,5-dimethyl-1,4,2-dioxazol-3-yl)phenol **(2b).**

Characterization of *N*-hydroxy-4-(hydroxymethyl)benzamide (3a)
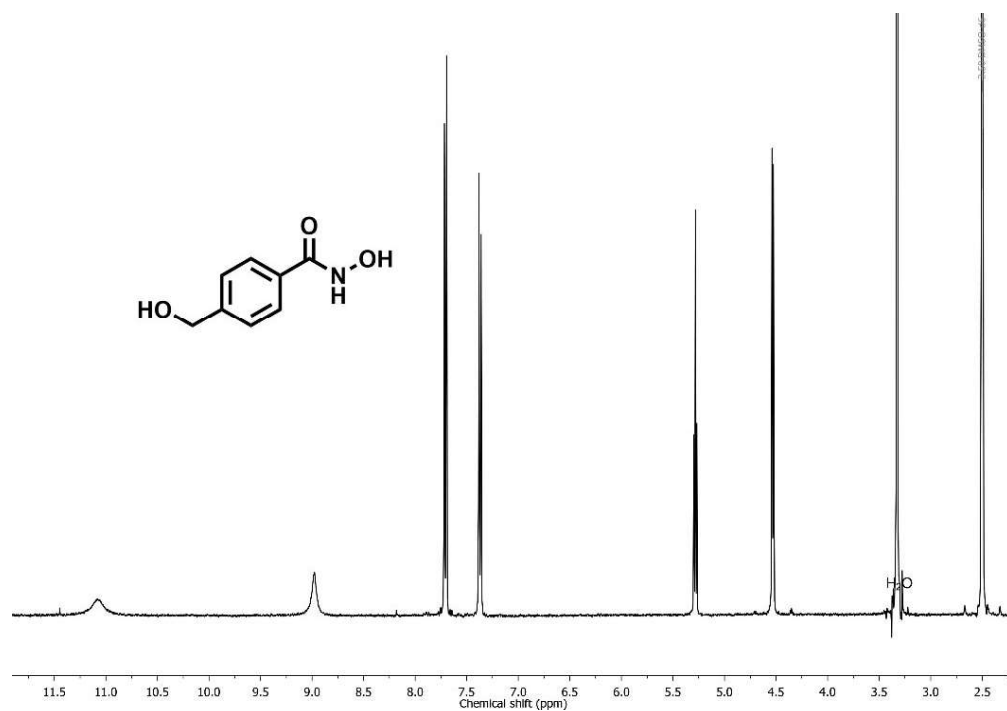
Figure S7a. ^{1}H NMR spectrum (400 MHz, DMSO-d_6) of *N*-hydroxy-4-(hydroxymethyl)benzamide **(3a).** See synthesis procedure for detailed assignment of the signals.
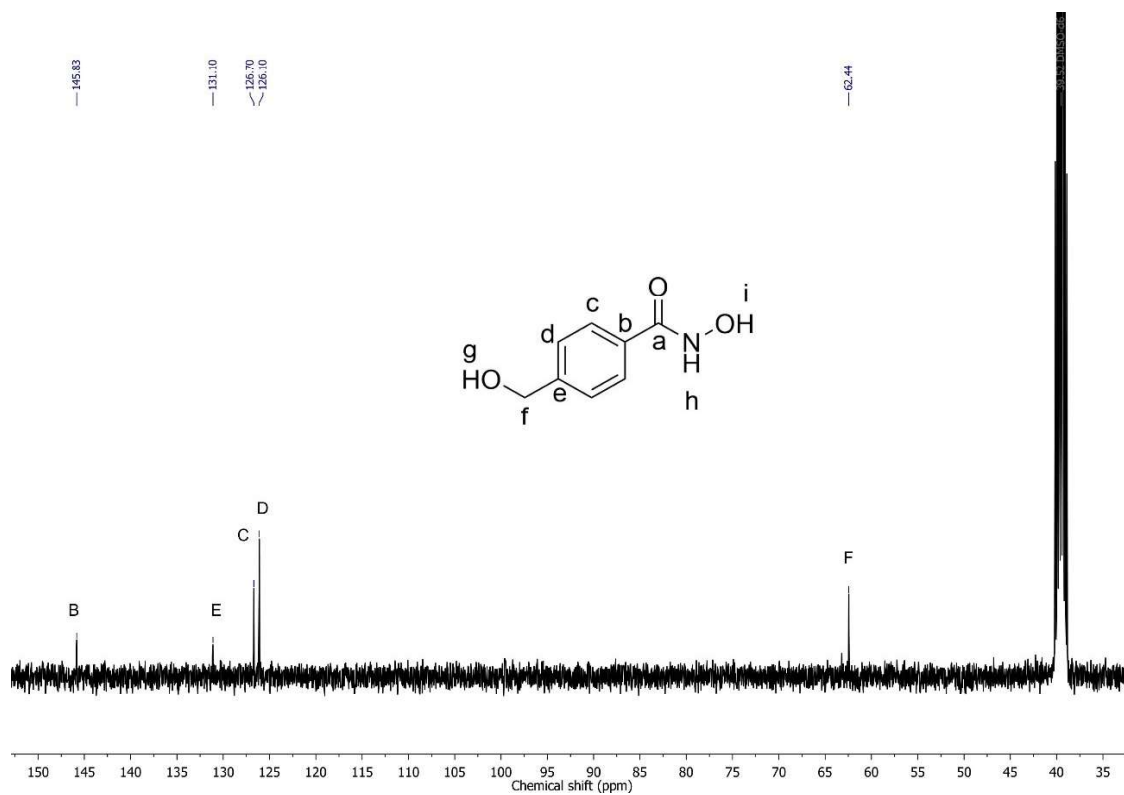
Figure S7b. ^{13}C NMR spectrum (100 MHz, DMSO-d_6) of *N*-hydroxy-4-(hydroxymethyl)benzamide **(3a).**
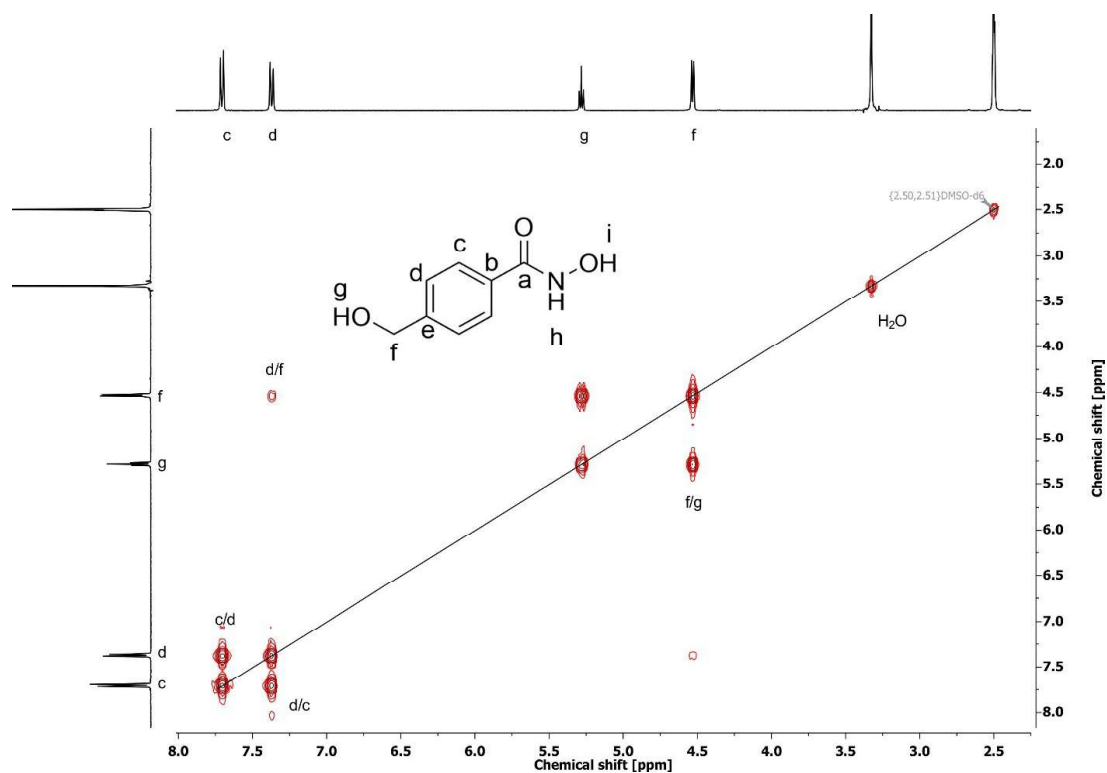
Figure S7c. ^{1}H-^{1}H COSY NMR spectrum (400 MHz, DMSO-d_6) of *N*-hydroxy-4-(hydroxymethyl)benzamide **(3a)**.
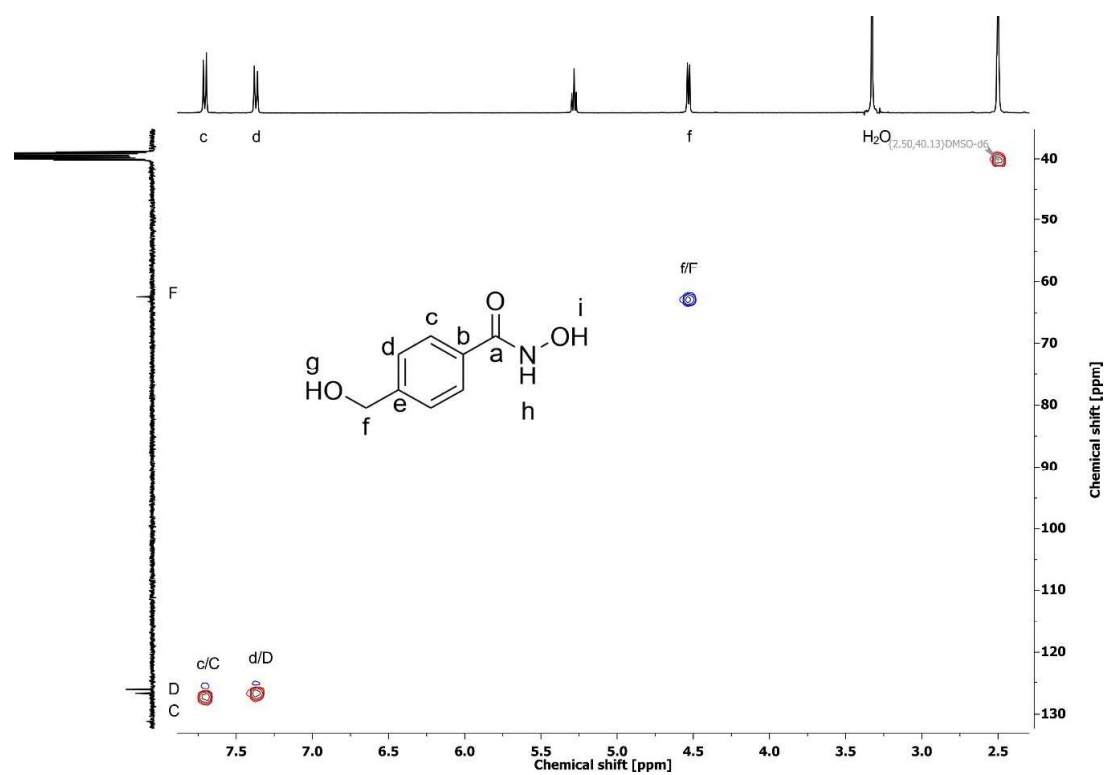
Figure S7d. ^{1}H-^{13}C HSQC NMR spectrum (400 MHz / 100 MHz, DMSO-d_6) of *N*-hydroxy-4-(hydroxymethyl)benzamide **(3a)**.
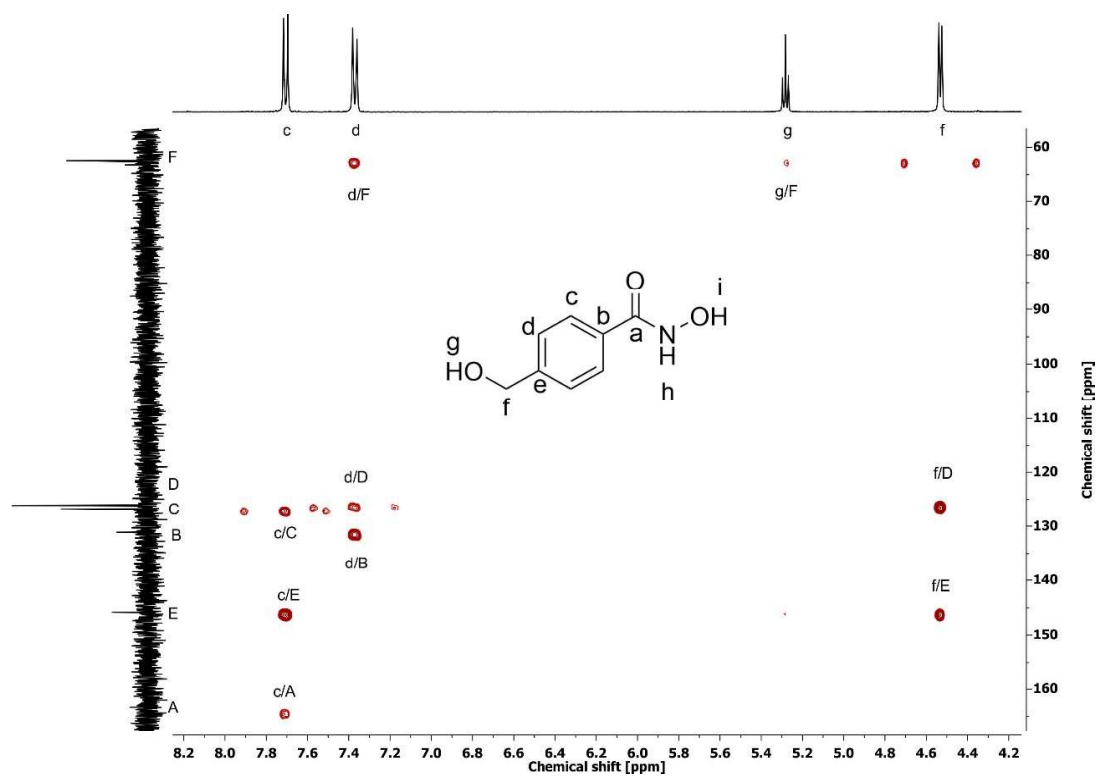
Figure S7e. ^{1}H-^{13}C HMBC NMR spectrum (400 MHz / 100 MHz, DMSO-d_6) of *N*-hydroxy-4-(hydroxymethyl)benzamide **(3a)**.

Characterization of (4-(5,5-dimethyl-1,4,2-dioxazol-3-yl)phenyl)methanol (3b) [benzyl]**HAA-OH**
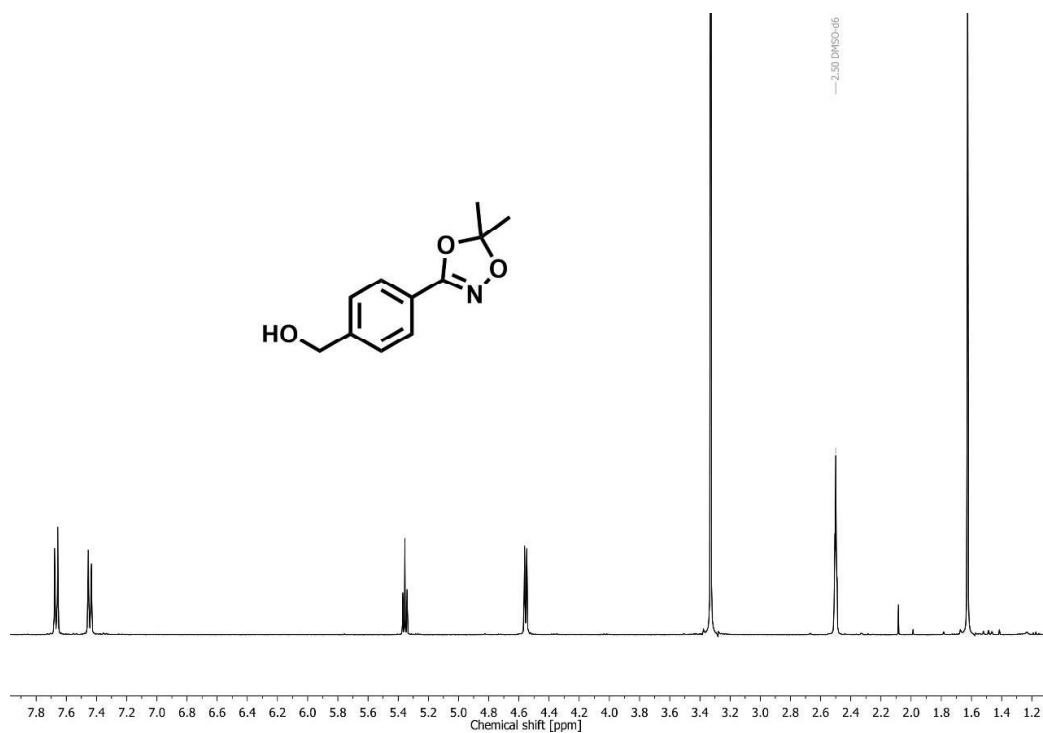
Figure S8a. ^{1}H NMR spectrum (400 MHz, DMSO-d_6) of (4-(5,5-dimethyl-1,4,2-dioxazol-3-yl)phenyl)methanol **(3b).** See synthesis procedure for detailed assignment of the signals.
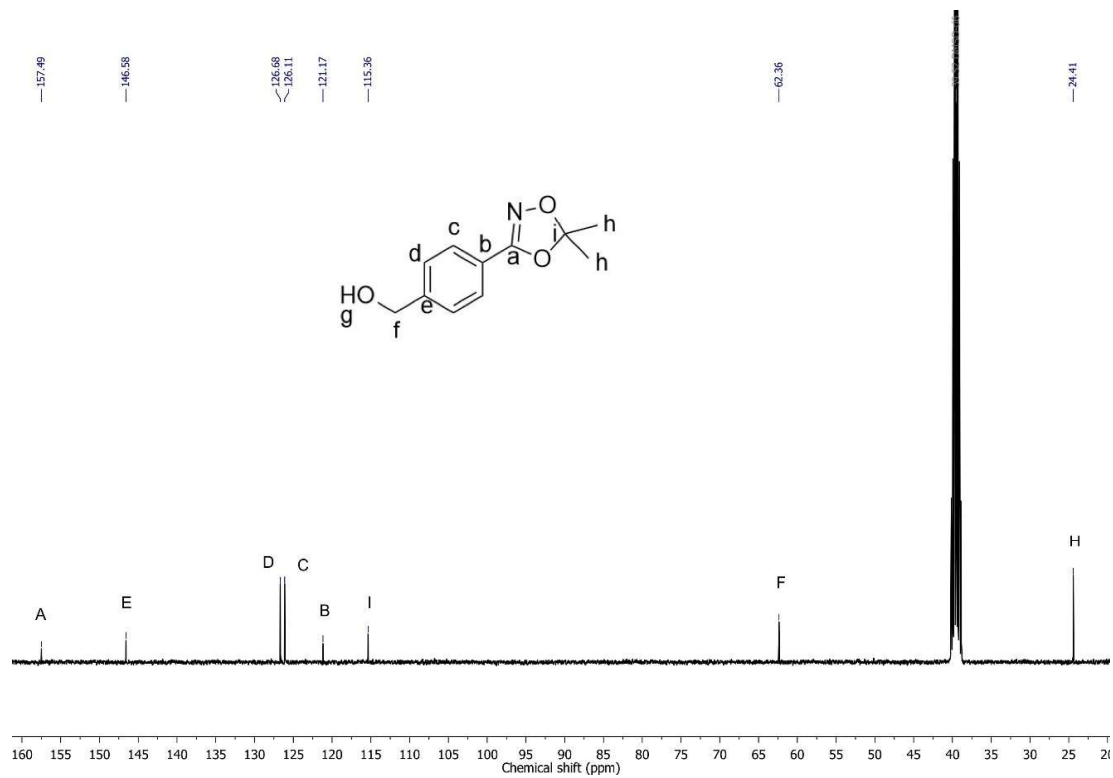
Figure S8b. ^{13}C NMR spectrum (100 MHz, DMSO-d_6) of (4-(5,5-dimethyl-1,4,2-dioxazol-3-yl)phenyl)methanol **(3b).**
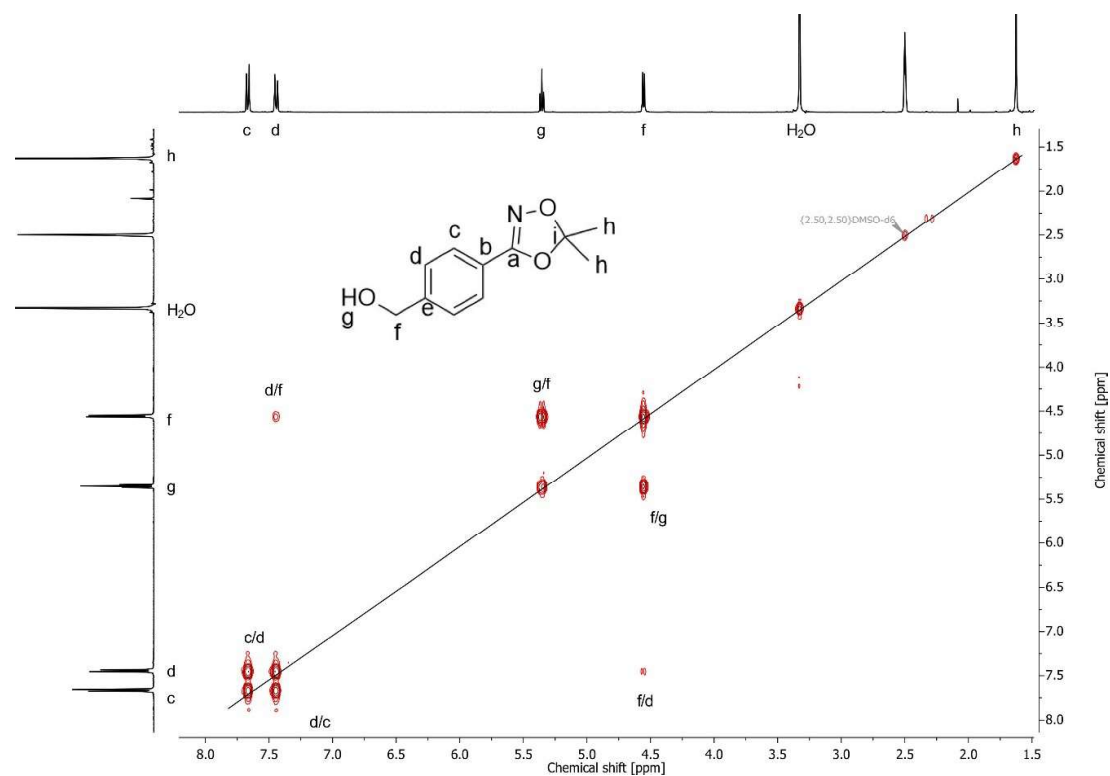
Figure S8c. ^{1}H-^{1}H COSY NMR spectrum (400 MHz, DMSO-d_6) of (4-(5,5-dimethyl-1,4,2-dioxazol-3-yl)phenyl)methanol **(3b).**
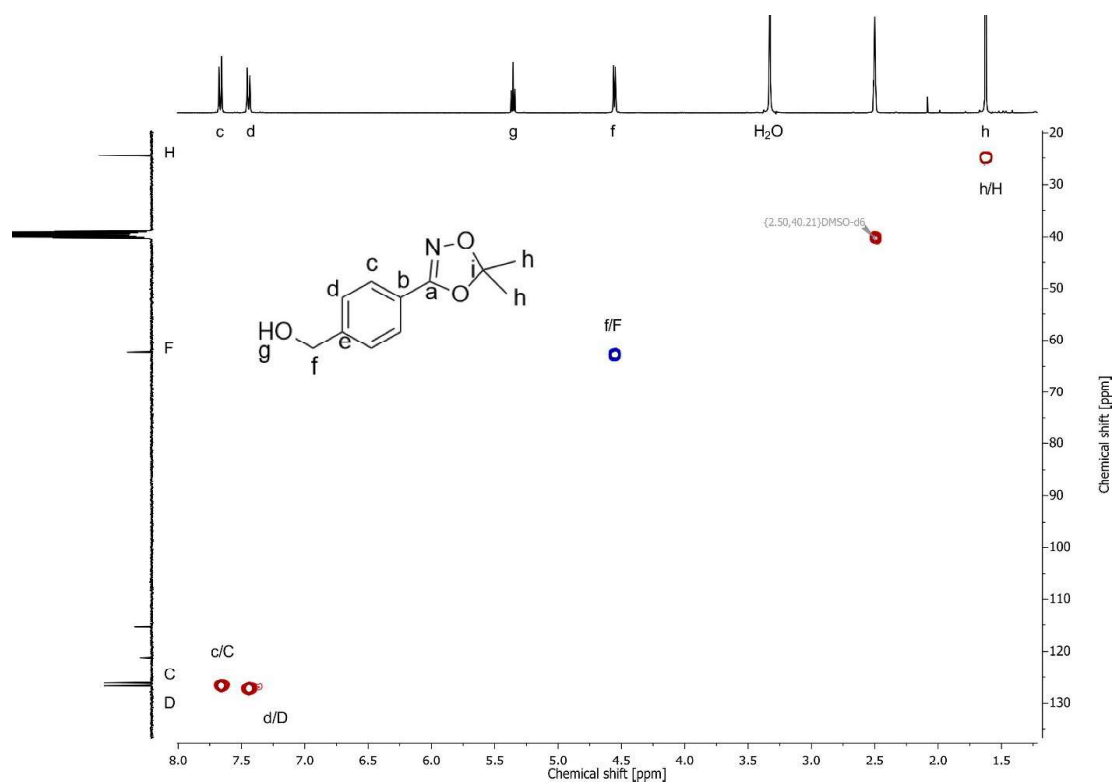
Figure S8d. ^{1}H-^{13}C HSQC NMR spectrum (400 MHz / 100 MHz, DMSO-d_6) of (4-(5,5-dimethyl-1,4,2-dioxazol-3-yl)phenyl)methanol **(3b).**

Figure S8e. ^{1}H-^{13}C HMBC NMR spectrum (400 MHz / 100 MHz, DMSO-d_6) of (4-(5,5-dimethyl-1,4,2-dioxazol-3-yl)phenyl)methanol **(3b).**

Characterization of *N*,6-dihydroxyhexanamide (4a)

Figure S9a. ^{1}H NMR spectrum (300 MHz, DMSO-d_6) of *N*,6-dihydroxyhexanamide **(4a)**.

Figure S9b. ^{13}C NMR spectrum (75 MHz, DMSO-d_6) of *N*,6-dihydroxyhexanamide **(4a)**.
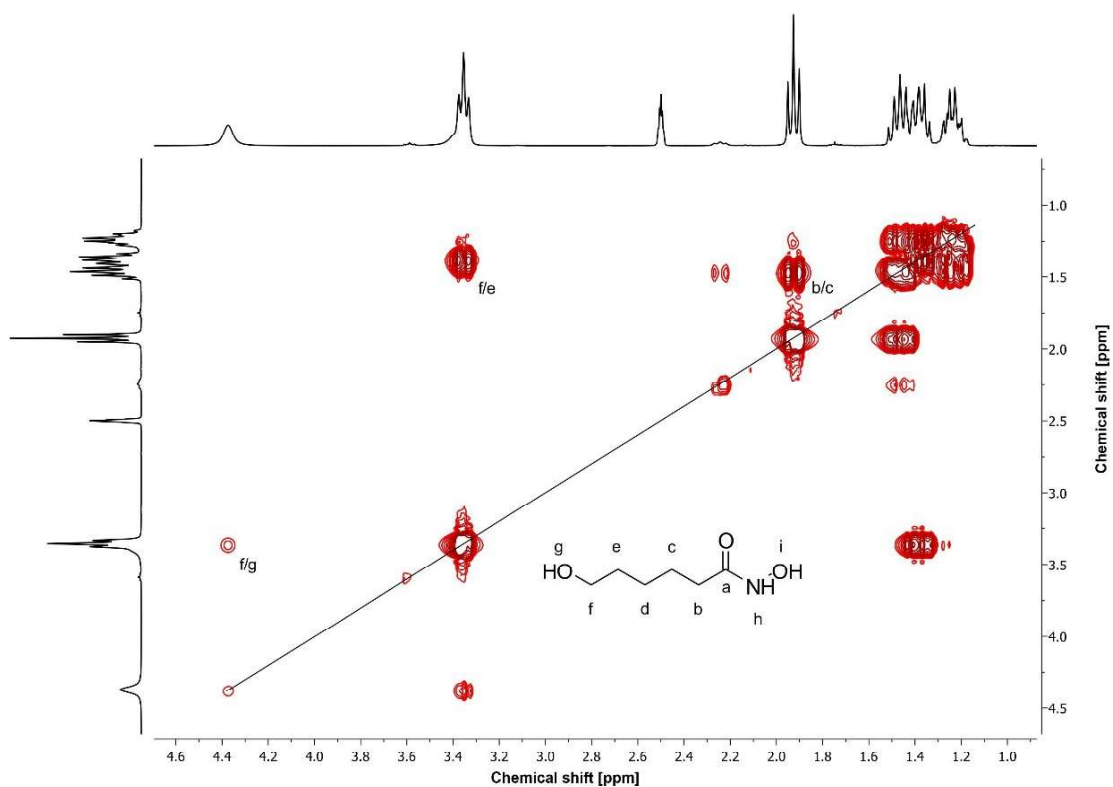
Figure S9c. ^{1}H-^{1}H COSY NMR spectrum (300 MHz, DMSO-d_6) of *N*,6-dihydroxyhexanamide **(4a)**.
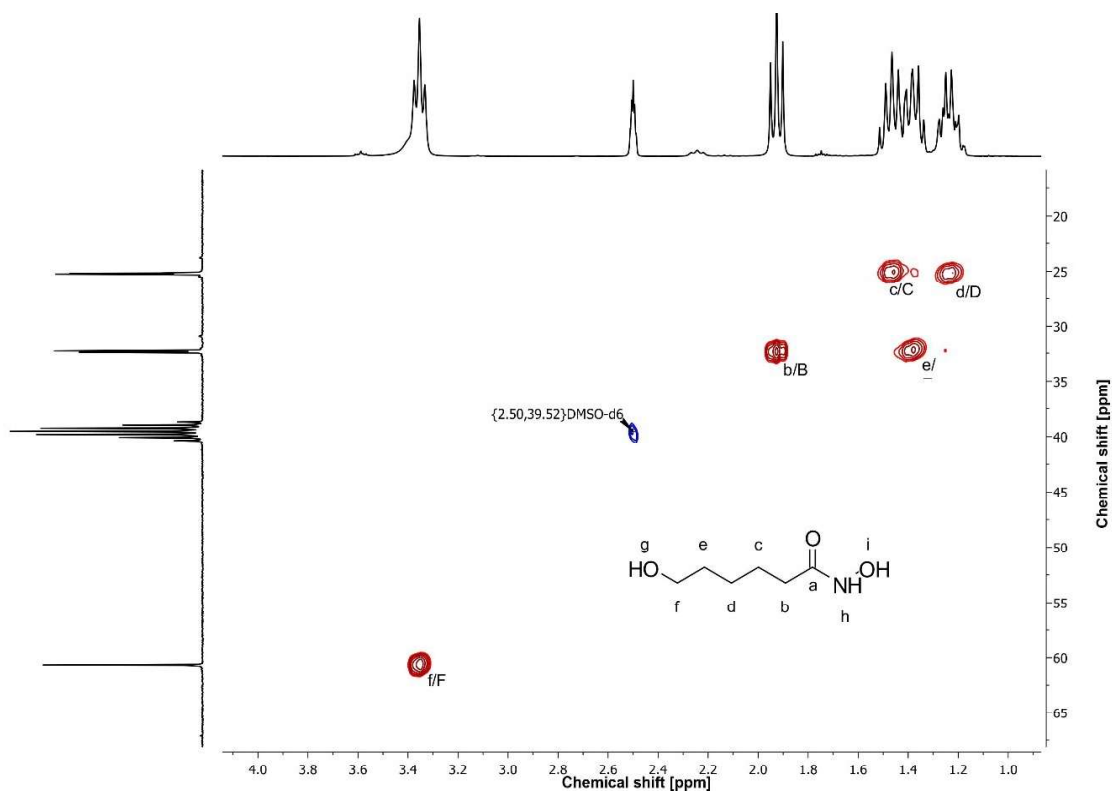
Figure S9d. ^{1}H-^{13}C HSQC NMR spectrum (300 MHz / 100 MHz, DMSO-d_6) of *N*,6-dihydroxyhexanamide **(4a)**.
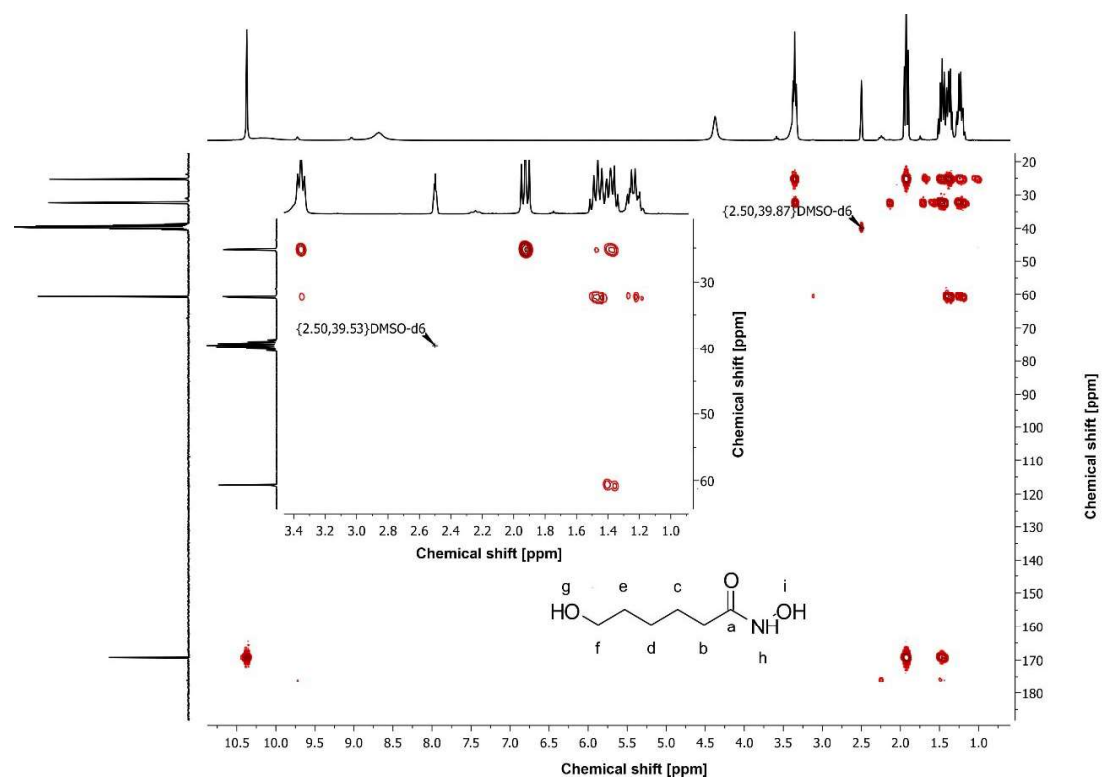
Figure S9e. ^{1}H-^{13}C HMBC NMR spectrum (300 MHz / 100 MHz, DMSO-d_6) of *N*,6-dihydroxyhexanamide **(4a).**
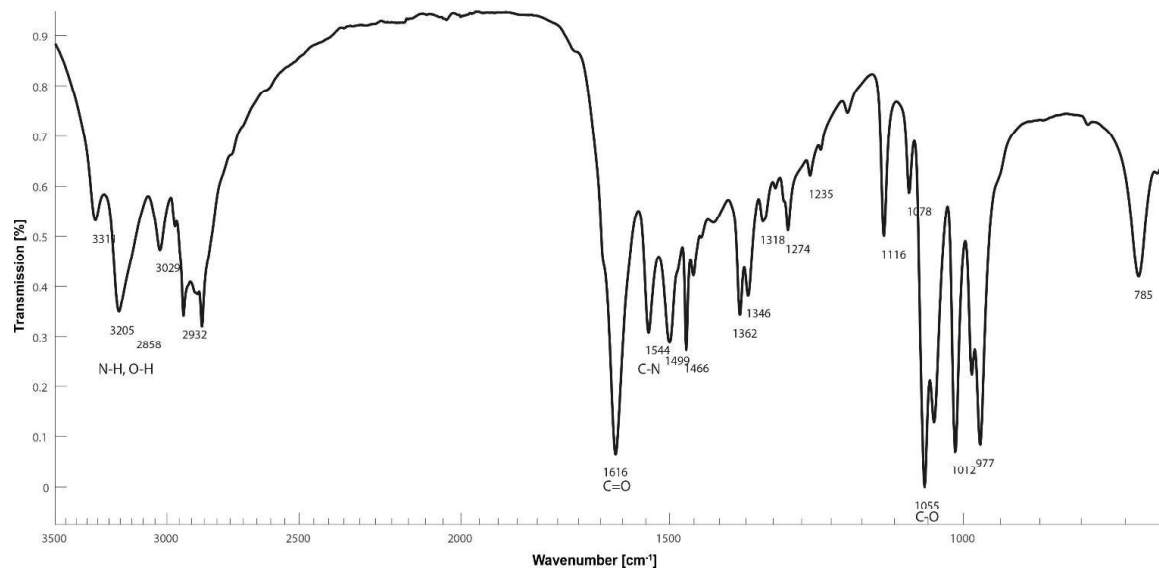
Figure S9f. FT-ATR-IR spectrum of *N*,6-dihydroxyhexanamide **(4a).**

Characterization of 5-(5,5-dimethyl-1,4,2-dioxazol-3-yl)pentan-1-ol (4b)
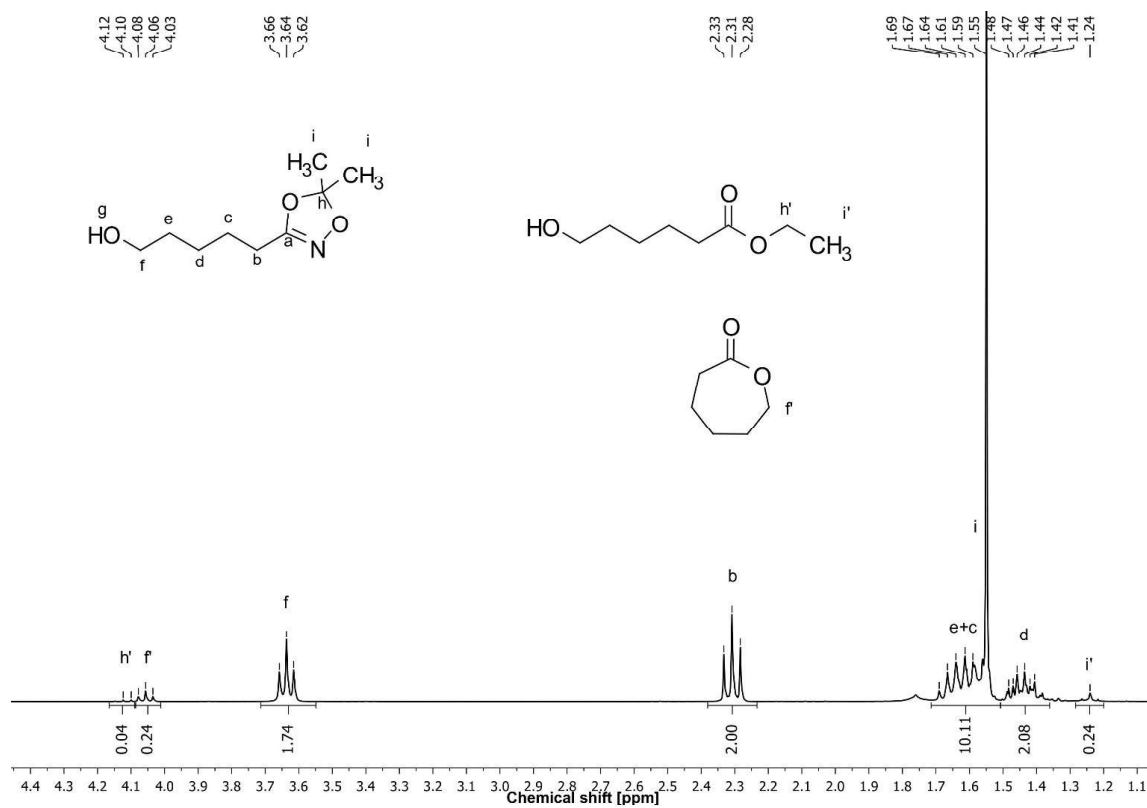
Figure S10. ^{1}H NMR spectrum (300 MHz, DMSO-d_6) of 5-(5,5-dimethyl-1,4,2-dioxazol-3-yl)pentan-1-ol **(4b).** The caprolactone signals originate from the side reaction during transketalization reaction.

Characterization of 5,5-dimethyl-3-(4-(2-(oxiran-2-ylmethoxy)ethoxy)phenyl) -1,4,2-dioxazole (1d)
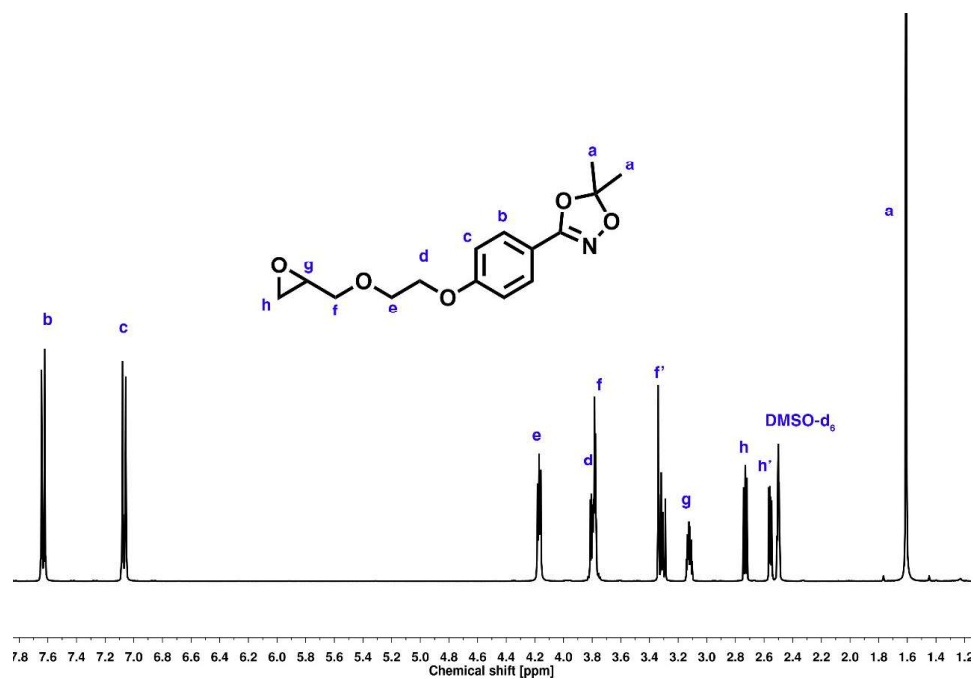
Figure S11. ^{1}H NMR spectrum (400 MHz, DMSO-d_6) of 5,5-dimethyl-3-(4-(2-(oxiran-2-ylmethoxy)ethoxy)phenyl) -1,4,2-dioxazole **(1d)**

Characterization of 2-(4-(5,5-dimethyl-1,4,2-dioxazol-3-yl)phenoxy)ethyl methacrylate (1e)
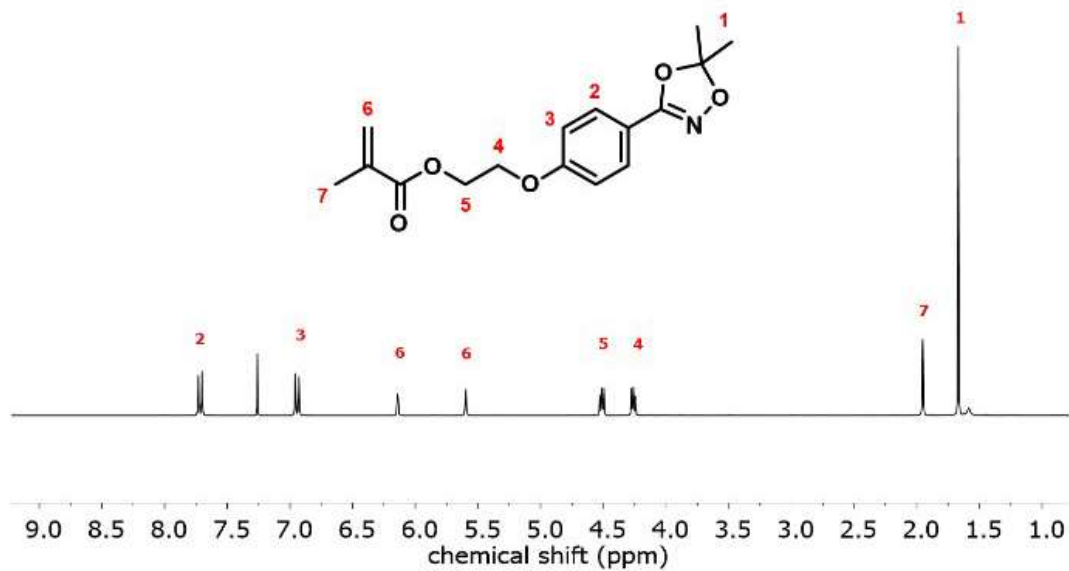
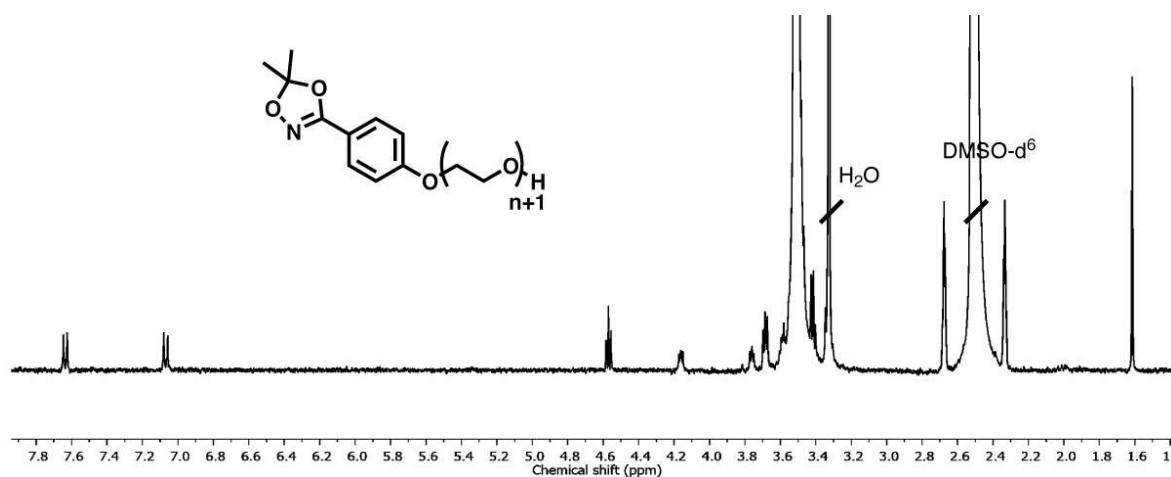**Figure S12.** ^{1}H NMR spectrum (300 MHz, DMSO-d_6) of 2-(4-(5,5-dimethyl-1,4,2-dioxazol-3-yl)phenoxy)ethyl methacrylate **(1e).**

Characterization of HAA-PEG (P1a), HA-PEG (P1b) and benzyl**HAA-PEG (P2a) polymers**

Figure S13a. Exemplary ^{1}H NMR spectrum (400 MHz, DMSO-d_6) of HAA-PEG (**P1a**). See synthesis procedure for detailed assignment of the signals.
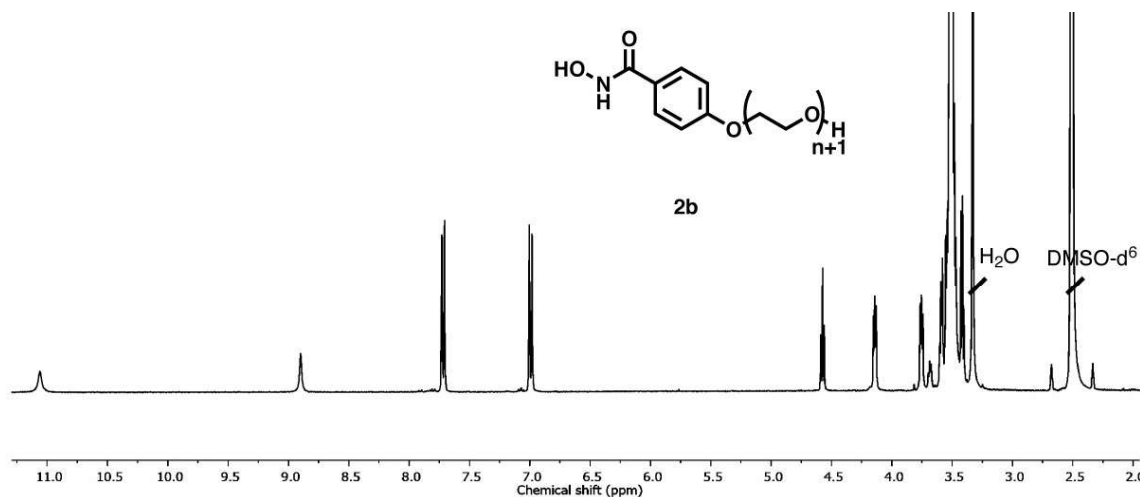

Figure S13b. Exemplary ^{1}H NMR spectrum (400 MHz, DMSO-d_6) of HA-PEG (**P1b**). See synthesis procedure for detailed assignment of the signals.
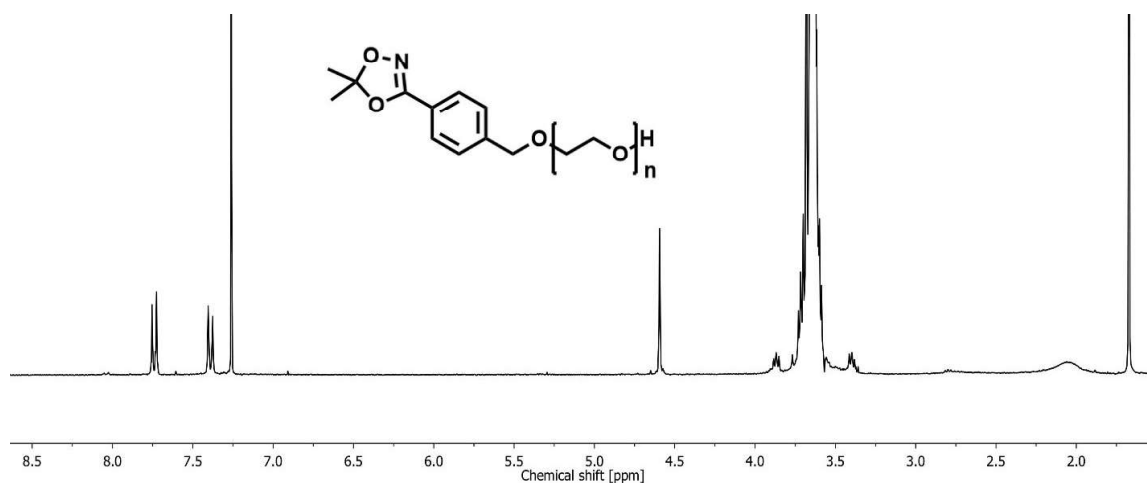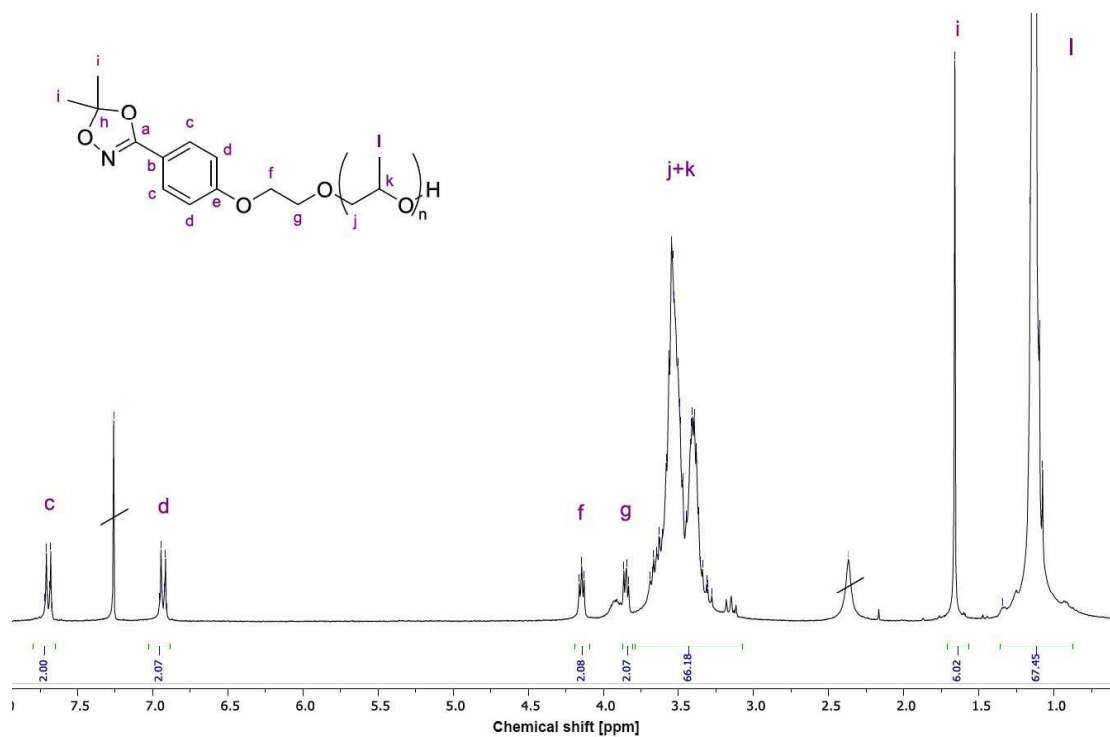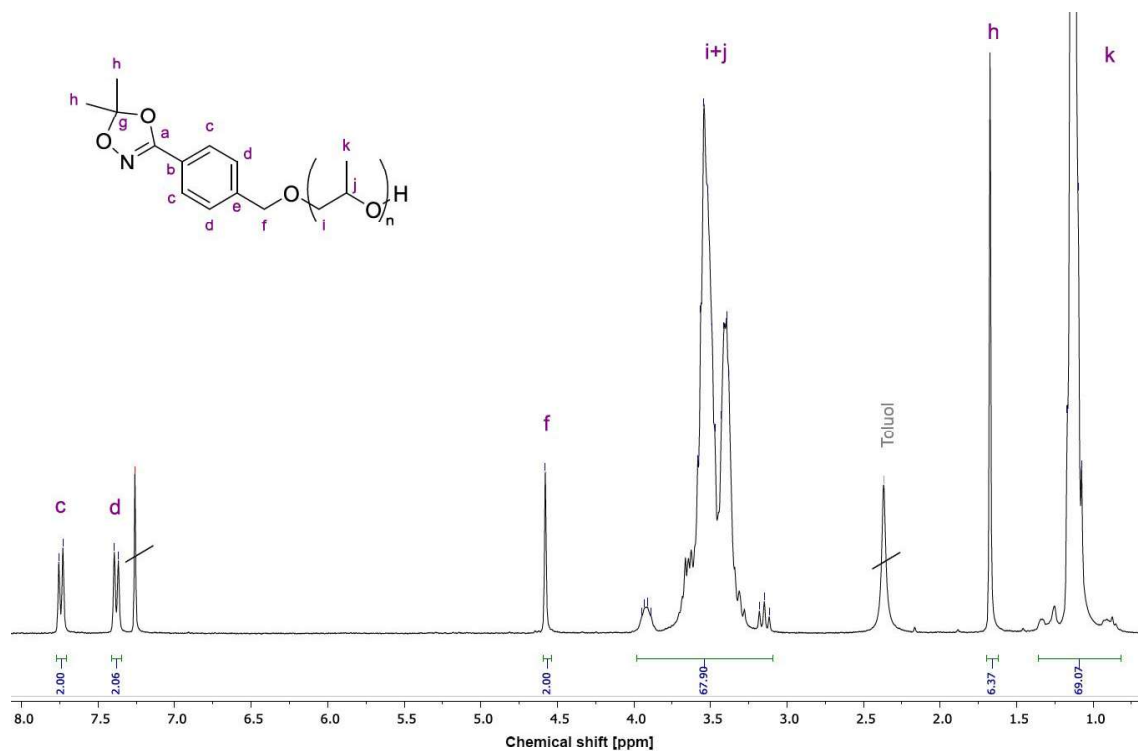

Figure S14. Exemplary ^{1}H NMR spectrum (300 MHz, CDCl$_3$) of benzyl HAA-PEG (**P2a**).

Characterization of HAA-PPO (P3a), benzylHAA-PPO (P4a), HAA-PEEGE (P5a) and benzylHAA-PEEGE (P6a) polymers

Figure S15. Exemplary ^{1}H NMR spectrum (300 MHz, CDCl$_3$) of HAA-PPO (**P3a**).

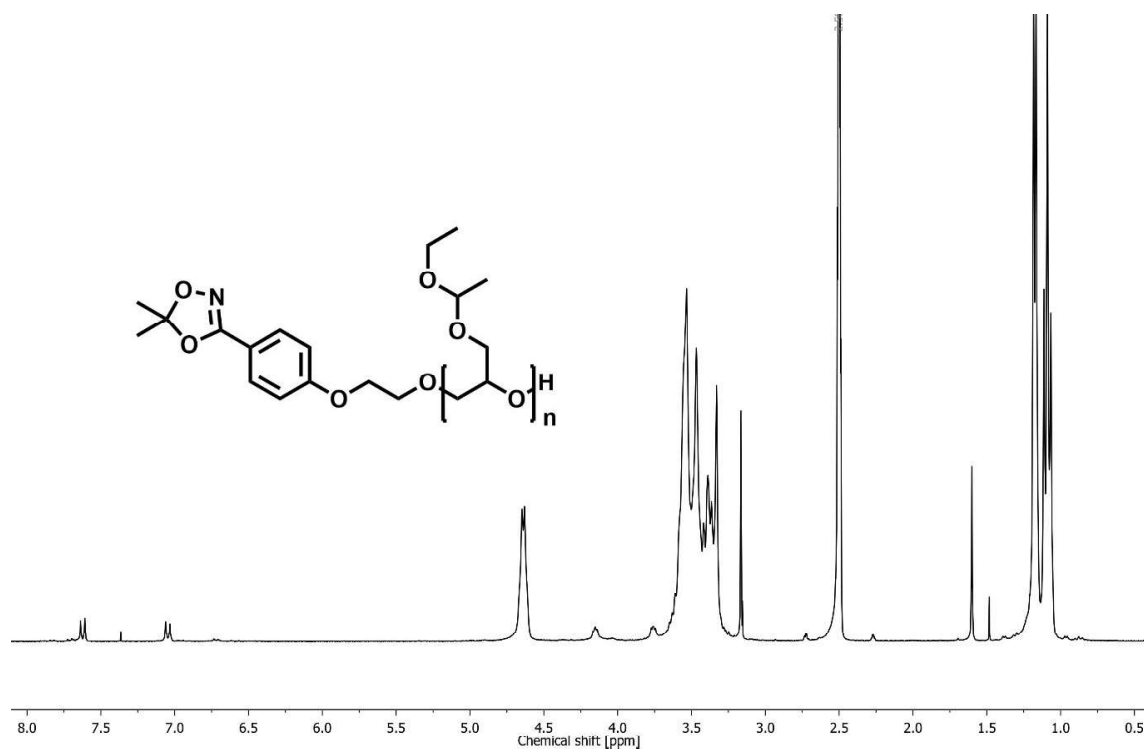**Figure S16.** Exemplary ^{1}H NMR spectrum (300 MHz, CDCl$_3$) of benzylHAA-PPO (**P4a**).

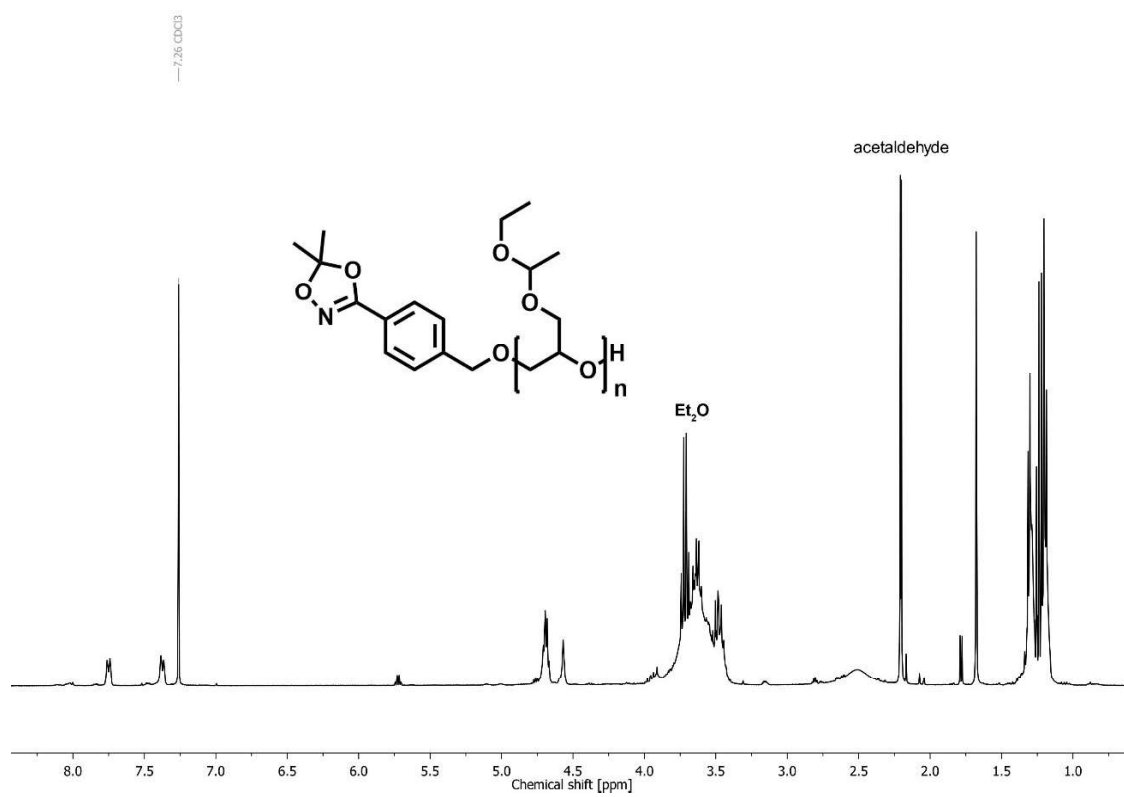**Figure S17.** Exemplary ¹H NMR spectrum (300 MHz, CDCl₃) of HAA-PEEGE (**P5a**).

Figure S18. Exemplary ¹H NMR spectrum (300 MHz, CDCl₃) of ᵇᵉⁿᶻʸˡHAA-PEEGE (**P6a**).

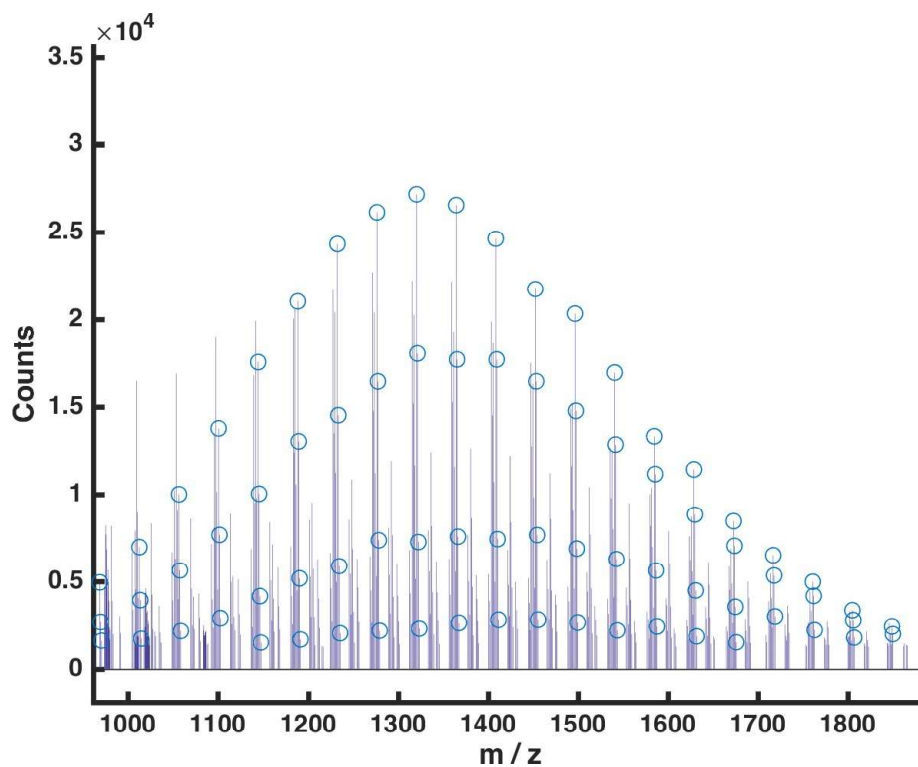## Polymer mass spectroscopy characterization

Figure S19. ESI-MS spectrum of HAA-PEG₃₁. The circles denote the HAA-PEG distribution with sodium as a counter ion.
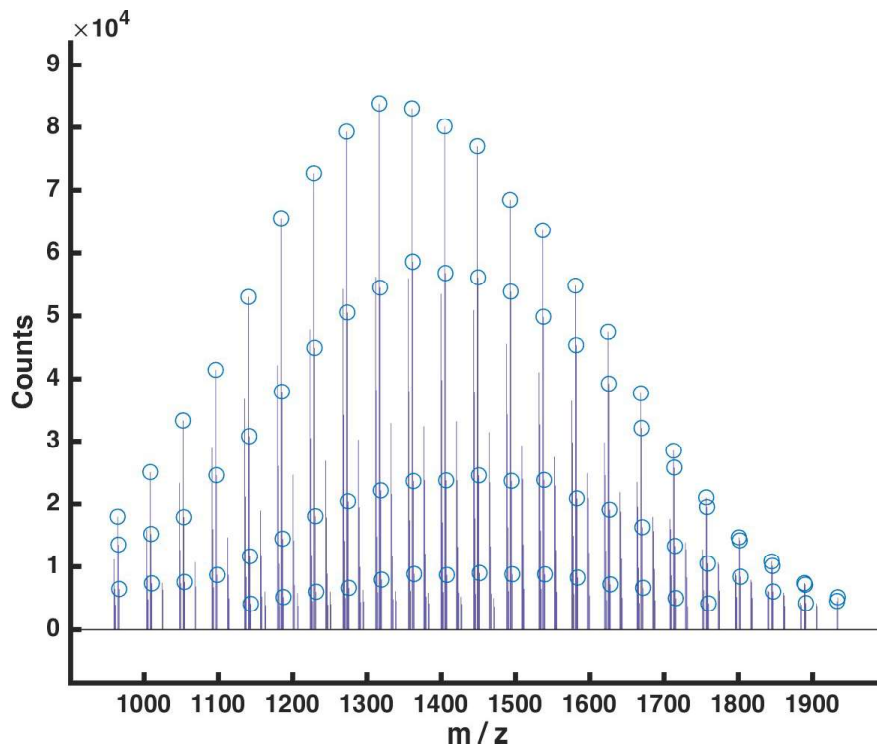

Figure S20. ESI-MS spectrum of HA-PEG₃₁. The circles denote the HA-PEG distribution with sodium as a counter ion.

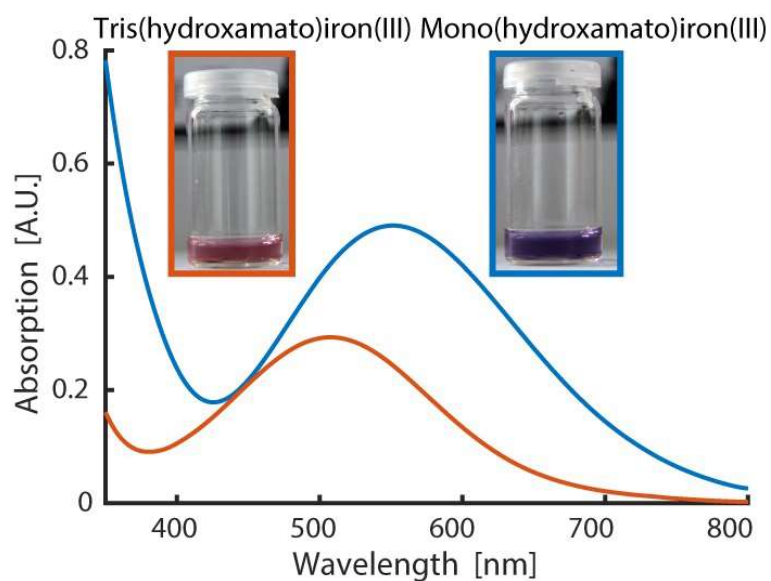## Complexation properties

Figure S21. UV-Vis spectra of tris(HA-PEG)iron(III) (red) and mono(HA-PEG)iron(III) (blue) complexes in methanol.

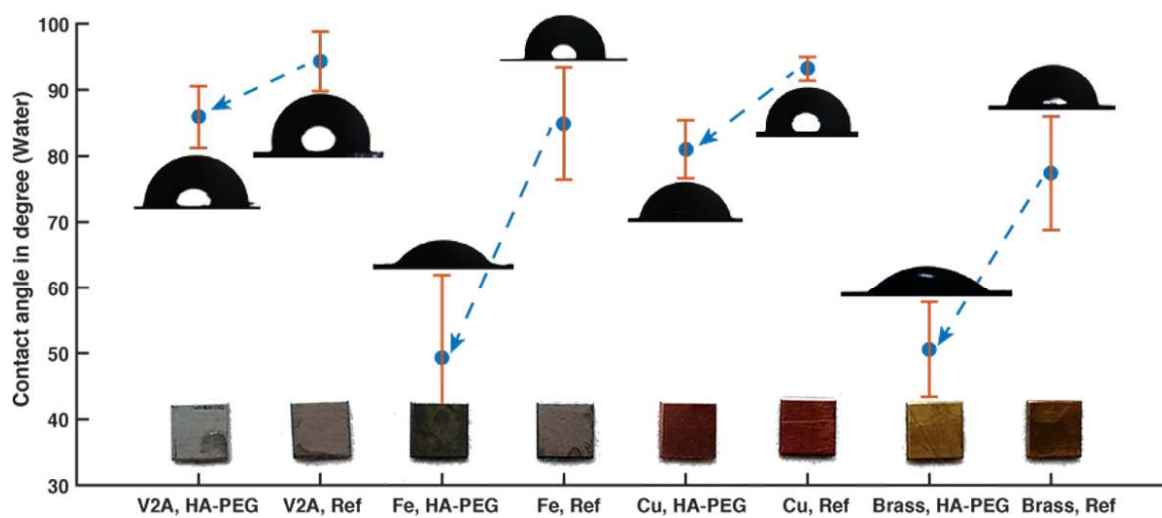**Figure S22.** Contact angle measurements by the sessile drop method. PEG_{44} was used as a reference. In all cases, increased hydrophilicity of the corresponding surface was detected when $HA\text{-}PEG_{188}$ was employed as a coating material.

Nanoparticle characterization
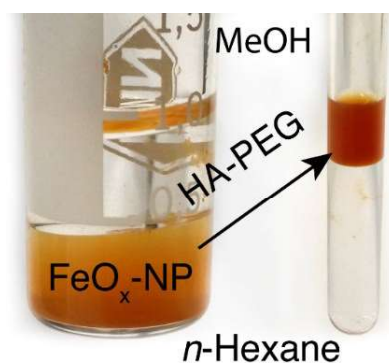
Figure S23. Proof of principle demonstration of the altered solubilisation behaviour of HA-PEG coated nanoparticles. Left image shows the non-modified nanoparticles solely soluble in n-hexane, while after coating with HA-PEG$_{188}$ the nanoparticles become freely soluble in methanol.

Table S1. Summary of DLS measurements.

Sample	Z_{avg} diameter [nm]	PDI	Peak diameter [nm]	Peak diameter standard deviation [nm]
NP-Oleat	20.9	0.10	21.3	4.5
NP-Oleat + PEG$_{44}$	22.2	0.10	23.7	6.7
NP-HA-PEG$_{21}$	25.8	0.08	27.1	6.5
NP-HA-PEG$_{80}$	35.8	0.07	38.9	9.7
NP-HA-PEG$_{188}$	49.4	0.09	53.4	12.3

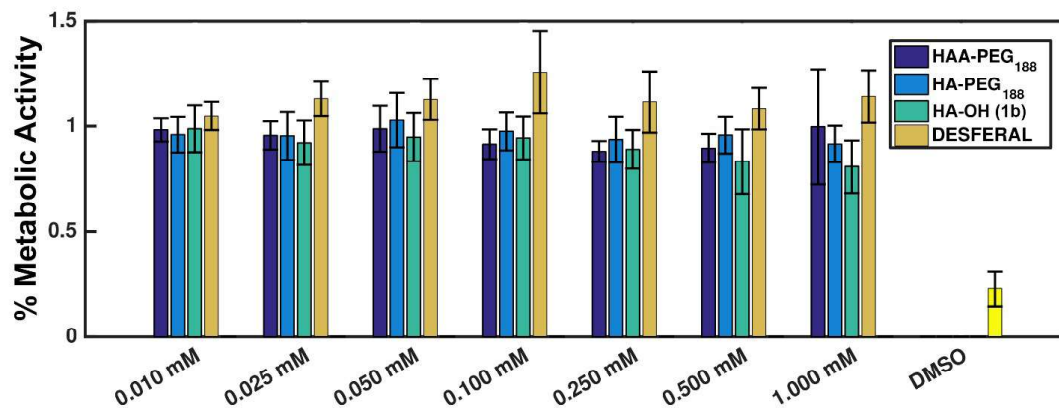## T-Cell proliferation assay and MTT metabolic activity analysis

Figure S24. MTT metabolic activity assay. In all cases no significant decrease in metabolic activity, translating to cell toxicity can be observed. Only in case of low MW HA "HA-OH" (1b) a subtle decrease in metabolic activity was detected, suggesting increased toxicity compared to HA-PEG$_{188}$. (Data denote the mean±SEM of values obtained for PBMC prepared from 4 different healthy donors and tested in triplicates.)
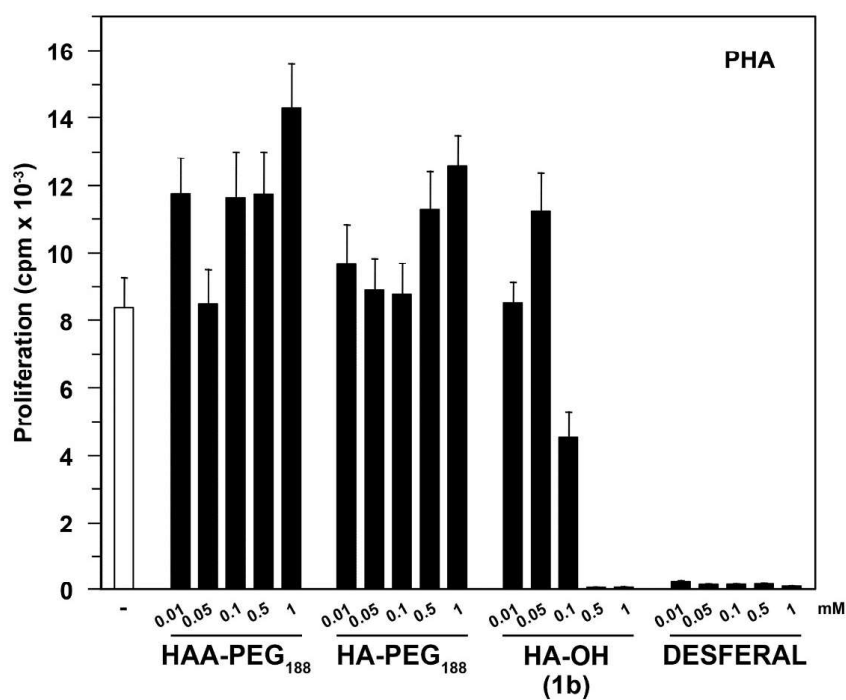
Figure S25. T-Cell proliferation assay. Human PBMC were stimulated with PHA to induce proliferation of T-cells in the presence of the different test compounds. In case of Desferal, proliferation was completely inhibited. Low MW HA compound "HA-OH" (1b) showed dose-dependent inhibition of proliferation. In contrast, no influence of HAA-PEG or HA-PEG was found regarding T-cell proliferation. (Data denote the mean±SEM of values obtained for PBMC prepared from 4 different healthy donors and tested in triplicates.)

Figure S26. T-Cell proliferation assay. Unstimulated human PBMC were incubated with different test compounds. No significant effect towards background proliferation were found. (Data denote the mean±SEM of values obtained for PBMC prepared from 4 different healthy donors and tested in triplicates.)

Jennifer Keth

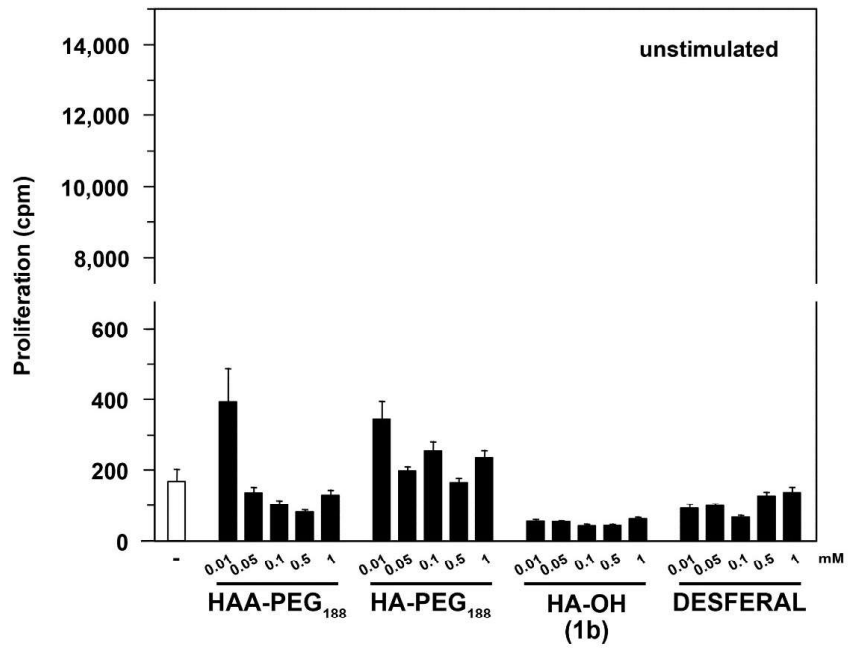## Education and Work Experience

10/2017 – now	**PhD candidate** Chemistry
	Johannes Gutenberg University (JGU), Mainz
	Research group of Prof. Dr. Holger Frey

Focus:
- Polymer chemistry and organic synthesis
- Reaction kinetics and spectroscopy

Collaborations:

Collaboration partners at 5 institutes

Supervision of:
- 2 Master students
- Bachelor students in 4 lab courses

10/2015 – 08/2017	**Master of Science (1.8)** Chemistry, JGU Mainz
	Research group of Prof. Dr. Holger Frey

Topic: "Anionic and radical polymerization of hydroxamic acid-functionalized vinyl based monomers"

12/2014 – 03/2015	**Semester abroad** Durham University, United Kingdom
	Research group of Prof. Dr. Lian Hutchings

Scholarship: ERASMUS+

*Topic: "*Synthesis and Temperature Gradient Interaction Chromatographic Characterization of end-functionalized Polymers*"*

10/2011 – 07/2015	**Bachelor of Science (2.4)** Chemistry, JGU Mainz
	Research group of Prof. Dr. Rudolf Zentel

Topic: "Synthesis and characterization of amphiphilic copolymer structures via controlled radical polymerization"

08/2002 – 03/2011	**High-school diploma (Abitur) (2.1)**
	Gauß-Gymnasium Worms

Specialized Skills

Organic Synthesis	Development of **metal chelating monomers** in multistep procedures
	Reversible blocking of functional groups
Polymer Synthesis	**Free** and **controlled radical polymerization**
	Carbanionic polymerization of **butadiene, styrene** and **functional derivatives**
Reaction kinetics and -monitoring	**Copolymerization kinetics** of **methacrylates** via *in situ* ^{1}H NMR spectroscopy
Spectroscopic Methods	**NMR** (1D- and 2D-techniques), **IR**, **UV-Vis**
Other Methods	**TLC**, **MALDI-ToF**, **SEC**, **TGIC**, **TEM**, **SEM**

Scientific Publications

Publications	**3 publications** in peer-reviewed journals See detailed list at: https://www.ak-frey.chemie.uni-mainz.de/jennifer-keth/
Conferences	**4 International conferences** with poster presentations

Languages and Skills

Languages	**German** (First language), **English** (Fluent), **Spanish** (Working knowledge), **French** (Working Knowledge)
IT	**Scientific Computing Software** *Office-Software, WinGPC Unichrom, MATLAB, ChemDraw, MestReNova, LaTeX* **Working Knowledge in Graphical Design** *Photoshop, Office Software*
Courses	Intercultural Communication, Project Management, Academic Writing, Presenting in English

Interests

Playing the trumpet, cooking, hiking

List of Publications

Contribution as first author or equally

2021

███████████████████████████████████

███████████████████████████████████████

███████████████████████████

2020

[4] <u>J. Keth</u>, T. Johann, H. Frey, Hydroxamic acid – An Underrated Moiety? Marrying Bioinorganic Chemistry and Polymer Science, *Biomacromolecules*, **2020**, DOI: 10.1021/acs.biomac.0c00449.

Contribution as coauthor

2019

[5] T. Johann, <u>J. Keth</u>, M. Bros, H. Frey, H. A general concept for the introduction of hydroxamic acids into polymers, *Chem. Sci*, **2019**, DOI: 10.1039/c9sc02557j.

2015

█████████████████████████████████████

Conferences

09/2019	**Ionic Polymerization, Beijing, China**
	Poster: Multifunctional hydroxamic acid-functionalized polymers as metal chelating agents
09/2018	**Meeting of the GDCh Division Macromolecular Chemistry, Karlsruhe, Germany**
	Poster: Hydroxamic acid-functionalized polymers for metal chelation obtained by controlled radical polymerization
05/2018	**Bordeaux Polymer Conference, Bordeaux, France**
	Poster: Hydroxamic acid-functionalized polymers for metal chelation obtained by radical polymerization
01/2015	**Separation and Characterization of Natural and Synthetic Macromolecules, Amsterdam (SCM-7), The Netherlands**
	Poster: Characterisation of High Molecular Weight End-Functionalised Polymers by Interaction Chromatography